Design, Synthesis and Characterization of Ruthenium Polypyridyl Complexes Towards Structural and Conformational Control of Intramolecular Electron Transfer

by

Mirvat Abdelhaq

B.S., University of New Mexico, 2006
B.A., University of New Mexico, 2006

A thesis submitted to the Faculty of the Graduate School of the University of Colorado in partial fulfillment of the requirements for the degree of Doctor of Philosophy
Department of Chemistry and Biochemistry
2012

This thesis entitled:
Design, Synthesis and Characterization of Ruthenium Polypyridyl Complexes Towards Structural and Conformational Control of Intramolecular Electron Transfer

written by Mirvat Abdelhaq

has been approved for the
Department of Chemistry and Biochemistry

by

_____
Niels H. Damrauer

_____
Gordana Dukovic

Date: _____

A final copy of this thesis has been approved by all signatories, and we find that both the content and the form meet acceptable presentation standards of scholarly work in the above mentioned discipline.

Mirvat Abdelhaq (Ph.D., Physical Chemistry)

Design, Synthesis and Characterization of Ruthenium Polypyridyl Complexes Towards Structural and Conformational Control of Intramolecular Electron Transfer

Thesis Directed by Niels H. Damrauer

Abstract

The demand for carbon neutral sources of energy has led researchers to turn toward strategies involving conversion of solar photons to produce electricity and fuels. Solar conversion is initiated by photoinduced electron transfer (ET) processes. Donor-Bridge-Acceptor (DBA) complexes are a common platform for investigating photoinduced intramolecular electron transfer processes.

In this work, two series of DBA complexes have been synthesized and characterized to investigate the role of structural elements on rates of photoinduced intramolecular electron transfer. The DBA complexes are comprised of a ruthenium polypyridyl donor covalently linked to a 4,4'-bipyridinium acceptor by a bridging aryl subunit. We hypothesize that the addition of steric bulk on the donor chromophore and the bridging subunit will alter the lifetimes for forward and back electron transfer processes.

New electroactive asymmetric ligands were synthesized in high yields and complexed to produce seven new DBA complexes which were characterized by absorption and emission spectroscopies, cyclic voltammetry and spectroelectrochemistry, electronic structure calculations and picosecond transient absorption techniques.

The first series of DBA complexes was prepared to investigate how lifetimes of intramolecular ET are affected by increased methylation on ancillary ligands which is expected to alter driving forces for ET. The electron lifetimes were measured for three complexes that share an electroactive ligand but differ in ancillary ligand. It was

determined that the lifetime for forward ET was not significantly altered but the lifetimes for back ET differed by a factor of two.

For the second DBA series, methyl groups were systematically introduced onto various positions of the bridging subunit to determine if steric bulk is effective at disrupting electron communication within the complex thereby altering ET lifetimes. Reductive spectroelectrochemistry and transient absorption spectra revealed that steric bulk was effective at localizing electron density onto the acceptor moiety. The measured ET lifetimes showed that the number of methyl substituents on the bridging subunit was more of a determining factor of ET lifetimes than the methyl substituent position.

To my family for understanding that this is what I wanted to do

Table of Contents

List of Tables

List of Figures and Schemes

Publications

Abdelhaq, M.; Damrauer, N.H., Synthesis and Characterization of a New Family of Asymmetric Electroactive Polypyridine Ligands for Investigating the Effect of Steric Bulk in Affecting Electron Delocalization. *In preparation*.

Abdelhaq, M.; Hewitt, J. T.; Damrauer, N. H. Ligand Platforms and their Coordination Complexes of Ru(II) for Observation and Structural control of Ultrafast Electron Transfer Photochemistry. *In preparation.*

Meylemans, H.A.; Hewitt, J.T.; Abdelhaq, M.; Vallett, P.J.; Damrauer, N.H. Exploiting Conformational Dynamics to Facilitate Formation and Trapping of Electron Transfer Photoproducts in Metal Complexes. *Journal of the American Chemical Society*. **132**, 11464-11466, (2010)

Acknowledgements

Working on this dissertation has been the most challenging, humbling and rewarding thing I have done. When I began this work so many years ago I had no idea what it would require and as I look back I realize that if were not for the support of so many people I would still be a confused second year student.

I would like to thank my advisor Niels Damrauer. Six years ago you had an idea about a molecular system and you patiently watched as I turned it into this body of work. Thank you for the patience. You taught me to pay attention to the schmutz in the baseline and to appreciate a good science story. I hope you are as proud of this work as I am. My committee members all had a hand in this work and I thank them. Tarek Sammakia, if you had not mentioned pinacol esters to me I do not think this dissertation would exist. Thank you for always answering my questions. Gordana Dukovic, thank you for appreciating the art of synthesis and understanding that someone has to do it. Veronica Bierbaum, for years you have passed on your encouragement and support, it has been always been greatly appreciated. Jerry Peterson, I am not sure what I did to earn your respect and support but thank you for everything; I will do my best to make you proud in DC.

For the past six years I have had the pleasure of sharing a lab with an incredible group of colleagues. Matthew Montgomery, Heather Meylemans and Erik Grumstrup- thank you for paving the way and proving it can be done. I would especially like to thank Heather for teaching me how to make a carbon-carbon bond. Josh you are my bmf and this work is as much yours as it is mine, thank you for everything. Paul Vallett, thank you for being as interested in my work as I was, I will always be grateful for all your help. Huan-Wei Tseng, Jamie Snyder and Karen Spettel- I hope I was a good teacher to you.

My family has been a constant source of support and encouragement. Thank you for understanding that this is what I wanted to do and for being there every step of the way. To my parents, who trusted me and the decisions I made, thank you for letting me forge my own path in life. To habibti Aminah- thank you for calling me everyday, your unconditional support has meant the world to me. To Mohammed, Omar, Jamilah, Serine, Moose, Noor and Ham- your support and encouragement were a constant. Finally, I'd like to thank habibi Ameen for always putting a smile on my face.

Throughout the years I have been surrounded by an excellent group of friends who reminded me that work was not the only thing in my life. I would especially like to thank the Garsts for welcoming me into their family. There were some crazy times but I will look back at the three years I was the 'nanny' fondly. Finally, I would like to thank Sydney Kaufman for always being there. Your support and motivation inspired me to aim big and I will always be thankful.

Chapter One

Introduction

1.1 Background and Research Plan

As the risks of a warming planet are established and communicated[1-4] the demand for carbon neutral sources of energy have risen. One strategy for solving the energy crisis involves conversion of solar photons to electricity and fuels.[1,5-20] This active area of research seeks to design and synthesize molecular systems whose structure permits the use of light absorption as a means of creating charge separated redox equivalents for energy storage or photocurrent generation.[18,21-42] Strategies for such exploration are initiated by photoinduced electron transfer processes rendering it essential to understand the fundamental elements of electron transfer as well as how to use light to drive and control them.

Our work focuses on understanding how to efficiently use light to create charge-separated species for energy conversion purposes. We strive to design systems of chromophores that will undergo photoinduced intramolecular electron transfer to produce and store charge-separated states. Within these systems of chromophores structural modifications are synthetically introduced to determine how photoinduced intramolecular electron transfer is affected while establishing which structural modifications are more amenable to forming longer-lived charge-separated states. The basis for this work is that structural modifications will manipulate nuclear coordinates that are not directly involved in the electron transfer process thereby altering parameters that affect electron transfer rate constants. Such parameters include the free energies of electron transfer (ΔG^0) and electronic coupling (H_{ab}) between the reactant and product.

In designing a system to address the effect of structural modifications on photoinduced intramolecular electron transfer rate constants we turn to donor-bridge-acceptor (DBA) complexes. The specific DBA platform chosen allows for systematic manipulation of structural elements of the donor chromophore (D) and the bridge (B). **Figure 1.1** summarizes the DBA platform described in this work where positions marked with R indicate where structural modifications have been introduced.

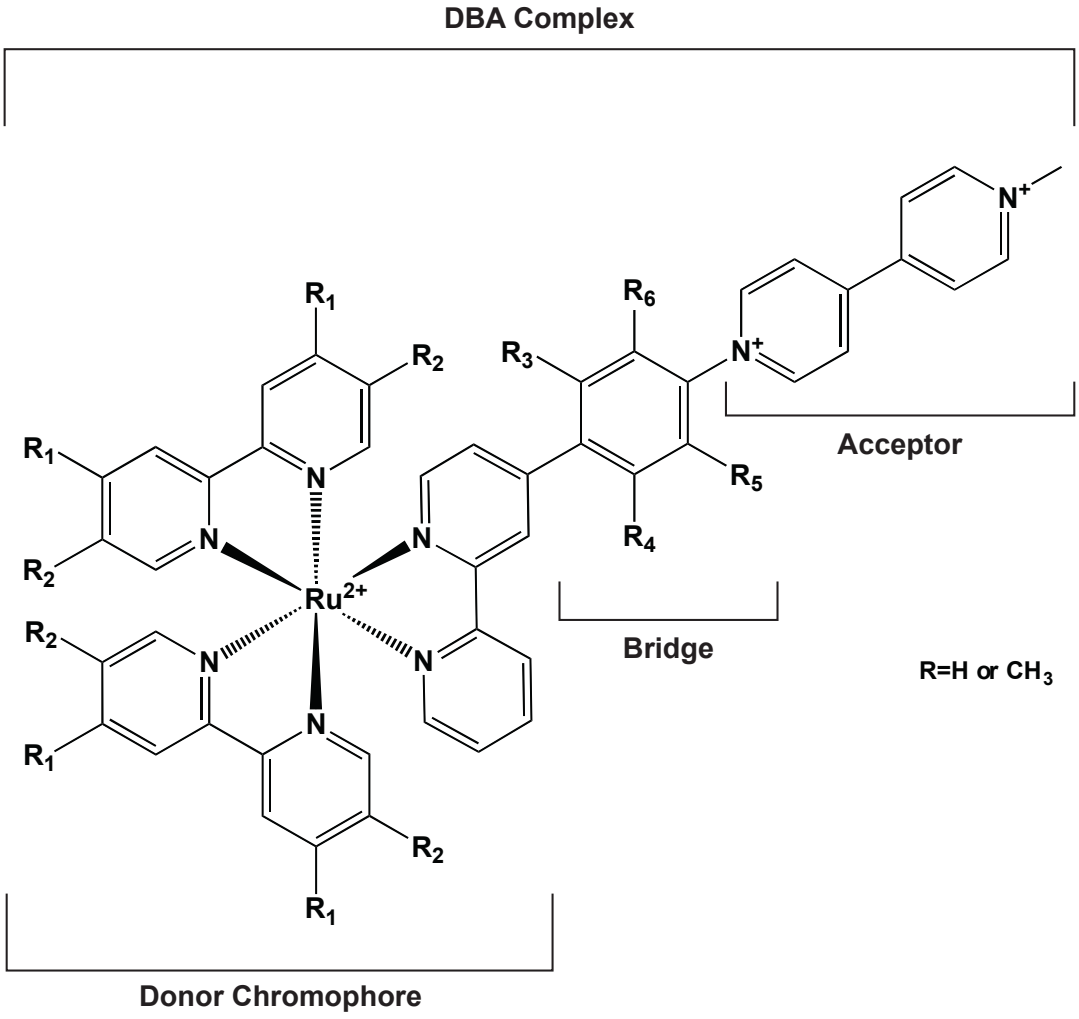

Figure 1.1 Donor-Bridge-Acceptor platform studied throughout this dissertation.

Ruthenium polypyridine complexes were chosen as donor chromophores, a conformationally active aryl group as the bridge and a 4,4'-bipyridinium derivative as the acceptor. Structural modifications in the form of methyl group substitutions were made in positions marked by R in **Figure 1.1**.

Ground and excited-state properties of ruthenium polypyridyl complexes make them appropriate choices as donor chromophores for photoinduced intramolecular electron transfer (ET) studies. The donor chromophores are bisheteroleptic derivatives of $[Ru(bpy)_3]^{2+}$ (see **Figure 1.2**) where bpy is 2,2'-bipyrdine. $[Ru(bpy)_3]^{2+}$ and hundreds of its derivatives have been well studied[43] and are prevalent in many applications of inorganic photochemistry. Such complexes find prominent use owing to properties of stability, excited-state lifetime, and an ability to undergo excited-state redox chemistry. These complexes are known for their long excited state lifetimes. $[Ru(bpy)_3]^{2+}$ has a reported excited state lifetime of $\sim$ 1 μs in degassed room temperature acetonitrile.[44] The photoinduced ET process requires the transfer of an electron from the excited state of the donor chromophore to the acceptor. Therefore, a long–lived excited state is advantageous for the formation of the ET photoproduct. $[Ru(bpy)_3]^{2+}$ and its derivatives are also known for their chemical stability; the choice of donor subunit must be chemically stable in order to reliably measure electron transfer lifetimes. Preparation of the DBA complexes is not trivial therefore utilizing a stable donor chromophore will aid in maintaining the integrity of the DBA complexes. $[Ru(bpy)_3]^{2+}$ and its derivatives are known for their intense metal-to-ligand charge transfer (MLCT) band upon absorption of a visible photon.[43,45] The MLCT process can be thought of as a simultaneous oxidation of the ruthenium and reduction of a polypyridine ligand. More specifically an electron is transferred from a dπ orbital on the

ruthenium to a π* orbital on a polypyridine ligand. The excitation is rapidly localized on the lower energy ancillary ligand. For $[Ru(bpy)_3]^{2+}$ the energy of the MLCT state is 2.1 eV.[43] The high energy MLCT state provides the donor chromophore with sufficient energy to do intramolecular electron transfer.

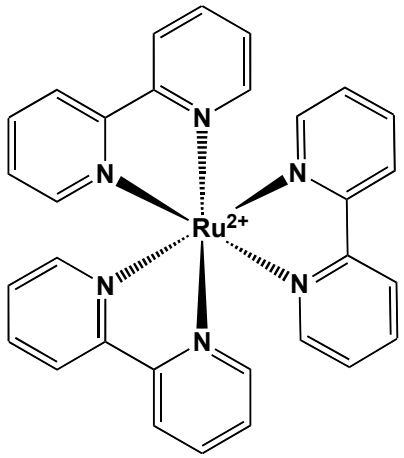

Figure 1.2 Structure of $[Ru(bpy)_3]^{2+}$

An additional reason for choosing ruthenium polypyridine complexes as donor chromophores is the ability to tune the energetics of the complexes. Substitution of ancillary ligands on $[Ru(bpy)_3]^{2+}$ has been shown to alter absorption and electrochemical properties of these complexes.[46] In our attempt to use structural modifications to affect ET rate constants DBA complexes were prepared with varying degrees of methylation on ancillary ligands. Methyl groups were introduced in positions R_1 and R_2 in **Figure 1.1**. By tuning the energetics of the complexes the free energies for ET are also tuned.[47] Thus, preparing DBA complexes with varying degrees of methylation on the ancillary ligands allows for studying the dependence of ET rate constants on structural modifications.

As stated above a conformationally active aryl group was selected as the bridging subunit (see **Figure 1.1**). The choice of bridging subunit is critical in our study of the effect of structural elements on the rates of photoinduced electron transfer. For our proposed DBA system the bridging subunit serves as the platform for introduction of steric bulk and therefore must be amenable to systematic functionalization with methyl groups. The aryl bridging subunit is appended onto a 2,2'-bipyridine ligand of the donor chromophore.

Transition metal complexes of aryl-substituted ligands are prevalent and their photophysics is well studied.[25,26,47-69] Increased molar extinction coefficients[51] and increased emission lifetimes[52-54,70] are explained by excited state intraligand delocalization of the charge-transferred electron onto the aryl-substituted polypyridine ligand after MLCT excitation. Delocalization of the charge-transferred electron is facilitated by ring rotation dynamics that allow the charge-transferred electron to delocalize over the π-system of the aryl-substituted polypyridine ligand. It is for this reason that the aryl subunit is referred to as conformationally active.

In order to understand the nature and timescale of ring rotation and excited state delocalization dynamics ultrafast experimental and theoretical studies were conducted on ruthenium (II) complexes with aryl-substituted polypyridine ligands by McCusker's group and others.[55,58,59,71,72] In the ground state the steric interactions between the hydrogen atoms on the polypyridyl ligand and aryl substituent prevent co-planarization between the two moieties. However, these studies concluded that upon excitation with a visible photon the ^{3}MLCT state will lie on the aryl-substituted ligand which has undergone nuclear rearrangement to assume a more coplanar geometry between the 2,2'-bipyridine and the aryl substituent. Co-planarization allows for maximization of the π-system in which the

charge-transferred electron from the excited ^{3}MLCT state lies. These dynamics are driven by the lowering of the energy of the excited state which can be explained by a reduction in the electron kinetic energy and by a reduction in inter-electron repulsions. When studying the ultrafast dynamics of $[Ru(dpb)_3]^{2+}$ (where dpb is 4,4'-diphenyl-2,2'-bipyridine) in room temperature acetonitrile the excited state delocalization and ring rotation dynamics were found to occur in ~ 1 ps. The ring rotation behavior in aryl-substituted polypyridine ligands is analogous to the ground and excited state behavior of neutral biphenyl.[73-76]

In our design of conformationally active electroactive ligands for studying the influence of structural elements on photoinduced intramolecular electron transfer we take advantage of the known inter-ring rotational dynamics that occur within the MLCT state of ruthenium (II) complexes with aryl-substituted polypyridyl ligands. We attempt to inhibit ring rotational dynamics by addition of steric bulk between the 2,2'-bipyridine moiety and the bridging aryl group (R_3 and R_4 in **Figure 1.1**). Unlike the addition of steric bulk on the ancillary ligands structural modifications of the bridging subunit are not expected to alter the energetics of the ET process but are expected to influence the excited-state dynamics of the DBA complexes. We speculate that hindering rotational dynamics will limit the extent of intraligand delocalization thereby reducing electronic coupling (H_{ab}). Electronic coupling is expected to change as the π*-system of the bridging subunit evolves with co-planarization. H_{ab} is governed by orbital overlap and orbital energies and as result it will be affected by intraligand delocalization. Therefore the rates of photoinduced ET are expected to be affected by structural modification to the bridging ligand.

Torsional motions, such as co-planarization between an aryl group and a 2,2'-bipyridine, have been found to play a significant role on intramolecular processes such as

electron transfer and energy transfer.[24,25,30,38,47,48,50,77-107] For a series of organic DBA systems which were designed to function as molecular wires Wasielewski and Ratner[30] found the intramolecular electron transfer process was gated by a low frequency torsional mode. Laine and co-workers have shown that conformational dynamics play a role in decoupling electroactive subunits in DBA complexes[48,108] where bulky substituents on the bridging ligand restricted conformational variability and as a result donor and acceptor moieties were electronically decoupled. Recent work by our group[77] has shown that a sterically encumbered conformationally active bridging subunit is responsible for more than an 8-fold increase in the lifetime of the electron transfer photoproduct in a series of ruthenium polypyridyl DBA complexes (see **Figure 1.3** below).

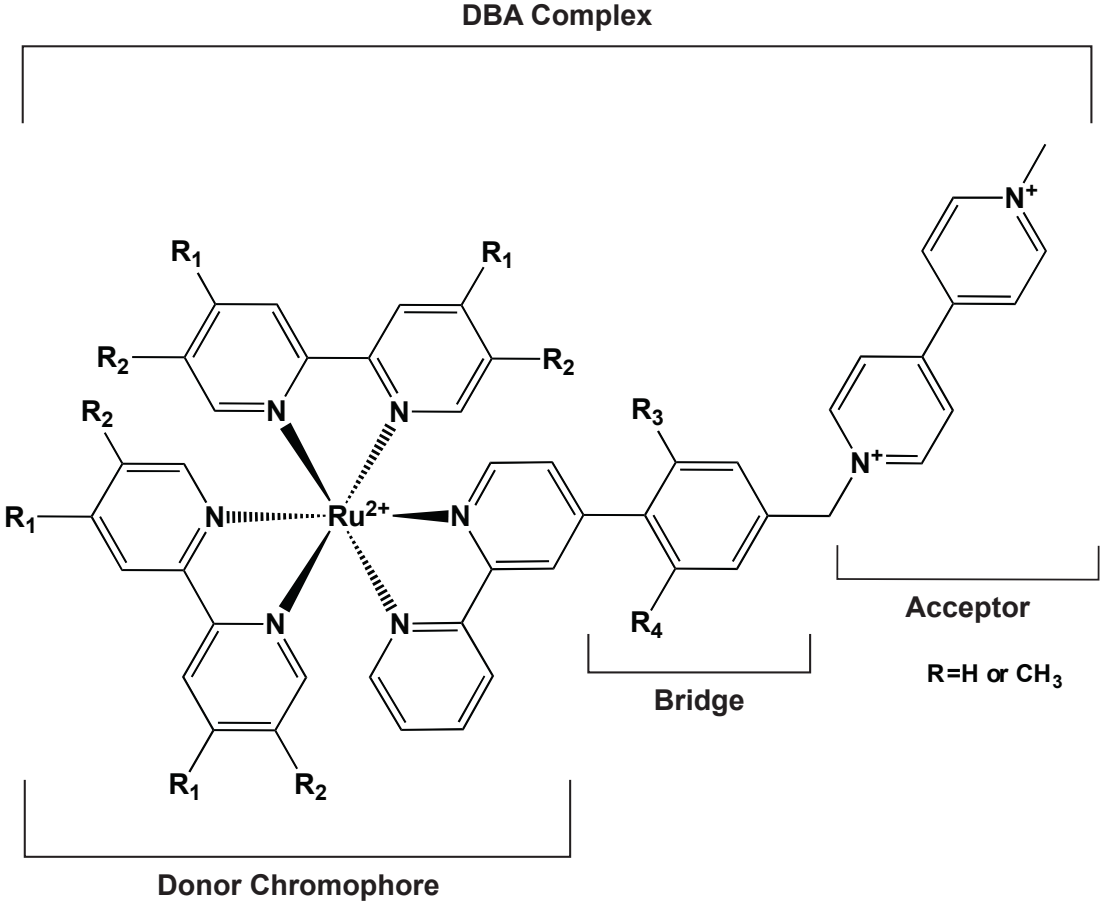

Figure 1.3 Donor-Bridge-Acceptor platform previously studied by our group.

For the acceptor a derivative of N,N'-dimethyl-4,4'-bipyridinium (methyl viologen, MV^{2+}) was chosen. Methyl viologen is widely used as an electron acceptor because of its striking color change upon reduction as well as the reversibility of radical cation formation.[109,110] Although examples of photoinduced intramolecular electron transfer from a ruthenium polypyridyl donor to methyl viologen acceptor exist in the literature,[36,47,77,111-116] this body of work is the first study of an electron acceptor that has been directly appended to an aryl-substituted 2,2'-bipyridine. For a majority of the reported studies the donor and acceptor moieties were separated by varying numbers of methylene (CH_2) spacers, which electronically decouple the π-systems of the donor chromophore and acceptor. By directly appending the electron acceptor the potential for conjugation throughout the electroactive ligand exists, thus enabling facile electronic communication across the electroactive ligand. Furthermore, the system of DBA complexes prepared allows for determining the role of steric bulk in inhibiting electronic coupling (H_{ab}) between the donor and bridging subunit as well as between bridging subunit and acceptor. The former has been achieved by the substitution of methyl groups in the R_3 and R_4 positions of the bridging subunit while the latter was achieved by substitution of steric bulk in positions R_5 and R_6 (see **Figure 1.1**). Methylation in the R_5 and R_6 positions allows us to address whether steric bulk in these positions can electronically isolate the acceptor from the remainder of the complex and to establish how this impacts rates of electron transfer.

The work described in this dissertation is centered on answering a fundamental question regarding the role of structural elements on photoinduced intramolecular electron transfer processes. Thus far it has been presented how steric bulk has been

utilized to alter the properties that determine electron transfer lifetimes such as free energy and electronic coupling. However, the systematic methylation of the bridging ligand also allows for establishing whether steric bulk can be utilized to create longer-lived ET photoproducts while not significantly altering the rate of which the photoproduct is formed. We speculate that methylation on R_5 and R_6 is more amenable to 'trapping' the electron transfer photoproduct on the acceptor. This body of work is rooted in understanding how structural elements affect photoinduced electron transfer. This process is the initial step for solar energy conversion therefore creating long-lived charge-separated states is desired within this field of research.

Towards answering these questions seven new DBA complexes were prepared and characterized. The complexes are classified into two categories. The first of these categories is referred to as the 'driving-force series' where the complexes share the same electroactive asymmetric ligand but differ in ancillary ligand. The second series known as the 'sterics series' consists of five DBA complexes which possess the same ancillary ligand but the electroactive ligands vary in the position and number of methyl substituents on the bridging ligand. Following synthesis and typical NMR analysis, the complexes were characterized by electrochemical techniques, absorption and emission spectroscopies, electronic structure calculations and picosecond transient absorption experiments.

Prior to preparing the DBA complexes asymmetric electroactive ligands were synthesized. Chapter Two describes in detail the synthetic routes utilized to prepare a series of methylated-aryl substituted polypyridine ligands. The synthesis of ligands with and without covalently linked electroactive acceptors is described. Synthesis of acceptor subunits is also described. The electroactive ligands and acceptor subunits are

characterized by electrochemical techniques. Cyclic voltammetry measures reduction potentials and reductive spectroelectrochemical measurements determines the absorption properties of the radical cations of both electroactive ligands and acceptor subunits. We find from the reductive spectroelectrochemical measurements that methylation on the bridging ligand influences the electronic properties of the ligands and can be used to 'subdivide' ligands into different regions for delocalization following reduction.

In Chapter Three the synthesis and purification of the metal complexes prepared from the asymmetric aryl substituted ligands is described. As mentioned above, seven DBA complexes alongside seven corresponding 'donor' complexes were prepared. These complexes are acceptor-less analogues of the DBA complexes and form a set of model compounds that cannot undergo photoinduced electron transfer. Cyclic voltammetry and spectroelectrochemical techniques are used to electrochemically characterize the complexes. Cyclic voltammetry measurements afford oxidation and reduction potentials of the complexes while oxidative and reductive spectroelectrochemistry experiments provide spectral information on the reduced and oxidized metal complex, respectively.

Chapters Four and Five describe the photophysical characterization of the metal complexes prepared in the 'driving-force series' and 'sterics series', respectively. Here steady state and time dependent techniques will be used to characterize the complexes. Steady state absorption and emission measurements will establish a foundation of the electronic properties of the complexes. Driving forces for photoinduced electron transfer are calculated and quantum calculations are used to aid in understanding the UV-visible spectra of the complexes. Lastly, picosecond transient absorption experiments that detect and measure the lifetimes for photoinduced intramolecular electron transfer are described.

In fact, intramolecular electron transfer is found to occur in these complexes and structural elements are found to play a role in controlling the electron transfer process.

This body of work describes a systematic approach to investigating the role of structural modifications on photoinduced intramolecular electron transfer processes. Steric bulk was methodically substituted on various positions of donor-bridge-acceptor complexes to specifically address the role of structural elements from three different perspectives. First, using structural elements to manipulate the energetics of electron transfer. Second, using structural elements to influence excited-state dynamics of DBA complexes. Third, using structural elements to potentially localize electron density and create long-lived charge separated states for energy conversion purposes. In preparing and characterizing the DBA complexes the importance of structural elements has been presented and illustrates the power of controlling electron transfer properties and processes with structural modifications.

1.2 References

(1) Lewis, N. S.; Nocera, D. G. *Proc. Natl. Acad. Sci. U.S.A.* **2006**, *103*, 15729.

(2) *IPCC Fourth Assessment Report; Climate Change 2007: The Physical Science Basis*; Cambridge University Press: Cambridge, 2007.

(3) Hoffert, M. I.; Caldeira, K.; Jain, A. K.; Haites, E. F.; Harvey, L. D. D.; Potter, S. D.; Schlesinger, M. E.; Schneider, S. H.; Watts, R. G.; Wigley, T. M. L.; Wuebbles, D. J. *Nature* **1998**, *395*, 881.

(4) *Basic Research Needs for Solar Energy Utilization*; Office of Science; US Department of Energy: Washington DC, 2005.

(5) Nozik, A. J. *Annu. Rev. Phys. Chem.* **1978**, *29*, 189.

(6) Gray, H. B.; Maverick, A. W. *Science* **1981**, *214*, 1201.

(7) Meyer, T. J. *Acc. Chem. Res.* **1989**, *22*, 163.

(8) O'Regan, B.; Gratzel, M. *Nature* **1991**, *353*, 737.

(9) Wasielewski, M. R. *Chem. Rev.* **1992**, *92*, 435.

(10) Kalyanasundaram, K.; Gratzel, M. *Coord. Chem. Rev.* **1998**, *177*, 347.

(11) Gosztola, D.; Niemczyk, M. P.; Svec, W.; Lukas, A. S.; Wasielewski, M. R. *J. Phys. Chem. A* **2000**, *104*, 6545.

(12) Gust, D.; Moore, T. A.; Moore, A. L. *Acc. Chem. Res.* **2001**, *34*, 40.

(13) Gratzel, M. *J. Photochem. Photobiol., C* **2003**, *4*, 145.

(14) Nozik, A. J. *Inorg. Chem.* **2005**, *44*, 6893.
(15) Wenger, O. S.; Leigh, B. S.; Villahermosa, R. M.; Gray, H. B.; Winkler, J. R. *Science* **2005**, *307*, 99.
(16) Alstrum-Acevedo, J. H.; Brennaman, M. K.; Meyer, T. J. *Inorg. Chem.* **2005**, *44*, 6802.
(17) Meyer, G. J. *Inorg. Chem.* **2005**, *44*, 6852.
(18) Wasielewski, M. R. *J. Org. Chem.* **2006**, *71*, 5051.
(19) Crabtree, G. W.; Lewis, N. S. *Physics Today* **2007**, *60*, 37.
(20) Kamat, P. V. *J. Phys. Chem. C* **2007**, *111*, 2834.
(21) Wasielewski, M. R. *Chem. Rev.* **1992**, *92*, 435.
(22) Balch, A. L.; Olmstead, M. M. *Chem. Rev.* **1998**, *98*, 2123.
(23) Barbara, P. F.; Meyer, T. J.; Ratner, M. A. *J. Phys. Chem.* **1996**, *100*, 13148.
(24) Benniston, A. C.; Harriman, A. *Chem. Soc. Rev.* **2006**, *35*, 169.
(25) Johansson, O.; Borgstrom, M.; Lomoth, R.; Palmblad, M.; Bergquist, J.; Hammarstrom, L.; Sun, L. C.; Akermark, B. *Inorg. Chem.* **2003**, *42*, 2908.
(26) Collin, J. P.; Guillerez, S.; Sauvage, J. P.; Barigelletti, F.; Decola, L.; Flamigni, L.; Balzani, V. *Inorg. Chem.* **1991**, *30*, 4230.
(27) Cukier, R. I.; Nocera, D. G. *Annu. Rev. Phys. Chem.* **1998**, *49*, 337.
(28) Damrauer, N. H.; Hodgkiss, J. M.; Rosenthal, J.; Nocera, D. G. *J. Phys. Chem. B* **2004**, *108*, 6315.
(29) Davis, W. B.; Svec, W. A.; Ratner, M. A.; Wasielewski, M. R. *Nature* **1998**, *396*, 60.
(30) Davis, W. B.; Ratner, M. A.; Wasielewski, M. R. *J. Am. Chem. Soc.* **2001**, *123*, 7877.
(31) Heimer, T. A.; Heilweil, E. J.; Bignozzi, C. A.; Meyer, G. J. *J. Phys. Chem. A* **2000**, *104*, 4256.
(32) Laine, P. P.; Loiseau, F.; Campagna, S.; Ciofini, I.; Adamo, C. *Inorg. Chem.* **2006**, *45*, 5538.
(33) Macqueen, D. B.; Schanze, K. S. *J. Am. Chem. Soc.* **1991**, *113*, 7470.
(34) Newton, M. D. *Chem. Rev.* **1991**, *91*, 767.
(35) Oevering, H.; Paddonrow, M. N.; Heppener, M.; Oliver, A. M.; Cotsaris, E.; Verhoeven, J. W.; Hush, N. S. *J. Am. Chem. Soc.* **1987**, *109*, 3258.
(36) Yonemoto, E. H.; Riley, R. L.; Kim, Y. I.; Atherton, S. J.; Schmehl, R. H.; Mallouk, T. E. *J. Am. Chem. Soc.* **1992**, *114*, 8081.
(37) Weller, A. *Z. Phys. Chem.* **1982**, *133*, 93.
(38) Weber, J. M.; Rawls, M. T.; MacKenzie, V. J.; Limoges, B. R.; Elliott, C. M. *J. Am. Chem. Soc.* **2007**, *129*, 313.
(39) Watson, D. F.; Meyer, G. J. *Annu. Rev. Phys. Chem.* **2005**, *56*, 119.
(40) Sauvage, J.-P.; Collin, J.-P.; Chambron, J.-C.; Guillerez, S.; Coudret, C. *Chem. Rev.* **1994**, *94*, 993.
(41) Rubtsov, I. V.; Susumu, K.; Rubtsov, G. I.; Therien, M. J. *J. Am. Chem. Soc.* **2003**, *125*, 2687.
(42) Opperman, K. A.; Mecklenburg, S. L.; Meyer, T. J. *Inorg. Chem.* **1994**, *33*, 5295.
(43) Juris, A.; Balzani, V.; Barigelletti, F.; Campagna, S.; Belser, P.; von Zelewsky, A. *Coord. Chem. Rev.* **1988**, *84*, 85.
(44) Demas, J. N.; Crosby, G. A. *J. Phys. Chem.* **1971**, *75*, 991.

(45) Kalyanasundaram, K. **1992**.
(46) Anderson, P. A.; Keene, F. R.; Meyer, T. J.; Moss, J. A.; Strouse, G. F.; Treadway, J. A. *J Chem Soc Dalton* **2002**, 3820.
(47) Meylemans, H. A.; Lei, C. F.; Damrauer, N. H. *Inorg. Chem.* **2008**, *47*, 4060.
(48) Laine, P. P.; Bedioui, F.; Loiseau, F.; Chiorboli, C.; Campagna, S. *J. Am. Chem. Soc.* **2006**, *128*, 7510.
(49) Sauvage, J. P.; Collin, J. P.; Chambron, J. C.; Guillerez, S.; Coudret, C.; Balzani, V.; Barigelletti, F.; Decola, L.; Flamigni, L. *Chem. Rev.* **1994**, *94*, 993.
(50) Laine, P. P.; Campagna, S.; Loiseau, F. *Coord. Chem. Rev.* **2008**, 2552.
(51) Phifer, C. C.; McMillin, D. R. *Inorg. Chem.* **1986**, *25*, 1329.
(52) Boyde, S.; Strouse, G. F.; Jones, W. E.; Meyer, T. J. *J. Am. Chem. Soc.* **1990**, *112*, 7395.
(53) Strouse, G. F.; Schoonover, J. R.; Duesing, R.; Boyde, S.; Jones, W. E.; Meyer, T. J. *Inorg. Chem.* **1995**, *34*, 473.
(54) Treadway, J. A.; Loeb, B.; Lopez, R.; Anderson, P. A.; Keene, F. R.; Meyer, T. J. *Inorg. Chem.* **1996**, *35*, 2242.
(55) Damrauer, N. H.; Boussie, T. R.; Devenney, M.; McCusker, J. K. *J. Am. Chem. Soc.* **1997**, *119*, 8253.
(56) Hammarstrom, L.; Barigelletti, F.; Flamigni, L.; Indelli, M. T.; Armaroli, N.; Calogero, G.; Guardigli, M.; Sour, A.; Collin, J. P.; Sauvage, J. P. *J. Phys. Chem. A* **1997**, *101*, 9061.
(57) Feliz, M. R.; Rodriguez-Nieto, F.; Ruiz, G.; Wolcan, E. *J Photochem Photobiol a-Chem* **1998**, *117*, 185.
(58) Damrauer, N. H.; McCusker, J. K. *J. Phys. Chem. A* **1999**, *103*, 8440.
(59) Damrauer, N. H.; McCusker, J. K. *Inorg. Chem.* **1999**, *38*, 4268.
(60) Miller, M. T.; Gantzel, P. K.; Karpishin, T. B. *Inorg. Chem.* **1999**, *38*, 3414.
(61) Michalec, J. F.; Bejune, S. A.; McMillin, D. R. *Inorg. Chem.* **2000**, *39*, 2708.
(62) Berg, K. E.; Tran, A.; Raymond, M. K.; Abrahamsson, M.; Wolny, J.; Redon, S.; Andersson, M.; Sun, L. C.; Styring, S.; Hammarstrom, L.; Toftlund, H.; Akermark, B. *Eur. J. Inorg. Chem.* **2001**, 1019.
(63) Michalec, J. F.; Bejune, S. A.; Cuttell, D. G.; Summerton, G. C.; Gertenbach, J. A.; Field, J. S.; Haines, R. J.; McMillin, D. R. *Inorg. Chem.* **2001**, *40*, 2193.
(64) Walters, K. A.; Ley, K. D.; Cavalaheiro, C. S. P.; Miller, S. E.; Gosztola, D.; Wasielewski, M. R.; Bussandri, A. P.; van Willigen, H.; Schanze, K. S. *J. Am. Chem. Soc.* **2001**, *123*, 8329.
(65) Walters, K. A.; Premvardhan, L. L.; Liu, Y.; Peteanu, L. A.; Schanze, K. S. *Chem. Phys. Lett.* **2001**, *339*, 255.
(66) Wang, Y. S.; Liu, S. X.; Pinto, M. R.; Dattelbaum, D. M.; Schoonover, J. R.; Schanze, K. S. *J. Phys. Chem. A* **2001**, *105*, 11118.
(67) Balazs, G. C.; del Guerzo, A.; Schmehl, R. H. *Photochem. Photobiol. Sci.* **2005**, *4*, 89.
(68) Goze, C.; Sabatini, C.; Barbieri, A.; Barigelletti, F.; Ziessel, R. *Inorg. Chem.* **2007**, *46*, 7341.
(69) Clark, M. L.; Diring, S.; Retailleau, P.; McMillin, D. R.; Ziessel, R. *Chem. Eur. J.* **2008**, *14*, 7168.

(70) Strouse, G. F.; Schoonover, J. R.; Duesing, R.; Boyde, S.; Jones, W. E.; Meyer, T. J. *Inorg. Chem.* **1995**, *34*, 473.
(71) Damrauer, N. H.; Weldon, B. T.; McCusker, J. K. *J. Phys. Chem. A* **1998**, *102*, 3382.
(72) Lyubimova, O. O.; Baranovskii, V. I. *Journal of Structural Chemistry* **2003**, *44*, 728.
(73) Almenningen, A.; Bastiansen, O.; Fernholt, L.; Cyvin, B. N.; Cyvin, S. J.; Samdal, S. *J Mol Struct* **1985**, *128*, 59.
(74) Brock, C. P.; Minton, R. P. *J. Am. Chem. Soc.* **1989**, *111*, 4586.
(75) Rubio, M.; Merchan, M.; Orti, E. *Theoretica Chimica Acta* **1995**, *91*, 17.
(76) Rubio, M.; Merchan, M.; Orti, E.; Roos, B. O. *Chem. Phys. Lett.* **1995**, *234*, 373.
(77) Meylemans, H. A.; Hewitt, J. T.; Abdelhaq, M.; Vallett, P. J.; Damrauer, N. H. *J. Am. Chem. Soc.* **2010**, *132*, 11464.
(78) Meylemans, H.; Damrauer, N. H., In preparation.
(79) Larsson, S. *J. Am. Chem. Soc.* **1981**, *103*, 4034.
(80) Helms, A.; Heiler, D.; McLendon, G. *J. Am. Chem. Soc.* **1991**, *113*, 4325.
(81) Gourdon, A. *New J. Chem.* **1992**, *16*, 953.
(82) Dong, T. Y.; Huang, C. H.; Chang, C. K.; Wen, Y. S.; Lee, S. L.; Chen, J. A.; Yeh, W. Y.; Yeh, A. *J. Am. Chem. Soc.* **1993**, *115*, 6357.
(83) Ward, M. D. *Chem. Soc. Rev.* **1995**, *24*, 121.
(84) Sachs, S. B.; Dudek, S. P.; Hsung, R. P.; Sita, L. R.; Smalley, J. F.; Newton, M. D.; Feldberg, S. W.; Chidsey, C. E. D. *J. Am. Chem. Soc.* **1997**, *119*, 10563.
(85) Newton, M. D. *International Journal of Quantum Chemistry* **2000**, *77*, 255.
(86) Toutounji, M. M.; Ratner, M. A. *J. Phys. Chem. A* **2000**, *104*, 8566.
(87) Nelsen, S. F.; Li, G. Q.; Konradsson, A. *Org. Lett.* **2001**, *3*, 1583.
(88) Nelsen, S. F.; Blomgren, F. *J. Org. Chem.* **2001**, *66*, 6551.
(89) Kyrychenko, A.; Albinsson, B. *Chem. Phys. Lett.* **2002**, *366*, 291.
(90) Benniston, A. C.; Harriman, A.; Li, P.; Sams, C. A.; Ward, M. D. *J. Am. Chem. Soc.* **2004**, *126*, 13630.
(91) Rubtsov, I. V.; Redmore, N. P.; Hochstrasser, R. M.; Therien, M. J. *J. Am. Chem. Soc.* **2004**, *126*, 2684.
(92) Joachim, C.; Ratner, M. A. *Nanotechnology* **2004**, *15*, 1065.
(93) Smalley, J. F.; Sachs, S. B.; Chidsey, C. E. D.; Dudek, S. P.; Sikes, H. D.; Creager, S. E.; Yu, C. J.; Feldberg, S. W.; Newton, M. D. *J. Am. Chem. Soc.* **2004**, *126*, 14620.
(94) Benniston, A. C.; Harriman, A.; Li, P. Y.; Patel, P. V.; Sams, C. A. *Phys. Chem. Chem. Phys.* **2005**, *7*, 3677.
(95) Holman, M. W.; Yan, P.; Ching, K. C.; Liu, R. C.; Ishak, F. I.; Adams, D. M. *Chem. Phys. Lett.* **2005**, *413*, 501.
(96) Weiss, E. A.; Tauber, M. J.; Kelley, R. F.; Ahrens, M. J.; Ratner, M. A.; Wasielewski, M. R. *J. Am. Chem. Soc.* **2005**, *127*, 11842.
(97) Welter, S.; Salluce, N.; Belser, P.; Groeneveld, M.; De Cola, L. *Coord. Chem. Rev.* **2005**, *249*, 1360.
(98) Valasek, M.; Pecka, J.; Jindrich, J.; Calleja, G.; Craig, P. R.; Michl, J. *J. Org. Chem.* **2005**, *70*, 405.
(99) Benniston, A. C.; Harriman, A.; Li, P. Y.; Patel, P. V.; Sams, C. A. *J. Org. Chem.* **2006**, *71*, 3481.

(100) Eng, M. P.; Ljungdahl, T.; Martensson, J.; Albinsson, B. *J. Phys. Chem. B* **2006**, *110*, 6483.

(101) Venkataraman, L.; Klare, J. E.; Nuckolls, C.; Hybertsen, M. S.; Steigerwald, M. L. *Nature* **2006**, *442*, 904.

(102) Albinsson, B.; Eng, M.; Pettersson, K.; Winters, M. *Phys. Chem. Chem. Phys.* **2007**, *9*, 5847.

(103) Kilsa, K.; Kajanus, J.; Martensson, J.; Albinsson, B. *J. Phys. Chem. B* **1999**, *103*, 7329.

(104) Indelli, M. T.; Chiorboli, C.; Flamigni, L.; De Cola, L.; Scandola, F. *Inorg. Chem.* **2007**, *46*, 5630.

(105) Albinsson, B.; Martensson, J. *J. Photochem. Photobiol. C-Photochem. Rev.* **2008**, *9*, 138.

(106) Benniston, A.; Harriman, A.; Li, P.; Patel, P.; Sams, C. *Chem. Eur. J.* **2008**, *14*, 1710.

(107) Eng, M.; Albinsson, B. *Chem. Phys.* **2009**, *357*, 132.

(108) Ciofini, I.; Laine, P. P.; Bedioui, F.; Adamo, C. *J. Am. Chem. Soc.* **2004**, *126*, 10763.

(109) Monk, P. M. S. *The viologens : physicochemical properties, synthesis, and applications of the salts of 4,4'-bipyridine*; Wiley: Chichester ; New York, 1998.

(110) *Electron Transfer in Chemistry*; Balzani, V., Ed.; Wiley-VCH: Weinheim, 2001.

(111) Cooley, L. F.; Headford, C. E. L.; Elliott, C. M.; Kelley, D. F. *J. Am. Chem. Soc.* **1988**, *110*, 6673.

(112) Cooley, L. F.; Larson, S. L.; Elliott, C. M.; Kelley, D. F. *J. Phys. Chem.* **1991**, *95*, 10694.

(113) Elliott, C. M.; Freitag, R. A.; Blaney, D. D. *J. Am. Chem. Soc.* **1985**, *107*, 4647.

(114) Kelly, L. A.; Rodgers, M. A. J. *J. Phys. Chem.* **1995**, *99*, 13132.

(115) Lomoth, R.; Haupl, T.; Johansson, O.; Hammarstrom, L. *Chem. Eur. J.* **2002**, *8*, 102.

(116) Yonemoto, E. H.; Saupe, G. B.; Schmehl, R. H.; Hubig, S. M.; Riley, R. L.; Iverson, B. L.; Mallouk, T. E. *J. Am. Chem. Soc.* **1994**, *116*, 4786.

Chapter Two

Synthesis and Characterization of Conformationally Active Asymmetric Electroactive Ligands

2.1 Introductory Remarks

In order to determine the role that nuclear motions play in the mechanism and rate constants of photoinduced intramolecular electron transfer (ET), molecular systems that allow for the introduction of systematic structural and electronic barriers to ET need to be designed and prepared. To achieve the goal of studying photoinduced intramolecular ET we rely on the well-known architecture of Donor-Bridge-Acceptor (DBA) molecular systems.[1-17] The donor moiety serves as the source of the electron following photo-excitation of the molecule, the acceptor moiety is the recipient, and the bridge covalently links the two portions. The bridge will also serve as the platform for which the aforementioned structural and electronic barriers are introduced into the systems.

The DBA structural motif has been a workhorse in the field of photoinduced intramolecular ET and many structural platforms exist. We have chosen ruthenium (II) polypyridyls as our DBA platform. This particular platform has been used by many groups to investigate photoinduced intramolecular ET.[2-18] Ruthenium (II) polypyridyls have been well studied and their photophysics is well documented.[19] Specifically, we have chosen $[Ru(bpy)_3]^{2+}$, where bpy is 2,2'-bipyridine, and its derivatives as donor chromophores, N,N'dimethyl-4,4'-bipyridinium, methyl viologen, derivatives as acceptors and methyl-substituted aryl rings as bridging ligands. $[Ru(bpy)_3]^{2+}$ and its derivatives are known for their chemical stability and long excited state lifetime in room temperature acetonitrile.[19]

Methyl viologen is commonly used as an electron acceptor because of its intense color change upon reduction to form a radical cation.[20]

Conformationally active asymmetric electroactive ligands will serve as the active site for the electron transfer events. Six structurally unique but related conformationally active electroactive ligands have been prepared. Electroactive ligand preparation was achieved utilizing the same synthetic methods and the ligands were afforded in high yields. The asymmetric electroactive ligands have the same general structure: to a polypyridyl subunit an aryl ring is appended and to that aryl ring a bipyridinium acceptor is appended. The general structure of the conformationally active ligands is shown below in **Scheme 2.1**.

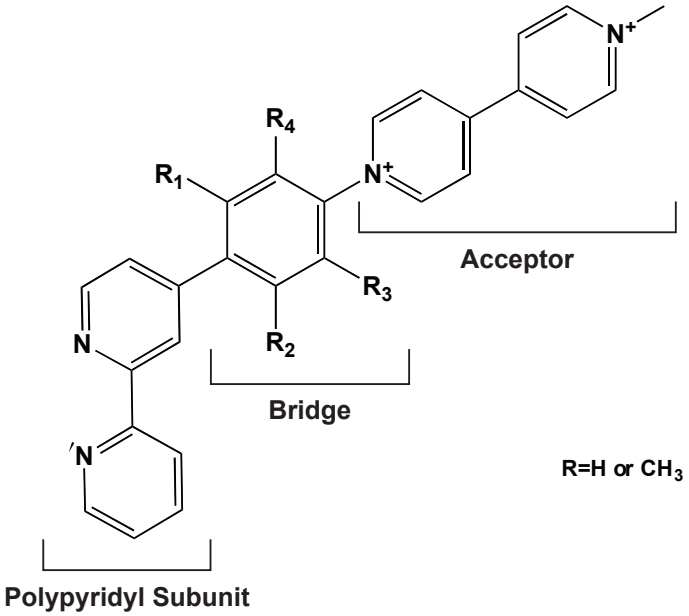

Scheme 2.1 General structure of the conformationally active asymmetric electroactive ligands. The R-groups represent positions where steric bulk is introduced.

Figure 2.1 below shows the six conformationally active electroactive ligands prepared for studying the role of nuclear motions on photoinduced electron transfer processes.

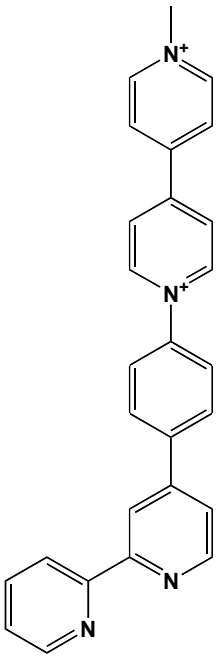

bpy- phenyl-MV (**L1**)

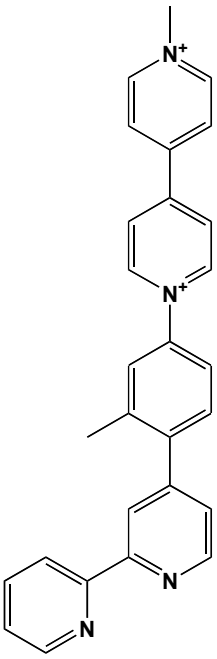

bpy-ortho-MV (**L2**)

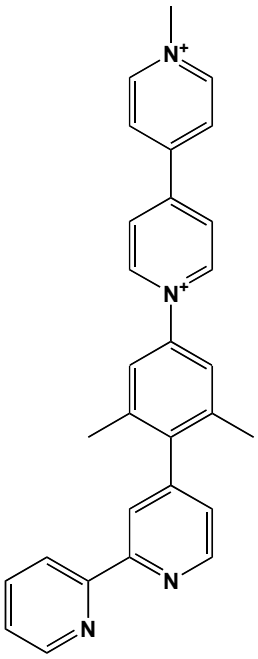

bpy-2,6-dimethylphenyl-MV (**L3**)

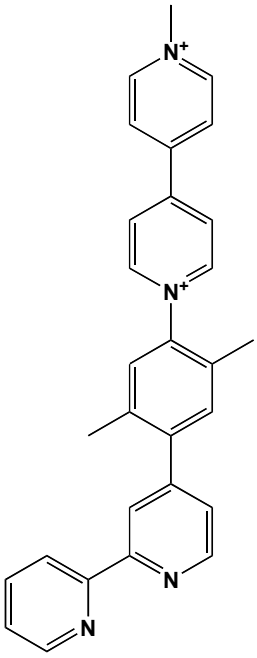

bpy-2,5-dimethylphenyl-MV (**L4**)

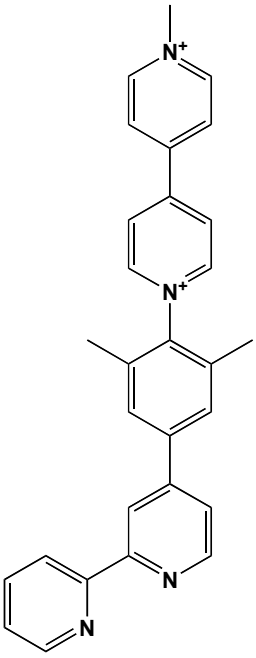

bpy-3,5-dimethylphenyl-MV (**L5**)

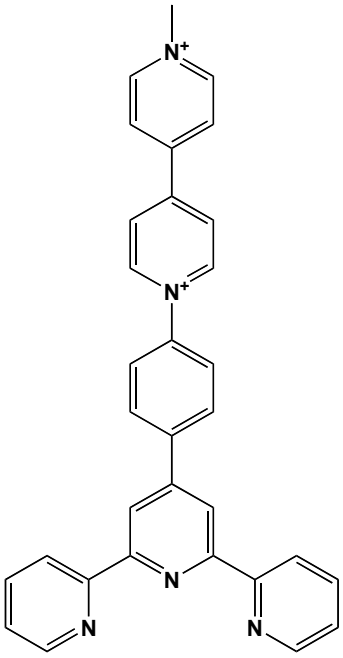

tpy-phenyl-MV (**L6**)

Figure 2.1 Structures of the novel asymmetric electroactive ligands. The ligands were isolated as PF_6^- salts.

The 2,2'-bipyridine-based ligands are comprised of five contiguously linked aryl rings while tpy-phenyl-MV (**L6**) is comprised of six. Building on what is known about the excited state delocalization dynamics of ruthenium complexes with aryl-substituted polypyridine ligands[21-25] we believe strong electronic communication will exist within the ligands after MLCT excitation. After photo-excitation with a visible photon the MLCT excited state will lie on the lower energy electroactive ligand and in order to maximize π-orbital overlap co-planarization will occur between the polypyridyl and bridging subunits. Upon addition of steric bulk in the form of methyl groups on the bridging ligand we believe co-planarization will be hindered and therefore electronic communication will be disrupted. It is this disruption in electronic communication brought on by nuclear motions that we believe will dictate intramolecular electron transfer. Steric bulk is systematically introduced onto the bridging phenyl not only to determine the effects of hindered ring rotations on intramolecular ET but to determine if the position of methylation also plays a role. This particular question will be addressed with DBA complexes prepared from (**L4**) and (**L5**).

Here we describe the preparation of six novel conformationally active electroactive ligands. Of the six electroactive ligands five are asymmetric aryl-substituted 2,2'-bipyridine ligands and one is an aryl-substituted terpyridine ligand (**L6**). In general asymmetric aryl-substituted 2,2'-bipyridine ligands are less studied than aryl-substituted terpyridine ligands due to the difficulty of their preparation and low yields resulting from multi-step syntheses.[2,3,11,13,26] For the asymmetric aryl-substituted 2,2'-bipyridine ligands prepared herein over fifty percent yields were obtained and the synthesis of the electroactive ligands was achieved in ~three steps. To the author's knowledge this is the only study on

electroactive ligands that systematically studies steric bulk on every position on the bridging ligand. The electroactive ligand tpy-phenyl-MV (**L6**) was prepared in order to demonstrate the robustness of the synthesis. Metal complexes descending from this electroactive ligand will not be discussed in this text.

In order to understand the role of the bipyridinium-acceptor both in the properties of the electroactive ligands and the DBA complexes, model complexes comprised only of 'donors' also need to be prepared. These donor complexes serve as standards in order to determine the photophysical behavior of these systems without the juxtaposed electron acceptor. The 'donor' ligands are asymmetric aryl-substituted 2,2'-bipridine ligands. The donor ligands complement their corresponding electroactive ligand in number and position of methylation on the appended aryl substituent. **Figure 2.2** below summarizes the structure of the donor ligands.

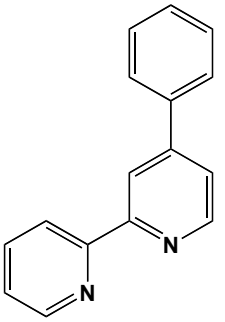

bpy- phenyl (**L1'**)

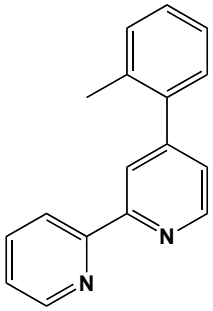

bpy-ortho (**L2'**)

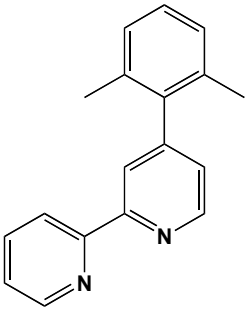

bpy-2,6-dimethylphenyl (**L3'**)

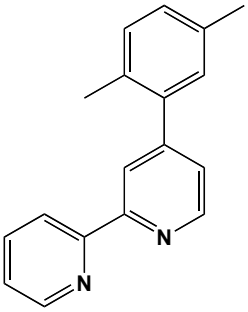

bpy-2,5-dimethylphenyl (**L4'**)

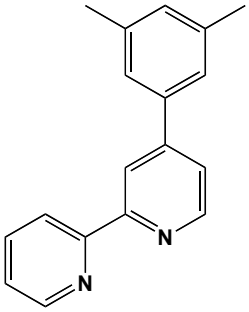

bpy-3,5-dimethylphenyl (**L5'**)

Figure 2.2 Structure of donor ligands prepared in order to determine the effect of the appended bipyridinium acceptor. They will be used to prepare donor complexes.

To fully understand the electrochemical behavior of the electroactive ligands the 'acceptor' subunits were also prepared and characterized. These acceptor ligands were prepared for the purpose of determining the contribution of the acceptor subunit to the overall electrochemical behavior of the electroactive ligand. The novel acceptor ligands are shown in **Figure 2.3**.

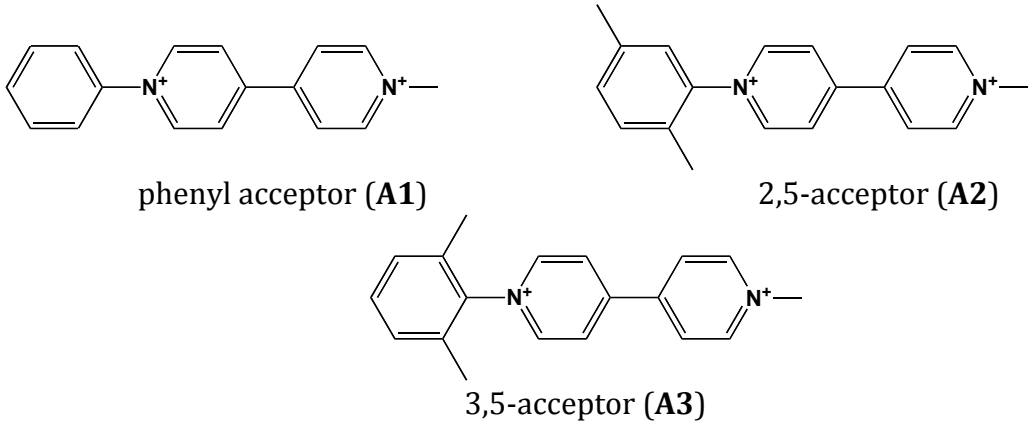

Figure 2.3 Structure of the acceptor subunits prepared and characterized. These ligands were isolated as PF_6^- salts.

2.2 Experimental

2.2.1 Synthesis

All reagents and materials from commercial sources were used as received. Solvents were purchased from Sigma-Aldrich Chemical Co. or Mallinckrodt Chemicals. All deuterated solvents were obtained from Cambridge Isotope Laboratories, Inc. Aniline, 2,5-dimethylaniline, 3,5-dimethylanaline, 2,4-dinitrochlorobenzene, 4,4'-bipyridine, methyl iodide, barium hydroxide, sodium carbonate and ammonium hexafluorophosphate were obtained from Sigma-Aldrich Chemical Co. All boronic acids were obtained from Combi-Blocks. 4-Bromo-2,2'-bipyridine was obtained from Shanghai Elittes Organics Co. Tetrakis(triphenylphosphine)palladium(0) was obtained from Strem Chemicals, Inc. All NMR spectra were recorded on a Varian Inova 500 MHz or Varian Inova 400 MHz spectrometer. Accurate mass measurements were obtained in house from the University of Colorado's Central Analytical Laboratory. The ligands 4-phenyl-2,2'-bipyridine[11] (**L1'**), 4-(4-aminophenyl)-2,2'-bipyridine[27], 4'-(4-aminophenyl)-2,2':6',2''-terpyridine[28] and N-(2,4-

dinitrophenyl)-4,4'-bipyridinium chloride[29] were prepared according to previously published procedures.

N-(Methyl)-N'-(2,4-dinitrophenyl)-4,4'-bipyridinium Chloride Iodide (modified Zincke Salt).

1.0 equivalent (1 mmol) of N-(2,4-dinitrophenyl)-4,4'-bipyridinium chloride was added to a round bottom flask equipped with a stir bar and dissolved in 20 mL of CH_3CN. To this flask 1.5 equivalents (1.5 mmol) of CH_3I was added. The flask was gently heated for 12 hours. The reaction mixture was allowed to cool and the desired product precipitated from solution. The product was collected by filtration. No further purification was needed. Yield: 60% (300 mg) . ^1H NMR (500 MHz, D_2O) δ 9.38 (m, 3H), 9.09 (d, J = 6.6 Hz, 2H), 8.91 (dd, J = 8.7, 2.4 Hz, 1H), 8.79 (d, J = 6.8 Hz, 2H), 8.60 (d, J = 6.4 Hz, 2H), 8.27 (d, J = 8.7 Hz, 1H), 4.50 (s, 3H).

General procedure for Suzuki couplings.

1.0 equivalent (1 mmol) of arylboronic acid and 0.90 equivalents (O.9 mmol) of 4-Bromo2,2'-bipyridine were reacted with 3 equivalents of $Ba(OH)_2$ (3 mmol) and 2.5 mol % of $Pd(PPh_3)_4$ in a degassed solution of 1:1 H_2O:CH_3CN at reflux under argon for 36 - 96 hours (progress was monitored by TLC). The solvent was removed and the residual oil extracted in H_2O/CH_2Cl_2. The organic layer was collected and dried by rotary evaporator. The crude product was purified on a 9:1 CH_2Cl_2: MeOH silica gel column unless otherwise noted.

Asymmetric aryl-Substituted 2,2'-bipyridines (donor ligands).

4-(2-methylphenyl)-2,2'-bipyrdine. (**L2'**)

Starting boronic acid: 2-methylphenyl boronic acid. Yield: 58% (128 mg). ^{1}H NMR (500 MHz, $CDCl_3$) δ 8.72 (dd, J = 5.0, 0.8 Hz, 1H), 8.67 (ddd, J = 4.8, 1.8, 0.9 Hz, 1H), 8.44 (dt, J = 8.0, 1.1 Hz, 1H), 8.41 (dd, J = 1.7, 0.8 Hz, 1H), 7.83 (ddd, J = 8.0, 7.5, 1.8 Hz, 1H), 7.32 – 7.27 (m, 6H), 2.32 (s, 3H).

4-(2,6-dimethylphenyl)-2,2'-bipyrdine. (**L3'**)

Starting boronic acid: 2,6-dimethylphenyl boronic acid. Yield: 64% (149 mg). ^{1}H NMR (400 MHz, $CDCl_3$ δ 8.76 (dd, J = 4.9, 0.9 Hz, 1H), 8.66 (ddd, J = 4.8, 1.8, 0.9 Hz, 1H), 8.48 (dt, J = 8.0, 1.1 Hz, 1H), 8.28 (dd, J = 1.6, 0.9 Hz, 1H), 7.83 (ddd, J = 8.0, 7.5, 1.8 Hz, 1H), 7.30 (ddd, J = 7.5, 4.8, 1.2 Hz, 1H), 7.20 (dd, J = 8.5, 6.5 Hz, 1H), 7.16 (dd, J = 4.9, 1.6 Hz, 1H), 7.14 – 7.10 (m, 2H), 2.07 (s, 6H).

4-(2,5-dimethylphenyl)-2,2'-bipyrdine. (**L4'**)

Starting boronic acid: 2,5-dimethylphenyl boronic acid. Yield: 68% (159 mg). ^{1}H NMR (500 MHz, $CDCl_3$) δ 8.71 (dd, J = 5.0, 0.8 Hz, 1H), 8.68 (ddd, J = 4.8, 1.8, 0.9 Hz, 1H), 8.45 (dt, J = 8.0, 1.1 Hz, 1H), 8.41 (dd, J = 1.7, 0.8 Hz, 1H), 7.8 (ddd, J = 8.0, 7.5, 1.8 Hz, 1H), 7.32 – 7.28 (m, 2H), 7.18 (d, J = 8.4 Hz, 1H), 7.12 (d, J = 6.6 Hz, 2H), 2.36 (s, 3H), 2.28 (s, 3H).

4-(3,5-dimethylphenyl)-2,2'-bipyrdine. (**L5'**)

Starting boronic acid: 3,5-dimethylphenyl boronic acid. Yield: 45% (105 mg). ^{1}H NMR (500 MHz, $CDCl_3$) δ 8.72 (ddd, J = 4.8, 1.8, 0.9 Hz, 1H), 8.70 (dd, J = 5.1, 0.8 Hz, 1H), 8.65 (dd, J = 1.8, 0.8 Hz, 1H), 8.46 (dt, J = 8.0, 1.1 Hz, 1H), 7.82 (ddd, J = 7.9, 7.5, 1.8 Hz, 1H), 7.51 (dd, J = 5.1, 1.9 Hz, 1H), 7.39 – 7.36 (m, 2H), 7.31 (ddd, J = 7.5, 4.8, 1.2 Hz, 1H), 7.11 – 7.02 (m, 1H), 2.39 (s, 6H).

Aminophenyl-substituted 2,2'-bipyridines

4-(4-amino-2-methylphenyl)-2,2'-bipyridine and 4-(4-amino-3,5-dimethylphenyl)-2,2'-bipyridine were prepared using the Suzuki coupling procedure described above. The compounds 4-(4-amino-2,6-dimethylphenyl)-2,2'-bipyridine and 4-(4-amino-2,5-dimethylphenyl)-2,2'-bipyridine required an additional step. They were prepared from N-Boc-protected boronic acids, where Boc is tert-butoxycarbonylamino, and required a deprotection step.

Deprotection:

The crude reaction mixture from the Suzuki coupling was dissolved in 20 mL of dichloromethane and excess (~1mL) CF_3COOH was added. The reaction mixture was refluxed for 12 hours. Water was added, the aqueous phase collected, and the pH of the solution was raised to 12 by slow addition of Na_2CO_3. Chloroform was added and the organic layer was extracted. A dark oil was obtained upon evaporation of the organic solvent. The crude oil was purified on a silica gel column with chloroform as the eluent. A yellow solid was obtained for all aminophenyl-substituted 2,2'-bipyridines.

4-(4-amino-2-methylphenyl)-2,2'-bipyridine

Starting boronic acid: 4-amino-2-methylphenylboronic acid, pinacol ester. Yield: 44% (103 mg). ^{1}H NMR (500 MHz, $CDCl_3$) δ 8.69 – 8.65 (m, 2H), 8.42 (dt, J = 8.0, 1.1 Hz, 1H), 8.37 (dd, J = 1.7, 0.8 Hz, 1H), 7.83 (ddd, J = 7.9, 7.5, 1.8 Hz, 1H) 7.31 (ddd, J = 7.5, 4.8, 1.2 Hz, 1H), 7.29 – 7.26 (m, 1H), 7.13 (d, J = 7.9 Hz, 1H), 6.62 (m, 2H), 3.80 (s, 2H), 2.29 (s, 3H).

4-(4-amino-2,6-dimethylphenyl)-2,2'-bipyridine

Starting boronic acid: 4-(t-butoxycarbonylamino)-2,6-dimethylphenylboronic acid. Yield: 73% (180 mg). ^{1}H NMR (400 MHz, $CDCl_3$) δ 8.70 (dd, J = 4.9, 0.8 Hz, 1H), 8.65 (ddd, J = 4.8, 1.8, 0.9 Hz, 1H), 8.45 (dt, J = 8.0, 1.1 Hz, 1H), 8.26 (dd, J = 1.6, 0.8 Hz, 1H), 7.79 (ddd, J = 8.0, 7.5, 1.8 Hz, 1H), 7.30 – 7.23 (m, 1H), 7.12 (dd, J = 4.9, 1.6 Hz, 1H), 6.45 – 6.42 (m, 2H), 3.74 (s, 2H), 1.98 (s, 6H).

4-(4-amino-2,5-dimethylphenyl)-2,2'-bipyridine

Starting boronic acid: 4-(t-butoxycarbonylamino)-2,5-dimethylphenylboronic acid. Yield: 55% (136 mg). ^{1}H NMR (500 MHz, $CDCl_3$) δ 8.68 (ddd, J = 4.8, 1.8, 0.9 Hz, 1H), 8.66 (dd, J = 5.0, 0.8 Hz, 1H), 8.43 (dt, J = 8.0, 1.1 Hz, 1H), 8.38 (dd, J = 1.8, 0.8 Hz, 1H), 7.82 (ddd, J = 8.0, 7.5, 1.8 Hz, 1H), 7.33 – 7.24 (m, 2H), 7.04 (s, 1H), 6.59 (s, 1H), 3.72 (s, 2H), 2.26 (s, 3H), 2.16 (s, 3H).

4-(4-amino-3,5-dimethylphenyl)-2,2'-bipyridine

Starting boronic acid: 4-amino-3,5-dimethylphenylboronic acid, pinacol ester. Yield: 58% (144 mg). ^{1}H NMR (500 MHz, $CDCl_3$) δ 8.68 (ddd, J = 4.8, 1.8, 0.9 Hz, 1H), 8.60 (dd, J = 5.8, 0.7 Hz, 2H), 8.42 (dt, J = 8.0, 1.1 Hz, 1H), 7.76 (ddd, J = 8.0, 7.5, 1.8 Hz, 1H), 7.45 (dd, J = 5.1, 2.0 Hz, 1H), 7.37 (s, 2H), 7.25 (ddd, J = 7.5, 4.8, 1.2 Hz, 1H), 3.79 (s, 2H), 2.17 (d, J = 0.5 Hz, 6H).

General procedure for Zincke reaction

When using this method to prepare the electroactive ligands the amount of starting materials varied because it was dependent on the quantity of aminophenyl-substituted polypyridines prepared in the previous step of the synthesis. However the ratio of starting materials was consistent for all reactions. 1.0 equivalent of N-(methyl)-N'-(2,4-

dinitrophenyl)-4,4'-bipyridinium chloride iodide and 2.0 equivalents of either the aniline derivative (1 mmol) or aminophenyl-substituted polypyridines were added to a flask equipped with a stir bar. Methanol was added and the reaction mixture was allowed to reflux for 50 hours. The reaction volume was reduced by rotary evaporator and water was added upon which the 2,4-dinitrolaniline side product precipitated. The side product was filtered and excess NH_4PF_6 was added and the desired product precipitated. The white solid was collected by filtration and recrystallized from a 1:1 mixture of ethanol and acetone. It should be noted tpy-phenyl-MV (**L6**) required no additional purification after salt metathesis.

N-Methyl-N'-phenyl-4,4'-bipyridinium Hexafluorophosphate (phenyl acceptor) (A1) Yield: 55% (296 mg). ^{1}H NMR (500 MHz, CD_3CN) δ 9.21 – 9.16 (m, 2H), 8.90 (d, J = 7.0 Hz, 2H), 8.58 (d, J = 7.1 Hz, 2H), 8.47 (d, J = 6.8 Hz, 2H), 7.85 – 7.78 (m, 5H), 4.44 (s, 3H). Accurate mass: As [A^{2+} PF_6^-] calcd. 393.0953 measured 393.0550

N-Methyl-N'-(2,5-dimethylphenyl-4,4'-bipyridinium Hexafluorophosphate (2,5-acceptor) (A2) Yield: 40% (226 mg). ^{1}H NMR (500 MHz, CD_3CN) δ 9.01 – 8.97 (m, 2H), 8.91 (d, J = 6.7 Hz, 2H), 8.60 – 8.55 (m, 2H), 8.46 (d, J = 6.8 Hz, 2H), 7.50 (dt, J = 14.8, 4.7 Hz, 2H), 7.38 (s, 1H), 4.45 (s, 3H), 2.46 (s,3H). Accurate mass: As [A^{2+} PF_6^-] calcd. 421.1263 measured 421.1257

N-Methyl-N'-(2,6-dimethylphenyl-4,4'-bipyridinium Hexafluorophosphate (3,5-acceptor) (A3) Yield 58% (328 mg). ^{1}H NMR (500 MHz, CD_3CN) δ 8.99 – 8.89 (m, 4H), 8.66 – 8.59 (m, 2H), 8.47 (d, J = 6.7 Hz, 2H), 7.60 – 7.53 (m, 1H), 7.45 – 7.40 (m, 2H), 4.45 (s, 3H), 2.09 (s, 6H). Accurate mass: As [A^{2+} PF_6^-] calcd. 421.1263 measured 421.1259

4-(1-(1'-Methyl-4,4'-bipyridinium-1-yl)-phenyl)-2,2'-bipyridine Hexafluorophosphate. (bpy-phenyl-MV) (**L1**) Yield: 52% (122 mg). ^{1}H NMR (500 MHz, CD_3CN) δ 9.29 – 9.21 (m, 2H), 8.92 (d, J = 7.0 Hz, 2H), 8.85 – 8.80 (m, 2H), 8.74 (d, J = 4.7 Hz, 1H), 8.64 – 8.61 (m, 2H), 8.50 (m, 3H), 8.24 – 8.18 (m, 2H), 7.99 – 7.93 (m, 3H), 7.80 (dd, J = 5.1, 1.9 Hz, 1H), 7.47 (ddd, J = 7.5, 4.7, 1.2 Hz, 1H), 4.45 (s, 3H). Accurate mass: As $[A^{2+}\,PF_6^-]$ calcd. 547.1486 measured 547.1481

4-(1-(1'-Methyl-4,4'-bipyridinium-1-yl)-3-methyphenyl)-2,2'-bipyridine Hexafluorophosphate. (bpy-ortho-MV) (**L2**) Yield: 54% (137 mg). ^{1}H NMR (400 MHz, CD_3CN) δ 9.26 – 9.21 (m, 2H), 8.92 (d, J = 6.6 Hz, 2H), 8.82 (dd, J = 5.0, 0.8 Hz, 1H), 8.70 (ddd, J = 4.8, 1.8, 0.9 Hz, 1H), 8.63 – 8.60 (m, 2H), 8.54 – 8.48 (m, 4H), 7.99 – 7.94 (m, 1H), 7.80 (dd, J = 1.7, 0.7 Hz, 1H), 7.77 – 7.71 (m, 2H), 7.50 (dd, J = 5.0, 1.8 Hz, 1H), 7.45 (ddd, J = 7.5, 4.8, 1.2 Hz, 1H), 4.45 (s, 3H), 2.49 (s, 3H). Accurate mass: As $[A^{2+}\,PF_6^-]$ calcd. 561.1641 measured 561.1643

4-(1-(1'-Methyl-4,4'-bipyridinium-1-yl)-3,5-dimethyphenyl)-2,2'-bipyridine Hexafluorophosphate. (bpy-2,6-dimethylphenylMV) (**L3**) Yield: 60% (140 mg). ^{1}H NMR (400 MHz, CD_3CN) δ 9.24 – 9.20 (m, 2H), 8.91 (d, J = 6.7 Hz, 2H), 8.85 (dd, J = 4.9, 0.9 Hz, 1H), 8.67 (ddd, J = 4.8, 1.8, 0.9 Hz, 1H), 8.63 – 8.59 (m, 2H), 8.53 (dt, J = 8.0, 1.1 Hz, 1H), 8.48 (d, J = 6.9 Hz, 2H), 8.31 (dd, J = 1.7, 0.9 Hz, 1H), 7.99 – 7.94 (m, 1H), 7.62 (s, 2H), 7.45 (ddd, J = 7.5, 4.8, 1.2 Hz, 1H), 7.31 (dd, J = 4.9, 1.7 Hz, 1H), 4.45 (s, 3H), 2.23 (s, 6H). Accurate mass: As $[A^{2+}\,PF_6^-]$ calcd. 575.1797 measured 575.1794

4-(1-(1'-Methyl-4,4'-bipyridinium-1-yl)-2,5-dimethyphenyl)-2,2'-bipyridine Hexafluorophosphate. (bpy-2,5-dimethylphenyl-MV) (**L4**) Yield: 70% (134 mg). ^{1}H NMR (500 MHz, CD_3CN) δ 9.08 – 9.05 (m, 2H), 8.94 (d, J = 6.9 Hz, 2H), 8.78 (dd, J = 5.0, 0.8 Hz, 1H), 8.69 (ddd, J = 4.7, 1.8, 0.9 Hz, 1H), 8.64 – 8.62 (m, 2H), 8.49 (m, 3H), 8.45 (dd, J = 1.7, 0.8 Hz, 1H), 7.97 – 7.92 (m, 1H), 7.54 (s, 1H), 7.50 (s, 1H), 7.48 (dd, J = 4.9, 1.8 Hz, 1H), 7.44 (ddd, J = 7.5, 4.7, 1.2 Hz, 1H), 4.47 (s, 3H), 2.38 (s, 3H), 2.24 (s, 3H). Accurate mass: As $[A^{2+}\,PF_6^-]$ calcd. 575.1802 measured 575.1794

4-(1-(1'-Methyl-4,4'-bipyridinium-1-yl)-2,6-dimethyphenyl)-2,2'-bipyridine Hexafluorophosphate. (bpy-3,5-dimethylphenyl-MV) (**L5**) Yield: 57% (20 mg). ^{1}H NMR (500 MHz, CD_3CN) δ 9.01 (d, J = 6.4 Hz, 2H), 8.92 (d, J = 5.9 Hz, 2H), 8.86 – 8.79 (m, 2H), 8.74 (d, J = 4.1 Hz, 1H), 8.65 (d, J = 6.3 Hz, 2H), 8.52 (d, J = 7.8 Hz, 1H), 8.47 (d, J = 6.0 Hz, 2H), 7.97 (t, J = 7.5 Hz, 1H), 7.89 (s, 2H), 7.78 (d, J = 3.4 Hz, 1H), 7.52 – 7.43 (m, 1H), 4.46 (s, 3H), 2.17 (s, 6H). Accurate mass: As $[A^{2+}\,PF_6^-]$ calcd. 575.1801 measured 575.1799

4-(1-(1'-Methyl-4,4'-bipyridinium-1-yl)-phenyl)-2,2':6',2''-terpyridine Hexafluorophosphate. (tpy-phenyl-MV) (L6) Yield 60% (140 mg). ^{1}H NMR (500 MHz, CD_3CN) δ 9.31 – 9.25 (m, 2H), 8.97 – 8.85 (m, 4H), 8.76 (d, J = 8.2 Hz, 4H), 8.64 (d, J = 7.0 Hz, 2H), 8.50 (d, J = 6.8 Hz, 2H), 8.32 (d, J = 8.5 Hz, 2H), 8.02 (dd, J = 20.3, 8.1 Hz, 4H), 7.51 (s, 2H), 4.45 (s, 3H). Accurate mass: As $[A^{2+}\,PF_6^-]$ calcd. 624.1746 measured 624.1751

2.2.2 Electrochemistry

Cyclic Voltammetry. Electrochemical measurements were carried out with a CH Instruments 601C electrochemical analyzer. Solutions of the compound were dissolved in

anhydrous CH_3CN containing 0.1 M $TBAPF_6$ (where TBA is tetrabutylammonium) as the supporting electrolyte. A standard three-electrode setup was used with a working Pt electrode, Pt wire counter electrode, and an $Ag/AgNO_3$ reference electrode. The reference electrode is comprised of a silver wire in the supporting electrolyte solution that is also 0.01 M in $AgNO_3$. Fresh electrolyte and reference solutions were prepared prior to each measurement. Before measuring the redox potentials of a new compound, a standard with known reduction potentials was measured to ensure proper preparation of the reference solution. All measurements were made after an argon purge and a 100mV/s scan rate. Adding 0.298 V to the experimentally obtained value converts $E_{1/2}$ values from $Ag/AgNO_3$ to SCE.[30]

Spectro-Electrochemistry. Spectra were recorded with a Hewlett-Packard HP8452A diode array UV-Vis spectrophotometer. The experiments were carried out in a home built OTTLE cell as previously reported[2,3] with the Pt mesh held at constant voltage using the CH Instruments 601C electrochemical analyzer, a platinum auxiliary electrode and an $Ag/AgNO_3$ reference electrode. The reference electrode is comprised of a silver wire in a 0.01 M $AgNO_3$ in the supporting electrolyte solution. Fresh electrolyte and reference solutions were prepared for every new measurement. An argon purge was maintained over the course of the experiment. For the reductive experiments compounds were held at -0.85 V vs. $Ag/AgNO_3$. The reductions were reversed (returned to their original state) by holding the voltage to 0 V vs. $Ag/AgNO_3$.

2.3 Results and Discussion

2.3.1 Electroactive Ligand Synthesis.

All electroactive ligands shown in **Figure 2.1** were prepared utilizing a similar synthetic method. A Zincke reaction was used to accomplish their preparation. The Zincke reaction is an amine exchange reaction that converts N-(2,4-dinitrophenyl)pyridinium salts (known as Zincke salts) to N-arylpyridiniums upon treatment with an appropriate aniline derivative.[31,32] The Zincke reaction is often utilized to prepare N-aryl 4,4'-bipyridinium salts.[29,31-36] **Scheme 2.2** below summarizes the general Zincke reaction. For simplicity, preparation of bpy-phenyl-MV (**L1**) is shown. Although not specified in **Scheme 2.2** PF_6^- serves as the counterion for the electroactive ligands while the Zincke salt is a mixed chloride iodide salt.

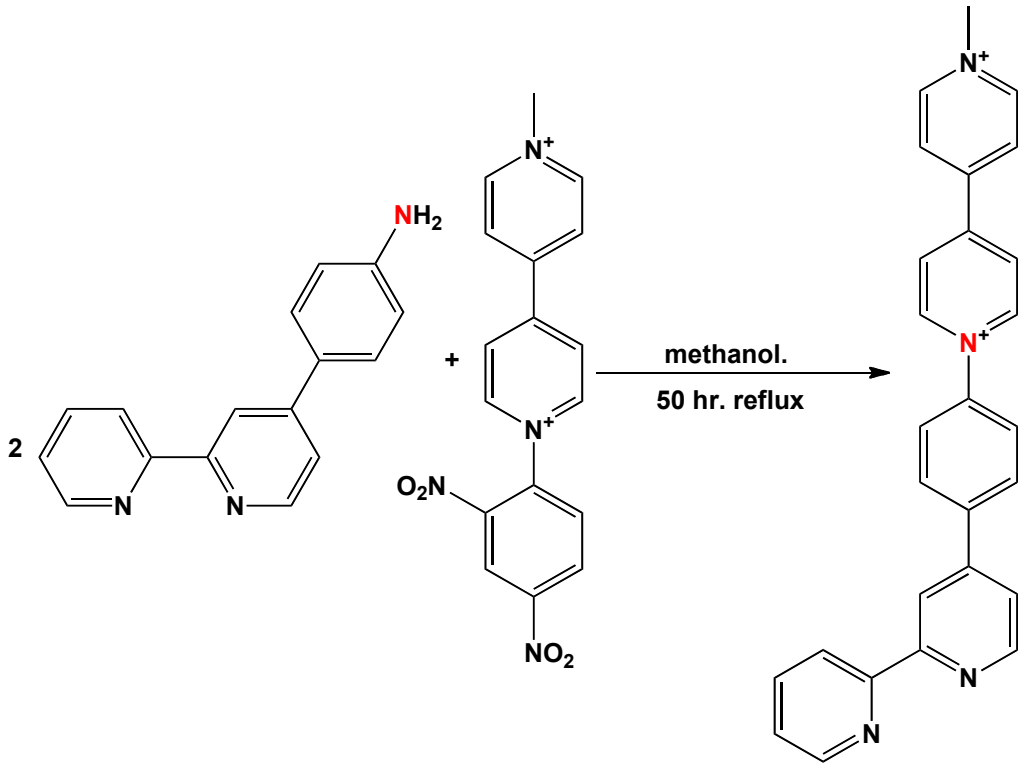

Scheme 2.2 Modified Zincke reaction highlighting the preparation of the asymmetric electroactive ligands. All six ligands were prepared under the same conditions but only bpy-phenyl-MV (**L1**) is shown. The ligands were isolated as PF_6^- salts. The nitrogen atoms in red highlight the connectivity and by inference the reaction mechanism.

In **Scheme 2.2** two nitrogen atoms are shown in red to highlight the reaction mechanism. The first step of the reaction mechanism is nucleophilic addition of the arylamine to the Zincke salt followed by ring opening, *cis-trans* interconversions and ring closing.[32,37-39] The byproduct of the reaction is 2,4-dinitroaniline. We find that the Zincke reaction is higher yielding for electroactive ligands with methyl groups on the bridging ligand. This observation is explained by the increased nucleophilicity of the arylamine-substituted polypyridines brought about by the electron donating character of the methyl substituents.

As stated above, the two components needed for the Zincke reaction are the Zincke salt and an aniline derivative. The modified Zincke salt required for the preparation of the electroactive ligands is N-(methyl)-N'-(2,4-dinitrophenyl)-4,4'-bipyridinium chloride iodide. This modified salt is one of two known doubly charged Zincke salts[31,32] (most known Zincke salts are singly charged). Preparation of the Zincke salt was achieved in two steps. First N-(2,4-dinitrophenyl)-4,4'-bipyridinium chloride was prepared by reacting 2,4-dintitrochlorobenzene with 4,4-bipyridine[29] (**Scheme 2.3**). Subsequent N-methylation was achieved by treatment with methyl iodide[5] to yield the full Zincke salt (**Scheme 2.4**).

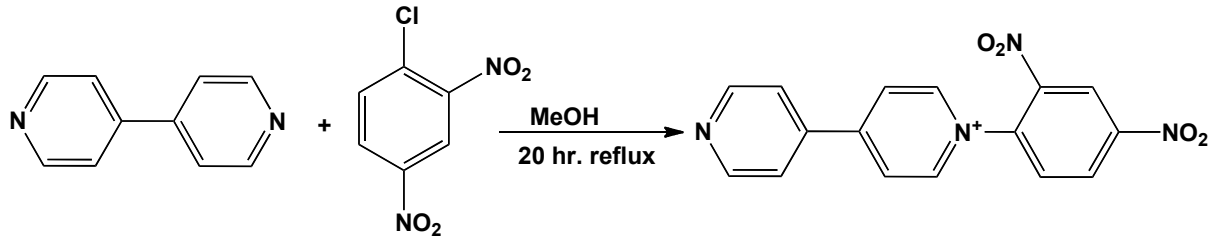

Scheme 2.3 First step of modified Zincke salt synthesis. Isolated as a Cl^- salt.

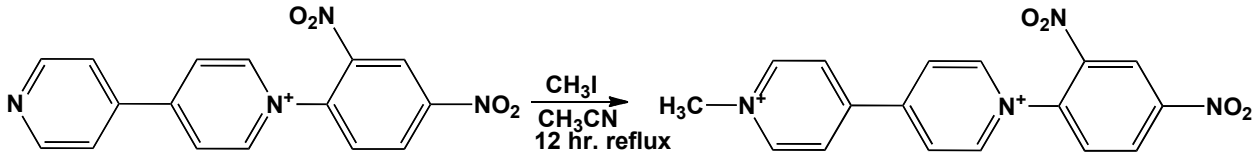

Scheme 2.4 Second step of modified Zincke salt synthesis; N-methylation was achieved using methyl iodide. Here the counterions of the product are Cl^- and I^-.

The second component needed for the Zincke reaction is an aniline derivative. For our purposes the required aniline derivatives must be arylamine-substituted polypyridines with varying degrees of methylation on the arylamine. The arylamine-substituted polypyridines prepared for the Zincke reaction are summarized in **Figure 2.4**

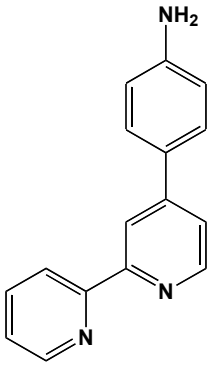

bpy- phenyl-amine

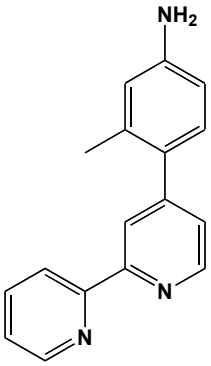

bpy-ortho-amine

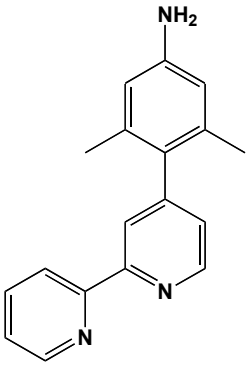

bpy-2,6-dimethylphenyl-amine

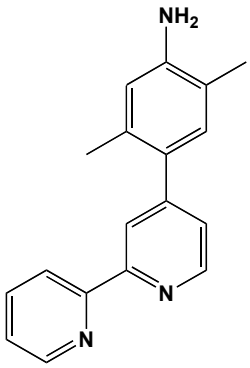

bpy-2,5-dimethylphenyl-amine

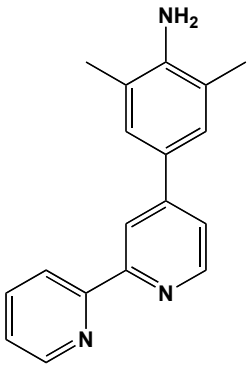

bpy-3,5-dimethylphenyl-amine

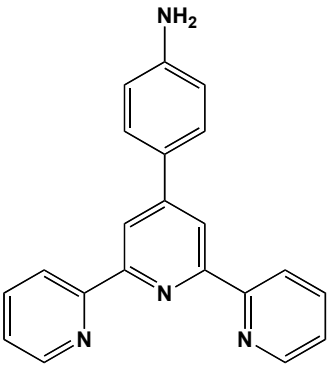

tpy-phenyl-amine

Figure 2.4 The arylamine-substituted polypyridines needed for the Zincke reaction

The preparation of two of these ligands, bpy-phenyl-amine[27] and tpy-phenyl-amine[28] have been previously reported. They were prepared by the Kröhnke condensation of pyridines. The remaining four arylamine-substituted 2,2'-bipyridines were prepared by Suzuki coupling strategies. A Suzuki coupling is a palladium-catalyzed carbon-carbon bond forming reaction between an aryl boronic acid and an aryl halide.[40-42] Our group has optimized the coupling conditions used.[3] In running the reactions, two synthetic routes were taken depending on the structure of the starting aryl boronic acid. The boronic acids used to prepare the arylamine-substituted polypyridines were obtained from commercial sources as custom synthons. For bpy-ortho-amine and bpy-3,5-dimethylphenyl-amine an unprotected aminophenyl boronic acid pinacol ester was coupled to 4-bromo-2,2'-bipyridine to give the desired product. This reaction is summarized in **Scheme 2.5** (for simplicity only the bpy-ortho-amine reaction is shown).

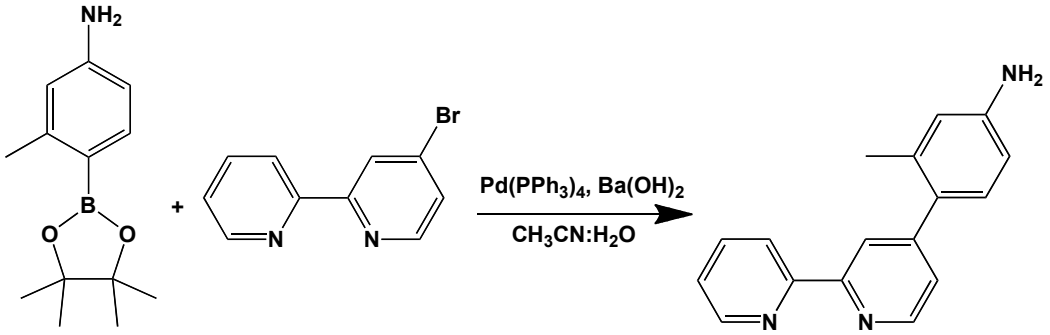

Scheme 2.5 Suzuki Coupling reaction used to prepare the bpy-ortho-amine and the bpy-3,5-dimethylphenyl- amines. For simplicity, only the bpy-ortho-amine is shown.

For bpy-2,6-dimethylphenyl-amine and bpy-2,5-dimethylphenyl-amine, N-boc protected aminophenyl boronic acids were coupled to 4-bromo-2,2'-bipyrdine. In order to isolate the desired free amine a second step, a deprotection step,[43] was required. This two-step synthesis is summarized in **Schemes 2.6** and **2.7**. For simplicity, preparation of the

bpy-2,6-dimethylphenyl-amine is shown. It should also be noted that the product from the first step was isolated but not purified and the semi-crude product was taken on to the deprotection step. The ligand was purified after deprotection.

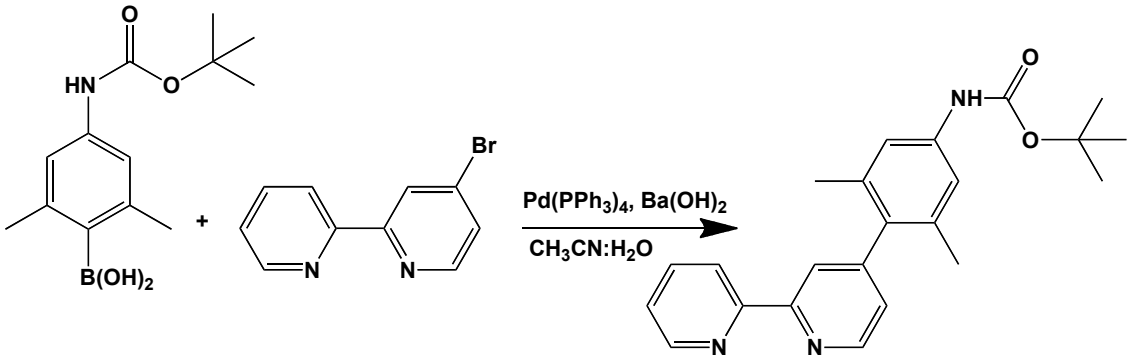

Scheme 2.6 Step 1: Suzuki Coupling reaction to yield coupled and protected product. Product was isolated but not purified. The semi-crude product was taken on to the deprotection step. For simplicity, preparation of the bpy-2,6-dimethylphenyl-amine is shown.

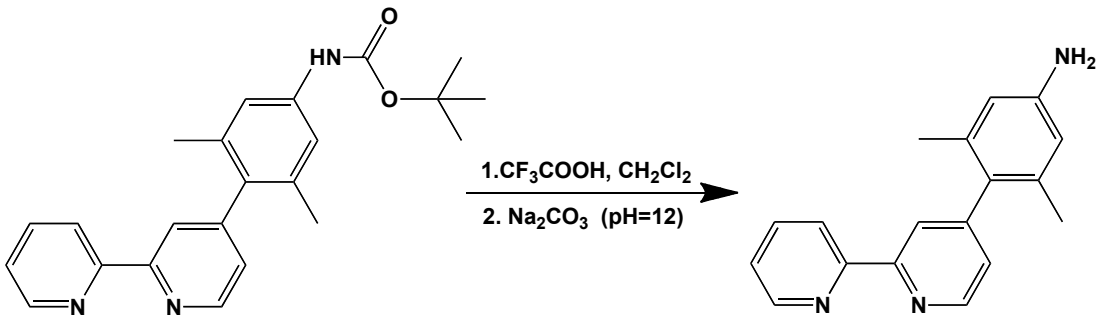

Scheme 2.7 Step 2: Deprotection of the Suzuki Coupling product to yield the primary amine required for the Zincke reaction. For simplicity, deprotection of the bpy-2,6-dimethylphenyl-amine is shown.

With both the arylamine-substituted 2,2'-bipyridines and the modified Zincke salt in hand the Zincke reaction can be performed. All six electroactive ligands were prepared from their respective arylamine-substituted 2,2'-bipyridine and the same modified Zincke salt. Purification was achieved from recrystallization in 1:1 ethanol: acetone solution. The ligand tpy-phenyl-MV (**L6**) required no purification after the Zincke reaction. The overall Zincke reaction is robust, versatile and reaction yields are not adversely affected by the

addition of steric bulk like other asymmetric ligands as was the case for other electroactive ligands previously prepared by our group.[3]

2.3.2 Acceptor Subunit Synthesis.

The acceptor subunits, phenyl acceptor (**A1**), 2,5-acceptor (**A2**) and 3,5-acceptor (**A3**) (see **Figure 2.3**), were also prepared utilizing the Zincke reaction. The phenyl acceptor has been previously reported.[44] The Zincke salt used to prepare the electroactive ligands was again used to prepare the acceptor subunits. Commercially available aniline, 2,5-dimethylaniline, and 3,5-dimethylaniline were used as the amine sources. **Scheme 2.8** shows the Zincke reaction used to prepare the N-methyl-N'-phenyl-4,4'-bipyridinium hexafluorophosphate (phenyl acceptor, (**A1**)). Again, for simplicity, only the phenyl acceptor (**A1**) is shown.

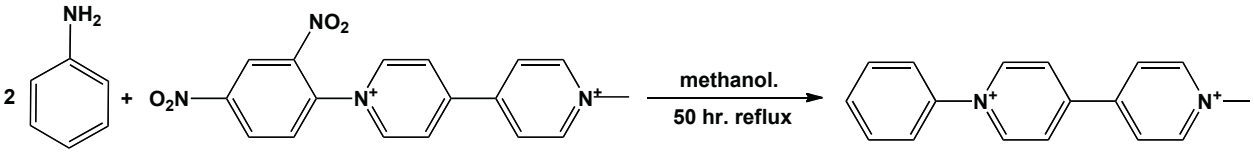

Scheme 2.8 Representative reaction for preparing the acceptor subunits. Preparation of the phenyl-acceptor (**A1**) is shown. Ligands were isolated as PF_6^- salts.

The acceptor subunits were purified via the same recrystallization conditions as the electroactive ligands, from a 1:1 solution of acetone: ethanol.

2.3.3 Donor Ligand Synthesis.

Suzuki couplings were also used to prepare the donor ligands. The synthesis of 4-phenyl-2,2'-bipyridine (bpy-phenyl) (**L1'**) has been reported.[11] The remaining donor ligands have not been previously reported. The syntheses of the remaining donor ligands were carried out with 4-bromo-2,2'-bipyridine and an appropriate methylated phenylboronic acid. **Scheme 2.9** highlights the synthesis of bpy-ortho (**L2'**) for simplicity.

It should be noted that the reaction conditions are the same as those of the amine coupling reactions described in **Section 2.2.1**.

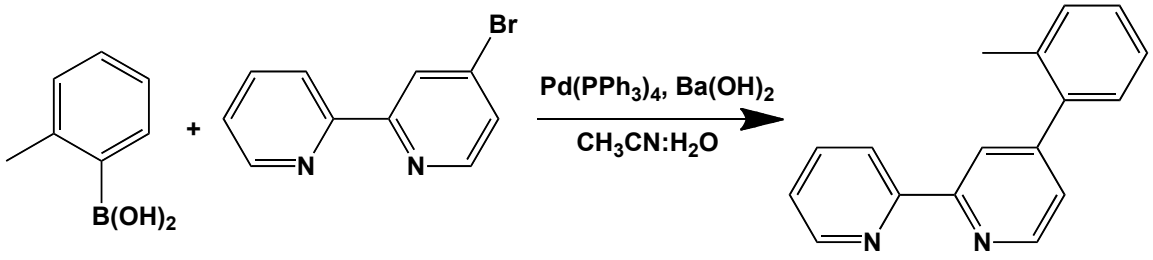

Scheme 2.9 Suzuki Coupling conditions used to prepare the donor ligands. For simplicity, the bpy-ortho (**L2'**) reaction is shown.

The donor ligands were not characterized electrochemically; the purpose for their synthesis is the eventual preparation of the donor metal complexes.

2.3.4 Electrochemistry: Cyclic Voltammetry

The electrochemical properties of the electroactive ligands and acceptor subunits were determined by cyclic voltammetry (CV) and reductive spectroelectrochemistry. In this section, results of the CV experiments will be discussed. CV is an experimental technique that measures reduction and oxidation potentials of an analyte in a supporting electrolyte solution. **Figure 2.5** below shows a representative cyclic voltammogram. The reported reduction potentials, $E_{red(1)}$ and $E_{red(2)}$, refer to the average of the anodic and cathodic ½-wave potentials for the two sequential one-electron ligand reduction events.

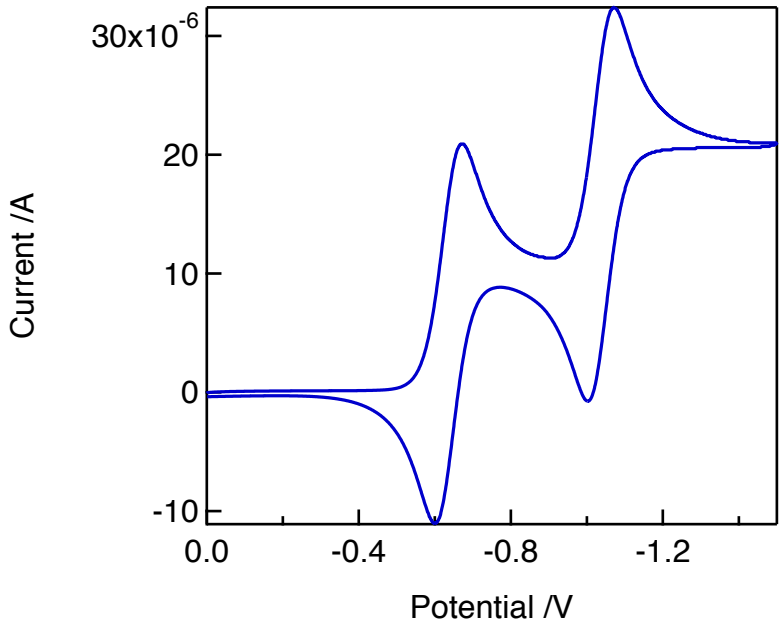

Figure 2.5 Representative cyclic voltammogram for the systems discussed here. For this particular scan (**L4**) was dissolved in the supporting electrolyte solution which is 0.1 M NH_4PF_6 in room temperature anhydrous acetonitrile. The measurements were recorded versus a 0.01 M $Ag/AgNO_3$ reference electrode. The measurements recorded with a 100 mV/s scan rate after an argon purge.

The CV results are summarized in **Table 2.1** below. For comparison, **Table 2.1** also contains reported[20] reduction potentials for methyl viologen (MV^{2+}) and two of its derivatives, benzyl viologen (BV^{2+}) and phenyl viologen (PV^{2+}) whose structures are shown in **Figure 2.6**.

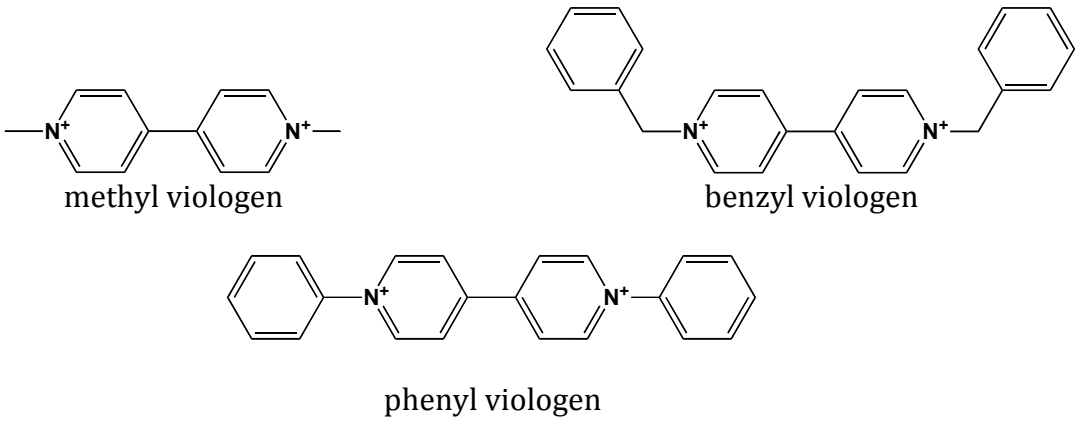

Figure 2.6 Methyl, benzyl and phenyl viologen. The reduction potentials of these known compounds are compared to the electroactive ligands and acceptor ligands in **Table 2.1**.

The reduction potentials were recorded in room temperature acetonitrile and are reported versus SCE.

Table 2.1 Electrochemical Data in Room Temperature CH_3CN vs. SCE

	$E_{red(1)}$ /V ($2^+/1^+$)	$E_{red(2)}$ /V ($1^+/0$)
methyl viologen[a]	-0.450	-0.850
benzyl viologen[a,b]	-0.370	--
phenyl viologen[a]	-0.247	-0.507
phenyl acceptor(**A1**)	-0.272	-0.650
2,5-acceptor (**A2**)	-0.396	-0.810
3,5-acceptor (**A3**)	-0.375	-0.809
bpy-phenyl-MV (**L1**)	-0.308	-0.665
tpy-phenyl-MV (**L6**)	-0.304	-0.668
bpy-ortho-MV (**L2**)	-0.318	-0.680
bpy-2,6-dimethylphenyl-MV (**L3**)	-0.325	-0.699
bpy-2,5-dimethylphenyl-MV (**L4**)	-0.338	-0.739
bpy-3,5-dimethylphenyl-MV (**L5**)	-0.334	-0.753

[a] Electrochemical Data reported in reference 16.
[b] The second reduction potential was not reported.

The reduction potentials of the electroactive ligands fall within the range of other 4,4'-disubstituted bipyridinium salts, namely MV^{2+} and PV^{2+}. The most common 4,4'-disubstituted bipyridinium salt is methyl viologen (MV^{2+}) where in acetonitrile the MV^{2+}/MV^{+} couple has a reported reduction potential of -450 mV versus SCE.[20] N,N'-diphenylbipyridinium (phenyl viologen (PV^{2+})) has a reported PV^{2+}/PV^{+} reduction potential of -247 mV versus SCE in room temperature acetonitrile.[20] Its reduction potential is less negative relative to MV^{2+} because the N-methyl substituents on MV^{2+} are electron donating in character and therefore lower the reduction potential (larger negative

number). Based on these reported values one would expect the first reduction potential of the newly synthesized ligands to fall within the range -450 to -247 mV.

The reduction potentials of the non-methylated electroactive ligands bpy-phenyl-MV (**L1**) and tpy-phenyl-MV (**L6**) are reduced at potentials closest to that of PV^{2+}. This is reasonable because (**L1**) and (**L6**) are structurally similar to phenyl viologen in that they possess a non-methylated N-aryl group. As described below, as sterics are introduced onto the bridging phenyl we see a gradual shift to reduction potentials that approach those of benzyl viologen indicating that the methyl group(s) are playing a role in determining the electronic properties of the ligands. Intuitively, upon addition of electron-donating methyl groups one would expect a decrease in reduction potential (larger negative number) this is observed experimentally. Across the series as methyl groups are added onto the bridging phenyl an ~35 mV shift to more negative reduction potential is observed where $E_{red(1)}$ for tpy-phenyl-MV (**L6**) is -0.304 V while that of bpy-2,5-dimethylphenyl-MV (**L4**) is -0.338 V. The reduction potentials of the di-methylated ligands approach that of benzyl viologen, BV^{2+}, a compound that has a methylene spacer between the quaternary nitrogen and a phenyl ring. In other words, by adding methyl groups onto the bridging phenyl of the electroactive ligands the reduction potentials approach that of an electronically insulated viologen. We can rationalize this as a demonstration of using structural elements via synthesis to isolate electron density onto the bipyridinium portion of the ligand rather than allowing it to delocalize onto the other parts of the ligand, which is what we speculate occurs with the bpy-phenyl-MV (**L1**) and tpy-phenyl-MV (**L6**).

To better understand the role of the juxtaposed electron acceptor in determining the reduction potentials of the electroactive ligands we prepared a series of acceptor

subunits that complement the acceptors of the electroactive ligands in methylation on the bridging phenyl. Three acceptor subunits were prepared, phenyl acceptor (**A1**), 2,5-acceptor (**A2**) and 3,5-acceptor (**A3**) (see **Figure 2.3**). By preparing the acceptor subunits we can examine the electronic properties of the acceptors in the absence of the electron donating polypyridine moiety as well as confirm the observed trend of decreased reduction potentials with increased methylation. The reduction potentials of the acceptor subunits are listed in **Table 2.1**. Comparing the reduction potentials of the phenyl acceptor (**A1**) with those of PV^{2+} and the non-methylated electroactive ligands, (**L1**) and (**L6**), we see that the first reduction potential of the phenyl acceptor (**A1**) is –272 mV. This values falls between the reduction potential of PV^{2+} (-247 mV) and the non-methylated electroactive ligands bpy-phenyl-MV (-308 mV) (**L1**) and tpy-phenyl-MV (-304 mV) (**L6**). Again, this is explained as being caused by an inductive effect. For the phenyl acceptor (**A1**) the N-methyl acts as a stronger electron-donating group when compared to the N-phenyl present in PV^{2+}. This causes the phenyl acceptor (**A1**) to have a 25 mV larger negative reduction potential than PV^{2+}. Comparing the phenyl acceptor (**A1**) to the full non-methylated electroactive ligands (**L1**) and (**L6**) we see that the former is more easily reduced. This is understandable because the bipyridine moiety of the full ligand (the ligation site) is electron rich due to the presence of the lone pair electrons on the nitrogen atoms.

The electrochemical behavior of the phenyl acceptor (**A1**) is predictable but that of the two methylated acceptor subunits 2,5-acceptor (**A2**) and 3,5-acceptor (**A3**) (see **Figure 2.3**) is more interesting. We find that the first reduction potential of these two compounds is now more negative than any of the electroactive ligands and even that of BV^{2+}. Electrochemically these two acceptors subunits, (**A2**) and (**A3**), behave more like BV^{2+} and

MV^{2+}, which in effect are two systems where the bipyridinium moiety is electronically isolated. For (**A2**) and (**A3**) we can assume that upon one-electron reduction the methylation on the N-aryl substituents prevents delocalization of electron density onto the N-dimethylphenyl causing the reduction potentials to be higher.

2.3.5 Electrochemistry*:* Reductive Spectroelectrochemistry

Reductive spectroelectrochemistry is a bulk electrolysis technique that combines absorption spectroscopy and electrochemistry to obtain the absorption spectrum of a species after one-electron reduction. Here the reductive spectroelectrochemistry of the electroactive ligands (see **Figure 2.1**) and the acceptor subunits (see **Figure 2.3**) will be presented. The reductive spectral data on the electroactive ligands provides preliminary 'optical tags'[45] for the electron transfer (ET) photoproduct since the absorption spectra of the radical cations can be used to approximate the absorption properties of the ET photoproduct. In general these data are obtained by recording UV-visible spectra of an analyte while the solution is held at a constant voltage. The electroactive ligands and the acceptor subunits were held at -0.850 V vs. $Ag/AgNO_3$ (-0.553 V vs. SCE). Running the experiments at this voltage will ensure the first ligand reduction has occurred but not the second.

Reductive spectral data are plotted as absorbance versus wavelength at several time points during the bulk electrolysis experiment. In the figures below time points are differentiated by colors. The arrows in the figures indicate the direction of absorption change. The absorption spectrum of reduced methyl viologen radical cation ($MV^{\bullet+}$) is well known (**Figure 2.7**).[20,46] There is a sharp absorption band centered at 394 nm corresponding to the $D_2 \leftarrow D_0$ transition (where D_0 is the ground state doublet of the

radical cation) and a broad absorption band between 550 and 800 nm that peaks at 605 nm corresponding to the $D_1 \leftarrow D_0$ transition.[47] The ligand MV^{2+} is not colored when dissolved in acetonitrile however the methyl viologen radical cation, $MV^{\bullet+}$, is known for its striking deep shade of blue (see **Figure 2.7**).

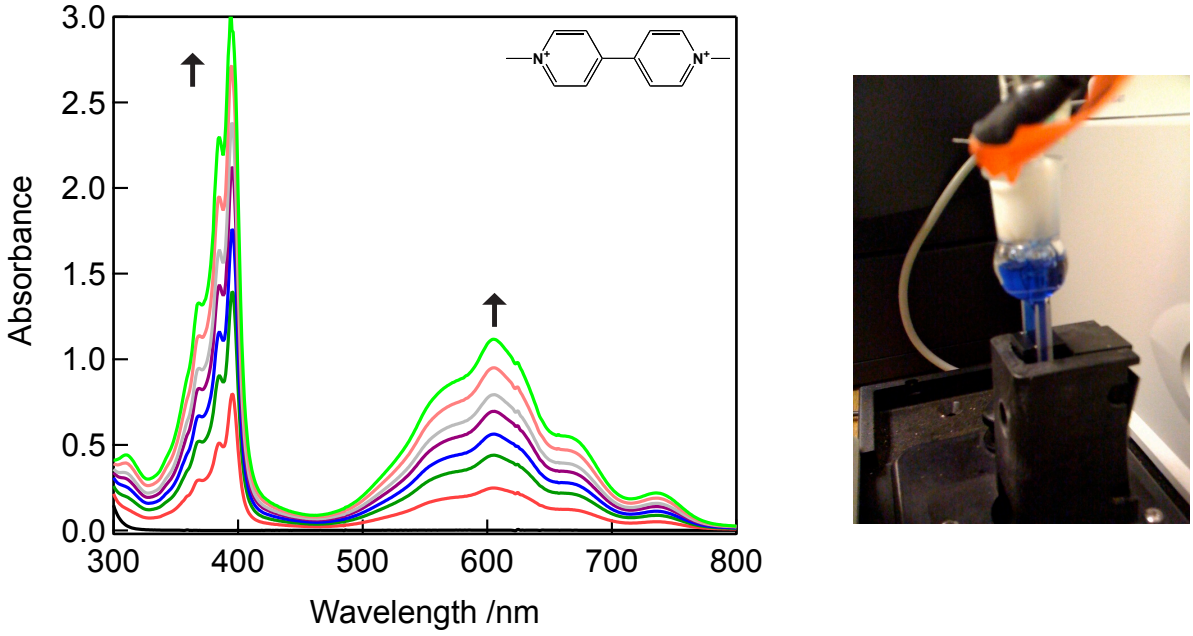

Figure 2.7 *Left*: One-electron reductive spectroelectrochemical data for $MV^{\bullet+}$. Spectrum was recorded in room temperature acetonitrile while held at a constant potential of -0.552 V vs. SCE. *Right*: Picture of $MV^{\bullet+}$ in acetonitrile taken during the experiment, note the blue color of the solution.

In comparing the absorption spectra of the reduced-electroactive ligands to that of $MV^{\bullet+}$ we will first look at absorption spectra of the non-methylated electroactive ligands bpy-phenyl-MV (**L1**) and tpy-phenyl-MV (**L6**) (see **Figure 2.8**). The reductive absorption spectra are similar to that of $MV^{\bullet+}$ but not identical. The same electronic transitions are observed, $D_1 \leftarrow D_0$ and $D_2 \leftarrow D_0$, however both band shape and peak maxima have changed. The radical cations of the non-methylated electroactive-ligands (**L1**) and (**L6**) have broader absorption bands with red-shifted absorption maxima. The $D_2 \leftarrow D_0$ peak red shifts from 394 nm in $MV^{\bullet+}$ to 424 nm in (**L1**$^{\bullet}$) and (**L6**$^{\bullet}$) representing a 0.22 eV shift to lower energy.

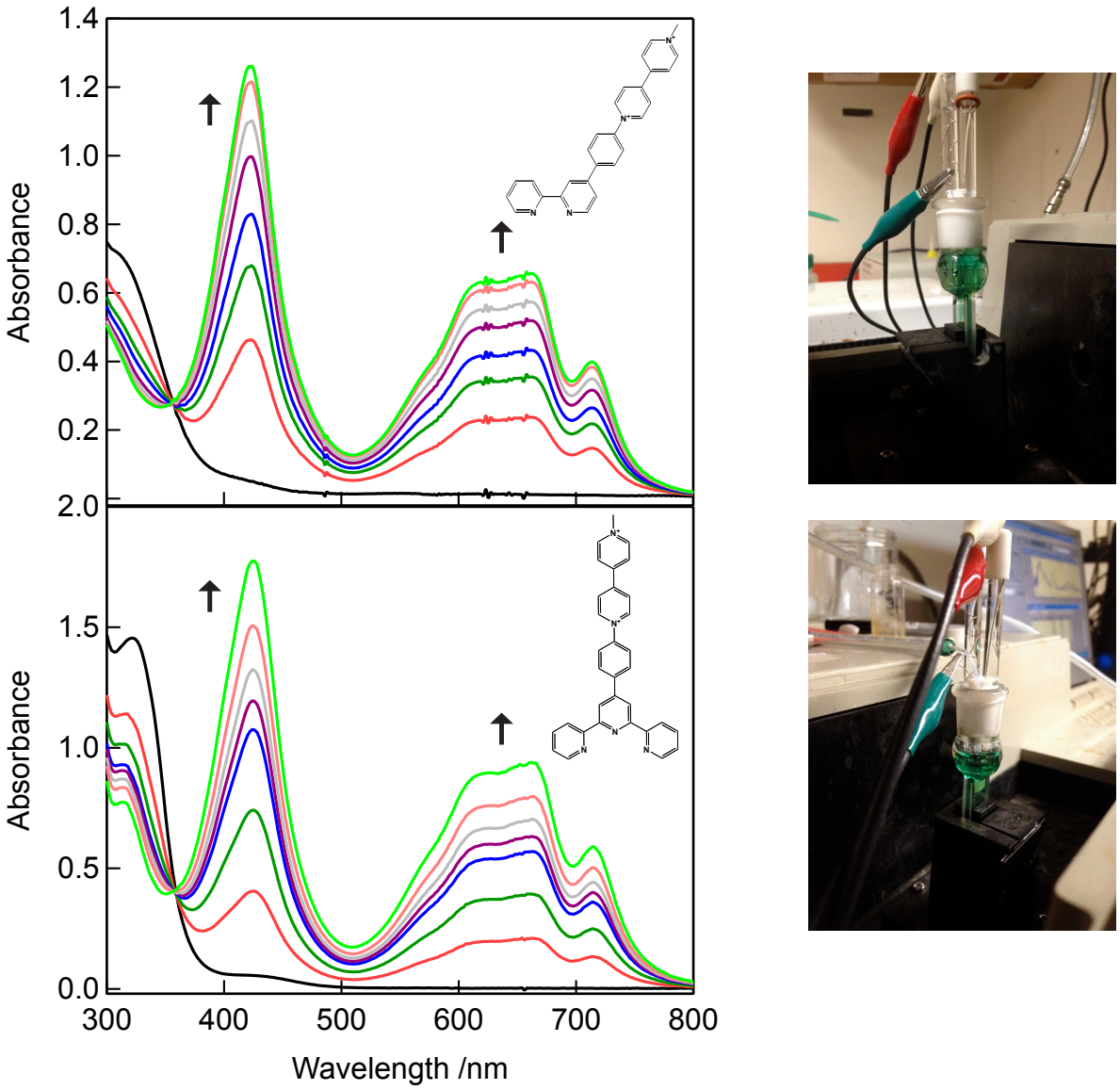

Figure 2.8 *Left*: Reductive spectroelectrochemical spectra for bpy-phenyl-MV (**L1**) (top) and tpy-phenyl-MV (**L6**)(bottom) in room temperature acetonitrile held at a potential of -0.522 V vs. SCE. When compared to $MV^{\bullet+}$, we see red shifting of absorption maxima. *Right*: Pictures corresponding to the reduced ligands in acetonitrile taken during the experiment.

Like $MV^{\bullet+}$ the new compounds discussed here are not colored in acetonitrile however the most striking and noticeable difference between $MV^{\bullet+}$ and the non-methylated reduced-electroactive ligands ((**L1**$^{\bullet}$) and (**L6**$^{\bullet}$)) is one that can be seen by eye, namely, the color of the solution. Unlike $MV^{\bullet+}$, the reduced non-methylated electroactive ligands (**L1**$^{\bullet}$)

and (**L6**$^{\bullet}$) turn green in acetonitrile, not blue. In order to determine if this observed color change is attributable to the appended N-phenyl alone or to the entirety of the ligand we prepared the phenyl acceptor (**A1**) and repeated the reductive spectroelectrochemical experiment. These spectra data are shown below in **Figure 2.9**. The experiment showed that the reduced phenyl acceptor also turns green in solution but spectral differences exist when comparing it to the radical cations of non-methylated electroactive ligands (**L1**) and (**L6**).

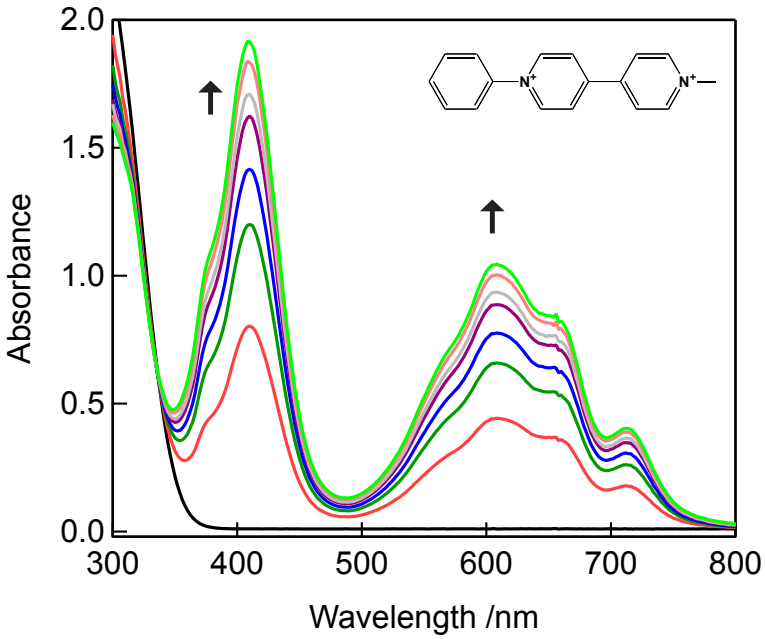

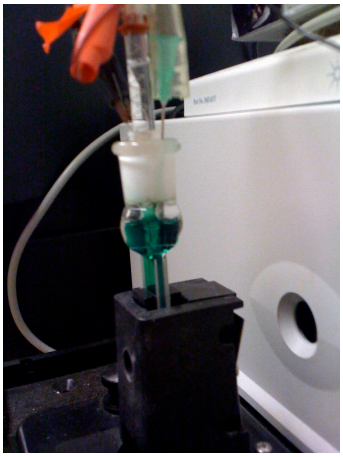

Figure 2.9 *Left*: Reductive spectroelectrochemical spectrum for the phenyl acceptor (**A1**) in room temperature acetonitrile held at a potential of -0.552 V vs. SCE. *Right*: Picture of the reduced phenyl acceptor (**A1**) in acetonitrile taken during the experiment.

For the phenyl acceptor we see the same two-band spectrum but here the $D_2 \leftarrow D_0$ absorption maximum now lies at 410 nm, red shifted by only 16 nm or 0.12 eV, when compared to $MV^{\bullet+}$, not 30 nm as was the case for the non-methylated ligands (**L1**) and (**L6**). We also see the return of spectral features in the $D_2 \leftarrow D_0$ transition. The spectral differences between $MV^{\bullet+}$ and compounds with an appended N-phenyl lead to the

conclusion that upon one-electron reduction compounds with appended aryl groups allow for delocalization of electron density onto these juxtaposed groups therefore altering the energetics of the system and red shifting the absorption maxima. Thinking in 'particle in a box' terms, delocalization onto the N-aryl group leads to lengthening of the 'box' and lowering of electronic energy levels. The conclusions from the reductive spectroelectrochemistry support our original claim for preparing directly linked electroactive ligands. We are effectively preparing highly coupled systems where electronic communication is facile. Furthermore the peak maxima are red shifted the most for the electroactive ligands (**L1**) and (**L6**) signifying that as additional aryl groups are appended (the polypyridine moieties) the reduced electron is delocalized over a 'longer box' implying that electron density is also delocalized on the polypyridine moiety.

Now we examine at the reductive spectra of the methylated electroactive ligands, particularly bpy-ortho-MV (**L2**) and bpy-2,6-dimethylphenyl-MV (**L3**) shown in **Figure 2.10** below. Here we begin to determine the effect of methyl substituents on the spectral properties of the reduced electroactive ligands. Our original claim was that methyl substituents on the bridging ligand would disrupt the ability of the electron density to delocalize over the ligand. When comparing the reductive spectra of (**L3**) and (**L4**) to those of the phenyl acceptor (**A1**) and the non-methylated electroactive ligands (**L1**) and (**L6**) we can determine to what extent the reduced electron is delocalized over the electroactive ligands. For bpy-ortho-MV (**L2**) and bpy-2,6-dimethylphenyl-MV (**L3**) we see that the reductive spectra more closely reproduce the spectral features of the phenyl acceptor (**A1**). We also see that the absorption maximum for the $D_2 \leftarrow D_0$ transition is 416 nm for bpy-ortho-MV (**L2**) and 414 nm for bpy-2,6-dimethylphenyl-MV (**L3**). Given the similarities in

spectral features and absorption maxima between (**A1**), (**L2**) and (**L3**) we conclude that for (**L2**) and (**L3**) electron delocalization is similar to that of (**A1**). In other words the methyl substituents are effectively preventing electron density from delocalizing onto the polypyridine moiety and are functioning as electronic insulators. These results validate our original claim that methyl substituents can disrupt electronic communication within the highly coupled directly linked electroactive ligands.

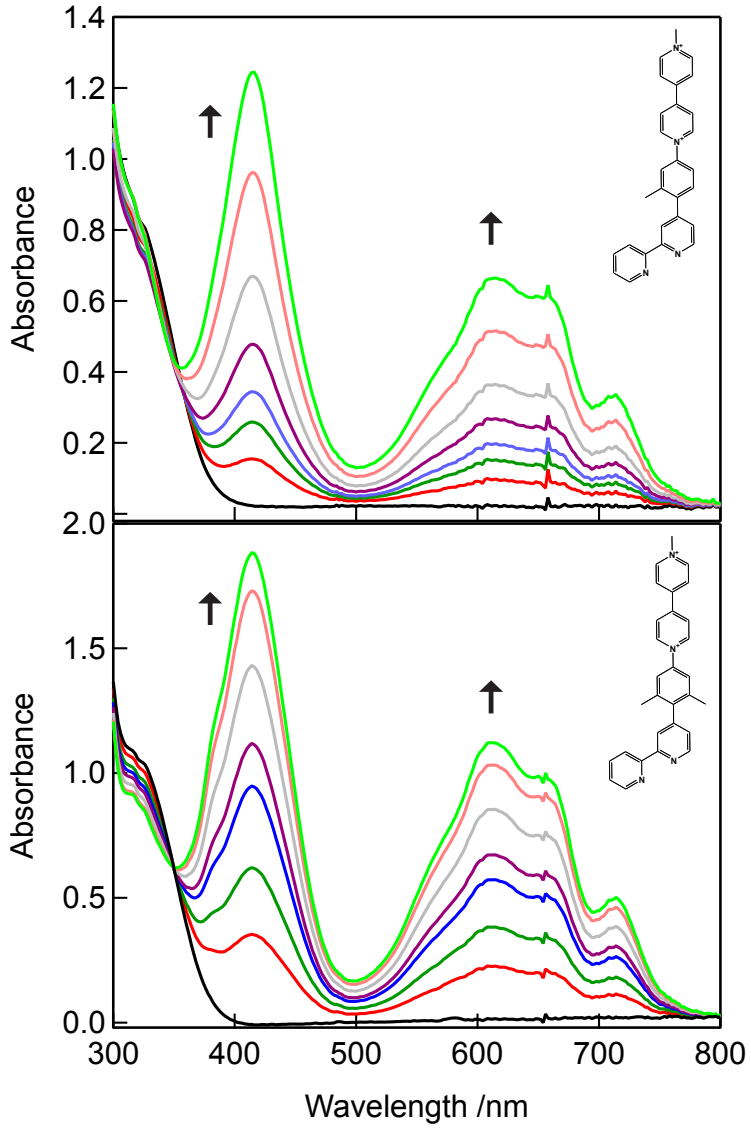

Figure 2.10 Reductive spectroelectrochemical spectra for bpy-ortho-MV (**L2**) (top) and bpy-2,6-dimethylphenyl-MV (**L3**) (bottom) in room temperature acetonitrile held at a potential of -0.522 V vs. SCE.

Taking a closer look at the spectrum of bpy-2,6-dimethylphenyl-MV (**L3**) it becomes evident that the spectral features are essentially indistinguishable from the phenyl acceptor (**A1**). Also the $D_2 \leftarrow D_0$ transition maximum for these two compounds is separated by only 4 nm. The $D_2 \leftarrow D_0$ peak maximum is 414 nm for (**L3**), 410 nm for (**A1**) while for (**L1**) it is 424 nm. **Figure 2.11** contains a normalized overlay of these three spectra for comparison. Where (**A1**) is shown in black, (**L3**) in red and (**L1**) is dotted. These observations support the argument that for (**L3**) and especially (**L4**) the methyl groups are effectively hindering electronic communication between the 2,2'-bipyridine and the 4,4'-bipyridinium moieties. The steric interactions between the methyl group(s) on the bridging ligand and the hydrogen atoms on the 2,2'-bipyridine inhibit ring rotation leading to a disruption in electronic communication and therefore electron density delocalization.

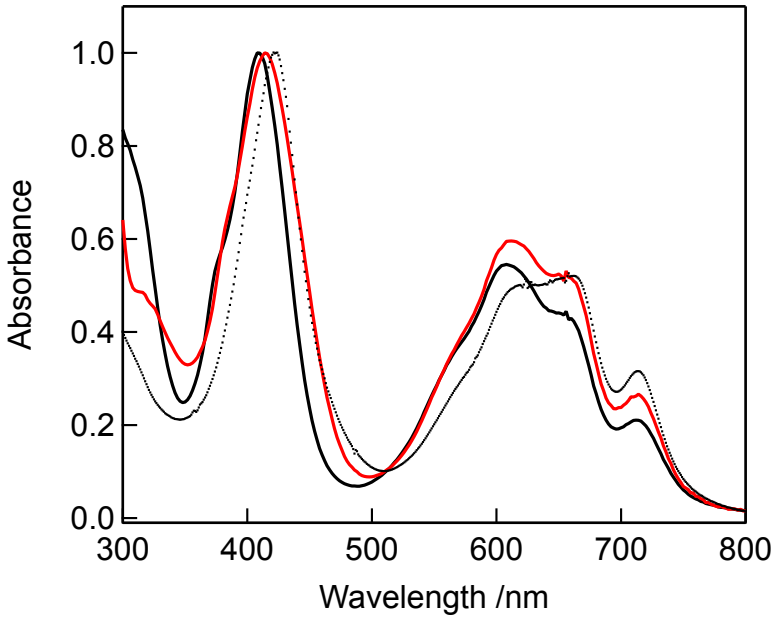

Figure 2.11 Overlay of phenyl acceptor (**A1**) (black), bpy-2,6-dimethylphenyl-MV (**L3**) (red) and bpy-phenyl-MV (**L1**) (dotted). Here we see that the spectral features for (**A1**) and (**L3**) are essentially indistinguishable. Leading to the conclusion that for (**L3**) steric bulk is effectively disrupting electronic communication across the entire ligand.

Clearly directly appending N-aryl groups to 4,4'-bipyrdinium derivatives has the ability to alter the electronic properties of this family of compounds. Methyl substitution in the 2 (**L2**) and 2,6 (**L3**) positions of the bridging phenyl has the effect of preventing the delocalization of electron density over the entire ligand, specifically, preventing electron density from reaching the 2,2'-bipyridine moiety. The next logical question is whether methylation in the 5 (**L4**) and 3,5 (**L5**) positions can be exploited to localize electron density onto the 4,4'-bipyridinium moiety. In other words can we effectively prevent electron delocalization onto the asymmetric aryl-substituted 2,2'-bipyridine moiety. Conducting the reductive spectroelectrochemical experiments on bpy-2,5-dimethylphenyl-MV (**L4**) and bpy-3,5-dimethylphenyl-MV (**L5**) alongside their respective acceptors subunits, (**A2**) and (**A3**), will allow us to address this issue. **Figure 2.12** below contains the reductive spectroelectrochemical data for bpy-2,5-dimethylphenyl-MV (**L4**) and 2,5-acceptor (**A2**) and **Figure 2.13** below contains that of bpy-3,5-dimethylphenyl-MV (**L5**) and 3,5-acceptor (**A3**).

Looking first at the reductive spectra of the 2,5 compounds shown in **Figure 2.12**, where (**A2**) is shown in the top panel and (**L4**) in the bottom panel we see that the reductive spectra have the same general features as those shown above wherein two bands are present, a $D_1 \leftarrow D_0$ transition and a $D_2 \leftarrow D_0$ transition. However the spectral features more closely resemble those of $MV^{\bullet+}$ not the N-aryl 4,4'-bipyridinium derivatives shown above. The $D_2 \leftarrow D_0$ transition in the absorption spectra of (**L4**) and (**A3**) peaks at 398 nm which is only 4 nm red-shifted from that of $MV^{\bullet+}$. Also the spectral features of the $D_1 \leftarrow D_0$ transition resemble that of the $MV^{\bullet+}$ in bandwidth and shape. Also upon one-electron reduction bpy-2,5-dimethylphenyl-MV (**L4**) and the 2,5-acceptor (**A2**) turn blue in solution,

like $MV^{\bullet+}$, not green like the compounds described above. The blue color of the solutions and spectral similarities between (**A3**), (**L4**) and $MV^{\bullet+}$ are leading indicators that steric bulk is disrupting electronic communication along the ligand and effectively restricting electron delocalization onto the 4,4'-bipyridinium moiety. This further validates our original claim for preparing these systems.

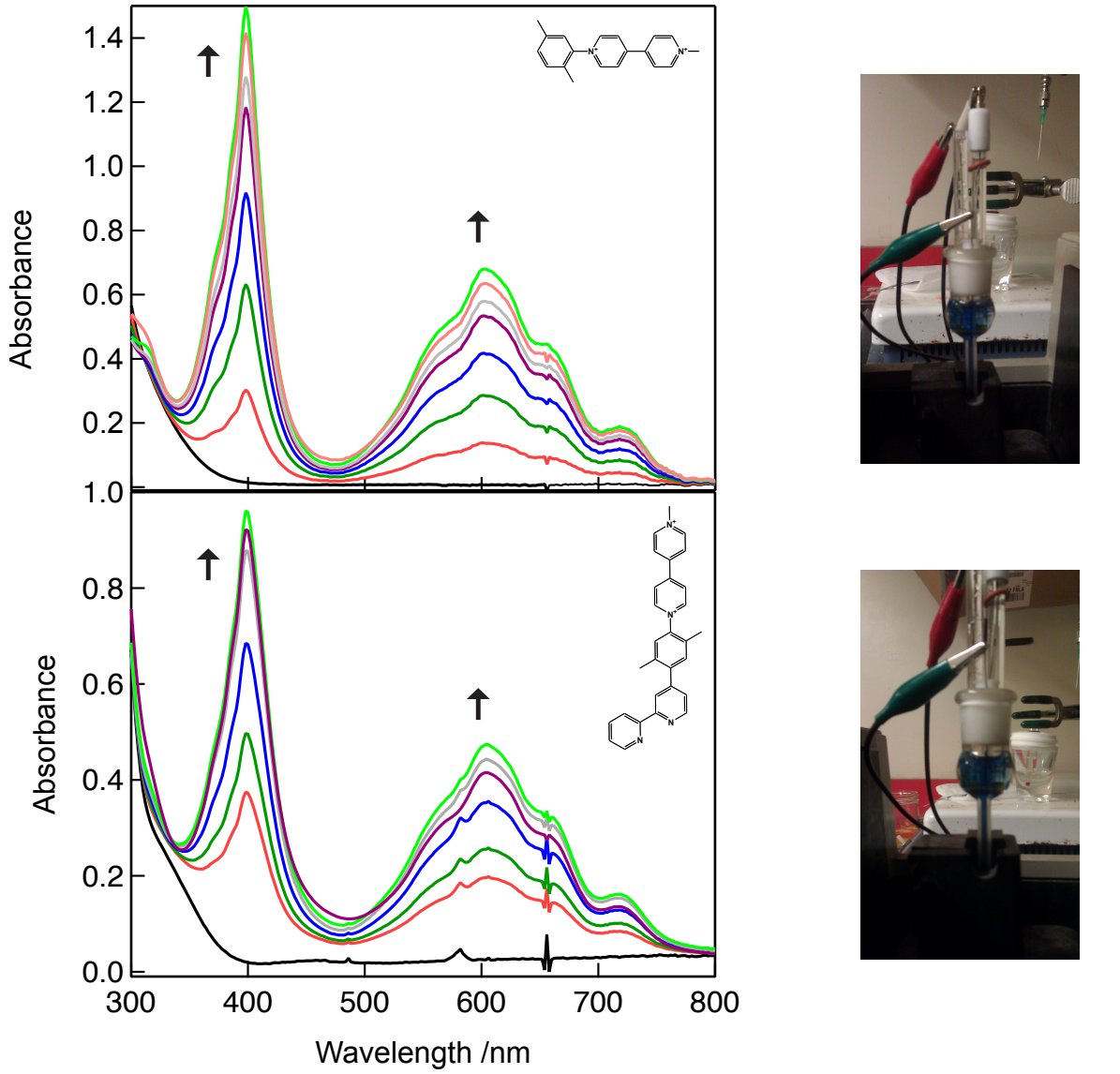

Figure 2.12 *Left*: Reductive spectroelectrochemical spectra for 2,5-acceptor (**A2**) (top) and bpy-2,5-dimethylphenyl-MV (**L4**) (bottom) in room temperature acetonitrile held at a potential of -0.522 V vs. SCE. *Right*: Pictures corresponding to the 2,5-acceptor (**A2**) and bpy-2,5-dimethylphenyl-MV (**L4**) in acetonitrile taken during the experiment.

Finally we discuss the reductive spectra of bpy-3,5-dimethylphenyl-MV (**L5**) and its corresponding acceptor subunit (**A3**). The spectra are shown in **Figure 2.13** below where (**A3**) is shown in the top panel and (**L5**) in the bottom panel.

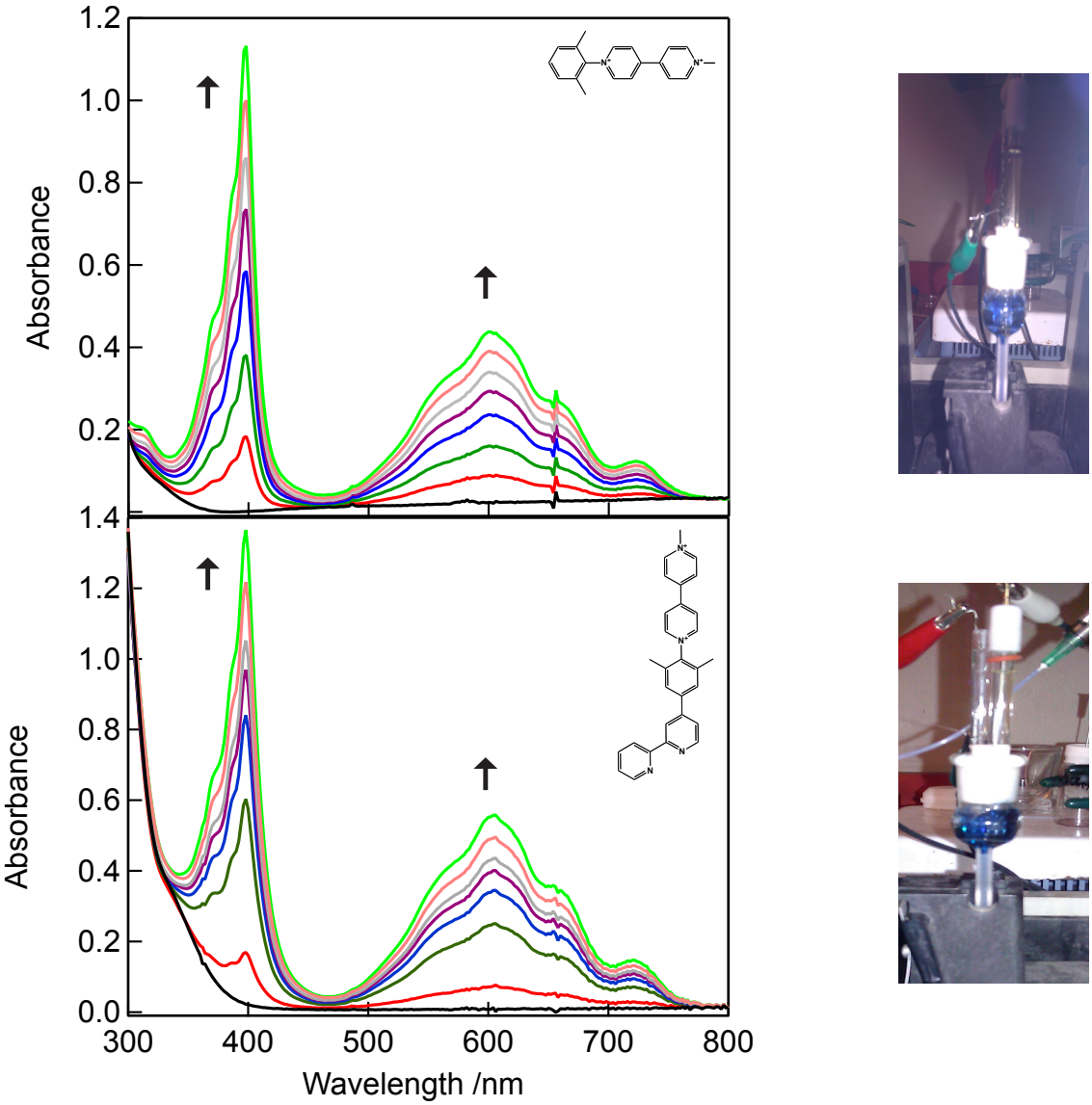

Figure 2.13 *Left*: Reductive spectroelectrochemical spectra for 3,5-acceptor (**A3**) (top) and bpy-3,5-dimethylphenyl-MV (**L5**) (bottom) in room temperature acetonitrile held at a potential of -0.522 V vs. SCE. *Right*: Pictures corresponding to the 3,5-acceptor (**A3**) and bpy-3,5-dimethylphenyl-MV (**L4**) in acetonitrile taken during the experiment.

Comparing these two spectra to each other we see that they are essentially indistinguishable. The $D_2 \leftarrow D_0$ transition peaks at 398 nm for both compounds. This is only

red shifted by 4 nm when compared to $MV^{\bullet+}$. Also we see the same vibronic structure (spectral features) for both compounds. The one-electron reduction absorption spectrum of bpy-3,5-dimethylphenyl-MV (**L5**) is electronically very similar to its acceptor subunit (**A3**) suggesting that upon one-electron reduction, the steric bulk within (**L5**) is preventing electron density from delocalizing onto the 2,2'-bipyridine moiety. Like (**L4**) and (**A2**) these compounds turn blue upon one-electron reduction in solution, like $MV^{\bullet+}$, not green like the non-methylated ligands electroactive ligands (**L1**) and (**L6**) or those methylated in the 2 **(L2**) and 2,6 positions (**L3**).

To highlight the spectral similarities between bpy-3,5-dimethylphenyl-MV (**L5**) and $MV^{\bullet+}$ a normalized overlay of the reductive absorption spectra is shown below in **Figure 2.14**. (**L5**) is shown in red and $MV^{\bullet+}$ in black.

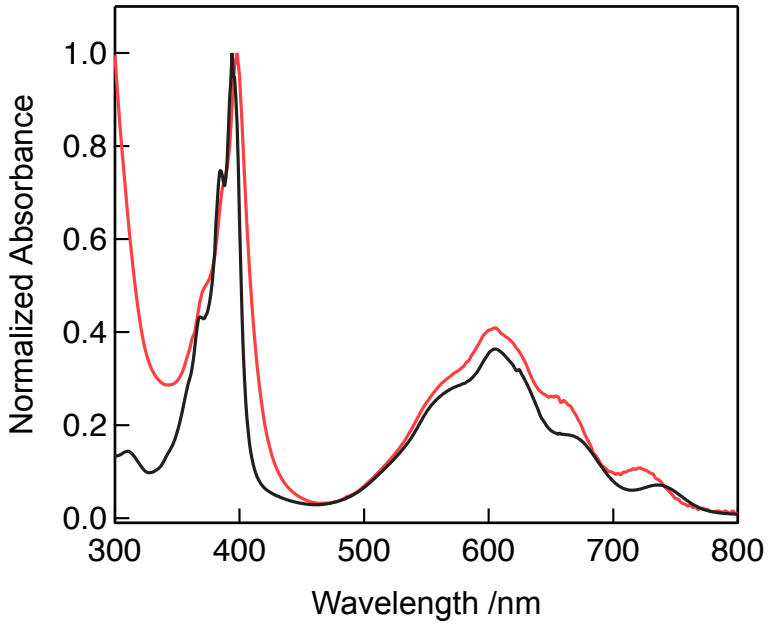

Figure 2.14 Normalized overlay of the $MV^{\bullet+}$ (black) and bpy-35-dimethylphenyl-MV (red) (**L5**) to highlight the spectral similarities between the two compounds when reduced by one electron.

When comparing the two spectra we find that they are not identical however they are very similar in band shape and absorption maxima. The spectral similarities between (**L5**) and $MV^{\bullet+}$ build on the evidence that methylation of the bridging ligand is disrupting electronic communication and can effectively determine extent of electron delocalization in these electroactive ligands.

It should be noted that the one-electron reduction process was reversible for all compounds described in this section. This means that the solutions were returned to their original color and absorption spectrum upon holding the voltage constant at 0 V vs. $Ag/AgNO_3$. This implies that over the course of the experiment the integrity of the compounds was not compromised. The reductive spectroelectrochemistry results discussed here will be used to interpret the analogous experimental data obtained when performing these experiments on the corresponding DBA complexes. The spectral features observed in the reductive experiments of the electroactive ligands and DBA complexes will be used to approximate spectral features of the photoinduced ET product.

2.4 Concluding Remarks

The synthesis and characterization of six new conformationally active electroactive ligands and their acceptor subunits have been described. A modified Zincke reaction was used to prepare these new compounds. This synthetic route has proven to be powerful since ~ 3 steps were needed to prepare the compounds. The compounds were isolated in high yields and purification was straightforward, only requiring recrystallization. The synthesis of the asymmetric aryl-substituted aminophenyl-2,2'-polypyrdines needed for the Zincke reaction as well as the asymmetric aryl-substituted-2,2'-bipyridine donor

ligands have also been described. These compounds were prepared via a Suzuki coupling in high yields.

The electrochemical characterization of these compounds was also described. Cyclic voltammetry and reductive spectroelectrochemistry were used to characterize the compounds. These experiments provided evidence that steric bulk on the bridging phenyl has the ability to alter the electronic properties of the compounds validating our original claim for preparing them. These electroactive ligands were prepared for the purpose of studying the role of nuclear motions in photoinduced intramolecular electron transfer. The electrochemistry experiments indicate that nuclear motions are playing a role in determining the electronic properties of the electroactive ligands.

2.5 References

(1) Davis, W. B.; Ratner, M. A.; Wasielewski, M. R. *J. Am. Chem. Soc.* **2001**, *123*, 7877.

(2) Meylemans, H. A.; Lei, C. F.; Damrauer, N. H. *Inorg. Chem.* **2008**, *47*, 4060.

(3) Meylemans, H. A.; Hewitt, J. T.; Abdelhaq, M.; Vallett, P. J.; Damrauer, N. H. *J. Am. Chem. Soc.* **2010**, *132*, 11464.

(4) Laine, P. P.; Bedioui, F.; Loiseau, F.; Chiorboli, C.; Campagna, S. *J. Am. Chem. Soc.* **2006**, *128*, 7510.

(5) Yonemoto, E. H.; Riley, R. L.; Kim, Y. I.; Atherton, S. J.; Schmehl, R. H.; Mallouk, T. E. *J. Am. Chem. Soc.* **1992**, *114*, 8081.

(6) Yonemoto, E. H.; Saupe, G. B.; Schmehl, R. H.; Hubig, S. M.; Riley, R. L.; Iverson, B. L.; Mallouk, T. E. *J. Am. Chem. Soc.* **1994**, *116*, 4786.

(7) Meylemans, H. A.; Damrauer, N. H. *Inorg. Chem.* **2009**, *48*, 11161.

(8) Ciofini, I.; Laine, P. P.; Bedioui, F.; Adamo, C. *J. Am. Chem. Soc.* **2004**, *126*, 10763.

(9) Elliott, C. M.; Freitag, R. A.; Blaney, D. D. *J. Am. Chem. Soc.* **1985**, *107*, 4647.

(10) Cooley, L. F.; Headford, C. E. L.; Elliott, C. M.; Kelley, D. F. *J. Am. Chem. Soc.* **1988**, *110*, 6673.

(11) Berg, K. E.; Tran, A.; Raymond, M. K.; Abrahamsson, M.; Wolny, J.; Redon, S.; Andersson, M.; Sun, L. C.; Styring, S.; Hammarstrom, L.; Toftlund, H.; Akermark, B. *Eur. J. Inorg. Chem.* **2001**, 1019.

(12) Lomoth, R.; Haupl, T.; Johansson, O.; Hammarstrom, L. *Chem. Eur. J.* **2002**, *8*, 102.

(13) Johansson, O.; Borgstrom, M.; Lomoth, R.; Palmblad, M.; Bergquist, J.; Hammarstrom, L.; Sun, L. C.; Akermark, B. *Inorg. Chem.* **2003**, *42*, 2908.

(14) Henrich, J. D.; Zhang, H. Y.; Dutta, P. K.; Kohler, B. *J. Phys. Chem. B* **2010**, *114*, 14679.

(15) BergBrennan, C.; Subramanian, P.; Absi, M.; Stern, C.; Hupp, J. T. *Inorg. Chem.* **1996**, *35*, 3719.

(16) Cooley, L. F.; Larson, S. L.; Elliott, C. M.; Kelley, D. F. *J. Phys. Chem.* **1991**, *95*, 10694.

(17) Kelly, L. A.; Rodgers, M. A. J. *J. Phys. Chem.* **1995**, *99*, 13132.

(18) Meylemans, H. a.; Lei, C.-F.; Damrauer, N. H. *Inorg. Chem.* **2008**, *47*, 4060.

(19) Juris, A.; Balzani, V.; Barigelletti, F.; Campagna, S.; Belser, P.; Vonzelewsky, A. *Coord. Chem. Rev.* **1988**, *84*, 85.

(20) Monk, P. M. S. *The viologens : physicochemical properties, synthesis, and applications of the salts of 4,4'-bipyridine*; Wiley: Chichester ; New York, 1998.

(21) Damrauer, N. H.; Boussie, T. R.; Devenney, M.; McCusker, J. K. *J. Am. Chem. Soc.* **1997**, *119*, 8253.

(22) Damrauer, N. H.; Weldon, B. T.; McCusker, J. K. *J. Phys. Chem. A* **1998**, *102*, 3382.

(23) Damrauer, N. H.; McCusker, J. K. *J. Phys. Chem. A* **1999**, *103*, 8440.

(24) Damrauer, N. H.; McCusker, J. K. *Inorg. Chem.* **1999**, *38*, 4268.

(25) Lyubimova, O. O.; Baranovskii, V. I. *Journal of Structural Chemistry* **2003**, *44*, 728.

(26) Cordaro, J. G.; McCusker, J. K.; Bergman, R. G. *Chem. Commun.* **2002**, 1496.

(27) Borgstrom, M.; Johansson, O.; Lomoth, R.; Baudin, H. B.; Wallin, S.; Sun, L. C.; Akermark, B.; Hammarstrom, L. *Inorg. Chem.* **2003**, *42*, 5173.

(28) Zhang, Z.; Dong, Y. W.; Wang, G. W. *Chem. Lett.* **2003**, *32*, 966.

(29) Coe, B. J.; Harris, J. A.; Harrington, L. J.; Jeffery, J. C.; Rees, L. H.; Houbrechts, S.; Persoons, A. *Inorg. Chem.* **1998**, *37*, 3391.

(30) Pavlishchuk, V. *Inorg. Chim. Acta* **2000**, *298*, 97.

(31) Li, J. J. *Name reactions in heterocyclic chemistry*; Wiley-Interscience: Hoboken, N.J., 2005.

(32) Cheng, W. C.; Kurth, M. J. *Org Prep Proced Int* **2002**, *34*, 585.

(33) Coe, B. J.; Harris, J. A.; Jones, L. A.; Brunschwig, B. S.; Song, K.; Clays, K.; Garin, J.; Orduna, J.; Coles, S. J.; Hursthouse, M. B. *J. Am. Chem. Soc.* **2005**, *127*, 4845.

(34) Freitag, M.; Gundlach, L.; Piotrowiak, P.; Galoppini, E. *J. Am. Chem. Soc.* **2012**, *134*, 3358.

(35) Coe, B. J.; Foxon, S. P.; Harper, E. C.; Helliwell, M.; Raftery, J.; Swanson, C. A.; Brunschwig, B. S.; Clays, K.; Franz, E.; Garin, J.; Orduna, J.; Horton, P. N.; Hursthouse, M. B. *J. Am. Chem. Soc.* **2010**, *132*, 1706.

(36) Coe, B. J.; Fielden, J.; Foxon, S. P.; Brunschwig, B. S.; Asselberghs, I.; Clays, K.; Samoc, A.; Samoc, M. *J. Am. Chem. Soc.* **2010**, *132*, 3496.

(37) Marvell, E. N.; Caple, G.; Shahidi, T. *J. Am. Chem. Soc.* **1970**, *92*, 5641.

(38) Ise, N.; Okubo, T.; Kitano, H.; Kunugi, S. *J. Am. Chem. Soc.* **1975**, *97*, 2882.

(39) Kunugi, S.; Okubo, T.; Ise, N. *J. Am. Chem. Soc.* **1976**, *98*, 2282.

(40) Miyaura, N.; Yamada, K.; Suzuki, A. *Tetrahedron Lett.* **1979**, *20*, 3437.

(41) Miyaura, N.; Suzuki, A. *J Chem Soc Chem Comm* **1979**, 866.

(42) Miyaura, N.; Suzuki, A. *Chem. Rev.* **1995**, *95*, 2457.

(43) Kocienski, P. J. *Protecting groups*; Corr. ed.; G. Thieme: Stuttgart ; New York, 2000.
(44) Saika, T.; Iyoda, T.; Shimidzu, T. *Chem. Lett.* **1990**, 1955.
(45) McCusker, J. K. *Acc. Chem. Res.* **2003**, *36*, 876.
(46) Watanabe, T.; Honda, K. *J. Phys. Chem.* **1982**, *86*, 2617.
(47) Haupl, T.; Lomoth, R.; Hammarstrom, L. *J. Phys. Chem. A* **2003**, *107*, 435.

Chapter Three

Synthesis and Electrochemical Characterization of Ruthenium (II) Polypyridyl Complexes with Conformationally Active Ligands.

3.1 Introductory Remarks

Chapter Two described the preparation and characterization of the conformationally asymmetric-electroactive ligands and their respective donor ligands. In this chapter the synthesis and electrochemical characterization of the metal complexes prepared from these ligands will be described. The complexes were prepared for the purpose of studying photoinduced intramolecular electron transfer (ET) in conformationally active directly linked ruthenium (II) polypyridyls. Photoinduced intramolecular electron transfer involves the transfer of charge from a donor chromophore to an acceptor moiety after photo-excitation. In preparing these complexes we seek to determine the role of nuclear motions on photoinduced intramolecular ET.

To study intramolecular ET the donor-bridge-acceptor (DBA) platform was chosen wherein the donor chromophore is covalently linked to the acceptor subunit via a bridging ligand. The proposed platform for these complexes is shown in **Scheme 3.1** below. We propose preparing a series of complexes with varying methylation on both the ancillary and asymmetric ligands. In **Scheme 3.1** R designates positions where methylation will be introduced. The asymmetric ligand will serve as the active site for the ET process. This ligand has a juxtaposed electroactive acceptor subunit that will function as the recipient of the transferred electron. In designing the DBA systems ruthenium (II) polypyridyls serve as the donor chromophores. Ruthenium (II) polypyridyls have frequently served as donor chromophores for studying intramolecular ET.[1-17] Aryl substituted polypyridine ligands

were chosen to serve as the asymmetric ligands because of their well documented excited-state ring rotational dynamics when chelated to ruthenium.[18-22]

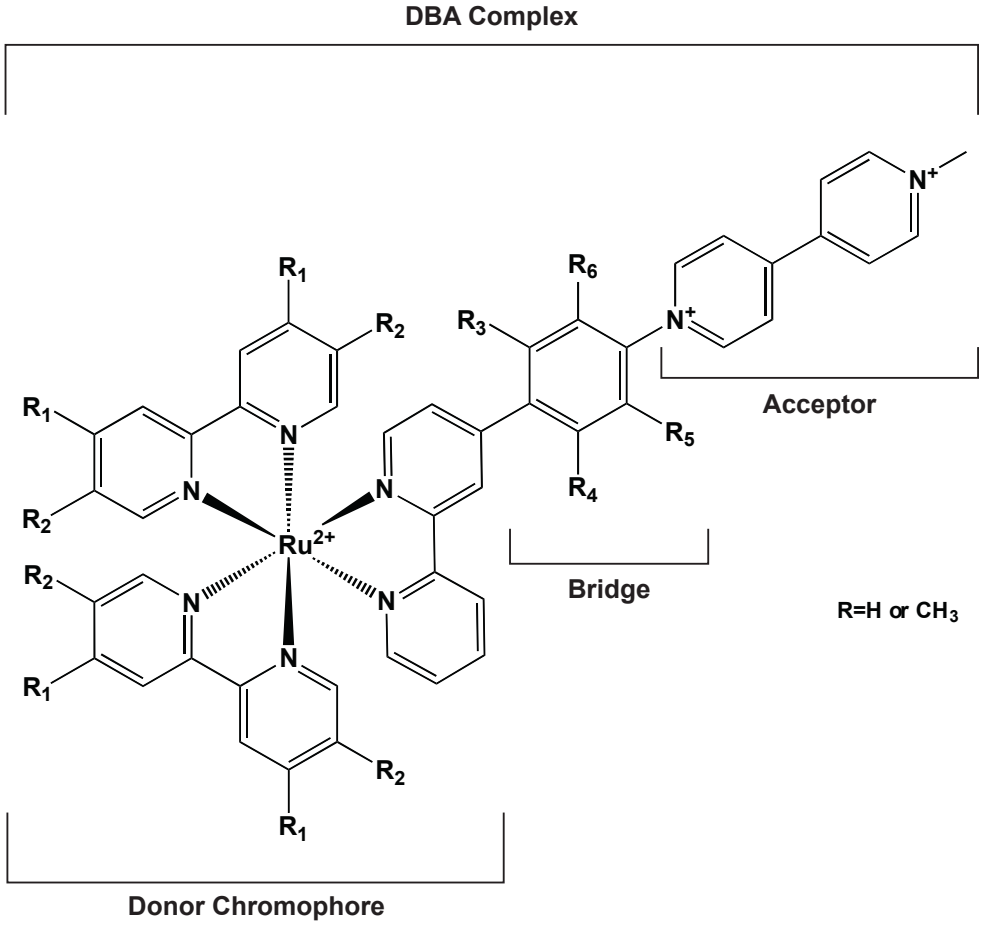

Scheme 3.1 Proposed donor-bridge-acceptor platform for studying conformationally gated intramolecular electron transfer.

Specifically $[Ru(bpy)_3]^{2+}$, where bpy is 2,2'-bipyridine, and its derivatives were chosen as donor chromophores. $[Ru(bpy)_3]^{2+}$ is shown below in **Figure 3.1**. Among the reasons for choosing these complexes is that the photophysics of $[Ru(bpy)_3]^{2+}$ and many of its derivatives is well known.[23-29] Ruthenium polypyridyl complexes are chemically stable, have long excited state lifetimes[30] and are known for their strong metal-to-ligand charge transfer (MLCT) band upon absorption of visible photon.[23,24] Simply put a MLCT absorption

event transfers an electron from a dπ-orbital on the metal into the π* system of one of the polypyridine ligands. After ^{1}MLCT ← GS (ground state) excitation a rapid intersystem crossing leads to the formation of a ^{3}MLCT excited state. The intersystem crossing reportedly occurs within 100 fs of excitation.[31-34]

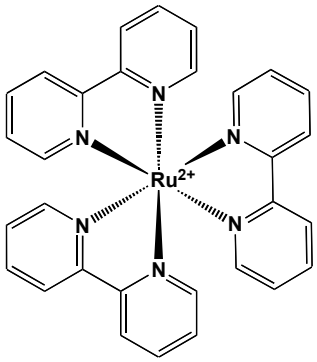

Figure 3.1 Structure of $[Ru(bpy)_3]^{2+}$. The metal complexes discussed in this text are derivatives of this complex due to its favorable photophysical properties. For our purposes, the complex is isolated as a PF_6^- salt.

$[Ru(bpy)_3]^{2+}$ can be derivatized by modifying the polypyridine ligands chelated to the metal center. Two derivatives with methylated polypyridine ligands are $[Ru(dmb)_3]^{2+}$ and $[Ru(tmb)_3]^{2+}$ where dmb is 4,4'-dimethyl-2,2'-bipyridine and tmb is 4,4',5,5'-tetramethyl-2,2'-bipyridine. These homoleptic complexes are shown in **Figure 3.2** below. $[Ru(bpy)_3]^{2+}$,$[Ru(dmb)_3]^{2+}$ and $[Ru(tmb)_3]^{2+}$ are the parent complexes for all new complexes reported herein. Derivatizing the polypyridine ligand allows for the manipulation of the photophysical properties of the complexes.[28,29] Introducing methyl groups onto the ancillary ligand alters the energetics of the complexes because methyl groups are electron donating. As a result driving forces for electron transfer will change.[5,17,29] This will be discussed in further detail in **Section 3.3.2** and Chapter Four.

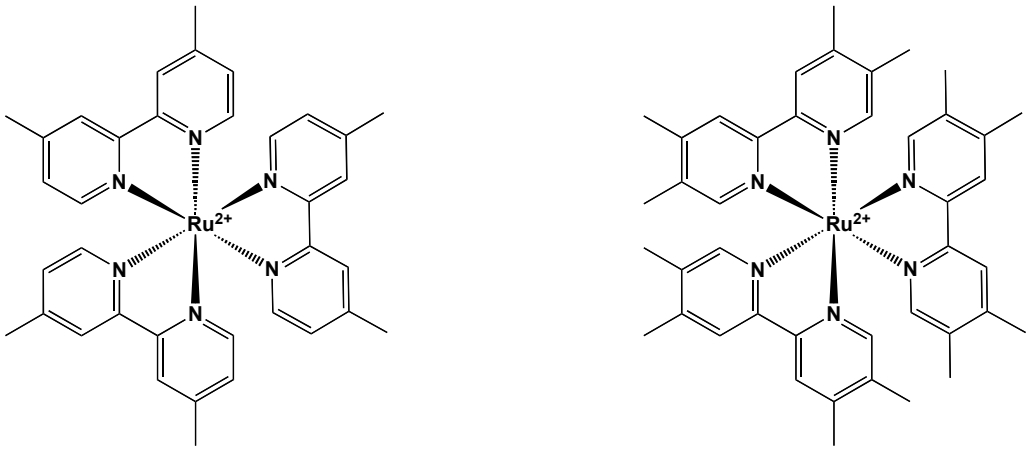

Figure 3.2 $[Ru(dmb)_3]^{2+}$ (left) and $[Ru(tmb)_3]^{2+}$ (right), these derivatives of $[Ru(bpy)_3]^{2+}$are also used as basses for the complexes prepared in this work. For our purposes, the complexes are isolated as PF_6^- salts.

Unlike the parent complexes, which are homoleptic species the new complexes discussed here are heteroleptic species. This means that the ligands chelating the metal center are not all the same. Specifically, one polypyridine ligand will be substituted for an asymmetric aryl-substituted 2,2'-bipyridine ligand. In addition to the DBA complexes we prepared 'donor' complexes. These complexes match the DBA complexes but lack an electroactive acceptor subunit. The donor complexes serve as photophysical models since they cannot do intramolecular ET. By studying the photophysics of the donor and DBA complexes the effect of the electroactive acceptor can be determined.

As mentioned in Chapter One the new complexes are classified into two categories: the 'driving-force' series and the 'sterics' series. In reference to **Scheme 3.1** the complexes in the driving-force series have the same asymmetric ligand but differ in ancillary ligand (positions R_1 and R_2). **Figure 3.3** below shows the structures of the complexes in this series. The non-methylated ligands bpy-phenyl (**L1'**) and bpy-phenyl-MV (**L1**) were used as the asymmetric ligands for the donor and DBA complexes, respectively.

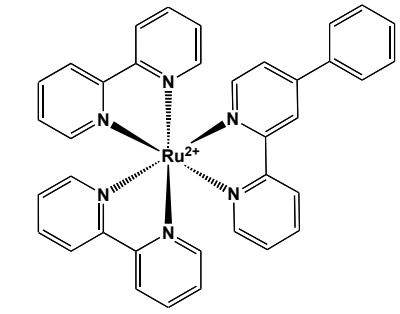

[Ru(bpy)$_2$(bpy-phenyl)]$^{2+}$(**1'**)

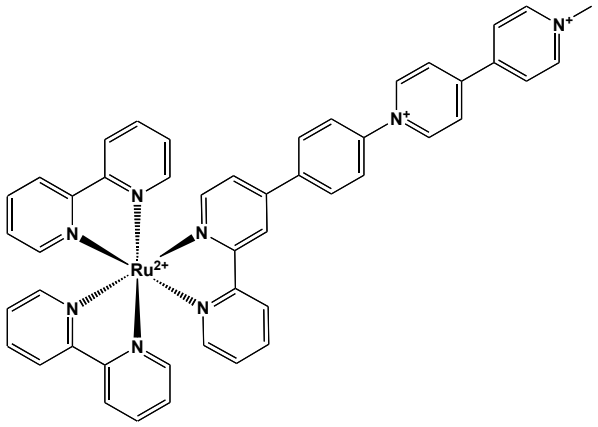

[Ru(bpy)$_2$(bpy-phenyl-MV)]$^{4+}$(**1**)

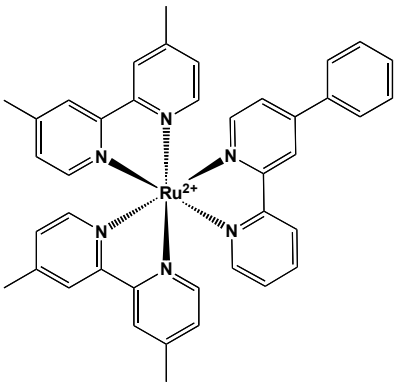

[Ru(dmb)$_2$(bpy-phenyl)]$^{2+}$(**2'**)

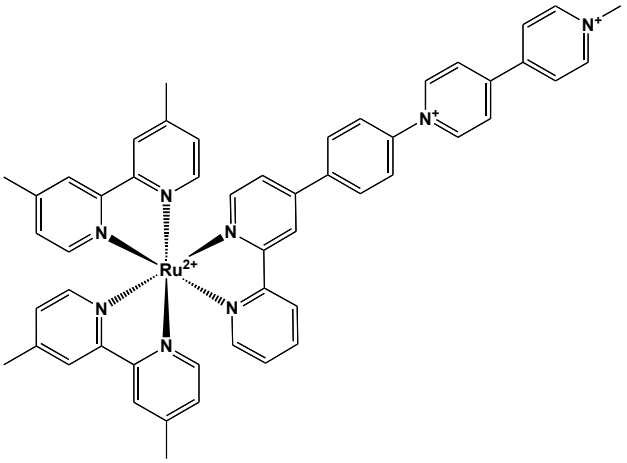

[Ru(dmb)$_2$(bpy-phenyl-MV)]$^{4+}$(**2**)

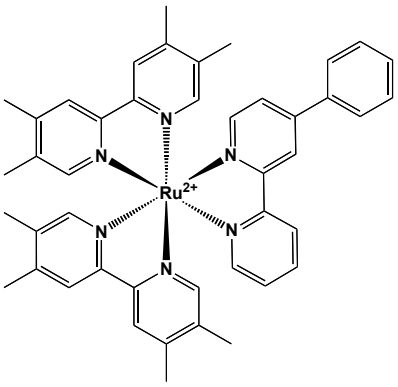

[Ru(tmb)$_2$(bpy-phenyl)]$^{2+}$(**3'**)

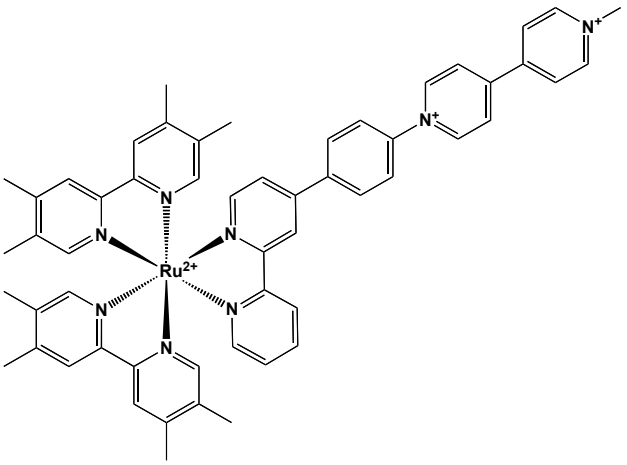

[Ru(tmb)$_2$(bpy-phenyl-MV)]$^{4+}$(**3'**)

Figure 3.3 Donor (left) and Donor-Bridge-Acceptor (right) complexes in the driving-forces series; which differ by ancillary ligand. The complexes were isolated as PF_6^- salts.

For the sterics series the same ancillary ligand is used to prepare the complexes but the asymmetric ligands differ in methylation on the aryl substituent (positions R_3, R_4, R_5 and R_6 in **Scheme 3.1**). 4,4',5,5'-tetramethyl-2,2'-bipyrdine (tmb) was used as the ancillary ligand for all the complexes. It is hypothesized that methylation of the aryl group on the ligands will not affect the energetics of the complexes significantly; therefore it is assumed that the complexes will have similar driving forces for photoinduced electron transfer and any differences in the photophysics may then be attributable to steric influences within the complex. The complexes in this series are shown in **Figure 3.4** below. Five sets of donor and DBA complexes were prepared in this series. By adding steric bulk to various positions on the aryl substituent not only can one determine the effect of methyl substituents on the photoinduced ET process but one can also examine if position of methylation plays a role.

In this chapter synthesis and electrochemical characterization of these complexes will be presented and discussed. Cyclic voltammetry (CV) and reductive and oxidative spectroelectrochemical experiments will be described. All of this information is needed in order to determine if photoinduced intramolecular ET is expected to be operative in these systems. Oxidation and reduction potentials of the DBA complex will be used in Chapters Four and Five to determine driving forces for ET. Spectroelectrochemical experiments are needed to approximate the absorption properties of the DBA upon one-electron reduction or oxidation. The photophysics of all these complexes will be discussed in subsequent chapters.

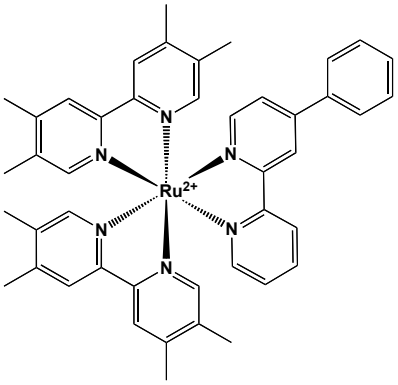

$[Ru(tmb)_2(bpy\text{-}phenyl)]^{2+}$(**3'**)

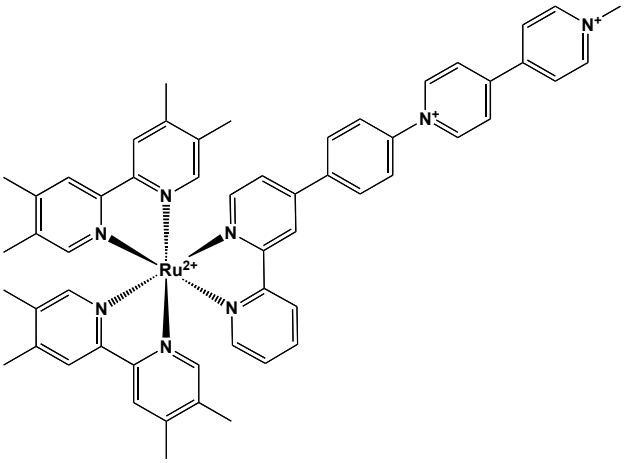

$[Ru(tmb)_2(bpy\text{-}phenyl\text{-}MV)]^{4+}$(**3**)

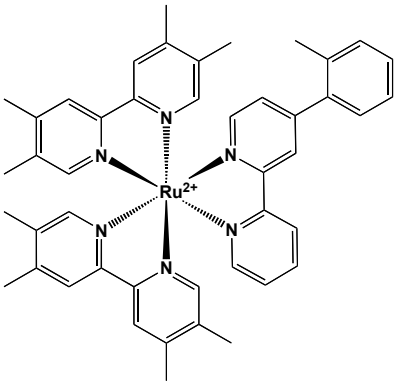

$[Ru(tmb)_2(bpy\text{-}ortho)]^{2+}$(**4'**)

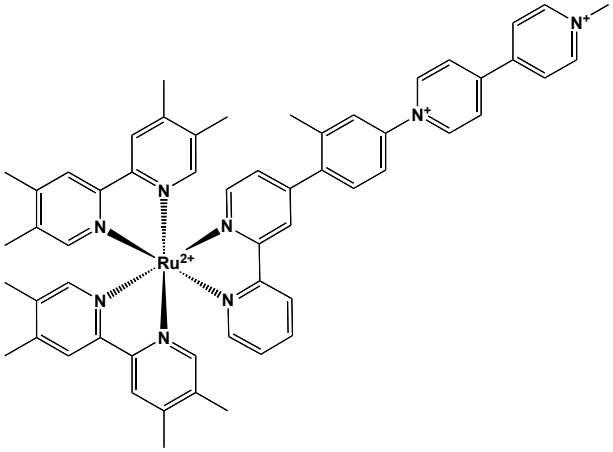

$[Ru(tmb)_2(bpy\text{-}ortho\text{-}MV)]^{4+}$(**4**)

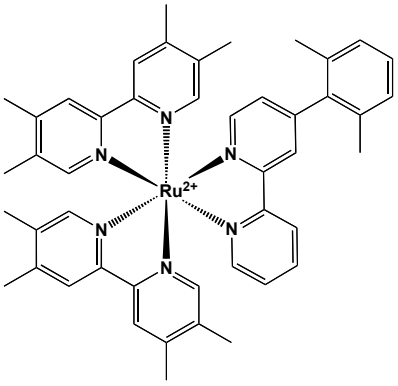

$[Ru(tmb)_2(bpy\text{-}2,6\text{-}dimethylphenyl)]^{2+}$(**5'**)

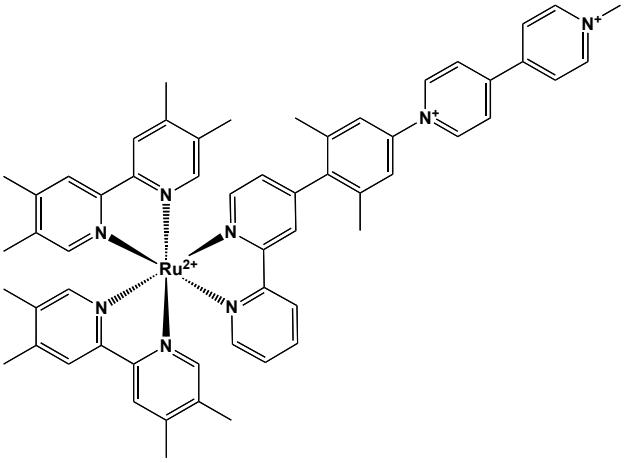

$[Ru(tmb)_2(bpy\text{-}2,6\text{-}dimethylphenyl\text{-}MV)]^{4+}$(**5**)

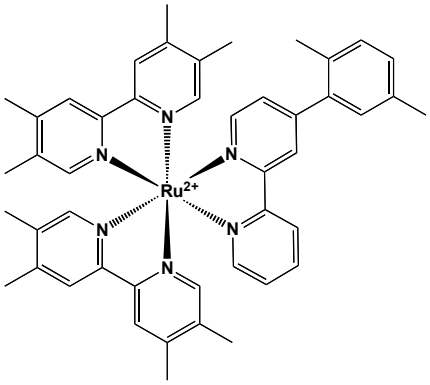

[Ru(tmb)$_2$(bpy-2,5-dimethylphenyl)]$^{2+}$(**6'**)

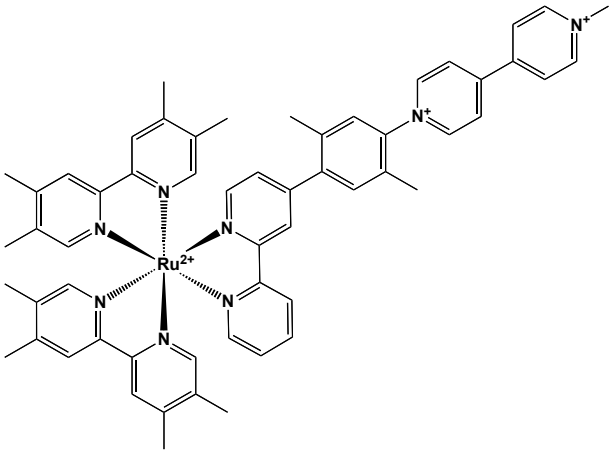

[Ru(tmb)$_2$(bpy-2,5-dimethylphenyl-MV)]$^{4+}$(**6**)

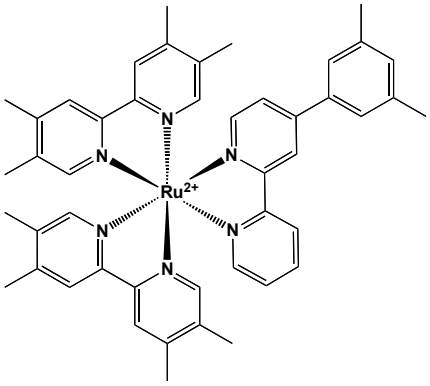

[Ru(tmb)$_2$(bpy-3,5-dimethylphenyl)]$^{2+}$(**7'**)

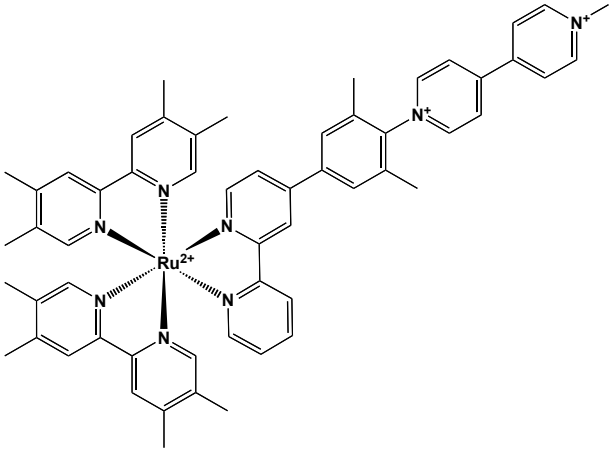

[Ru(tmb)$_2$(bpy-3,5-dimethylphenyl-MV)]$^{4+}$(**7**)

Figure 3.4 Donor (left) and Donor-Bridge-Acceptor (right) complexes in the sterics series. The complexes share ancillary ligands differ but differ by asymmetric aryl substituted ligand. The complexes were isolated as PF_6^- salts.

3.2 Experimental

3.2.1 Synthesis

All reagents and materials from commercial sources were used as received. Solvents were purchased from Sigma-Aldrich Chemical Co. or Mallinckrodt Chemicals. All deuterated solvents were obtained from Cambridge Isotope Laboratories, Inc. 2,2'-bipyridine, 4,4'-dimethyl-2,2'-bipyridine, ammonium hexafluorophosphate, and potassium

nitrate were obtained from Sigma-Aldrich Chemical Co. Ruthenium (III) chloride hydrate was obtained from Strem Chemicals, Inc 4,4',5,5'-tetramethyl-2,2'-bipyrdine (tmb) was prepared according to a previously published procedure.[35] All NMR spectra were recorded on a Varian Inova 500 MHz or Varian Inova 400 MHz spectrometer. Accurate mass measurements were obtained in house from the University of Colorado's Central Analytical Laboratory.

General procedure for metal complex preparation

The method used to prepare all fourteen metal complexes has been previously described.[5,17,35,36] A RuL_2CO_3 precursor was used where L is the ancillary ligand and corresponds to bpy, dmb or tmb. To a flask equipped with a stir bar, were added 15 mL of EtOH:H_2O solution saturated with KNO_3. To this flask 1 equivalent of ligand (donor or electroactive) and 0.80 equivalents of metal precursor were added and the contents stirred at room temperature for five days. The excess salt was filtered and the reaction mixture dried via rotary evaporator. The residues were purified on silica using an 8:1:1 CH_3CN: H_2O: sat. KNO_3 solution for DBA complexes and 9:1 CH_2Cl_2: MeOH for the donor complex. Salt metathesis to PF_6^- was achieved by dissolving the compounds in water and added excess NH_4PF_6. The orange precipitate was collected on a frit and washed with water and ether. The complexes were characterized by NMR and accurate mass spectrometry experiments. ^1H NMR and 2D COSY were used to aid in proton assignment and DOESY experiments were used to confirm the presence of a single complex.

[Ru(bpy)$_2$(bpy-phenyl)](PF$_6$)$_2$ (**1'**) Yield: 70% (47 mg) ^{1}H NMR (500 MHz, CD_3CN) δ 8.69 (d, J = 1.7 Hz, 1H), 8.63 (d, J = 8.2 Hz, 1H), 8.51 – 8.43 (m, 4H), 8.08 – 7.98 (m, 5H), 7.87 – 7.80 (m, 2H), 7.76 (d, J = 5.6 Hz, 1H), 7.74 – 7.66 (m, 5H), 7.60 (dd, J = 6.0, 2.0 Hz, 1H), 7.59 – 7.51 (m, 3H), 7.41 – 7.32 (m, 5H). Accurate Mass: As [A^{2+} PF_6^-] calcd. 791.1065 measured 791.1077

[Ru(dmb)$_2$(bpy-phenyl)](PF$_6$)$_2$ (**2'**) Yield: 68% (43 mg) ^{1}H NMR (500 MHz, CD_3CN) δ 8.71 (d, J = 1.8 Hz, 1H), 8.65 (d, J = 8.3 Hz, 1H), 8.34 (m, 4H), 8.05 (td, J = 7.9, 1.5 Hz, 1H), 7.90 – 7.84 (m, 2H), 7.74 (dd, J = 10.2, 5.8 Hz, 2H), 7.64 – 7.53 (m, 8H), 7.42 – 7.37 (m, 1H), 7.29 – 7.16 (m, 4H), 2.53 (dd, J = 5.9, 2.1 Hz, 12H). Accurate mass: As [A^{2+} PF_6^-] calcd. 847.1692 measured 847.1709

[Ru(tmb)$_2$(bpy-phenyl)](PF$_6$)$_2$ (**3'**) Yield: 65% (43 mg) ^{1}H NMR (500 MHz, CD_3CN) δ 8.72 (d, J = 1.8 Hz, 1H), 8.67 (d, J = 8.3 Hz, 1H), 8.25 (dd, J = 12.7, 8.3 Hz, 4H), 8.03 (td, J = 8.0, 1.4 Hz, 1H), 7.90 – 7.86 (m, 2H), 7.72 (d, J = 5.9 Hz, 2H), 7.62 – 7.53 (m, 4H), 7.35 (ddd, J = 34.2, 14.4, 3.8 Hz, 5H), 2.44 – 2.41 (m, 12H), 2.07 (dd, J = 10.8, 3.2 Hz, 12H). Accurate mass: As [A^{2+} PF_6^-] calcd. 903.2319 measured 903.2354

[Ru(tmb)$_2$(bpy-ortho)](PF$_6$)$_2$ (**4'**) Yield: 72% (48 mg) ^{1}H NMR (400 MHz, CD_3CN) δ 8.51 (d, J = 8.0 Hz, 1H), 8.46 (d, J = 1.4 Hz, 1H), 8.27 – 8.21 (m, 4H), 8.02 – 7.96 (m, 1H), 7.75 – 7.69 (m, 2H), 7.44 – 7.32 (m, 10H), 2.44 (dd, J = 6.0, 3.4 Hz, 12H), 2.34 (s, 3H), 2.09 (d, J = 4.6 Hz, 12H). Accurate mass: As [A^{2+} PF_6^-] calcd. 917.2444 measured 917.2476

[Ru(tmb)$_2$(bpy-2,6-dimethylphenyl)](PF$_6$)$_2$ (**5'**) Yield: 66% (44 mg) ^{1}H NMR (500 MHz, CD_3CN) δ 8.43 (d, J = 8.1 Hz, 1H), 8.33 (d, J = 1.5 Hz, 1H), 8.24 (dd, J = 19.5, 6.0 Hz, 4H), 8.00 – 7.95 (m, 1H), 7.78 – 7.72 (m, 2H), 7.41 (s, 1H), 7.36 (t, J = 6.5 Hz, 3H), 7.30 – 7.18 (m, 5H), 2.46 (s, 3H), 2.46 – 2.40 (m, 12H), 2.13 – 2.04 (m, 15H). Accurate mass: As [A^{2+} PF_6^-] calcd. 393.1493 measured 393.1490

[Ru(tmb)$_2$(bpy-2,5-dimethylphenyl)](PF$_6$)$_2$ (**6'**) Yield: 70% (47 mg) ^{1}H NMR (500 MHz, CD_3CN) δ 8.51 (d, J = 8.1 Hz, 1H), 8.44 (d, J = 1.5 Hz, 1H), 8.22 (dd, J = 13.0, 8.0 Hz, 4H), 7.99 (td, J = 8.0, 1.5 Hz, 1H), 7.73 (d, J = 5.7 Hz, 1H), 7.69 (d, J = 5.8 Hz, 1H), 7.37 – 7.22 (m, 8H), 7.19 (s, 1H), 2.44 (dd, J = 7.4, 4.1 Hz, 12H), 2.36 (s, 3H), 2.29 (s, 3H), 2.09 (d, J = 5.1 Hz, 12H). Accurate mass: As [A^{2+} PF_6^-] calcd. 393.1493 measured 393.1489

[Ru(tmb)$_2$(bpy-3,5-dimethylphenyl)](PF$_6$)$_2$ (**7'**) Yield: 73% (49 mg) ^{1}H NMR (500 MHz, CD_3CN) δ 8.68 (dd, J = 14.1, 4.9 Hz, 2H), 8.25 (dd, J = 11.2, 7.5 Hz, 4H), 8.04 (td, J = 7.9, 1.5 Hz, 1H), 7.75 – 7.68 (m, 2H), 7.59 (dd, J = 6.0, 2.0 Hz, 1H), 7.51 (s, 2H), 7.41 – 7.31 (m, 5H), 7.20 (s, 1H), 2.46 – 2.43 (m, 12H), 2.40 (s, 6H), 2.09 (dd, J = 10.8, 3.2 Hz, 12H). Accurate mass: As [A^{2+} PF_6^-] calcd. 393.1493 measured 393.1488

[Ru(bpy)$_2$(bpy-phenyl-MV)](PF$_6$)$_4$ (**1**) Yield: 12% (8 mg) ^{1}H NMR (500 MHz, CD_3CN) δ 9.24 – 9.20 (m, 2H), 8.90 (d, J = 6.9 Hz, 2H), 8.82 (d, J = 1.7 Hz, 1H), 8.72 (d, J = 8.3 Hz, 1H), 8.63 – 8.60 (m, 2H), 8.53 (t, J = 7.9 Hz, 4H), 8.47 (d, J = 6.9 Hz, 2H), 8.25 – 8.21 (m, 2H), 8.09 (dddd, J = 8.1, 5.8, 5.3, 1.4 Hz, 5H), 8.00 – 7.97 (m, 2H), 7.84 (d, J = 6.0 Hz, 1H), 7.82 – 7.72 (m, 6H), 7.47 – 7.40 (m, 5H), 4.43 (s, 3H). Accurate mass: As [A^{4+} $2PF_6^-$] calcd. 553.0774 measured 553.0799

[Ru(dmb)$_2$(bpy-phenyl-MV)](PF$_6$)$_4$ (**2**) Yield: 15% (10 mg) ^{1}H NMR (500 MHz, CD_3CN) δ 9.25 (d, J = 7.1 Hz, 2H), 8.91 (d, J = 6.8 Hz, 2H), 8.81 (d, J = 1.8 Hz, 1H), 8.71 (d, J = 8.1 Hz, 1H), 8.63 (d, J = 7.1 Hz, 2H), 8.50 (d, J = 6.9 Hz, 2H), 8.37 (d, J = 7.3 Hz, 4H), 8.25 – 8.21 (m, 2H), 8.10 – 8.06 (m, 1H), 8.01 – 7.97 (m, 2H), 7.84 (d, J = 6.0 Hz, 1H), 7.78 (d, J = 4.8 Hz, 1H), 7.71 (dd, J = 6.0, 2.0 Hz, 1H), 7.60 – 7.54 (m, 4H), 7.45 – 7.41 (m, 1H), 7.24 (dd, J = 13.0, 5.9 Hz, 4H), 4.44 (s, 3H), 2.54 (dd, J = 5.5, 2.3 Hz, 12H). Accurate mass: As [A^{4+} 2PF_6^-] calcd. 581.1088 measured 581.1079

[Ru(tmb)$_2$(bpy-phenyl-MV)](PF$_6$)$_4$ (**3**) Yield: 17% (11 mg) ^{1}H NMR (400 MHz, CD_3CN) δ 9.18 (d, J = 7.2 Hz, 2H), 8.87 (d, J = 7.0 Hz, 2H), 8.78 (s, 1H), 8.68 (d, J = 8.3 Hz, 1H), 8.57 (d, J = 7.1 Hz, 2H), 8.45 (d, J = 7.0 Hz, 2H), 8.26 – 8.20 (m, 6H), 8.03 (t, J = 7.9 Hz, 1H), 7.95 (d, J = 8.9 Hz, 2H), 7.81 (d, J = 5.9 Hz, 1H), 7.74 (d, J = 5.6 Hz, 1H), 7.69 (dd, J = 6.1, 2.0 Hz, 1H), 7.44 – 7.27 (m, 5H), 4.41 (s, 3H), 2.44 – 2.41 (m, 12H), 2.09 – 2.06 (m, 12H). Accurate mass: As [A^{4+} 2PF_6^-] calcd. 609.1401 measured 609.1431

[Ru(tmb)$_2$(bpy-ortho-MV)](PF$_6$)$_4$ (**4**) Yield: 22% (15 mg) ^{1}H NMR (500 MHz, CD_3CN) δ 9.24 – 9.18 (m, 2H), 8.90 (d, J = 6.8 Hz, 2H), 8.61 (d, J = 7.1 Hz, 2H), 8.55 (d, J = 8.2 Hz, 1H), 8.51 (d, J = 1.5 Hz, 1H), 8.48 (d, J = 6.9 Hz, 2H), 8.28 – 8.24 (m, 4H), 8.03 (td, J = 7.9, 1.4 Hz, 1H), 7.83 – 7.71 (m, 5H), 7.44 – 7.34 (m, 6H), 4.43 (s, 3H), 2.48 (s, 3H), 2.45 (t, J = 3.5 Hz, 12H), 2.11 (d, J = 4.0 Hz, 12H). Accurate mass: As [A^{4+} 2PF_6^-] calcd. 616.1468 measured 616.1480

[Ru(tmb)$_2$(bpy-2,6-dimethylphenyl-MV)](PF$_6$)$_4$ (**5**) Yield: 24% (16 mg) ^{1}H NMR (400 MHz, CD_3CN) δ 9.18 (d, J = 6.9 Hz, 2H), 8.90 (d, J = 6.7 Hz, 2H), 8.59 (d, J = 6.9 Hz, 2H), 8.46 (d, J = 7.0 Hz, 3H), 8.36 (d, J = 1.1 Hz, 1H), 8.25 (dd, J = 15.3, 4.2 Hz, 4H), 8.01 (t, J = 7.9 Hz, 1H), 7.83 (d, J = 5.8 Hz, 1H), 7.78 (d, J = 5.4 Hz, 1H), 7.63 (d, J = 10.8 Hz, 2H), 7.39 (dd, J = 16.4, 8.7 Hz, 4H), 7.26 (dd, J = 5.8, 1.6 Hz, 1H), 7.22 (s, 1H), 4.43 (s, 3H), 2.46 (t, J = 5.6 Hz, 12H), 2.30 (s, 3H), 2.11 (d, J = 4.2 Hz, 12H), 2.09 (s, 3H). Accurate mass: As [A^{4+} 2PF_6^-] calcd. 623.1569 measured 623.1558

[Ru(tmb)$_2$(bpy-2,5-dimethylphenyl-MV)](PF$_6$)$_4$ (**6**) Yield: 24% (16 mg) ^{1}H NMR (400 MHz, CD_3CN) δ 9.18 (d, J = 6.9 Hz, 2H), 8.90 (d, J = 6.7 Hz, 2H), 8.59 (d, J = 6.9 Hz, 2H), 8.46 (d, J = 7.0 Hz, 3H), 8.36 (d, J = 1.1 Hz, 1H), 8.25 (dd, J = 15.3, 4.2 Hz, 4H), 8.01 (t, J = 7.9 Hz, 1H), 7.83 (d, J = 5.8 Hz, 1H), 7.78 (d, J = 5.4 Hz, 1H), 7.63 (d, J = 10.8 Hz, 2H), 7.39 (dd, J = 16.4, 8.7 Hz, 4H), 7.26 (dd, J = 5.8, 1.6 Hz, 1H), 7.22 (s, 1H), 4.43 (s, 3H), 2.46 (t, J = 5.6 Hz, 12H), 2.30 (s, 3H), 2.11 (d, J = 4.2 Hz, 12H), 2.09 (s, 3H). Accurate mass: As [A^{4+} 2PF_6^-] calcd. 623.1569 measured 623.1559

[Ru(tmb)$_2$(bpy-3,5-dimethylphenyl-MV)](PF$_6$)$_4$ (**7**) Yield: 31% (20 mg) ^{1}H NMR (500 MHz, CD_3CN) δ 9.00 – 8.96 (m, 2H), 8.92 (d, J = 6.8 Hz, 2H), 8.77 (d, J = 1.8 Hz, 1H), 8.71 (d, J = 8.2 Hz, 1H), 8.66 – 8.63 (m, 2H), 8.47 (d, J = 6.9 Hz, 2H), 8.26 (t, J = 4.4 Hz, 4H), 8.07 (td, J = 7.7, 1.2 Hz, 1H), 7.91 (s, 2H), 7.81 (d, J = 6.0 Hz, 1H), 7.75 (dd, J = 5.6, 0.7 Hz, 1H), 7.69 (dd, J = 6.0, 2.0 Hz, 1H), 7.43 – 7.31 (m, 5H), 4.44 (s, 3H), 2.48 – 2.44 (m, 12H), 2.19 (s, 6H), 2.10 (dd, J = 9.4, 4.1 Hz, 12H). Accurate mass: As [A^{4+} 2PF_6^-] calcd. 623.1569 measured 623.1559

3.2.2 Electrochemistry

Cyclic Voltammetry. Electrochemical measurements were carried out with a CH Instruments 601C electrochemical analyzer. Solutions of the compound were dissolved in anhydrous CH_3CN containing 0.1 M $TBAPF_6$ (where TBA is tetrabutylammonium) as the supporting electrolyte. A standard three-electrode setup was used with a working Pt electrode, Pt wire counter electrode, and an $Ag/AgNO_3$ reference electrode. The reference electrode is comprised of a silver wire in the 0.1 M $TBAPF_6$ supporting electrolyte solution that is also 0.01 M in $AgNO_3$. Fresh electrolyte and reference solutions were prepared prior to each measurement. Before measuring the redox potentials of a new compound, a standard with known reduction potentials was measured to ensure proper preparation of the reference solution. All measurements were made after an argon purge and a 100mV/s or 200 mV/s scan rate. Adding 0.298 V to the experimentally obtained value converts $E_{1/2}$ values from $Ag/AgNO_3$ to SCE.[37]

Spectro-Electrochemistry. Spectra were recorded with a Hewlett-Packard HP8452A diode array UV-Vis spectrophotometer. The experiments were carried out in a home built OTTLE cell as previously reported[5,17] with the Pt mesh held at constant voltage using the CH Instruments 601C electrochemical analyzer a platinum auxiliary electrode and an $Ag/AgNO_3$ reference electrode. The reference electrode is comprised of a silver wire in the 0.1 M $TBAPF_6$ supporting electrolyte solution that is also 0.01 M in $AgNO_3$. Fresh electrolyte and reference solutions were prepared for every new measurement. An argon purge was maintained over the course of the experiment. Both oxidative and reductive experiments were reversed (returned to their original state) by holding the constant voltage at 0 V vs. $Ag/AgNO_3$.

3.3 Results and Discussion

3.3.1 Metal Complex Synthesis

All fourteen of the new complexes presented in this work were prepared via the same synthetic route; from a known RuL_2CO_3 precursor,[36,38] where L is the either bpy, dmb or tmb. The precursor complex is ancillary-ligand specific meaning that three different precursors were prepared (one for each ancillary ligand). This synthetic method is versatile and efficient since the same precursor is used to prepare complexes with the same ancillary ligands. Preparation of the precursor is summarized in **Equation 3.1**.

$$RuCl_3 \cdot 3H_2O \xrightarrow[\substack{2.\ \text{conc. HCl} \\ 1.8\ \text{eq. L}}]{1.\ H_2O/EtOH} [RuL_2Cl_2]Cl \xrightarrow[H_2O]{Na_2CO_3} RuL_2CO_3 \qquad \text{Equation 3.1}$$

The reaction to yield the heteroleptic complexes from the RuL_2CO_3 precursor is simple but time consuming. The procedure calls for stirring a solution of RuL_2CO_3 and asymmetric ligand, donor or electroactive, in a 1:1 EtOH: H_2O saturated KNO_3 solution for five days at room temperature.[5,17] The reaction is performed at room temperature to prevent the formation of mixed species. The reaction is not oxygen sensitive and was performed under atmospheric conditions but as a precaution the reaction mixtures were kept in the dark to prevent any adverse reactions with light. The reaction progress was monitored visually (since the RuL_2CO_3 is purple in solution and the desired complexes are orange) and by thin-layer chromatography (TLC). Preparation of the asymmetric complexes is summarized in **Equation 3.2**.

$$RuL_2CO_3 \xrightarrow[\substack{EtOH/H_2O \\ \text{Sat. } KNO_3}]{1.2\ \text{eq. L'}} [RuL_2L']^{2+\text{ or }4+} \qquad \text{Equation 3.2}$$

This synthetic route is synthetically robust and can be used to prepare complexes that are both doubly charged (2+, donor complexes) or quadruply charged (4+, DBA complexes). It should be noted that the preparation of the donor complexes was much higher yielding. This is explained by the electrostatics of the reaction. The ruthenium precursor more readily reacts with the neutral donor ligands than doubly charged electroactive ligands.

The purification of the metal complexes was accomplished by column chromatography. Silica gel columns were used to purify the complexes. For donor compounds optimum separation was achieved using a 9:1 CH_2Cl_2: MeOH solvent combination. For the DBA complexes optimum separation was achieved using an 8:1:1 CH_3CN:H_2O: saturated KNO_3 solvent combination. The highly charged nature of the DBA complexes required very polar column conditions.

3.3.2 Electrochemistry: Cyclic Voltammetry

Cyclic Voltammetry (CV) experiments were conducted on all complexes in order to determine oxidation and reduction potentials. These values will be used to determine the effect of methylating both the ancillary and asymmetric ligands on the oxidation and reduction potentials of the complexes. To begin this analysis the complexes in the driving-force series will be discussed; **Table 3.1** contains the reduction potentials for these complexes as well as the respective parent complexes. Examining the $Ru^{III/II}$ couple for all complexes it is evident that the ancillary ligand affects the potential required to oxidize the metal center. For the parent complexes a ~200 mV shift to less positive values in the $Ru^{III/II}$ couple is observed going from bpy complexes to tmb complexes. However the donor and DBA complexes exhibit smaller shifts in the $Ru^{III/II}$ couple going from bpy complexes to tmb

complexes, 110 mV for the donors and 140 for the DBA complexes. These shifts in the $Ru^{III/II}$ couple indicate that for the three types of complexes (parent, donor and DBA) oxidizing a tmb complex requires less potential than a bpy complex. This phenomenon is commonly explained by the electron-donating character of the methyl groups on the dmb and tmb ligands which stabilize the hole on the Ru^{III} metal center after oxidation.

Table 3.1 Electrochemical Data in Room Temp. CH_3CN vs. SCE for the Driving-Force Series

	($Ru^{III/II}$) /V	$MV^{2+/1+}$ /V	$MV^{1+/0}$ /V	1st Ligand Red. /V	2nd Ligand Red. /V
Complex	$E_{1/2}$	$E_{1/2}$	$E_{1/2}$	$E_{1/2}$	$E_{1/2}$
$[Ru(bpy)_3](PF_6)_2$[a]	1.24	--	--	-1.38	-1.57
$[Ru(bpy)_2(bpy\text{-}phenyl)](PF_6)_2$ (**1'**)	1.22	--	--	-1.36	-1.54
$[Ru(bpy)_2(bpy\text{-}phenyl\text{-}MV)](PF_6)_4$ (**1**)	1.27	-0.29	-0.63	-1.32	-1.54
$[Ru(dmb)_3](PF_6)_2$[a]	1.14	--	--	-1.44	-1.61
$[Ru(dmb)_2(bpy\text{-}phenyl)](PF_6)_2$ (**2'**)	1.18	--	--	-1.35	-1.59
$[Ru(dmb)_2(bpy\text{-}phenyl\text{-}MV)](PF_6)_4$ (**2**)	1.19	-0.29	-0.62	-1.40	-1.60
$[Ru(tmb)_3](PF_6)_2$[b]	1.04	--	--	-1.60	-1.80
$[Ru(tmb)_2(bpy\text{-}phenyl)](PF_6)_2$ (**3'**)	1.11	--	--	-1.37	-1.74
$[Ru(tmb)_2(bpy\text{-}phenyl\text{-}MV)](PF_6)_4$ (**3**)	1.13	-0.29	-0.61	-1.38	-1.76

[a] Electrochemical Data reported in reference 1.
[b] Electrochemical Data reported in reference 19.

From **Table 3.1** it is also evident that the $Ru^{III/II}$ couple is more positive for all new complexes except (**1'**) when compared to respective parent complexes signifying that the asymmetric ligands are not as effective at stabilizing the hole on the Ru^{III} metal center after oxidation. This suggests that all aryl-substituted ligands (except (**L1'**)) are more electron withdrawing than bpy, dmb or tmb. For the DBA complexes we see that all three have a more positive $Ru^{III/II}$ couple than both respective parent and donor complex. This implies that the hole on the Ru^{III} metal center is even more destabilized for the DBA complexes. The electroactive ligand bpy-phenyl-MV (**L1**) must be more electron withdrawing than bpy-

phenyl (**L1'**). Also the $MV^{2+/1+}$ couple occurs at the same potential, -0.29 V, for the three complexes signifying that the ancillary ligand does not impact the $MV^{2+/1+}$ couple.

The reduction potentials for the complexes in the sterics series are reported in **Table 3.2** below where dimethylphenyl has been abbreviated with dmp. The reduction potentials are also represented in the energy level diagram in **Figure 3.5** below. In extension of the analysis above we see that all complexes in this series have a more positive $Ru^{III/II}$ couple than $[Ru(tmb)_3](PF_6)_2$ suggesting that the asymmetric ligands are not as effective as tmb at stabilizing the hole on the Ru^{III} metal center after oxidation. In extension of the analysis above the asymmetric ligands are electron withdrawing with respect to tmb.

Table 3.2 Electrochemical Data in Room Temperature CH_3CN vs. SCE for the Sterics Series

	$(Ru^{III/II})$ /V	$MV^{2+/1+}$ /V	$MV^{1+/0}$ /V	1st Ligand Red. /V	2nd Ligand Red. /V
Complex	$E_{1/2}$	$E_{1/2}$	$E_{1/2}$	$E_{1/2}$	$E_{1/2}$
$[Ru(tmb)_3](PF_6)_2$[a]	1.04	--	--	-1.60	-1.80
$[Ru(tmb)_2$(bpy-phenyl)$](PF_6)_2$ (**3'**)	1.11	--	--	-1.37	-1.74
$[Ru(tmb)_2$(bpy-phenyl-MV)$](PF_6)_4$ (**3**)	1.13	-0.29	-0.61	-1.38	-1.76
$[Ru(tmb)_2$(bpy-ortho)$](PF_6)_2$ (**4'**)	1.10	--	--	-1.41	-1.77
$[Ru(tmb)_2$(bpy-ortho-MV)$](PF_6)_4$ (**4**)	1.12	-0.28	-0.65	-1.44	-1.77
$[Ru(tmb)_2$(bpy-2,6-dmp)$](PF_6)_2$ (**5'**)[b]	1.11	--	--	-1.40	-1.76
$[Ru(tmb)_2$(bpy-2,6-dmp-MV)$](PF_6)_4$ (**5**)[b]	1.13	-0.29	-0.67	-1.41	-1.78
$[Ru(tmb)_2$(bpy-2,5-dmp)$]$ $(PF_6)_2$ (**6'**)[b]	1.10	--	--	-1.42	-1.76
$[Ru(tmb)_2$(bpy-2,5-dmp-MV)$](PF_6)_4$ (**6**)[b]	1.06	-0.37	-0.76	-1.45	-1.81
$[Ru(tmb)_2$(bpy-3,5-dmp)$](PF_6)_2$ (**7'**)[b]	1.09	--	--	-1.41	-1.77
$[Ru(tmb)_2$(bpy-3,5-dmp-MV)$](PF_6)_4$ (**7**) [b]	1.08	-0.35	-0.78	-1.43	-1.82

[a] Electrochemical Data reported in reference 19. [b]dimethylphenyl has been abbreviated by dmp

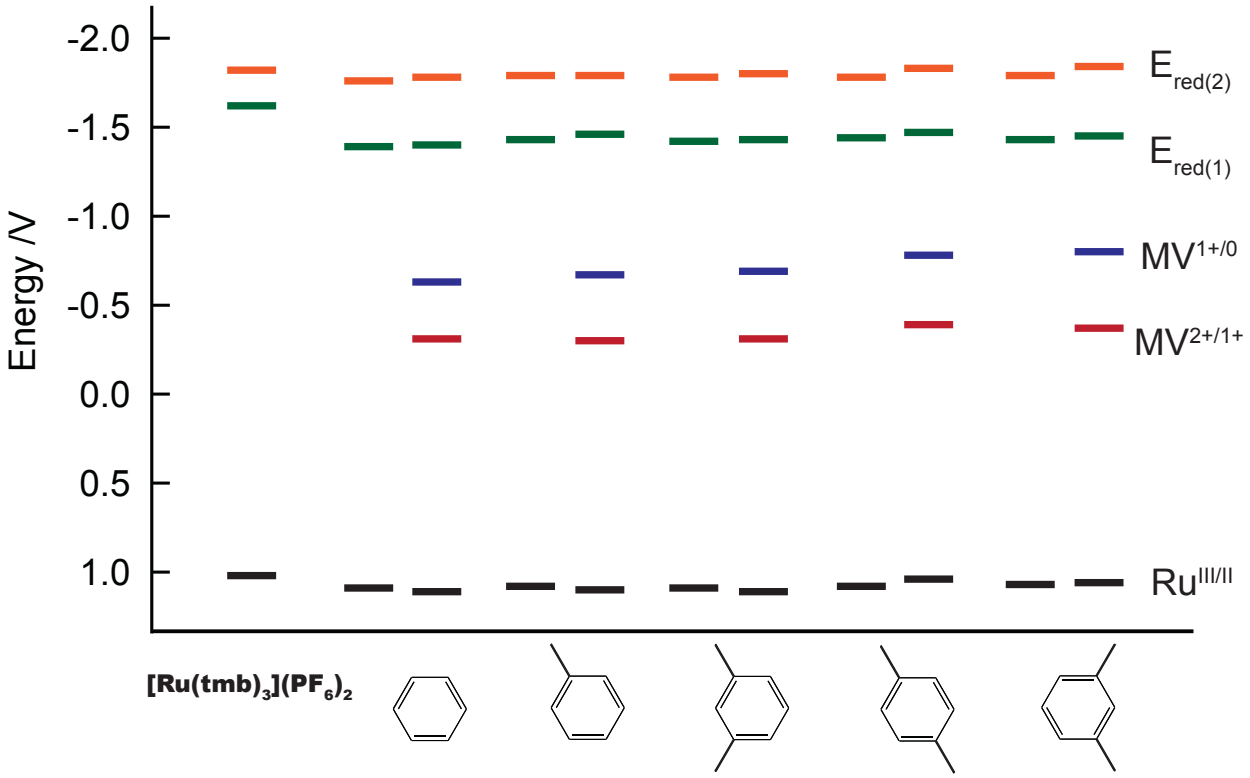

Figure 3.5 Energy level diagram summarizing the reduction potentials of complexes in the sterics series.

Across the DBA complexes in this series we see a 70 mV difference in $Ru^{III/II}$ couple where $[Ru(tmb)_2(bpy\text{-}phenyl\text{-}MV)](PF_6)_4$ (**3**) is harder to oxidize than $[Ru(tmb)_2(bpy\text{-}2,5\text{-}dimethylphenyl\text{-}MV)](PF_6)_4$ (**6**). The general trend is that as additional methyl groups are appended onto the electroactive ligand it becomes easier to oxidize the complex. This is explained by the fact the electron-donating character of the methyl groups helps to stabilize the $1e^-$-oxidized complex. Looking at the three doubly methylated complexes $[Ru(tmb)_2(bpy\text{-}2,6\text{-}dimethylphenyl\text{-}MV)](PF_6)_4$ (**5**), $[Ru(tmb)_2(bpy\text{-}2,5\text{-}dimethylphenyl\text{-}MV)](PF_6)_4$ (**6**) and $[Ru(tmb)_2(bpy\text{-}3,5\text{-}dimethylphenyl\text{-}MV)](PF_6)_4$ (**7**) it is evident that position of methylation is playing a role in determining $Ru^{III/II}$ couple. Where (**5**) is 70 mV harder to oxidize than (**6**) and 50 mv harder to oxidize than (**7**). Methylation in positions proximal to the bipyridinium moiety act as stabilizers making (**L4**) and (**L5**) less electron

withdrawing than (**L3**) thereby shifting the $Ru^{III/II}$ couple of (**6**) and (**7**) to less positive values.

Looking at the $MV^{2+/1+}$ couple within the DBA complexes of this series it is evident that there is a divide in these values. The $MV^{2+/1+}$ couple for $Ru(tmb)_2$(bpy-phenyl-MV)]$(PF_6)_4$ (**3**), $Ru(tmb)_2$(bpy-ortho-MV)]$(PF_6)_4$ (**4**) and $Ru(tmb)_2$(bpy-2,6-dimethylphenyl-MV)]$(PF_6)_4$ (**5**) is ~-0.29 V whereas for $Ru(tmb)_2$(bpy-2,5-dimethylphenyl-MV)]$(PF_6)_4$ (**6**) it is -0.37 V and for [$Ru(tmb)_2$(bpy-3,5-dimethylphenyl-MV)]$(PF_6)_4$ (**7**) it is -0.35 V. It is 60 mV more difficult to reduce (**6**) and 80 mV harder to reduce (**7**) than (**3**), (**4**) and (**5**). This trend is consistent with the results from the CV experiments on the electroactive ligands and the acceptor subunits (see **Table 2.1**) where (**L4**) and (**L5**) have lower $MV^{2+/1+}$ couples than the other ligands and (**A2**) and (**A3**) are greater than 100 mV more difficult to reduce than (**A1**). As with the ligands electron density delocalization is invoked to account for the differences in $MV^{2+/1+}$ couple of the complexes. The methyl substituents on the 3- and 5- positions of the bridging ligand in (**6**) and (**7**) are preventing electron density from delocalization onto the 2,2'-bipyridne moiety thereby lowering the $MV^{2+/1+}$ couple. As with the ligands the methyl substituents are affecting the electronic properties of the DBA complexes whereby we observe differences in the $Ru^{III/II}$ and $MV^{2+/1+}$ couples brought upon by steric bulk.

3.3.3 Electrochemistry: Spectroelectrochemistry

Both oxidative and reductive spectroelectrochemical experiments were conducted on all metal complexes. These experiments allow for monitoring the absorption spectra of the complexes upon one electron reduction or oxidation. These spectra are useful as they are an approximation of absorption properties of critical components of the electron

transfer reaction. Reductive spectroelectrochemical data will be shown for all DBA complexes and the donor complex $[Ru(bpy)_2(bpy\text{-}phenyl)](PF_6)_2$ (**1'**). Oxidative spectroelectrochemical data are presented for $[Ru(bpy)_2(bpy\text{-}phenyl\text{-}MV)](PF_6)_4$ (**1**) and the donor complex $[Ru(bpy)_2(bpy\text{-}phenyl)](PF_6)_2$ (**1'**). The reductive spectra of the remaining donor complexes will not be shown since they exhibit similar spectral features upon reduction as $[Ru(bpy)_2(bpy\text{-}phenyl)](PF_6)_2$ (**1'**). Similarly the oxidative spectra of the remaining complexes will not be shown since they produce spectral features similar to that of (**1**) or (**1'**) upon oxidation.

The spectroelectrochemical experimental results for $[Ru(bpy)_2(bpy\text{-}phenyl\text{-}MV)](PF_6)_4$ (**1**) are summarized in **Figure 3.6** below where the reductive data are shown in the top panel and oxidative in the bottom panel. Upon one-electron reduction at -0.40 V vs. SCE the spectral features attributable to bpy-phenyl-MV (**L1**) radical cation are observed where bands corresponding to the $D_1 \leftarrow D_0$ (between 500-800 nm) and $D_2 \leftarrow D_0$ (400-500 nm) transitions are observed (see **Figure 2.8**, top panel). Upon oxidation at 1.50 V vs. SCE the Ru^{II} species is converted to Ru^{III} which manifests in the spectral data as a loss of the MLCT band signifying loss of the $^1MLCT \leftarrow GS$ absorption. The reductive and oxidative spectral data will be used to aid in assignment of spectral features attributed to the electron transfer photoproduct.

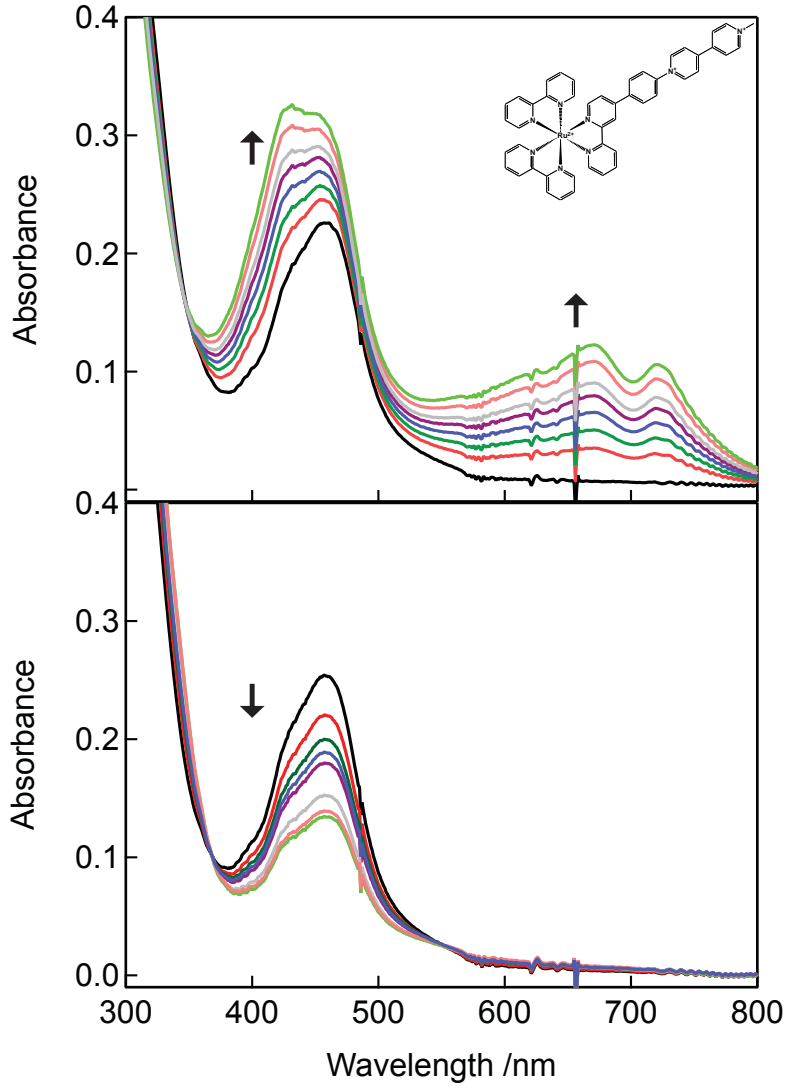

Figure 3.6 Reductive (top, held at -0.40 V vs. SCE) and oxidative (bottom, held at 1.50 V vs. SCE) spectroelectrochemical data for $[Ru(bpy)_2(bpy\text{-}phenyl\text{-}MV)](PF_6)_4$ (**1**) in room temperature acetonitrile. Upon reduction we observe spectral features attributable to bpy-phenyl-MV (**L1**) radical cation. Upon oxidation we see a decrease in the MLCT band.

The proposed photoinduced intramolecular electron transfer (ET) mechanism involves the formation of the ET photoproduct from the excited state of the donor chromophore after absorption of a visible photon. Performing the reductive and oxidative spectroelectrochemical experiments on the donor compounds will provide approximations of the spectral features of the excited state of the donor formed after photo-excitation. The

reductive spectra of $[Ru(bpy)_2(bpy\text{-}phenyl)](PF_6)_2$ (**1'**) collected at -1.45 V vs. SCE are reported in the top panel of **Figure 3.7** below while oxidative spectra collected at -1.50 V vs. SCE are shown in the bottom panel.

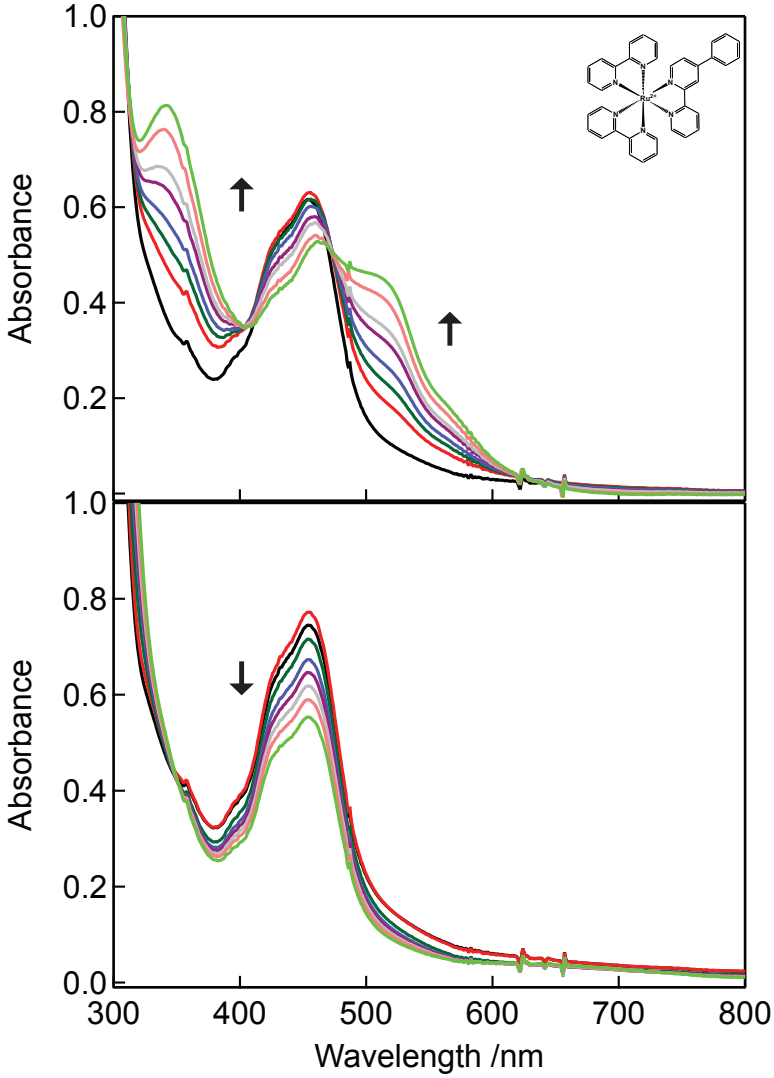

Figure 3.7 Reductive (top, held at -1.45 V vs. SCE) and oxidative (bottom, held at 1.50 V vs. SCE) spectroelectrochemical data for $[Ru(bpy)_2(bpy\text{-}pheny](PF_6)_2$ (**1'**) in room temperature acetonitrile. Upon reduction we see features that are attributable to the radical anion of an aryl-substituted 2,2'-bipyrdine. Upon oxidation we primarily observe the loss of the MLCT band.

For the oxidation, behavior similar to that of $[Ru(bpy)_2(bpy\text{-}phenyl\text{-}MV)](PF_6)_4$ (**1**) is observed where loss of the ^{1}MLCT ← GS absorption is demonstrated by an elimination of

the MLCT band. However, the reductive spectra are different than those of (**1**) where signatures of a ligand-reduced polypyridyl species[39] with absorption in the near-UV and mid-visible regions of the spectrum are observed. The reductive and oxidative data will be used to assign spectral features of the donor chromophore after photo-excitation.

In continuing the analysis of the reductive spectroelectrochemistry experiments on the DBA complexes the spectra of $[Ru(dmb)_2(bpy\text{-}phenyl\text{-}MV)](PF_6)_4$ (**2**) and $[Ru(tmb)_2(bpy\text{-}phenyl\text{-}MV)](PF_6)_4$ (**3**) collected at -0.40 V vs. SCE are shown below in the top and bottom panels of **Figure 3.8**, respectively. While those of $[Ru(bpy)_2(bpy\text{-}ortho\text{-}MV)](PF_6)_4$ (**4**) and $[Ru(bpy)_2(bpy\text{-}2,6\text{-}dimethylphenyl\text{-}MV)](PF_6)_4$ (**5**) collected -0.40 V vs. SCE are shown below **in Figure 3.9**. The spectra of (**4**) are shown in the top panel and (**5**) in the bottom panel. As was observed for (**1**) spectral features attributed to the radical cation of the asymmetric electroactive ligands are observed, namely the presence of the bands assigned to the $D_1 \leftarrow D_0$ and $D_2 \leftarrow D_0$ transitions. The information provided in these spectra will be used to assign the spectral features of the ET photoproduct.

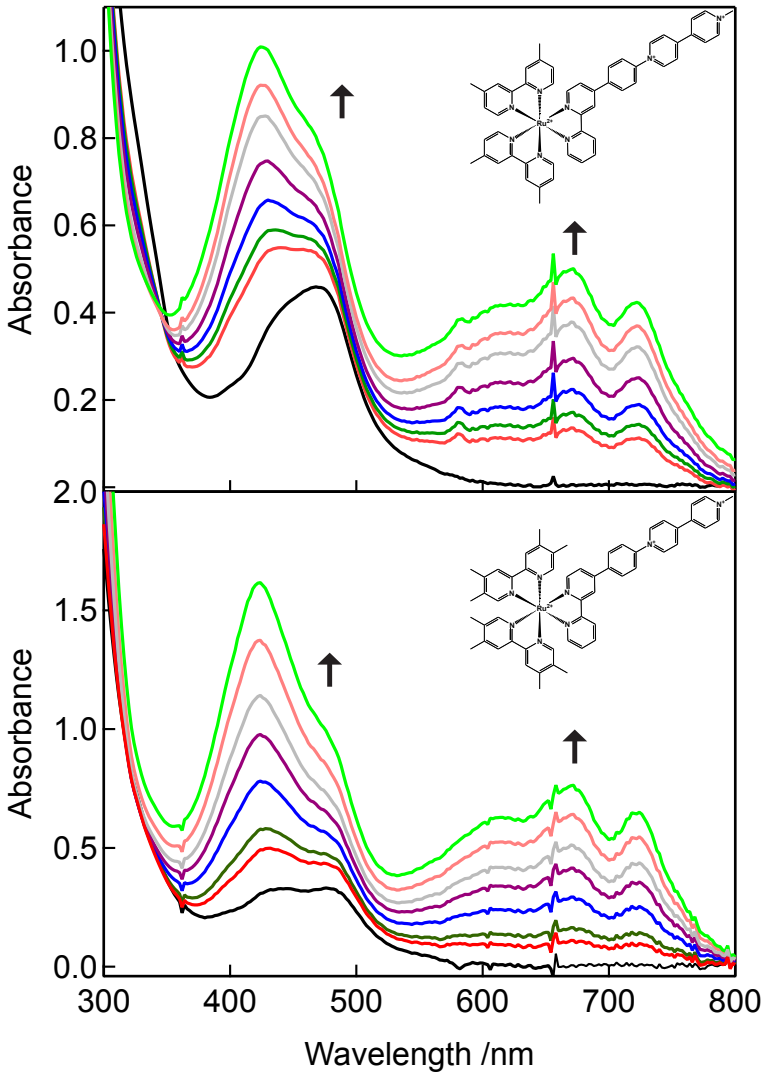

Figure 3.8 Reductive spectra held at -0.40 V vs. SCE for $[Ru(dmb)_2(bpy\text{-}phenyl\text{-}MV)](PF_6)_4$ (**2**) (top) and $[Ru(tmb)_2(bpy\text{-}phenyl\text{-}MV)](PF_6)_4$ (**3**) (bottom) in room temperature acetonitrile. Upon reduction the spectral features attributable to bpy-phenyl-MV (**L1**) radical cation are observed.

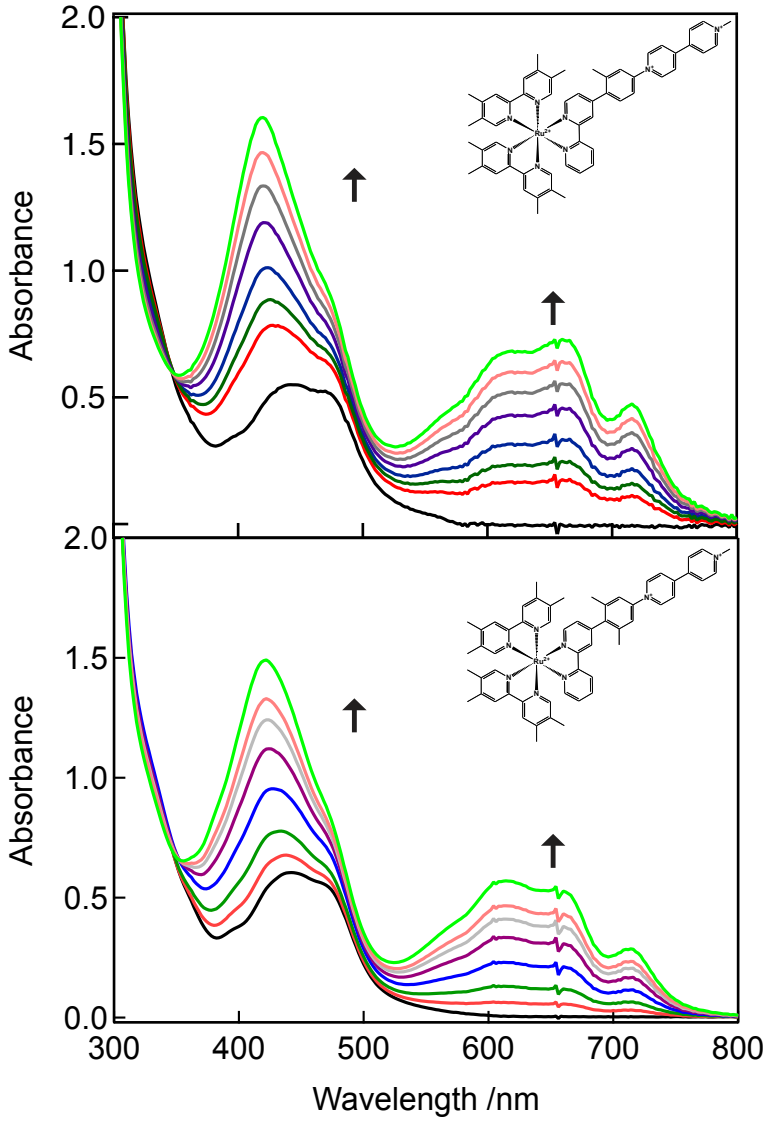

Figure 3.9 Reductive spectra held at -0.40 V vs. SCE for $[Ru(tmb)_2(bpy\text{-}ortho\text{-}MV)](PF_6)_4$ (**4**) (top) and $[Ru(tmb)_2(bpy\text{-}2,6\text{-}dimethylphenyl\text{-}MV)](PF_6)_4$ (**5**) (bottom) in room temperature acetonitrile.

When reductive spectroelectrochemical experiments were conducted on the electroactive ligands in Chapter Two the spectral features of ligands methylated in the 2,5- (**L4**) and 3,5- (**L5**) positions resembled those of methyl viologen radical cation as opposed to an N-arylated pyridinium, namely that the $D_1 \leftarrow D_0$ transition is narrower for these ligands and peaks at 398 nm (see bottom panels in **Figures 2.12 and 2.13**). The same trend is observed in the reductive spectroelectrochemistry spectra of the corresponding

DBA complexes as seen in **Figure 3.10** where the spectra of $[Ru(bpy)_2(bpy\text{-}2,5\text{-}dimethylphenyl\text{-}MV)](PF_6)_4$ (**6**) and $[Ru(bpy)_2(bpy\text{-}3,5\text{-}dimethylphenyl\text{-}MV)](PF_6)_4$ (**7**) collected at -0.60 V vs. SCE are shown in the top and bottom panels, respectively.

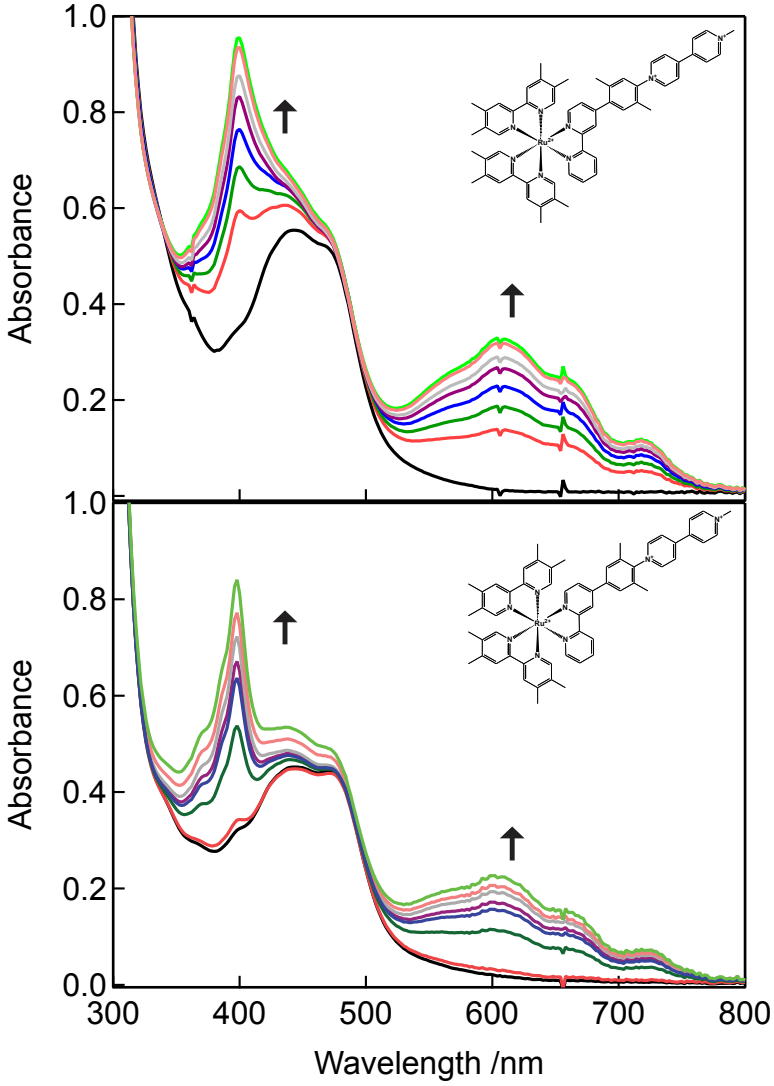

Figure 3.10 Reductive spectra held at -0.60 V vs. SCE for $[Ru(tmb)_2(bpy\text{-}2,5\text{-}dimethylpenyl\text{-}MV)](PF_6)_4$ (**6**) (top) and $[Ru(tmb)_2(bpy\text{-}3,5\text{-}dimethylphenyl\text{-}MV)](PF_6)_4$ (**7**) (bottom) in room temperature acetonitrile

From the electrochemistry experiments we conclude that the electronic properties of the electroactive ligands are carried through to the DBA complexes. The effects of steric bulk impeding electron delocalization in the electroactive ligands are also observed in the metal

complexes. For (**6**) and (**7**) the reductive spectroelectrochemistry data show that when an electron is added to the asymmetric ligand of these complexes steric bulk is restricting delocalization over the ligand. Our original claim for preparing these complexes was to use steric bulk in the form of methyl groups to inhibit electronic communication in DBA complexes and to affect intramolecular ET. We find from the reductive spectroelectrochemistry that steric bulk is effectively achieving this thus validating the original claim.

In concluding the spectroelectrochemistry section it should be noted that for all complexes the reductions and oxidations were reversible. In other words, after bulk electrolysis was complete the solutions were held at 0 V vs $Ag/AgNO_3$ to allow for the return of the original (pre-electrolysis) absorption spectrum. The reversibility of the bulk electrolysis experiments signifies that the complexes do not decompose during the spectroelectrochemical experiments. These reversed spectra are not shown.

3.4 Concluding Remarks

In this chapter the preparation and electrochemical characterization of seven donor complexes and seven corresponding donor-bridge-acceptor complexes has been described. The fourteen complexes were prepared in relatively high yields via the same synthetic route but purification conditions were different for donor and DBA complexes. The versatile synthetic method allowed for preparation of a family of complexes with varying degrees of methylation on the ancillary or asymmetric ligand.

Electrochemical experiments showed methyl substitution on the ancillary and asymmetric ligands affects the redox properties of the complexes. Addition of methyl groups on the ancillary ligand tends to shift the $Ru^{III/II}$ couple to more positive values while

the addition of methyl groups on the asymmetric aryl-substituted 2,2'-bipyrdine ligand tends to shift the $Ru^{III/II}$ couple to less positive values. The $MV^{2+/1+}$ couple of the DBA complexes is also affected by the electroactive ligand. Methylation of the bridging ligand tends to lower the $MV^{2+/1+}$ couple.

The spectroelectrochemistry experiments were performed in order to determine optical tags for the ET photoproduct. When the DBA complexes were reduced the spectral features of the corresponding electroactive ligands were obtained. In performing the reductive spectroelectrochemistry experiments we find validation for our hypothesis that steric bulk can be used to inhibit nuclear motions thereby affecting electronic properties of the complexes and limiting electron delocalization onto the electroactive ligand.

With metal complexes and electrochemical characterization in hand the photophysical characterization of the complexes can be completed. This will be discussed in subsequent chapters. Chapter Four will discuss the photophysics and ET properties of the complexes in the driving-force series while Chapter Five will discuss the photophysics and ET properties of the complexes in the sterics series.

3.5 References

(1) Yonemoto, E. H.; Riley, R. L.; Kim, Y. I.; Atherton, S. J.; Schmehl, R. H.; Mallouk, T. E. *J. Am. Chem. Soc.* **1992**, *114*, 8081.

(2) Yonemoto, E. H.; Saupe, G. B.; Schmehl, R. H.; Hubig, S. M.; Riley, R. L.; Iverson, B. L.; Mallouk, T. E. *J. Am. Chem. Soc.* **1994**, *116*, 4786.

(3) Meylemans, H. a.; Lei, C.-F.; Damrauer, N. H. *Inorg. Chem.* **2008**, *47*, 4060.

(4) Meylemans, H. A.; Damrauer, N. H. *Inorg. Chem.* **2009**, *48*, 11161.

(5) Meylemans, H. A.; Hewitt, J. T.; Abdelhaq, M.; Vallett, P. J.; Damrauer, N. H. *J. Am. Chem. Soc.* **2010**, *132*, 11464.

(6) Laine, P. P.; Bedioui, F.; Loiseau, F.; Chiorboli, C.; Campagna, S. *J. Am. Chem. Soc.* **2006**, *128*, 7510.

(7) Ciofini, I.; Laine, P. P.; Bedioui, F.; Adamo, C. *J. Am. Chem. Soc.* **2004**, *126*, 10763.

(8) Elliott, C. M.; Freitag, R. A.; Blaney, D. D. *J. Am. Chem. Soc.* **1985**, *107*, 4647.
(9) Cooley, L. F.; Headford, C. E. L.; Elliott, C. M.; Kelley, D. F. *J. Am. Chem. Soc.* **1988**, *110*, 6673.
(10) Berg, K. E.; Tran, A.; Raymond, M. K.; Abrahamsson, M.; Wolny, J.; Redon, S.; Andersson, M.; Sun, L. C.; Styring, S.; Hammarstrom, L.; Toftlund, H.; Akermark, B. *Eur. J. Inorg. Chem.* **2001**, 1019.
(11) Lomoth, R.; Haupl, T.; Johansson, O.; Hammarstrom, L. *Chem. Eur. J.* **2002**, *8*, 102.
(12) Johansson, O.; Borgstrom, M.; Lomoth, R.; Palmblad, M.; Bergquist, J.; Hammarstrom, L.; Sun, L. C.; Akermark, B. *Inorg. Chem.* **2003**, *42*, 2908.
(13) Henrich, J. D.; Zhang, H. Y.; Dutta, P. K.; Kohler, B. *J. Phys. Chem. B* **2010**, *114*, 14679.
(14) BergBrennan, C.; Subramanian, P.; Absi, M.; Stern, C.; Hupp, J. T. *Inorg. Chem.* **1996**, *35*, 3719.
(15) Cooley, L. F.; Larson, S. L.; Elliott, C. M.; Kelley, D. F. *J. Phys. Chem.* **1991**, *95*, 10694.
(16) Kelly, L. A.; Rodgers, M. A. J. *J. Phys. Chem.* **1995**, *99*, 13132.
(17) Meylemans, H. A.; Lei, C. F.; Damrauer, N. H. *Inorg. Chem.* **2008**, *47*, 4060.
(18) Damrauer, N. H.; Boussie, T. R.; Devenney, M.; McCusker, J. K. *J. Am. Chem. Soc.* **1997**, *119*, 8253.
(19) Damrauer, N. H.; Weldon, B. T.; McCusker, J. K. *J. Phys. Chem. A* **1998**, *102*, 3382.
(20) Damrauer, N. H.; McCusker, J. K. *J. Phys. Chem. A* **1999**, *103*, 8440.
(21) Damrauer, N. H.; McCusker, J. K. *Inorg. Chem.* **1999**, *38*, 4268.
(22) Lyubimova, O. O.; Baranovskii, V. I. *Journal of Structural Chemistry* **2003**, *44*, 728.
(23) Juris, A.; Balzani, V.; Barigelletti, F.; Campagna, S.; Belser, P.; von Zelewsky, A. *Coord. Chem. Rev.* **1988**, *84*, 85.
(24) Kalyanasundaram, K. *Photochemistry of Polypyridine and Porphyrin Complexes*; Academic Press Inc.: San Diego, 1992.
(25) Lever, A. B. P. *Inorg. Chem.* **1990**, *29*, 1271.
(26) Sauvage, J.-P.; Collin, J.-P.; Chambron, J.-C.; Guillerez, S.; Coudret, C. *Chem. Rev.* **1994**, *94*, 993.
(27) Vos, J. G.; Kelly, J. M. *Dalton T* **2006**, 4869.
(28) Anderson, P. A.; Keene, F. R.; Meyer, T. J.; Moss, J. A.; Strouse, G. F.; Treadway, J. A. *J Chem Soc Dalton* **2002**, 3820.
(29) Ghosh, B. K.; Chakravorty, A. *Coord. Chem. Rev.* **1989**, *95*, 239.
(30) Demas, J. N.; Crosby, G. A. *J. Phys. Chem.* **1971**, *75*, 991.
(31) Damrauer, N. H.; Cerullo, G.; Yeh, A.; Boussie, T. R.; Shank, C. V.; McCusker, J. K. *Science* **1997**, *275*, 54.
(32) Bhasikuttan, A. C.; Suzuki, M.; Nakashima, S.; Okada, T. *J. Am. Chem. Soc.* **2002**, *124*, 8398.
(33) Cannizzo, A.; van Mourik, F.; Gawelda, W.; Zgrablic, G.; Bressler, C.; Chergui, M. *Angew Chem Int Ed* **2006**, *45*, 3174.
(34) Yoon, S.; Kukura, P.; Stuart, C. M.; Mathies, R. A. *Mol. Phys.* **2006**, *104*, 1275.

(35) Mines, G. A.; Bjerrum, M. J.; Hill, M. G.; Casimiro, D. R.; Chang, I. J.; Winkler, J. R.; Gray, H. B. *J. Am. Chem. Soc.* **1996**, *118*, 1961.
(36) Togano, T.; Nagao, N.; Tsuchida, M.; Kumakura, H.; Hisamatsu, K.; Howell, F. S.; Mukaida, M. *Inorg. Chim. Acta* **1992**, *195*, 221.
(37) Pavlishchuk, V. *Inorg. Chim. Acta* **2000**, *298*, 97.
(38) Sullivan, B. P.; Salmon, D. J.; Meyer, T. J. *Inorg. Chem.* **1978**, *17*, 3334.
(39) McCusker, J. K. *Acc. Chem. Res.* **2003**, *36*, 876.

Chapter Four

Photophysical Characterization and Photoinduced Electron Transfer Analysis for Complexes in the Driving-Force Series.

4.1 Introductory Remarks

The main purpose of this body of work is to determine how structural elements of donor-bridge-acceptor complexes (DBA) affect the lifetimes of photoinduced intramolecular electron transfer (ET). To investigate the role of structural elements methyl groups have been systematically substituted onto various positions of DBA complexes. Two series of complexes have been prepared, a driving-force series and a steric series, which allow for an investigation of this question from two perspectives. The driving force series warrants an examination of how steric bulk on the ancillary ligands affects ET while the steric series looks at the effect steric bulk on the bridging ligand. In Chapter Three the preparation and electrochemical characterization of the DBA complexes was presented. The electrochemical analysis indicated that methylation affects the $Ru^{III/II}$ and the $MV^{2+/1+}$ couples while also determining the spectral features of the complexes upon one-electron reduction.

In this chapter, and the next, the focus will shift to the photophysical and ET studies conducted on these systems. In this chapter the focus will be on complexes in the driving-force series where complexes were prepared with minimal steric bulk on the bridging ligand. The complexes were prepared from the same non-methylated asymmetric aryl-substituted ligand but varied in methylation of the ancillary ligands. The donor and DBA complexes are summarized below in **Figure 4.1**. Recall that donor complexes were prepared as acceptor-less analogues of corresponding DBA complexes.

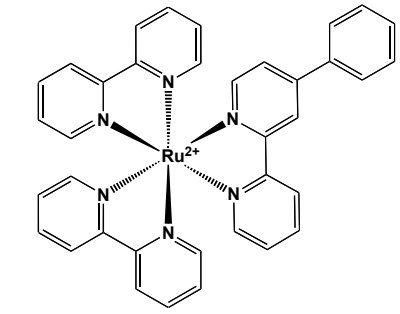

$[Ru(bpy)_2(bpy\text{-}phenyl)]^{2+}$(**1'**)

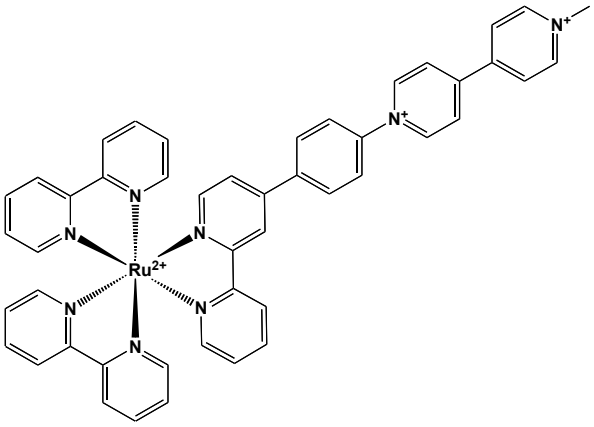

$[Ru(bpy)_2(bpy\text{-}phenyl\text{-}MV)]^{4+}$(**1**)

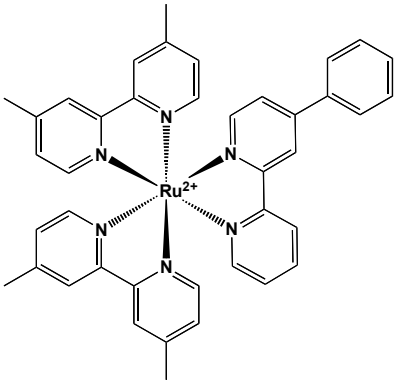

$[Ru(dmb)_2(bpy\text{-}phenyl)]^{2+}$(**2'**)

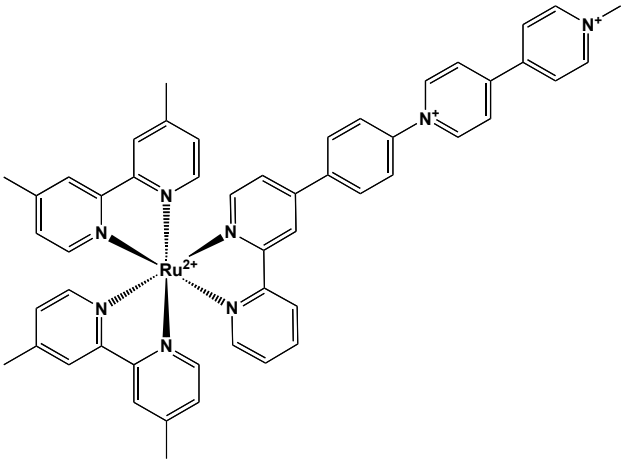

$[Ru(dmb)_2(bpy\text{-}phenyl\text{-}MV)]^{4+}$(**2**)

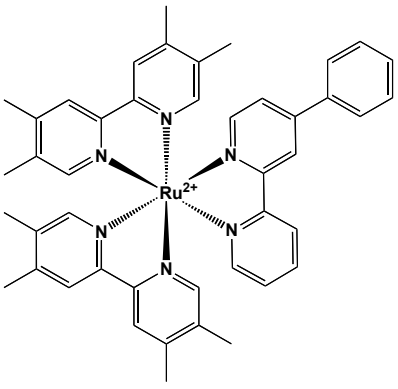

$[Ru(tmb)_2(bpy\text{-}phenyl)]^{2+}$(**3'**)

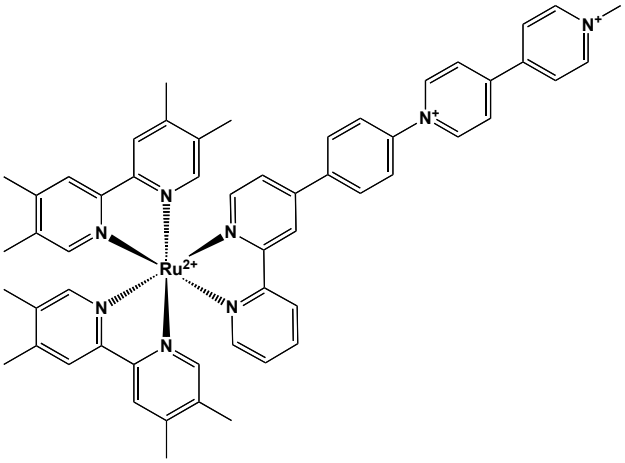

$[Ru(tmb)_2(bpy\text{-}phenyl\text{-}MV)]^{4+}$(**3'**)

Figure 4.1 Donor (left) and Donor-Bridge-Acceptor (right) complexes in the driving forces series; which differ by ancillary ligand. The complexes were isolated as PF_6^- salts.

The photophysics and photochemistry of ruthenium polypyridine complexes have been the subject of much research over many decades and as a result the complexes are well characterized.[1-7] Preparing a series of ruthenium (II) polypyridine complexes with different ancillary ligands allows for systematic tuning of the excited-state energetics of the complexes as a function of ligand substitution.[1,6] Specifically, tuning the driving forces available for photoinduced intramolecular ET processes.[8,9] For our purposes driving forces for intramolecular ET can be thought of as the amount of energy available in the ^{3}MLCT excited (metal-to-ligand charge transfer) state of the 'donor' complex that can reduce the covalently bound electroactive acceptor. Driving forces are calculated from a combination of photophysical and electrochemical measurements. A detailed explanation of these quantities and the equations utilized to calculate them can be found in **Section 4.3.2**. Determinations of driving force are necessary in order to determine if ET will be operative in these systems.

Prior to measuring rates for ET in these systems photophysical characterization of these complexes must be undertaken. UV-visible absorption spectra of the complexes will determine the effect of ancillary and asymmetric ligands on the characteristic MLCT band of these complexes. For the donor complexes emission spectra are needed to determine the energy of the lowest lying ^{3}MLCT state within the excited-sate triplet manifold as well as quantum yields for phosphorescence. In conjunction with emission spectra, emission lifetimes of the donor complexes will be measured. From these measurements and the redox potentials provided in Chapter Three, driving forces for forward electron transfer (ΔG^0_{ET}) and back electron transfer (ΔG^0_{BET}) will be calculated. Lastly, ultrafast transient

absorption measurements will be used to confirm the formation of the electron transfer product as well as measure the lifetimes for forward ET (τ_{ET}) and back ET (τ_{BET}).

4.2 Experimental

4.2.1 Steady State Absorption and Emission Spectroscopy

Experimental parameters for absorption and emission measurements have been described in detail previously.[8,9] However they are summarized here. All spectroscopic data were obtained on samples dissolved in anhydrous CH_3CN. Absorption spectra were measured with a Hewlett-Packard HP8452A diode array UV-Vis spectrophotometer. Emission spectra were collected for deoxygenated solutions of each complex having an optical density of ca. 0.1 (1 cm path length) at the excitation wavelength using a PTI QM-4 fluorometer. Samples were deoxygenated using a diffusion pump setup in which 5 freeze-pump-thaw cycles were performed on each sample.

4.2.2 Nanosecond Time-Resolved Emission

The nanosecond time-resolved emission setup has been described elsewhere[10] but is summarized here. Sample solutions were prepared and deoxygenated in the same manner as described above for emission spectra and quantum yields measurements. The measurements were done at 23-24^{o}C. Each sample was excited with 355 nm laser pulses (10 Hz; ~0.3 μJ/pulse) generated by a Continuum Minilite II Q-Switched Nd:YAG Laser. Two dielectric mirrors and one bandpass filter (300-360 nm) in front of the sample were used to eliminate residual 532 nm and 1064 nm laser radiation. The emitted light was detected at 90^o with respect to the excitation laser using a Hamamatsu H9305-02 photomultiplier tube (PMT) operating at –900 Vdc. A notch filter (640 ± 5 nm) was placed within a lens-tube assembly (two back-to-back plano-convex lenses, f_o =25.4 mm/diameter

= 25.4 mm) in front of the detector and the emission intensity was monitored. The PMT signal was terminated with a 50 Ω resistor into a LeCroy 9384L Oscilloscope. Maximum signal levels were kept well below the measured linearity of the PMT response. Each emission transient was acquired by averaging 5000 scans with a time window of 0 to 10 μs. The data from the oscilloscope were transferred to a personal computer and fit with a single exponential decay model using Labview code of local origin to obtain the lifetimes.

4.2.3 Computational Details

All calculations were performed in the Q-Chem 4.0 program package.[11] Gas-phase geometry optimizations used the long range corrected ωB97X exchange-correlation functional.[12] First row elements employed a 6-31g(d) basis set[13,14] and ruthenium atoms were described using a triple-ζ Stuttgard-Dresden (SDD)[15,16] electron core potential. Geometries were fully optimized without symmetry constraints.

Time Dependent Density Functional Theory (TD-DFT) techniques were used to calculate electronic transitions for metal complexes.[17] Simulated absorption spectra were constructed by summing Gaussians proportional in height to the oscillator strength of each transition and assuming a constant FWHM of 0.25 eV. Transitions with oscillator strength less than 0.02 were excluded. Transitions for donor complexes were red shifted by 1.3 eV while those of the DBA complexes were red shifted by 1.4 eV for easier comparison with experimental spectra.[18] Attachment-Detachment electron density calculations were used to visualize the character and localization of electronic transitions calculated by TD-DFT. All surfaces were visualized using Molekel version 5.4.0.8[19] and were plotted with isovalues of 0.001 or 0.002.

4.2.4 Picosecond Transient Absorption Kinetics and Spectra

Transient Absorption Kinetics. This experimental description is an excerpt from the dissertation of Joshua T. Hewitt which is in preparation. A majority of the transient kinetics presented in this thesis were collected using a homebuilt spectrometer built upon a commercially available Ti:Sapphire laser system (Clark CPA-1000) with the regenerative amplifier pumped by a nanosecond YLF (Quantronix; Darwin). The output of the regenerative amplifier (Clark MXR CPA1000, ~ 800 nm +/- 10 nm, ~150 fs temporal FWHM, 1kHz, 500 mJ/ pulse) was split using a 70:30 beam splitter where ~ 350 mJ was sent to a home built NOPA[20,21] in order to generate pump pulses centered between 495 - 525 nm that were prism compressed (Thorlabs; AFS-FS) to a FWHM of less than 80 fs. The remaining output of the regenerative amplifier, ~ 150 mJ, was used to generate the probe pulse and travels along a path containing two computer controlled linear delay stages (Newport MM3000 .049 fs/step time resolution, 14 inches of travel; Velmex 169 fs/step time resolution, 48 inches of travel) which are used to control the relative time delay between the pump and probe pulses. The probe beam is generated by attenuating the fundamental to ~1 μJ with neutral density filters and then focusing it into a 3 mm thick disk of calcium fluoride (Thorlabs, WG50530, mounted on a moving translational stage) resulting in a single filament continuum with nearly Gaussian spatial profile. An off-axis parabolic mirror was used to collimate the white light after its generation. The probe pulse train was then directed towards the sample cell (2 mm quartz cuvette) and focused with a 100 mm achromatic lens and spatially overlapped with the pump. For all experiments the power of the pump at the sample was attenuated to less than 260 nJ/ pulse (~1.7 x 10^{10} W/cm) with neutral density filters. Analyte concentrations and pump powers were

adjusted to rigorously maintain an excitation probability of less than 1 in 100 per pump pulse[22] with the typical sample absorbance at the pump laser central frequency being equal to approximately 0.5 (~0.5 μM). The angle between the pump and probe beams in this configuration is ~ 14^0. Kinetics were collected at parallel-parallel, parallel-perpendicular and the magic angle (54.7^o) by rotating the pump beam polarization relative to the probe with an achromatic half-wave plate (Thorlabs; AHWP05M-600) just before entering the sample. For all three cases the DBA complexes were found to have essentially identical kinetics –i.e. the extracted electron transfer lifetimes were independent of polarization. After the sample, the broad-band probe was passed through a collimating lens and coupled into a 220 mm scanning monochromator (Spex; 220M, 0.5 mm entrance and exit slits) and spectrally dispersed by a 1200 grooves/mm grating resulting in a resolution of ~ 3 nm at the exit slit. An amplified Si photodiode (Thor labs; PDA-55) placed at the exit slit of the monochromator was used to collect the signal which was sent to a digital lock-in amplifier (Stanford Research; SR830 DSP) synchronized to the frequency of an optical chopper used to modulated the pump beam. The lockin reports a change in transmittance as excited state absorption or bleach transitions are produced by the probe pulse. Kinetics traces were collected by monitoring this signal as a function of the position of the motorized translation stage and the data are reported as a normalized change in transmittance ($-\Delta T$) and can be read in the same way as a ΔA signal with positive signals corresponding to net transient absorbance and negative signals corresponding to a net transient bleach. The kinetics traces reported herein represent an average of 3 - 6 scans of positions in the forward direction of the translation stage. The data collection software was written in house (National Instruments, Labview 2010). Plotting and fitting of the data relied on the

commercially available data analysis software Igor Pro 6.0 (WaveMetrics). A small number of the transient kinetics presented in this manuscript were collected using an alternate ultrafast spectrometer available in our lab which has been described in detail elsewhere.[8,23]

Transient Absorption Spectra. . This experimental description is an excerpt from the dissertation of Joshua T. Hewitt which is in preparation. The transient spectra presented herein relied upon the same commercially available Ti:Sapphire laser system (Clark CPA-1000) albeit with slightly different optics and geometry at the sample, to minimize the effects of chromatic aberration, and a different detection scheme. With respect to the former, after generation of the probe a 50:50 beam splitter (Thor Labs; BSW26) was used to split the pulse train with both beams directed towards and focused into the sample by a 50 mm achromatic lens to a measured spot diameter of ~92 μm inside the sample volume. One of these continuum beams was spatially overlapped with the pump while the other traveled through an un-pumped portion of the sample cell and functions as a reference. The pump beam was focused into the sample cell with a 200 mm lens yielding an experimentally measured beam diameter of ~ 200 μm inside the sample volume, thereby ensuring all the probe photons are within the pumped volume in the sample cell. The angle between the pump and probe beams in this configuration is ~ 3^0. After both the probe and reference pulse trains had traveled through the sample they were coupled into a 220 mm scanning monochromator (Spex; 220M, 0.5 mm entrance and exit slits) and spectrally dispersed by a 1200 grooves/mm grating resulting in a resolution of ~ 3 nm at the exit slit. Both the probe and reference beams were monitored with a differential detector (ThorLabs, PDB210) placed after the exit slit of the monochromator with the output being sent to a boxcar amplifier (Stanford Research, SRS250), an analog to digital converter

digital (NI PCI-6036E), and a computer based lock-in program (LabVIEW 2010) synchronized to the frequency of a mechanical chopper wheel that was used to modulate the pump beam. The transient spectra are plotted in terms of -ΔT/T and can be interpreted in the same way as a ΔA signal with positive features corresponding to a net transient absorption and negative signals corresponding to overall transient bleach. Chirp correction of the data was accomplished by setting the peak of the pump-probe cross-correlation in neat acetonitrile to t_o.[24]

4.3 Results and Discussion

4.3.1 Steady-State Absorption and Emission Spectroscopy

Ruthenium (II) polypyridyl complexes are known for their intense metal-to-ligand charge transfer (MLCT) absorption bands in the visible region of the spectrum.[1,2] These spin-allowed transitions have molar absorption coefficients on the order of $\sim 10^{4.}$ Upon absorption of a visible photon an electron is promoted from a dπ orbital on the ruthenium to a π*-orbital on a polypyridine ligand thereby formally oxidizing the metal while simultaneously reducing the ligand, **Equation 4.1** summarizes this absorption process.

$$[Ru^{n+}L_3] \xrightarrow{h\upsilon} [Ru^{(n+1)+}(L^{-})L_2]^{*} \qquad \textbf{Equation 4.1}$$

The complexes prepared for this work are no different from their ruthenium (II) polypyridine predecessors. Upon absorption of a visible photon an intense ^{1}MLCT ← ^{1}GS band is observed. **Figure 4.2** shows the normalized absorption and emission spectra of the donor complexes (red and blue traces, respectively) overlaid with the normalized absorption spectrum of the corresponding DBA complex (black) for the bpy, dmb and tmb complexes, respectively. It should be noted that all DBA complexes prepared are non-emissive. This is indicative that the DBA complexes are utilizing other excited state decay

pathways. The non-emissive behavior of the DBA complexes is the first indication that the complexes are undergoing photoinduced ET.

In examining the UV-visible spectra in **Figure 4.2** above we find that the spectra of the DBA complexes are not fully superimposable with those of the corresponding donor complexes. For all three DBA complexes we see an increase in absorption at the red edge of the spectrum (between 500-600 nm) as well as red shifting of the absorption maximum when compared to both respective donor and parent complex. This is most pronounced for $Ru(tmb)_2(bpy\text{-}phenyl\text{-}MV](PF_6)_4$ (**3**) where we see the growth of a second peak at the red edge of the spectrum. This observation leads to the conclusion that the directly appended electroactive ligand is perturbing the energetics of the MLCT transition. UV-visible spectra of DBA complexes previously prepared in our group[8,9] (see **Figure 1.3**) where a methylene spacer (a CH_2 group) in the bridging ligand separates the asymmetric aryl-substituted 2,2'-bipyridine from the methyl viologen acceptor showed that the appended electroactive acceptor does not perturb the MLCT band and that the UV-visible spectra of donor and DBA complexes were virtually superimposable. Clearly, the methylene spacer acts as an electronic insulator and removing it affects the electronic properties of the complex.

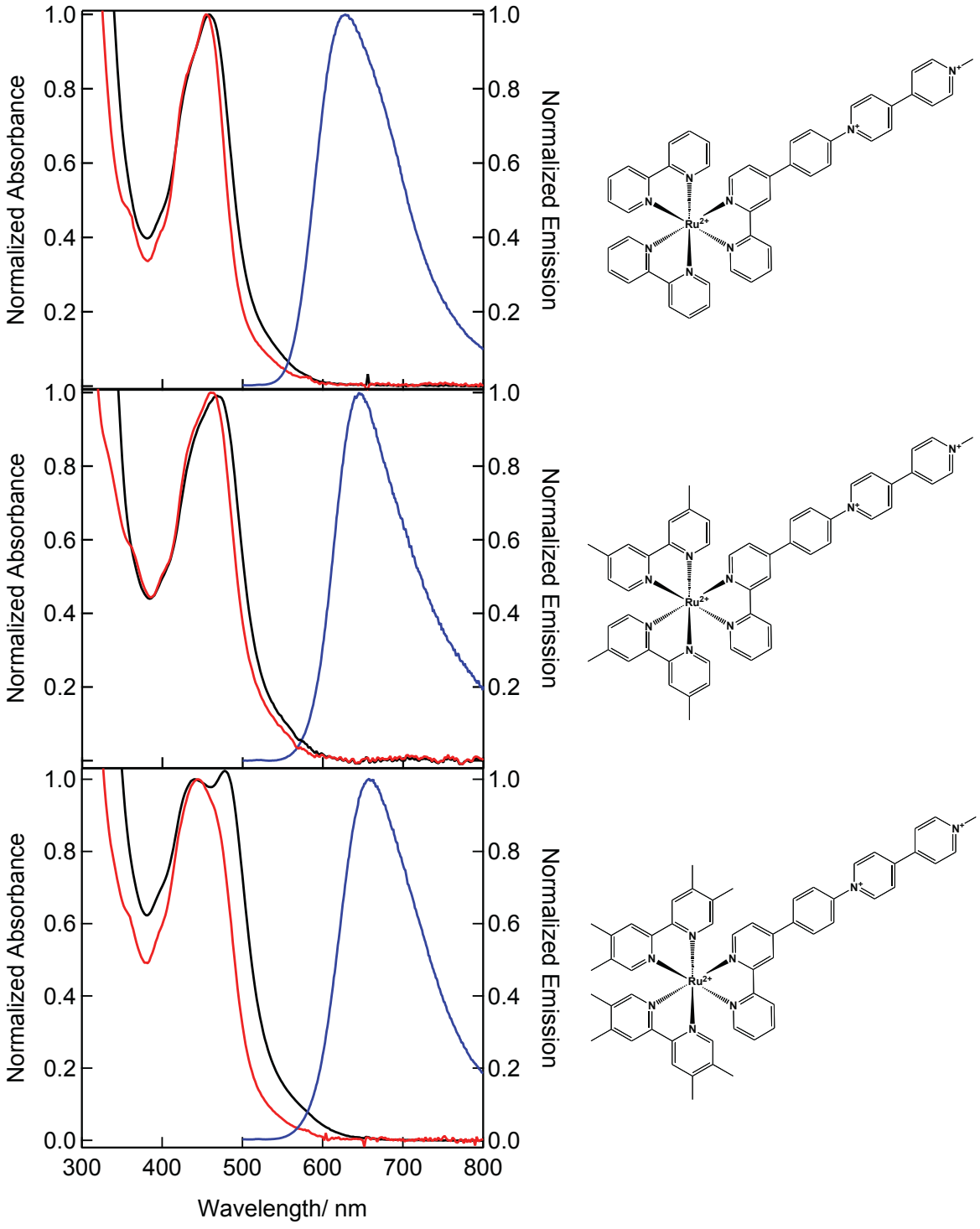

Figure 4.2 Normalized UV-visible absorption spectra of DBA (black) and donor (red) complexes in room temperature CH_3CN .The corrected emission spectra of the donor complexes recorded in room temperature CH_3CN are shown (blue) Top: $[Ru(bpy)_2(bpy\text{-}phenyl\text{-}MV)](PF_6)_4$ (**1**) and $[Ru(bpy)_2(bpy\text{-}phenyl)](PF_6)_2$ (**1'**) Middle:$[Ru(dmb)_2(bpy\text{-}phenyl\text{-}MV)](PF_6)_4$ (**2**) and $[Ru(dmb)_2(bpy\text{-}phenyl)](PF_6)_2$ (**2'**) Bottom:$[Ru(tmb)_2(bpy\text{-}phenyl\text{-}MV)](PF_6)_4$ (**3**) and $[Ru(tmb)_2(bpy\text{-}phenyl)](PF_6)_2$ (**3'**)

There are several examples in the literature of MLCT band red shifting upon appendage of a ligand with an extended π-system.[25-30] Particularly, Henrich and co-workers[28] observed a red shifting of ~50 nm compared to $[Ru(bpy)_3](PF_6)_2$ of a complex containing a quaternized asymmetric ligand. The new band in our systems reveals that the electroactive ligand significantly interacts with the ruthenium and that the lowest energy MLCT transition will be to the electroactive ligand.

It has been established that the electroactive ligand does perturb the MLCT transitions of the DBA complexes but what the source of this perturbation is unclear. In an attempt to understand the nature and composition of these new transitions we turned to quantum calculations. In **Section 4.3.3** the results of the quantum calculations will be addressed. The calculations shed light on the character of the transitions that are bringing about the increase in red-edge absorption in the DBA complexes. It will also be shown in **Section 4.3.4** that the increase in red-edge absorption plays a role in the photoinduced ET of the complexes.

The emission spectra of the donor complexes, which were collected after electronic excitation at 450 nm, show a broad and featureless emission band, which is characteristic of the $^3MLCT \rightarrow {}^1GS$ transition of other ruthenium polypyridyl complexes[1] and of the homoleptic parent complexes, $[Ru(bpy)_3](PF_6)_2$, $[Ru(dmb)_3](PF_6)_2$ and $[Ru(tmb)_3](PF_6)_2$. **Table 4.1** lists relevant ground state and excited state properties of these complexes. It should be noted that for the three donor complexes the emission maximum is red shifted when compared to the parent complex suggesting that the lowest-lying ^3MLCT state must lie on the lower energy asymmetric donor ligand and not the ancillary ligands.

Table 4.1 Photophysical Properties of Complexes in Room Temperature CH_3CN

Complex	λ^{MLCT}_{max} /nm	ε /M^{-1} cm^{-1}	λ_{em} $_{max}$ /nm	Φ_{em}[a]	τ_{obs} $1/k_0$ /μs	k_r /10^5 s^{-1}	k_{nr} /10^5 s^{-1}
$[Ru(bpy)_3](PF_6)_2$	452	13000[b]	615	0.095[b]	1.00	0.95	9.1
$[Ru(bpy)_2(bpy\text{-}phenyl)](PF_6)_2$ (**1'**)	454	17100	631	0.126	1.26	1.00	6.9
$Ru(bpy)_2(bpy\text{-}phenyl\text{-}MV)](PF_6)_4$ (**1**)	458	19000	--	--	--	--	--
$[Ru(dmb)_3](PF_6)_2$	450	17000[b]	630	0.083	0.91	0.91	10.0
$[Ru(dmb)_2(bpy\text{-}phenyl)](PF_6)_2$ (**2'**)	464	14800	648	0.097	1.19	0.81	7.6
$[Ru(dmb)_2(bpy\text{-}phenyl\text{-}MV)](PF_6)_4$ (**2**)	468	15000	--	--	--	--	--
$[Ru(tmb)_3](PF_6)_2$	448	8100	600	0.067	0.41	1.64	22.7
$[Ru(tmb)_2(bpy\text{-}phenyl)](PF_6)_2$ (**3'**)	444	12600	658	0.064	0.85	0.76	11.0
$[Ru(tmb)_2(bpy\text{-}phenyl\text{-}MV)](PF_6)_4$ (**3**)	478	15800	--	--	--	--	--

[a] The error bars on these measurements are ±0.003; they represent reproducibility within 2σ for three separate measurements for each complex. [b] These data were taken from reference 32.

Listed in **Table 4.1** are the ^{3}MLCT excited-state lifetimes of the donor complexes, τ_{obs}. From these lifetimes the rate constant k_0 ($1/\tau_{obs}$) is obtained. This rate constant is the sum of all deactivation pathways, radiative and nonradiative, from the ^{3}MLCT → ^{1}GS. Effectively, this is the rate of ground state recovery in the absence of an electron acceptor. We see that for all donor complexes the emission lifetimes are longer than the respective parent compound.

Radiative quantum yields (Φ_{em}) were also measured for the donor complexes; these values are reported in **Table 4.1**. We see that within the error of the measurement Φ_{em} is larger for the donor complexes than respective parent complex. This is attributed to the decrease in the radiative rate constant (k_{nr}) between parent and donor complex. The values of (k_{nr}) and (k_r) were calculated from experimentally measured emission lifetimes (τ_{obs}) and radiative quantum yields. Radiative quantum yields were calculated relative to the standard $[Ru(bpy)_3](PF_6)_2$ via **Equation 4.2**.[31]

$$\phi_{unk} = \phi_{std}\left(\frac{I_{unk}}{A_{unk}}\right)\left(\frac{A_{std}}{I_{std}}\right)\left(\frac{\eta_{unk}}{\eta_{std}}\right)^2 \qquad \textbf{Equation 4.2}$$

Where ϕ_{std} is the known radiative quantum yield of $[Ru(bpy)_3](PF_6)_2$, (0.095),[32] I_{unk} and I_{std} are the integrated emission intensities of the unknown and standard, respectively, A_{unk} and A_{std} are the absorbances of the unknown and standard, respectively, at the excitation wavelength (450 nm), lastly η_{unk} and η_{std} are the refractive indices of the unknown and standard solutions, respectively. However, since the standard and unknown were both measured in acetonitrile this ratio it set to 1.

Before measuring the rates of photoinduced ET one must first determine if there is sufficient driving force for charge separation to occur. In calculating the driving force for forward electron transfer, ΔG^0_{ET}, and back electron transfer, ΔG^0_{BET}, two experimentally derived values need to be obtained. The first is ΔG^0_{IP} which is the free energy associated with forming the ion-pair state, D^+-B-A^-. A detailed explanation of how this value is calculated is in **Section 4.3.2**. The second quantity is the so-called ΔG^0_{MLCT}, which can be thought of as the amount of energy that is stored in lowest-lying ^{3}MLCT state of the photo-excited 'donor', D^*-B-A, prior to ET. ΔG^0_{MLCT} is calculated from quantities obtained from a fit of spectral emission data.

Since the DBA complexes do not emit, the spectral emission data of the respective donors will be fit. The Parker and Rees correction was applied to the corrected data in order to convert the data from units of wavelength to energy.[33] The spectra were fit by a multi-parameter least square minimization to **Equation 4.3** where the best fit was determined by minimization of the root-mean-square-deviation and visual inspection.[34-36]

$$I(\bar{\nu}) = \sum_{\nu''=0}^{n} \left\{ \left(\frac{E_0 - \nu'' h\omega}{E_0} \right)^3 \left(\frac{S^{\nu''}}{\nu''!} \right) \exp\left[-4\ln(2) \left(\frac{\bar{\nu} - E_0 + \nu'' h\omega}{\Delta\bar{\nu}_{0,1/2}} \right) \right]^2 \right\} \quad \textbf{Equation 4.3}$$

For our purposes we consider three fit parameters, E_0 which is the energy difference between the emissive ^{3}MLCT state and the ground state, $\Delta\bar{\nu}_{0,1/2}$ which refers to the homogenously broadened linewidth of the zeroth vibronic transition ($\nu' = 0 \rightarrow \nu'' = 0$) and S_M, the Huang-Rhys factor, which is a unitless quantity that reflects the extent of vibronic coupling between the initial and final states in the emission process. Alternatively, S_M can be viewed as the extent of nuclear distortion between the emissive triplet state and ground state surfaces. S_M values range from 0-1 where a lower value is indicative of decreased nuclear distortion (more nested surfaces) along a single coordinate with a frequency of $h\omega_M$. Where $h\omega_M$ is taken to be the average energy of a vibrational mode coupling the ground and excited-state surfaces, usually a ring stretching frequency. For the spectral fits $h\omega_M$ was held at a constant value of 1350 cm^{-1}; this is the reported $h\omega_M$ value for $[Ru(bpy)_3]^{2+}$ and we expect it to be similar for our complexes.[37]

With the required fit parameters in hand ΔG^0_{MLCT} can be calculated from **Equation 4.4.**[37,38]

$$\Delta G^{\circ}_{MLCT} = E_0 + \frac{\left(\Delta\bar{\nu}_{0,1/2}\right)^2}{16 k_B T \ln 2} \quad \textbf{Equation 4.4}$$

Where E_0 and $\Delta\bar{\nu}_{0,1/2}$ are obtained directly from the fit, k_B is the Boltzmann constant and T is the temperature in Kelvin. Calculated values of ΔG^0_{MLCT} as well as results from the spectral emission fitting are summarized in **Table 4.2** below. When comparing E_0 values with the parent complexes we see that all donor compounds have a lower E_0 value than the corresponding parent complex. This implies that the lowest lying ^{3}MLCT state is on the

asymmetric aryl-substituted ligand since it is lower in energy than respective ancillary ligands, bpy, dmb or tmb. This result is consistent with CV results from Chapter Three (see **Table 3.1**) where for (**1'**), (**2'**) and (**3'**) the first ligand reductions were shifted to less negative values (easier to reduce) than those of the respective parent complexes. Where the differences in first ligand reductions between parent and donor for (**1'**), (**2'**) and (**3'**) between are 20 mV, 90 mV and 230 mV, respectively.

Table 4.2 Emission Spectra Fitting Data for Complexes in Room Temperature CH_3CN

Complex	E_0 /cm^{-1}	ΔG^0_{MLCT} /cm^{-1}	$h\omega_M$ /cm^{-1}	S_M	$\Delta\overline{\nu}_{0,1/2}$ /cm^{-1}
$[Ru(bpy)_3](PF_6)_2$[a]	16310±70	17630±70	1350	0.98±0.05	1740±40
$[Ru(bpy)_2(bpy\text{-}phenyl)](PF_6)_2$ (**1'**)	16107±70	17580±70	1350	0.94±0.05	1860±40
$[Ru(dmb)_3](PF_6)_2$[b]	15990±70	17410±70	1350	1.01±0.05	1805±40
$[Ru(dmb)_2(bpy\text{-}phenyl)](PF_6)_2$ (**2'**)	15545±70	17100±70	1350	0.85±0.05	1850±40
$[Ru(tmb)_3](PF_6)_2$[a]	16580±70	17810±70	1350	0.97±0.05	1680±40
$[Ru(tmb)_2(bpy\text{-}phenyl)](PF_6)_2$ (**3'**)	15315±70	16780±70	1350	0.81±0.05	1840±40

The error bars for the parameters reported in this table represent 2σ determined from five separate measurements and fittings of emission of $[Ru(bpy)_2(bpy\text{-}phenyl](PF_6)_2$. [a] These data were taken from reference 8. [b] These data were taken from reference 9.

From **Table 4.2** the values of S_M are lower for the donor complexes than those of the respective parent complexes. From the discussion above this indicates that the excited state and ground state surfaces for the donor complexes are more nested than those of the parent complexes. In other words there is less nuclear distortion between ground and excited state surfaces for the donor compounds than respective parent complex. The Energy Gap Law predicts that more nested surfaces lead to a decrease in the nonradiative rate of decay from the ^{3}MLCT state. As we can see from **Table 4.1** this is what we see when comparing k_{nr} between the parent and donor complexes.[34,39-42]

4.3.2 Determination of Driving Forces for Photoinduced Electron Transfer

As stated above, two quantities are needed to determine driving forces for ET, ΔG^0_{MLCT} and ΔG^0_{IP}. ΔG^0_{MLCT} was determined above and ΔG^0_{IP} is determined, in part, from electrochemical data. We use Weller's formulation[43] for finding ΔG^0_{IP}; summarized in **Equation 4.5**.

$$\Delta G^{\circ}_{IP} = E_{ox} - E_{red} - \frac{e^2}{4\pi\varepsilon_0\varepsilon_S R_{DA}} \times 6.242\times10^{18}\,\frac{eV}{J} \qquad \textbf{Equation 4.5}$$

It should be noted that Weller's electrochemical work term has been omitted since electrochemical and ET measurement were taken in the same solvent, acetonitrile. Here E_{ox} and E_{red} refer to the $5^+/4^+$ and $4^+/3^+$ half-wave reduction potentials of the DBA complexes, respectively. These values are tabulated in Chapter Three (**Table 3.1)**. Also, e is the fundamental charge, ε_0 is the permittivity of free space, ε_s is the static dielectric constant of the solvent in which the ET will be measured and R_{DA} is an estimate of the donor-to-acceptor distance. This distance is a through-space measurement from the Ru center to 4,4'-carbon bond in the acceptor. These values were estimated from the geometry-optimized structures obtained from DFT calculations performed in Q-Chem 4.0.

Equation 4.6 and **Equation 4.7** summarize how driving forces for forward ET and back ET (BET) are calculated, respectively.

$$\Delta G^{\circ}_{ET} = -\Delta G^{\circ}_{MLCT} + \Delta G^{\circ}_{IP} \qquad \textbf{Equation 4.6}$$

$$\Delta G^{\circ}_{BET} = -\Delta G^{\circ}_{IP} \qquad \textbf{Equation 4.7}$$

Values for R_{DA}, ΔG^0_{IP}, ΔG^0_{ET} and ΔG^0_{BET} are summarized in **Table 4.3**

Table 4.3 Calculated Driving Forces for Photoinduced ET

Complex	R_{DA}/Å	ΔG^0_{IP}/eV	ΔG^0_{ET}/eV	ΔG^0_{BET}/eV
$[Ru(bpy)_2(bpy\text{-}phenyl\text{-}MV)](PF_6)_4$ (**1**)	14.1	1.53	-0.65	-1.53
$[Ru(dmb)_2(bpy\text{-}phenyl\text{-}MV)](PF_6)_4$ (**2**)	14.1	1.45	-0.67	-1.44
$[Ru(tmb)_2(bpy\text{-}phenyl\text{-}MV)](PF_6)_4$ (**3**)	14.1	1.39	-0.70	-1.38

These calculations support our initial reasoning in preparing the complexes, namely that by substituting the ancillary ligand one alters the energetics of the complex therefore altering driving forces for ET. We see an increase of 50 meV in the exothermicity of forward ET for $[Ru(tmb)_2(bpy\text{-}phenyl\text{-}MV)](PF_6)_4$ (**1**) compared to $[Ru(bpy)_2(bpy\text{-}phenyl\text{-}MV)](PF_6)_4$ (**3**). This is due to the fact that the tmb-containing complex, (**3**), has a lower value of ΔG^0_{MLCT} and a lower $Ru^{III/II}$ oxidation potential. The latter effect contributes to the reduction of exothermicity of the reverse reaction (BET) of the tmb complex (**3**) by 150 meV. The reorganization energy for similar systems prepared by our group[8] were estimated to be ~1.0 eV which leads us to speculate that the forward ET process occurs in the Marcus normal region while the back ET occurs in the Marcus inverted region, see **Section 4.3.4** for further discussion.

4.2.3 Time-Dependent Density Functional Theory to Explain Absorption Spectra

As discussed in **Section 4.3.1** when compared to the corresponding donor complexes the visible absorption spectra of the DBA complexes exhibit increased absorbance at the red edge of the spectrum (between 500-600 nm). This effect is most pronounced for $[Ru(tmb)_2(bpy\text{-}phenyl\text{-}MV)](PF_6)_4$ (**3**) where the growth of a second peak is observed. This increased absorbance must be due to electronic perturbations caused by the appended electroactive acceptor. In order to understand the nature of the increased absorbance and therefore the new transitions we turned to quantum calculations,

specifically Density Functional Theory (DFT) and Time-Dependent Density Functional Theory (TD-DFT). The use of DFT and TD-DFT to understand charge transfer processes in d^6 transition metals have become more prevalent in the literature.[44-48] Here we use DFT to optimize ground-state geometries of the donor and DBA complexes followed by TD-DFT to predict the absorption spectra of the donor and DBA complexes.

Figure 4.3 is a comparison of the experimental absorption spectra (top panel) to the computed spectra (bottom panel) of the donor complexes. The calculated spectra have been red shifted by 1.4 eV for better comparison with experimental spectra.[18] DFT has been known to incorrectly predict charge transfer bands.[44] However the use of long-range corrected functionals such as ωB97-X have been shown to correctly predict charge transfer bands but tend to overestimate singlet states.[49] Song et al. calculated the transition energies of perylene dyes utilizing a range corrected functional and computed spectra required red shifting by ~0.5 eV for agreement with experimental spectra.[50]

For the calculated spectra (bottom panel in **Figure 4.3**) the solid lines are representative of the absorption envelope and the so-called sticks represent transitions within the envelope. As we can see when comparing the experimental visible absorption spectra (top panel above) with the calculated spectra there is good qualitative agreement between the two sets of data. Namely, that the calculated spectra reproduce the spectral features of the experimental spectra where no significant increase in absorption between 500-600 nm is observed. However the trend in absorption maxima is not correctly reproduced by the calculations. This can be attributed to the exclusion of solvent effects from the calculations; undoubtedly inclusion of solvation would alter absorption maxima.

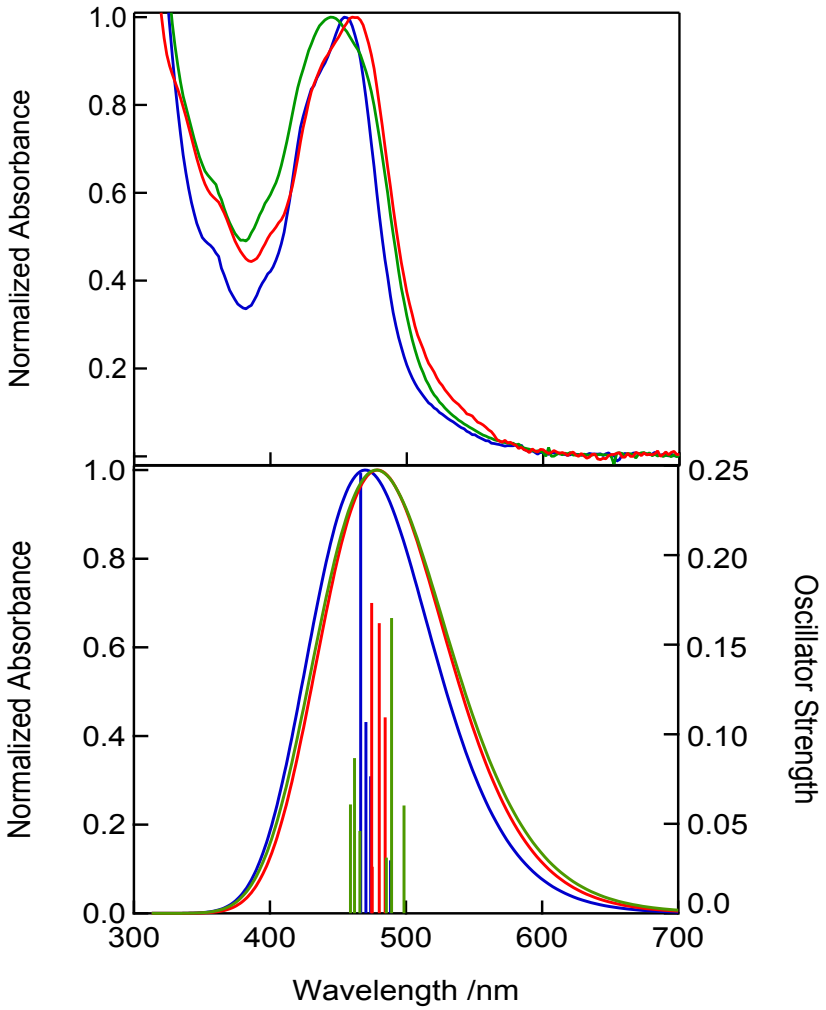

Figure 4.3 Comparison of experimental (top) and calculated (bottom) absorption spectra for $[Ru(bpy)_2(bpy\text{-}phenyl](PF_6)_2$ (**1'**) (blue), $[Ru(dmb)_2(bpy\text{-}phenyl](PF_6)_2$ (**2'**) (red) and $[Ru(tmb)_2(bpy\text{-}phenyl)](PF_6)_2$ (**3'**) (green). The calculated spectra have been red shifted by 1.4 eV for better comparison with experimental spectra. The long-range corrected ωB97X exchange-correlation functional was used for gas phase geometry observations.

Figure 4.4 below compares the experimental UV-visible absorption spectra of the DBA complexes (top) with calculated spectra (bottom). We see the calculated spectra for the DBA complexes qualitatively agree with the experimental absorption spectra. The calculated spectra are broader than the experimental spectra but the increase in red edge absorption is correctly reproduced by the calculations. Consistent with experiment, the red edge absorption becomes more prominent as we move across the series and eventually

grows into a second peak for $[Ru(tmb)_2(bpy\text{-}phenyl\text{-}MV)](PF_6)_4$ (**3**) (green data set in **Figure 4.4**).

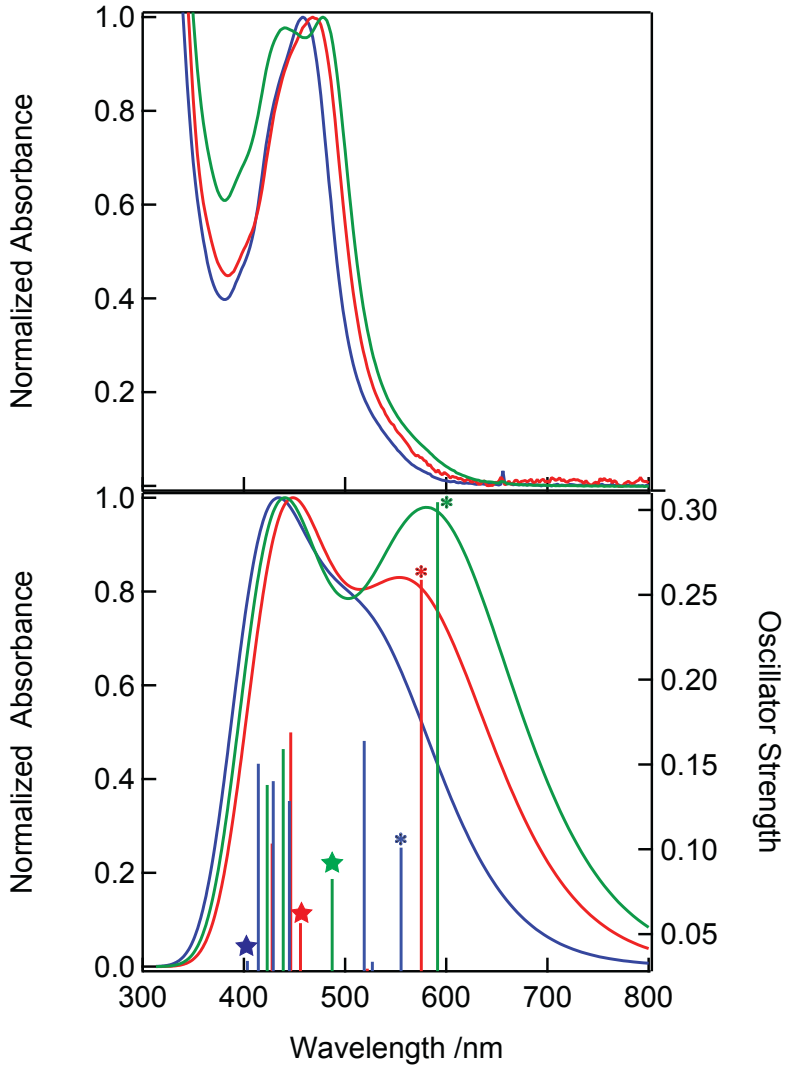

Figure 4.4 Comparison of experimental (top) and calculated (bottom) absorption spectra for $[Ru(bpy)_2(bpy\text{-}phenyl\text{-}MV)](PF_6)_4$ (**1**) (blue), $[Ru(dmb)_2(bpy\text{-}phenyl\text{-}MV)](PF_6)_4$ (**2**) (red) and $[Ru(tmb)_2(bpy\text{-}phenyl\text{-}MV)](PF_6)_4$ (**3**) (green). The calculated spectra have been red shifted by 1.4 eV for better comparison with experimental spectra. The long-range corrected ωB97X exchange-correlation functional was used for gas phase geometry observations.

The so-called stick spectra provide information about the transitions that are occurring upon excitation. To visually represent the transitions we turned to

detachment/attachment densities which are plots of regions depopulated and populated, respectively, after excitation.[18,44] Using these densities eliminates the need to represent different orbital components of the transitions and allows for the simplicity of viewing a single density representing the ground state or the excited state. For the donor complexes the stick spectra show the expected MLCT transitions where the detachment density is metal centered and the attachment density is localized on a polypyridine ligand. In analyzing the attachment and detachment densities for the DBA complexes we find that a majority of the transitions between 400 and 500 nm are MLCT in character where the detachment density is centered on the metal center and the attachment density on a polypyridine ligand.

Now we turn to the stick spectra to help explain the observed increase in red-edge absorption for the DBA complexes in this series. Specifically we will look at the transition at 555 nm for $[Ru(bpy)_2(bpy\text{-}phenyl\text{-}MV)](PF_6)_4$ (**1**), 575 nm for $[Ru(dmb)_2(bpy\text{-}phenyl\text{-}MV)](PF_6)_4$ (**2**) and 591 nm for $[Ru(tmb)_2(bpy\text{-}phenyl\text{-}MV)](PF_6)_4$ (**3**)(marked with asterisks in **Figure 4.4**). The attachment densities in blue and detachment densities in red for these respective transitions are shown in **Figure 4.5** below where the top panel is (**1**), the middle panel (**2**) and the bottom panel (**3**). As expected the detachment density is metal centered for each of the complexes and the attachment density is ligand localized. For (**2**) and (**3**) the attachment densities are not only localized on 2,2'-bipyrdine moiety of the ligand but also over the bridging ligand with density on the acceptor moiety for (**3**). However for (**1**) the attachment density is localized on both the ancillary ligands and the asymmetric ligand. We speculate that this result is attributed to the fact that calculations were performed in the gas phase. From CV data in Chapter Three (see **Table 3.1**) we find

that the first ligand reduction of the aryl-substituted 2,2'-bipyrine ligand is only 20 mV less negative than that of an un-substituted 2,2'-bipyridine signaling that the two ligands are similar in energy. We believe performing the calculations in a polar continuum whereby reproducing the conditions in which the UV-visible spectra were recorded (in acetonitrile) the attachment density would localize onto the lower energy substituted ligand. For (**1**), as with (**3**), electron density is also present on the acceptor. Therefore we attribute the delocalization of the attachment density onto the asymmetric ligand as the source of the increased absorption in the red edge of the spectra (between 500 and 600 nm). We also see that this red-edge transition has the highest oscillator strength for $[Ru(tmb)_2(bpy\text{-}phenyl\text{-}MV)](PF_6)_4$ (**3**) which supports the experimental results in that the increase in absorbance is most pronounced for this complex.

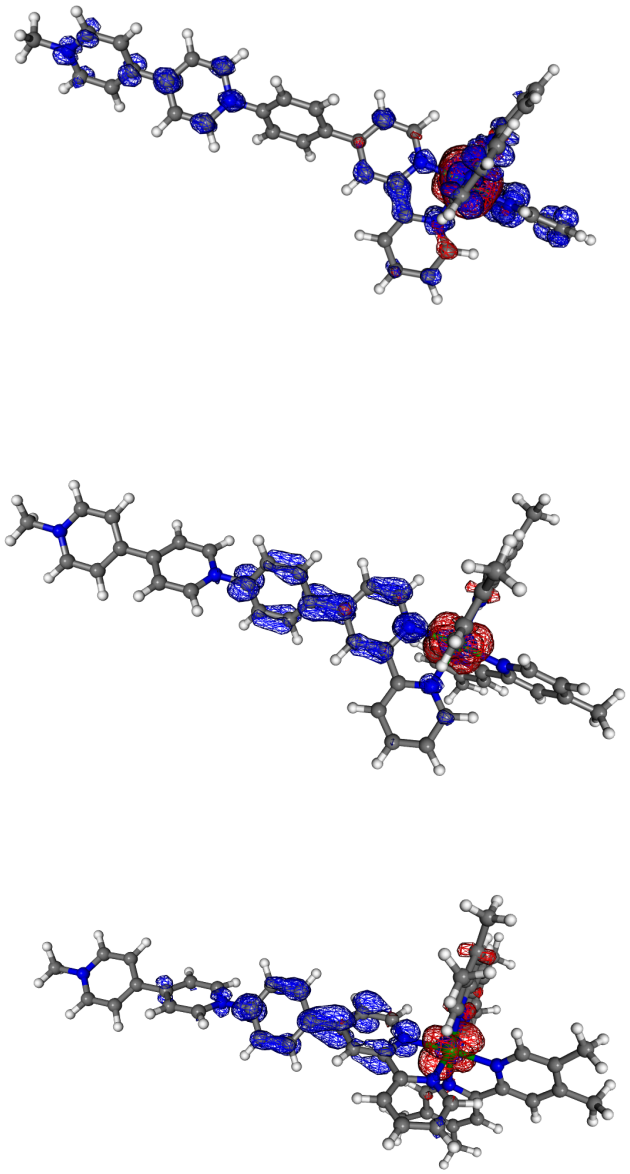

Figure 4.5 Attachment (blue) and detachment (red) densities for the red edge transitions of $Ru(bpy)_2(bpy\text{-}phenyl\text{-}MV)](PF_6)_4$ (**1**) (top, 555 nm), $[Ru(dmb)_2(bpy\text{-}phenyl\text{-}MV)](PF_6)_4$ (**2**) (middle, 575 nm) and $[Ru(tmb)_2(bpy\text{-}phenyl\text{-}MV)](PF_6)_4$ (**3**) (bottom, 591 nm). An isovalue of 0.001 was plotted for (**1**) and 0.002 for (**2**) and (**3**). The long-range corrected ωB97X exchange-correlation functional was used for gas phase geometry observations.

Continuing to analyze the stick spectra for these three complexes one comes across evidence for direct excitation from the metal center to the acceptor. These attachment/detachment densities are summarized in **Figure 4.6** where the top panel shows the attachment/detachment densities for the transition at 401 nm for $[Ru(bpy)_2(bpy\text{-}phenyl\text{-}MV)](PF_6)_4$ (**1**), the middle panel shows the attachment/detachment densities for the transition at 456 nm for $[Ru(dmb)_2(bpy\text{-}phenyl\text{-}MV)](PF_6)_4$ (**2**) and the bottom panel shows the attachment/detachment densities for the transition at 487 nm for $[Ru(tmb)_2(bpy\text{-}phenyl\text{-}MV)](PF_6)_4$ (**3**) these transitions are marked with stars in **Figure 4.4**. For (**1**) the transition at 410 nm also has ~15% direct excitation character. Across the series (from (**1**) to (**3**)) these transitions red shift and oscillator strengths increase. In general these transitions indicate that it is possible upon absorption of a visible photon to promote an electron from the ruthenium directly to the π^* orbitals of the acceptor moiety of the asymmetric ligand. As we will see in the discussion of the picosecond transient absorption kinetics below (**Section 4.3.4**) this direct excitation plays a role in the photoinduced electron processes of these complexes.

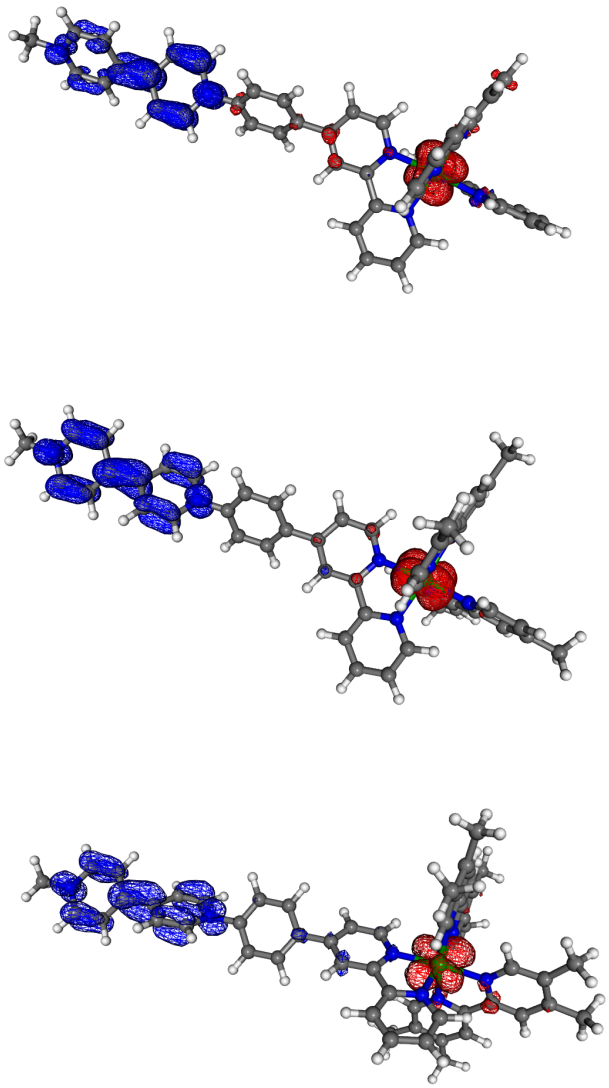

Figure 4.6 Attachment (blue) and detachment (red) densities for the direct acceptor excitation transitions of $Ru(bpy)_2(bpy\text{-}phenyl\text{-}MV)](PF_6)_4$ (**1**) (top, 414 nm), $[Ru(dmb)_2(bpy\text{-}phenyl\text{-}MV)](PF_6)_4$ (**2**) (middle, 456 nm) and $[Ru(tmb)_2(bpy\text{-}phenyl\text{-}MV)](PF_6)_4$ (**3**) (bottom, 487 nm). An isovalue of 0.002 was plotted. The long-range corrected ωB97X exchange-correlation functional was used for gas phase geometry observations.

4.3.4 Picosecond Transient Absorption Kinetics and Spectra

At the heart of this is body of work is the aspiration to determine the role structural elements play on the rates of the photoinduced intramolecular electron transfer in directly-linked conformationally-active ruthenium (II) polypyridyl DBA complexes. From calculated

driving forces we concluded that forming the charge-separated electron transfer product, D^+-B-A^-, from the excited state donor, D*-B-A, is a downhill process. The reductive spectrorelectrochemical data presented in Chapter Three provide optical tags[51] for the absorptive properties of the electron transfer product. In this section, picosecond transient absorption techniques will be utilized to detect and measure the rates of photoinduced electron transfer for this series of DBA complexes. A discussion of transient absorption spectra will be followed by transient absorption single wavelength kinetics.

Transient absorption is a two pulse experimental technique where the first pulse, a pump pulse, excites the sample and a second pulse, the probe pulse, interrogates the absorptive properties of the excited state. Time resolution is introduced by motorized translational stages that create delays between the two pulses. Transient absorption spectra look at the absorptive properties of the excited state over a range of wavelengths at certain time slices over the excited state lifetime. Experimental data is plotted as a change in absorbance (or transmittance) versus wavelength per time slice.

We begin our analysis of transient absorption (TA) spectra by first discussing the TA spectrum of the donor complex $[Ru(bpy)_2(bpy\text{-}phenyl)](PF_6)_2$ (**1'**). This will provide us with information on the spectral properties of a ^{3}MLCT-excited state of a heteroleptic ruthenium polypyridyl complex with an asymmetric ligand that lacks an appended electroactive acceptor. The TA spectra of $[Ru(bpy)_2(bpy\text{-}phenyl)](PF_6)_2$ (**1'**) collected at -5.0 ps (black), 0.2 ps (red) and 3.0 ps (green) after excitation are shown below in **Figure 4.7**. The spectra were acquired in room temperature acetonitrile with a 480 nm pump pulse (~80 fs fwhm). Data from 475-485 nm has been removed since it was contaminated with scatter from the pump pulse. As we can see from the spectra there are two absorptive

features, between ~350-400 nm and 500-600 nm. We also see a bleach feature from 400-500 nm that is attributed to the loss of ^{1}MLCT ← ^{1}GS absorption. Based on TA experiments of $[Ru(bpy)_3](PF_6)_2$ and other ruthenium complexes with aryl-substituted ligands[52-55] we have assigned the absorption feature centered at 370 nm as intraligand transitions within the reduced polypyridine ligand. The absorption feature between 500-600 nm has contributions from Ligand-to-Metal Charge Transfer (LMCT) transitions as well as intraligand transitions within the reduced polypyridine ligand.[56] It should be noted that these three spectral features are consistent with both the reductive and oxidative spectroelectrochemistry reported for this compound in Chapter Three; the reductive spectroelectrochemistry data is inset in **Figure 4.7**. Upon reduction two absorptive bands were observed from 300-400 nm and 500-600 nm. Upon oxidation a decrease in MLCT band intensity was observed. The spectral features observed in the TA spectra of $[Ru(bpy)_2(bpy\text{-}phenyl)](PF_6)_2$ (**1'**) are consistent with those of $[Ru(dmb)_2(bpy\text{-}phenyl)](PF_6)_2$ (**2'**) and $[Ru(tmb)_2(bpy\text{-}phenyl)](PF_6)_2$ (**3'**).

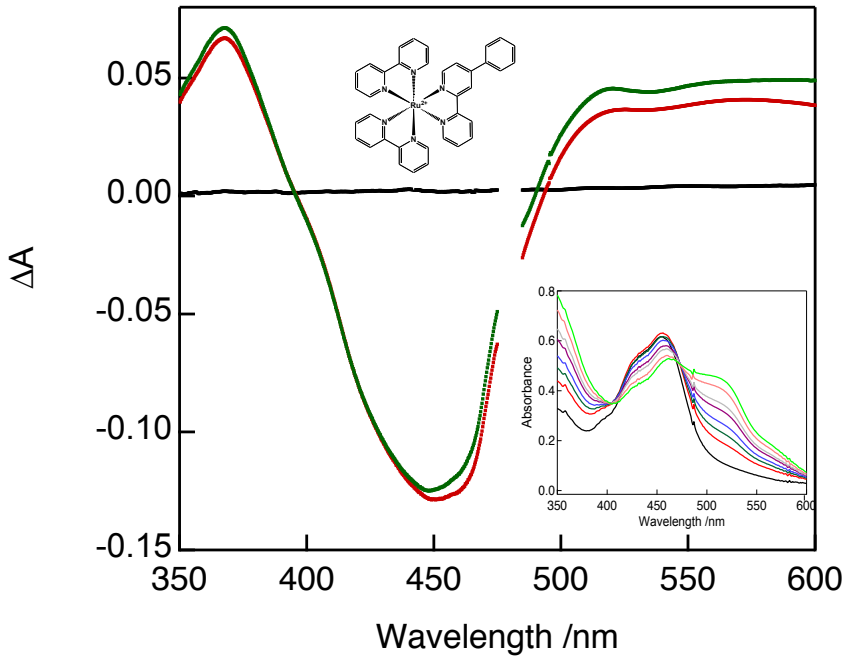

Figure 4.7 Transient Absorption Spectra of $[Ru(bpy)_2(bpy\text{-}phenyl)](PF_6)_2$ (**1'**) in room temperature acetonitrile collected at -5 ps (black) 0.2 ps (red) and 3.0 ps (green) following excitation with a 480 nm, ~80 fs pump pulse. Data between 475 and 485 nm has been removed since it was contaminated with scatter from the pump pulse. Inset: reductive spectroelectrochemistry data from Chapter Three.

The TA spectra of the DBA complex $[Ru(bpy)_2(bpy\text{-}phenyl\text{-}MV](PF_6)_4$ (**1**) are shown below in **Figure 4.8**. The spectra were collected at -5.0 ps (black), 0.2 ps (red), 0.6 ps (blue) and 3.0 ps (green) in room temperature acetonitrile after excitation with a 480 nm pulse (~80 fs). The data between 465 and 490 nm has been removed due to scatter from the pump pulse. Looking at the early time spectrum (0.2 ps, red trace in **Figure 4.8**) we see spectral features consistent with those of the donor (**1'**), an absorption feature centered at 370 nm assigned to intraligand transitions of the reduced polypyridine ligand, an intense bleach feature between 400 and 500 nm corresponding to a loss of $^1MLCT \leftarrow {}^1GS$ absorbance and an absorption feature between 600 and 700 nm ascribed to LMCT and intraligand transitions. However, unlike the donor compound the spectral features of the DBA complex evolve over the same time period. As can be seen from the intermediate time

point (0.6 ps, blue trace in **Figure 4.8**) the growth of a shoulder that peaks at 404 nm is observed while at the long time point (3.0 ps, green trace in **Figure 4.8**) we observe that the 370 nm peak has decreased in intensity while the data now peaks at 404 nm. Concomitant with the growth of the peak centered at 404 nm we see an increase in the absorption feature between 500 and 600 nm. Clearly, the appended electroactive acceptor is bringing about the changes in the TA spectra of the DBA complex.

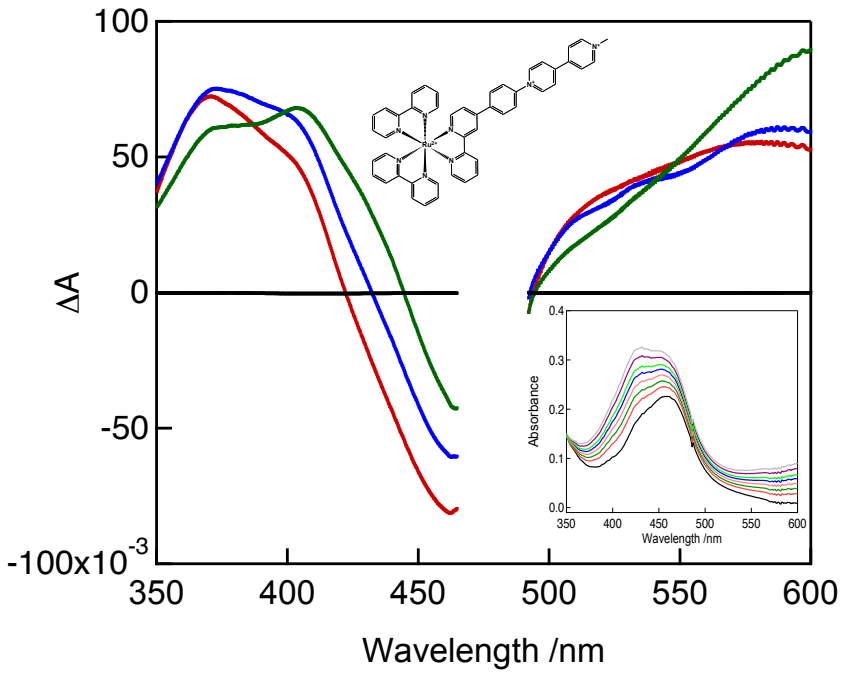

Figure 4.8 Transient Absorption Spectra of $[Ru(bpy)_2(bpy\text{-}phenyl\text{-}MV)](PF_6)_4$ (**1**) in room temperature acetonitrile collected at -5 ps (black) 0.2 ps (red) 0.6 ps (blue) and 3.0 ps (green) following excitation with a 480 nm, ~80 fs pump pulse. Data between 465 and 490 nm has been removed since it was strongly contaminated with scatter from the pump pulse. Inset: reductive spectroelectrochemistry data from Chapter Three

When comparing the reductive and oxidative spectroelectrochemistry results presented in Chapter Three of $[Ru(bpy)_2(bpy\text{-}phenyl\text{-}MV)](PF_6)_4$ (**1**) to the TA spectra above there are similarities between the two kinds of measurement. The reductive

spectroelectrochemistry data for this complex is shown as an inset in **Figure 4.8**. The oxidative spectroelectrochemistry data showed a decrease in ^{1}MLCT ← ^{1}GS absorbance that corresponds to the observed bleach feature. The reductive spectroelectrochemistry data showed the growth of a band centered at 429 nm and a broad absorptive feature between 500 and 600 nm, these absorptive features match those seen above in the TA spectra. The correspondence of the TA spectra with the reductive spectroelectrochemistry is direct evidence for the formation of the ET product. Recall in our case reductive spectroelectrochemistry measurements approximate the absorption properties of the ET product.

The TA spectra of $[Ru(dmb)_2(bpy\text{-}phenyl\text{-}MV)](PF_6)_4$ (**2**) and $[Ru(tmb)_2(bpy\text{-}phenyl\text{-}MV)](PF_6)_4$ (**3**) support the conclusions reached above for $[Ru(bpy)_2(bpy\text{-}phenyl\text{-}MV)](PF_6)_4$ (**1**), in that ET is operative in these complexes and the spectral features of the ET product include an absorptive feature centered at ~400 nm and a broad absorbance between 500 and 600 nm. **Figures 4.9** and **4.10** contain the TA spectra for $[Ru(dmb)_2(bpy\text{-}phenyl\text{-}MV)](PF_6)_4$ (**2**) and $[Ru(tmb)_2(bpy\text{-}phenyl\text{-}MV)](PF_6)_4$ (**3**), respectively where data between 475-515 nm has been removed due to contamination from pump scatter. It should be noted that the TA experimental setup used to acquire the TA spectra for $[Ru(dmb)_2(bpy\text{-}phenyl\text{-}MV)](PF_6)_4$ (**2**) and $[Ru(tmb)_2(bpy\text{-}phenyl\text{-}MV)](PF_6)_4$ (**3**) was outlined in detail in **Section 4.2.4** whereas the experimental setup utilized to acquire the spectra for $[Ru(bpy)_2(bpy\text{-}phenyl)](PF_6)_2$ (**1'**) and $[Ru(bpy)_2(bpy\text{-}phenyl\text{-}MV)](PF_6)_4$ (**1**) have been outlined in detail elsewhere.[8,23] The TA spectra of $[Ru(dmb)_2(bpy\text{-}phenyl\text{-}MV)](PF_6)_4$ (**2**) reported in **Figure 4.9** were collected at 0.5 ps (red), 1.5 ps (blue) and 5.0 ps (green) and were measured in room temperature acetonitrile pumping with a ~500 nm (~80 fs fwhm)

pulse. Again we see at early times (0.5 ps, red trace) that spectral features correspond to those of an excited donor complex, which peaks at 370 nm, and at longer times (5.0 ps, green) the spectral features assigned to the electron transfer product are observed, a sharp absorption band that peaks at 410 nm and broad absorption band between 500 and 650 nm. This again corresponds with reductive and oxidative spectroelectrochemical data for this complex.

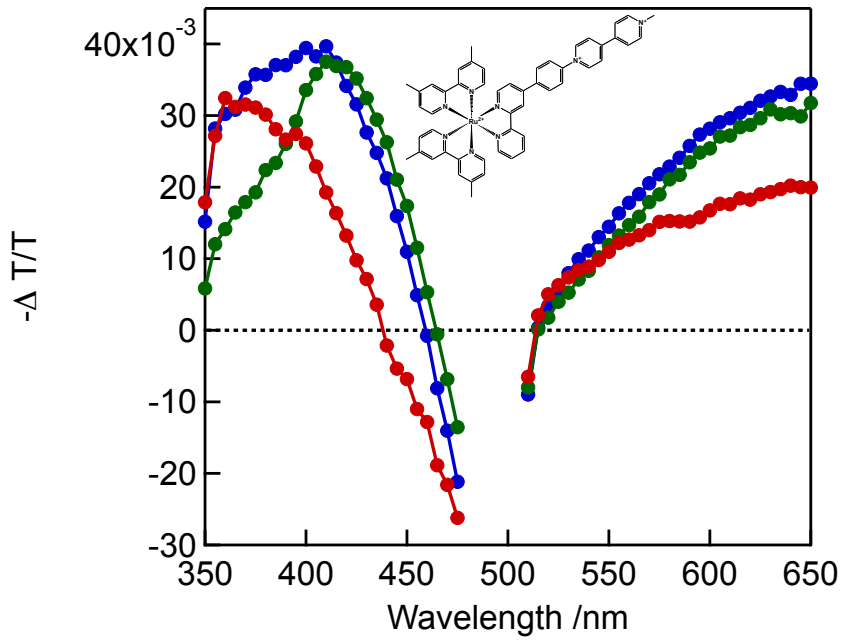

Figure 4.9 Transient Absorption Spectra of $[Ru(dmb)_2(bpy\text{-}phenyl\text{-}MV)](PF_6)_4$ (**2**) in room temperature acetonitrile collected 0.5 ps (red) 1.5 ps (blue) and 5.0 ps (green) following excitation with a 500 nm, ~80 fs pump pulse. Data between 475 and 515 nm has been removed since it was strongly contaminated with scatter from the pump pulse.

In **Figure 4.10** below the TA spectra for $[Ru(tmb)_2(bpy\text{-}phenyl\text{-}MV)](PF_6)_4$ (**3**) are reported. The TA spectra were collected at 0.5 ps (red), 1.5 ps (blue) and 5.0 ps (green) and were measured in room temperature acetonitrile pumping with a ~500 nm (~80 fs fwhm) pulse. Comparing these spectra to those shown above for $[Ru(bpy)_2(bpy\text{-}phenyl\text{-}$

MV)](PF$_6$)$_4$ (**1**) and [Ru(dmb)$_2$(bpy-phenyl-MV)](PF$_6$)$_4$ (**2**) we arrive at the same conclusions, that at early times (0.5 ps, red trace) spectral features attributable to a reduced donor complex, which peaks at 380 nm, are present and at long times (5.0 ps, green trace) spectral features attributable to the ET product are present: an absorptive feature that peaks at 410 nm and a broad absorption between 500 and 650 nm.

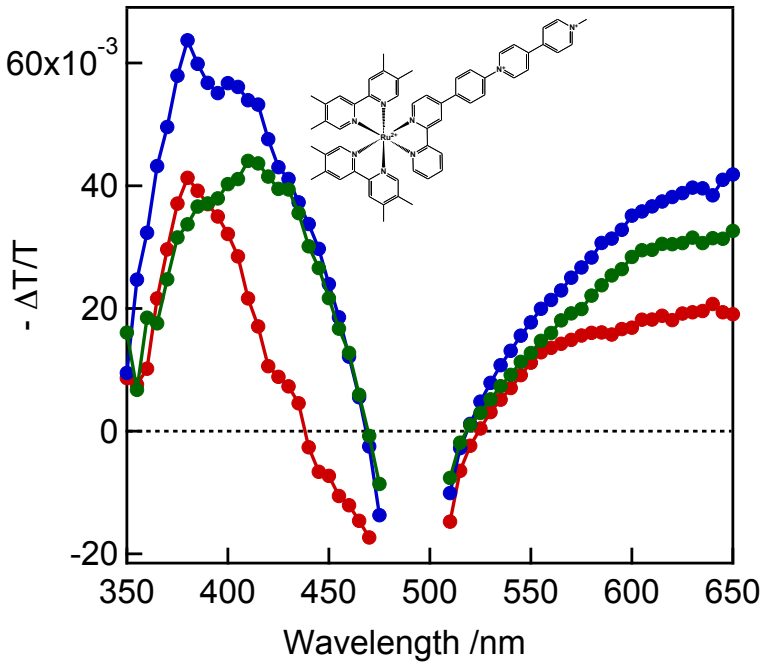

Figure 4.10 Transient Absorption Spectra of [Ru(tmb)$_2$(bpy-phenyl-MV)](PF$_6$)$_4$ (**3**) in room temperature acetonitrile collected 0.5 ps (red) 1.5 ps (blue) and 5.0 ps (green) following excitation with a 500 nm, ~80 fs pump pulse. Data between 475 and 510 nm has been removed since it was strongly contaminated with scatter from the pump pulse.

The TA spectra confirmed the formation of the ET product now we turn to TA single wavelength kinetics which will be used to extract the lifetimes for forward electron transfer (ET) and back electron transfer (BET). Where these data differ from TA spectra is that they allow for monitoring excited state dynamics at a single probe wavelength as a function of time and the data is fit to obtain ET and BET lifetimes (or rate constants). These

data are generally plotted as a negative change in transmittance versus time for each probe wavelength. The TA spectra are also used a means of determining which probe wavelengths will be best for determining electron transfer lifetimes. Ideally, one would choose probe wavelengths where all transient signal is attributed to the ET photoproduct however as evidenced from TA spectra of the donor and the DBA complexes there are no wavelengths available within our experimental setup that will allow for uniquely probing the ET photoproduct. From the discussion of the TA spectra above, probe wavelengths of 370, ~400 nm and 607 nm were selected. Probing at ~400 nm and 607 nm allow for monitoring the dynamics at wavelengths where the ET product has significant absorbance. While probing at 370 nm allows for probing at a wavelength where the excited state donor absorbs at early times and then ET photoproduct at later times.

The single wavelength kinetic data for $[Ru(bpy)_2(bpy\text{-}phenyl\text{-}MV)](PF_6)_4$ (**1**) collected in room temperature acetonitrile with an ~500 nm (80 fs fwhm) pump pulse are shown below in **Figure 4.11**. The raw data is shown in blue and a fit of the data is shown in red. Where the data were fit with a multi-exponential function. What is seen from the data probing at 400 nm (middle panel) and 607 nm (middle panel) is that the dynamics are similar at these probe colors. A rise feature at early times is assumed to be the build up of the ET photoproduct followed a decay that can be attributed to the subsequent decay of the photoproduct to the ground state. This assignment will be discussed further below. However the data probing at 370 nm is qualitatively different where no rise feature is observed and only a decay feature is observed. What is clear from the insets in **Figure 4.11** is that a majority of the dynamics occur within the first 20 ps indicating the ET process is occurring rapidly for these complexes.

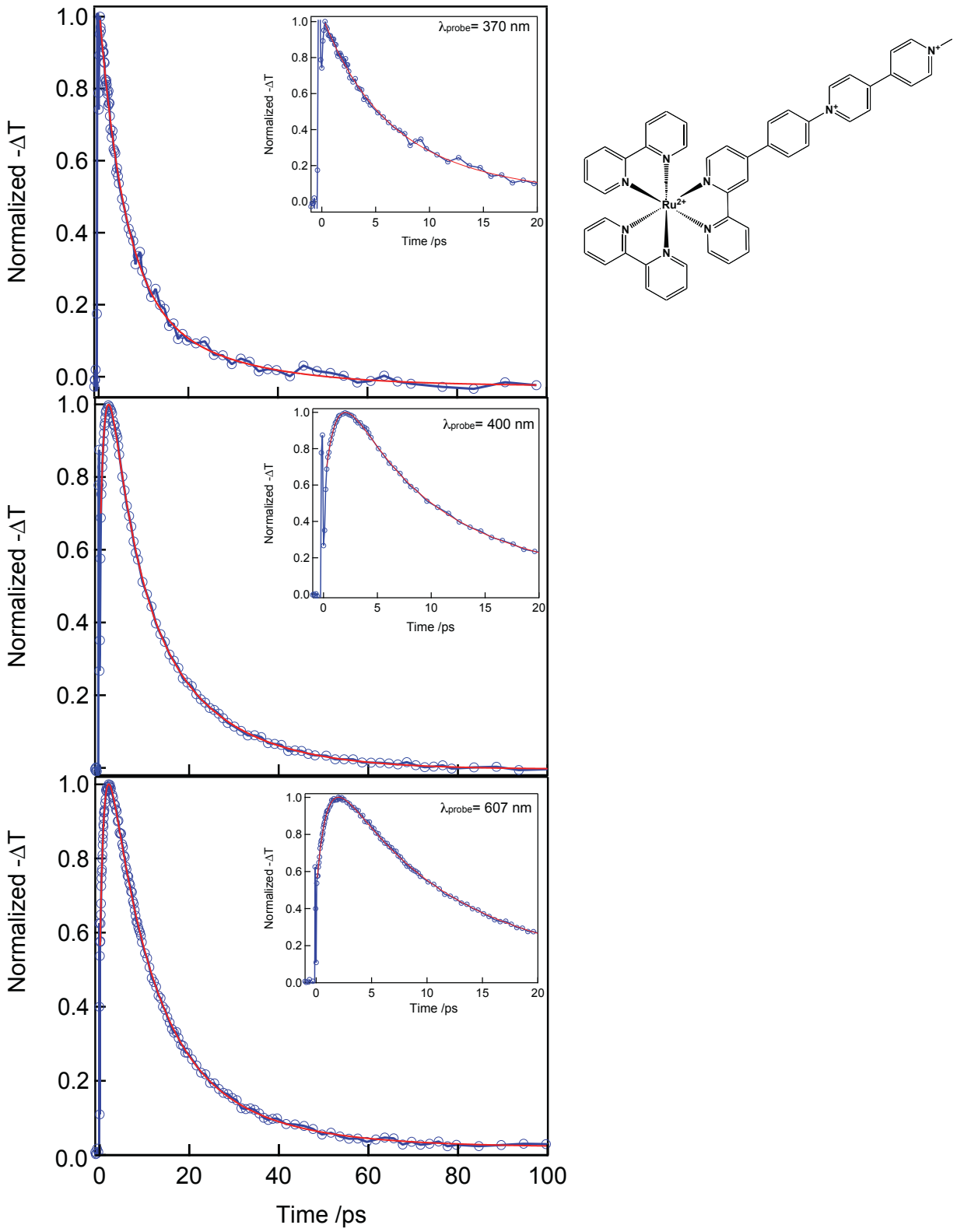

Figure 4.11 Transient absorption kinetics for (**1**) in room temperature acetonitrile collected with ~500 nm pump pulse and at a probe wavelength of 370 nm (top), 400 nm (middle) and 607 nm (bottom). The raw data (blue) was fit with a multi-exponential function (red).

The ET systems were designed with an initial expectation that they would follow the simple kinetic scheme shown below in **Scheme 4.1**. Absorption of a visible photon followed by rapid intersystem crossing leads to the formation of the ^{3}MLCT excited state, D*-B-A. From this state the charge separated state or the ET photoproduct, D^+-B-A^-, is formed with the rate constant k_{ET}. Recovery of the ground state, D-B-A, from the ET state, D^+-B-A^-, is described by the rate constant k_{BET}. Assuming that the ^{3}MLCT state is formed prior to the electron transfer step, which is a valid assumption since this process is known to occur within 100 fs,[57-61] one would expect to fit the single wavelength TA data with a bi-exponential function where one exponential describes the forward ET process and the second the back ET process.

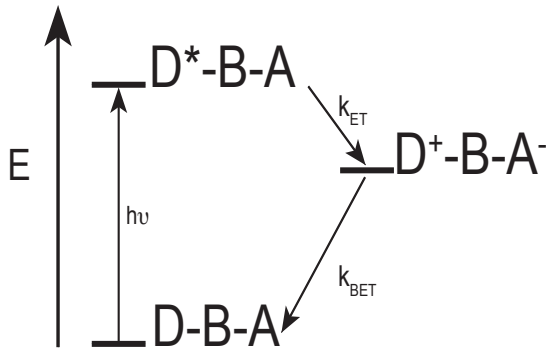

Scheme 4.1 Proposed kinetic scheme for DBA complexes upon absorption of a visible photon (hυ) where kET is the rate constant for forward electron transfer and kBET the rate constant for back electron transfer. The intersystem from crossing from ^{1}MLCT to ^{3}MLCT is not shown in the scheme.

However the single wavelength kinetic data probing at 400 nm and 607 nm does not fit to a bi-exponential function. A third exponential component is needed to properly fit the data.

The details of the fitting process can be found in Appendix Two; briefly the fits were performed using Igor Pro 6.0 where fitting functions were programmed in-house. The

initial and final data points to be fit were chosen manually. The starting point was selected as the first data point after the coherent solvent spike (which was manually set as t_0). The last data point at 100 ps was set as final data point to be fit. The best fit was determined by visual inspection and by minimizing the error from the extracted lifetimes. From the fits of the data probing at 400 nm and 607 nm three similar lifetimes were extracted, a fast component τ_1= ~1ps, and an intermediate component τ_2=~8 ps and a long component τ_3=~20 ps. When fitting the λ_{probe}=370 nm data a bi-exponential function is needed and the extracted lifetimes are commensurate with τ_2 and τ_3 stated above. Admittedly, the need to fit the λ_{probe}=400 nm and λ_{probe}=607 nm data with a third exponential component was unexpected. Before attempting to assign the ET lifetimes and identify the third component, the single wavelength kinetic data of $[Ru(dmb)_2(bpy\text{-}phenyl\text{-}MV)](PF_6)_4$ (**2**) and $[Ru(tmb)_2(bpy\text{-}phenyl\text{-}MV)](PF_6)_4$ (**3**) will be presented. By doing this one can determine if a third exponential component is needed to also fit these data or if it is unique to $[Ru(bpy)_2(bpy\text{-}phenyl\text{-}MV)](PF_6)_4$ (**1**).

The single wavelength kinetic data for $[Ru(dmb)_2(bpy\text{-}phenyl\text{-}MV)](PF_6)_4$ (**2**) and $[Ru(tmb)_2(bpy\text{-}phenyl\text{-}MV)](PF_6)_4$ (**3**) recorded in room temperature acetonitrile with an ~500 nm pump pulse (80 fs fwhm) and probing at 370 nm (top panel), 420 nm (middle) panel) and 607 nm (bottom panel) are shown below in **Figures 4.12** and **4.13**, respectively. The raw data are shown in blue and the fit of the data is shown in red. Multi-exponential functions were used to fit the data.

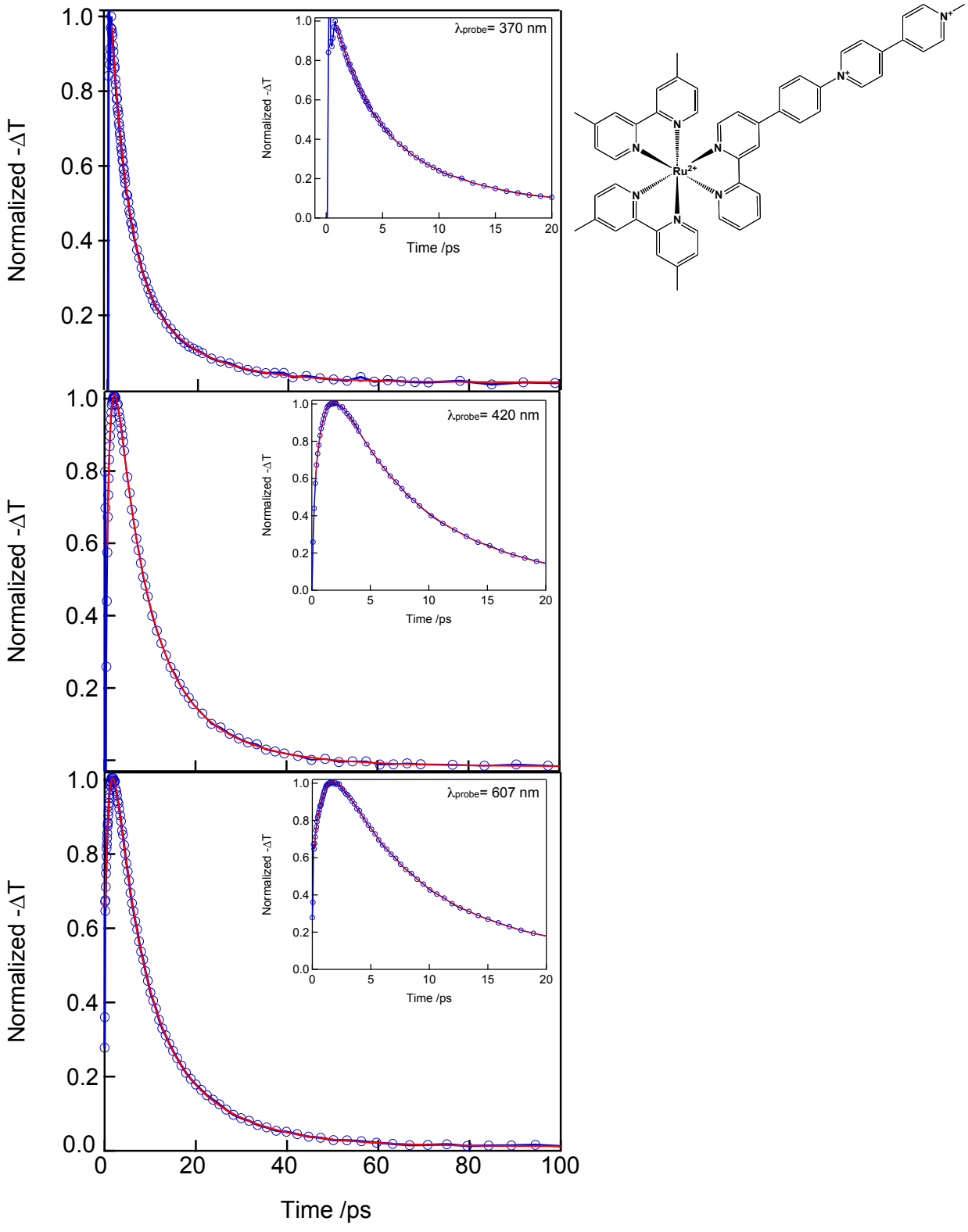

Figure 4.12 Transient absorption kinetics for (**2**) in room temperature acetonitrile collected with ~500 nm pump pulse and at a probe wavelength of 370 nm (top), 420 nm (middle) and 607 nm (bottom). The raw data (blue) was fit with a multi-exponential function (red).

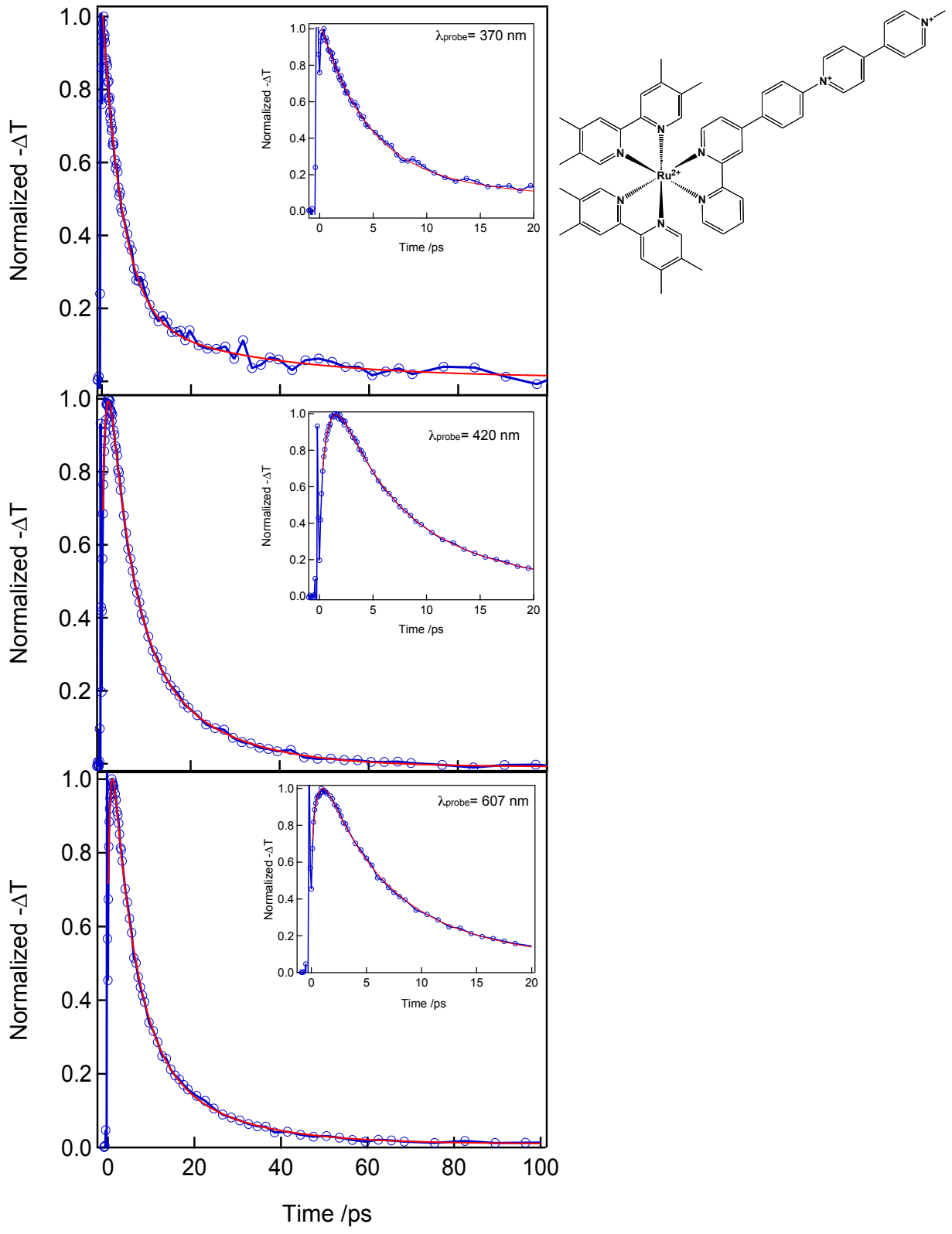

Figure 4.13 Transient absorption kinetics for (**3**) in room temperature acetonitrile collected with ~500 nm pump pulse and at a probe wavelength of 370 nm (top), 420 nm (middle) and 607 nm (bottom). The raw data (blue) was fit with a multi-exponential function (red).

Consistent with data for $[Ru(bpy)_2(bpy\text{-}phenyl\text{-}MV)](PF_6)_4$ (**1**) the data probing at 420 nm and 607 nm shows a rise and a decay feature while the data probing at 370 nm shows a decay feature. Also, like that of $[Ru(bpy)_2(bpy\text{-}phenyl\text{-}MV)](PF_6)_4$ (**1**) a majority of the dynamics occur within the first 20 ps after excitation as evidenced by the insets. For both complexes, (**2**) and (**3**), satisfactory fits of the data probing at 420 nm and 607 nm required three exponentials. For $[Ru(dmb)_2(bpy\text{-}phenyl\text{-}MV)](PF_6)_4$ (**2**) the values of the extracted lifetimes are a fast component τ_1= ~0.9 ps, an intermediate component τ_2=~6 ps and a long component τ_3=~16 ps. When fitting 370 nm probe data for (**2**) two exponential components are required and the extracted lifetimes are on the order of τ_2 and τ_3 for (**2**) presented above. In accordance with the other two compounds in the series, fitting the single wavelength kinetic data of $[Ru(tmb)_2(bpy\text{-}phenyl\text{-}MV)](PF_6)_4$ (**3**) yielded a similar result. The data probing at 420 nm and 607 nm required three exponential components to be fit satisfactorily. The extracted lifetimes are a fast component τ_1= ~0.7 ps, an intermediate component τ_2=~4 ps and a long component τ_3=~16 ps. As with (**1**) and (**2**) the data probing at 370 nm for (**3**) required a bi-exponential function to be fit where the extracted lifetimes were commensurate with τ_2 and τ_3 for (**3**).

With the fits of the single wavelength data in hand one can begin to look for similarities among the components and assign them. **Table 4.4** contains the extracted lifetimes for each complex probing at 607 nm. The data at this probe wavelength was chosen because of the three wavelengths analyzed this is the lone wavelength where the ground state of the complexes does not absorb. It should be stated that **Table 4.4** is only an attempt to organize the extracted lifetimes. **Table 4.5** below contains detailed ET data with

lifetime assignments and error bars determined from three independent measurements of the single wavelength kinetics probing at 607 nm.

Table 4.4 Lifetimes from Single Wavelength Kinetic Data Probing at 607 nm.

Complex/Lifetime	τ_1 /ps	τ_2 /ps	τ_3/ps
$[Ru(bpy)_2(bpy\text{-}phenyl\text{-}MV)](PF_6)_4$ (**1**)	1	8	20
$[Ru(dmb)_2(bpy\text{-}phenyl\text{-}MV)](PF_6)_4$ (**2**)	0.87	6.3	16
$[Ru(tmb)_2(bpy\text{-}phenyl\text{-}MV)](PF_6)_4$ (**3**)	0.74	4.5	16.4

From **Table 4.4** we see that the lifetimes for the complexes are similar. There is a fast component on the order of a picosecond, an intermediate component between 4 and 8 ps, and a long-time component of ~20 ps for (**1**) and ~16 ps for both (**2**) and (**3**). Since the long-time component shows no significant driving force dependence it is taken that this component does not arise from either of the two electron transfer steps (forward or back ET) and must be attributed to another excited state process. It is necessary to note that in Chapter Five the TA experiments performed on DBA complexes with steric bulk on the bridging ligand will be presented and it will be established that a third component is not required to fit the single wavelength kinetics data probing at ~400 and ~600 nm. So not only is the long-time component generally insensitive to driving force it is only present for DBA complexes where (**L1**) is the electroactive ligand. From this we conclude that τ_3 must be related to the structural feature that is unique to only these three DBA complexes, the non-methylated electroactive asymmetric ligand (**L1**).

However to ensure that τ_3 does not originate from a relaxation process within the donor, D*-B-A, we will examine the processes that are known to occur in the early time dynamics of $[Ru(bpy)_3]^{2+}$ and its derivatives upon photo-excitation with a visible photon. The initial Franck-Condon state (^{1}MLCT) formed upon photo-excitation with a visible photon undergoes an intersystem crossing within 100 fs to form the ^{3}MLCT state.[57-61] From

transient absorption data from McCusker's group it is known that the ^{3}MLCT is vibrationally relaxed within 300 fs after excitation.[51,59,62] However, the timescale for vibrational cooling from the hot ^{3}MLCT state in $[Ru(bpy)_3]^{2+}$ and other polypyridyl complexes has been determined to occur on a 5-20 ps timescale.[63-65] Based on this it is possible to assign τ_3 as vibrational cooling within the ^{3}MLCT. However, what seems unlikely is that the vibrational cooling component would not be present in the excited state dynamics of the DBA complexes with steric bulk. Therefore, we conclude that vibrational cooling within the ^{3}MLCT is not a viable assignment for the long-time component.

Within the community that studies homoleptic polypyridyl complexes of d^6 transition metal complexes (of Fe, Ru and Os) there is much contention surrounding the nature of the initial MLCT excitation. The contention is centered on the question regarding whether the initial excitation is localized onto one ligand or if it is delocalized on all three ligands and if it is delocalized what is the time scale for localization onto one ligand.[66-72] Many different types of experiments in polar solvents have been conducted to solve this problem including Stark spectroscopy,[69,73,74] resonance Raman,[75] solvatochromism[76] and ultrafast experiments.[55,62] The Stark spectroscopy, resonance Raman and solvatochromism experiments supported the finding that the initial excitation is localized onto one ligand however more recent ultrafast experiments find that the initial excitation is localized onto one ligand on a sub 100 fs timescale. Regardless of the nature of the initial excitation it is clear that the sub 100 fs localization dynamics are not the origin of the observed long-time component in the excited state dynamics of the DBA complexes.

Lastly, interligand electron transfer (ILET) is known to occur in the excited states of $[Ru(bpy)_3]^{2+}$ and $[Os(bpy)_3]^{2+}$and their derivatives. This process is commonly referred to as

electron hopping and can be thought of an electron hopping from one bpy ligand to another. The timescale for ILET was thought to occur on the order of ~50 ps[64] however recent theoretical and experimental measurements have found this process to occur on a sub-picosecond timescale for both homo- and heteroleptic derivatives of $[Ru(bpy)_3]^{2+}$ [55,77,78] and $[Os(bpy)_3]^{2+}$. [79] Also, the DBA complexes have different ancillary ligands that vary in energy and because of this one would expect differences in ILET lifetimes. However, no significant differences in τ_3 are observed within the series. For these two reasons we conclude that it is unlikely for ILET to be the excited state process described by the long-time component, τ_3.

It has been shown that τ_3 is not attributed to a relaxation process with the ^{3}MLCT state. It is possible for τ_3 to be related to a ligand-centered triplet (^{3}LC) formed via a triplet-triplet energy transfer process (E_nT). Ruthenium polypyridyl dyads and triads have been shown to undergo intramolecular $^3LC \leftarrow {}^3MLCT$ as a deactivation pathway from the ^{3}MLCT.[80-83] The E_nT process can be thought of as the transfer of excitation energy between donor and acceptor moieties (where charges are not transferred). However using quantum calculations to estimate the energy of the ^{3}LC of the DBA complexes it was established that ^{3}LC lies ~0.8 eV above the ^{3}MLCT. Therefore rendering the ^{3}LC state inaccessible from the ^{3}MLCT state. Furthermore, the fact that τ_3 exhibits no significant dependence on ancillary ligand signifies the process responsible for this component must not involve the metal center.

Now that the possible excited state processes of ruthenium (II) polypyridine complexes and other potential triplet excited states have been eliminated as possible explanations for the long-time component, we return to the proposed origin of this

component stated above that τ_3 must be the lifetime of a process involving the non-methylated electroactive asymmetric ligand (**L1**). Recall that the TD-DFT calculations for these complexes predicted direct excitations from the metal center to the acceptor moieties of these complexes (**Figure 4.6** above). This implies that upon absorption of a visible photon a fraction of the excitation produces an excited state that electronically resembles the ET photoproduct. Alternatively, the electroactive ligand has been reduced upon photo-excitation. This excitation process is summarized in **Equation 4.8** where anc. L denotes an ancillary ligand and asymm. L denotes the asymmetric ligand. Recall for a MLCT transition the excited state is expected to lie on the 2,2'-bipyridine moiety of the asymmetric ligand.

$$[Ru^{2+}(\text{anc. L})_2(\text{asymm. L})^{2+}] \xrightarrow{h\upsilon} [Ru^{3+}(\text{anc. L})_2(\text{asymm. L})^{+}]^* \qquad \textbf{Equation 4.8}$$

Although MV^{2+} is very commonly used as an electron acceptor[84] very few studies describe the excited state dynamics of the methyl viologen radical cation, $MV^{\bullet+}$. Hammarström and co-workers[85] conducted ultrafast pump-probe experiments on methyl viologen radical cation ($MV^{\bullet+}$) in room temperature acetonitrile. Following formation of the radical cation from bulk electrolysis the sample was excited with a 730 nm pump pulse and probed at 430 and 600 nm. The experiment revealed a 16 ps component that was assigned as the lifetime of the vibrationally excited ground state of $MV^{\bullet+}$. We expect that the direct excitation would create an electronic excited state on the acceptor moiety similar to the radical cation of the asymmetric ligand (**L1**) and excitation would undoubtedly be to a hot vibrational state of the acceptor. Since the value assigned to τ_3 is essentially that of the vibrationally excited state of $MV^{\bullet+}$ we assign τ_3 as the vibrationally excited lifetime of the

directly excited acceptor. Recall when fitting the probe data at 370 for these complexes the long-lived component was also extracted. Upon investigation of the reductive spectroelectrochemical data for these DBA complexes we find that radical cation of the asymmetric ligand absorbs at this wavelength and it is not surprising to find that dynamics probed at this color would include a contribution from the ET product.

With τ_3 assigned as the vibrationally excited lifetime of the directly excited acceptor this leaves τ_1 and τ_2 as the electron transfer lifetimes. There are two plausible scenarios when assigning electron transfer lifetimes. The first is known as normal kinetics where $\tau_{BET} > \tau_{ET}$ (or $k_{BET} < k_{ET}$), this is the intuitive assignment that the rise feature observed in the TA single wavelength kinetic data is attributed to the build up of the ET photoproduct and the decay to the subsequent recovery of the ground state from D^+-B-A^-. For similar DBA systems prepared where a methylene spacer separated the donor moiety from the MV^{2+} acceptor the kinetics were assigned as normal.[8,9,86,87] However, others who have measured photoinduced intramolecular ET rates from a ruthenium polypyridine donor to a MV^{2+} acceptor covalently linked through an ethyl spacer or longer carbon chains[88-91] observed the second scenario known as inverted kinetics[92] where $\tau_{BET} < \tau_{ET}$ (or $k_{BET} > k_{ET}$). In this scenario there is no build up of the ET photoproduct since the rate of decay to the ground state is greater than that for forming the ET photoproduct.

As stated above one way to unambiguously assign normal or inverted kinetics of ET would be to probe at a wavelength where the TA signal was uniquely attributed to either D*-B-A or D^+-B-A^+. However, this is not possible given our current experimental setup because both the Ru donor and ET photoproduct have TA signals at the probe wavelengths. Another way to independently measure τ_{ET} would be through time-resolved emission

experiments of the DBA complexes. Unfortunately these measurements would be very difficult for this system. Based on a comparison with the donor complexes the radiative lifetimes of the DBA complexes would be on the order of 10 μs (see **Table 4.1**). This means that very few photons will be emitted over the course of the very rapid ET process (<20 ps). Therefore to assign the kinetics as normal or inverted we turn to simulating the TA spectra and kinetics for both scenarios. The simulations unambiguously show that the ET kinetics are, in fact, normal. A detailed presentation of these simulations can be found in Appendix 2 but the main points will be presented here.

As seen above, the TA spectra for these complexes between 350 nm and 500 nm are distinctive and in our attempt to simulate these dynamics we chose to focus on the data in this wavelength region. Since τ_3 was found to be a component that is independent of the ET process it has not been included in the simulation. Simulations of the TA spectra were performed in Mathematica 8 utilizing the basic functions available in the software. Below, the simulated TA spectra for $[Ru(bpy)_2(bpy\text{-}phenyl\text{-}MV)](PF_6)_4$ (**1**) are presented. Analysis for $[Ru(dmb)_2(bpy\text{-}phenyl\text{-}MV)](PF_6)_4$ (**2**) and $[Ru(tmb)_2(bpy\text{-}phenyl\text{-}MV)](PF_6)_4$ (**3**) yield the same results, these simulations are reported in detail in Appendix Two. To begin the simulation, two Gaussian functions were defined to describe the experimental peak centered at 370 nm assigned to absorbance of the ^{3}MLCT of the donor and the experimental peak centered at 402 nm which corresponds to the absorbance from the ET photoproduct (see **Figure 4.8** above). To generate accurate Gaussians the peak widths and heights were estimated from the experimental spectra. For better qualitative agreement with experimental TA spectra the Gaussians were centered at their respective experimental maxima (370 nm and 402 nm for donor and ET, respectively). To introduce time

dependence each Gaussian was multiplied by the solution to the kinetic equation describing its respective state. Specifically, the Gaussian centered at 370 nm was multiplied the kinetic equation describing the depletion of the ^{3}MLCT and the peak centered at 402 was multiplied by the kinetic solution describing the formation and subsequent loss of the ET photoproduct. Finally, to simulate normal kinetics τ_{ET} was set as the fast time component (1 ps) and τ_{BET} set to the intermediate component (8 ps). For the inverted kinetics simulations assignment of these lifetimes was reversed. The simulated spectra for both normal and inverted kinetics are shown below in **Figures 4.14** and **4.15**, respectively. As can be clearly seen from **Figure 4.14** the dynamics simulated from assuming normal kinetics match those of the experimental spectra while those of the inverted do not. From this τ_{ET} is assigned as the fast component (τ_1) and τ_{BET} as the intermediate component (τ_2).

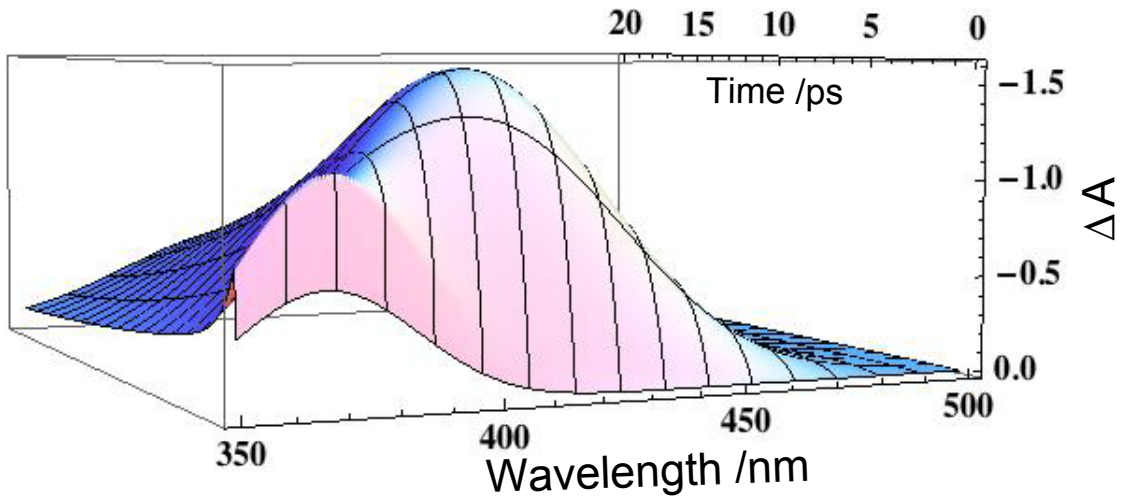

Figure 4.14 Simulation of TA spectra for [Ru(bpy)$_2$(bpy-phenyl-MV)](PF$_6$)$_4$ (**1**) between 350 -500 nm over a 20 ps time window assuming normal kinetics. The simulation details are described fully in Appendix Two.

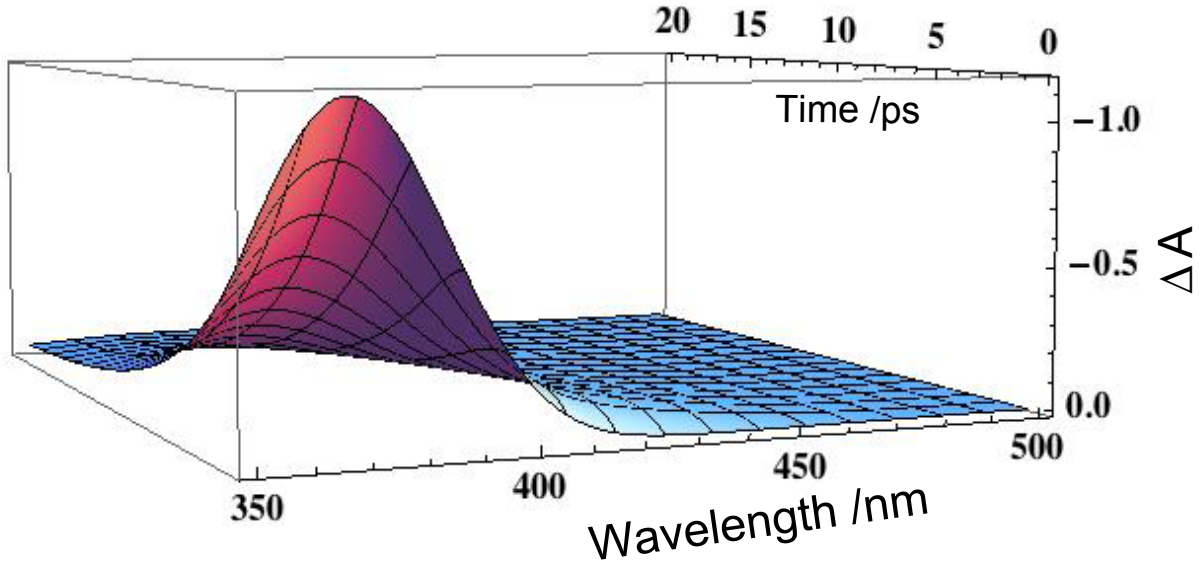

Figure 4.15 Simulation of TA spectra for $[Ru(bpy)_2(bpy\text{-}phenyl\text{-}MV)](PF_6)_4$ (**1**) between 350 -500 nm over a 20 ps time window assuming inverted kinetics. The simulation details are described fully in Appendix Two.

The assigned lifetimes and respective experimental error bars are listed in **Table 4.5**. The error bars were determined from three independent measurements of single wavelength kinetic data probing at 607 nm for each complex.

Table 4.5 Electron Transfer Data of Complexes in Room Temperature Acetonitrile.

Fit parameter/Complex	(**1**)	(**2**)	(**3**)
$k_{ET}/10^{12}\ s^{-1}$	1	1.1	1.4
τ_{ET} /ps	1±0.4	0.87±0.2	0.74±0.1
$k_{BET}/10^{12}\ s^{-1}$	0.13	0.16	0.22
τ_{BET} /ps	8±2	6.3±0.6	4.5±1.0
$k_3/10^{10}\ s^{-1}$	5.0	6.3	6.09
τ_3/ps	20±1.2	16±2.0	16.4±2.2

The error bars reported in this table represent 2σ determined from fitting three separate measurements of kinetics collected at λ_{probe} =607 nm for each complex.

From **Table 4.5** we see that the forward electron transfer process occurs rapidly and becomes faster for complexes (**2**) and (**3**). This is expected as driving force for forward ET increases from -0.65 eV for (**1**) to -0.70 eV for (**3**). The measured values for τ_{ET} validate our original claim for preparing the complexes in this series, namely, that structural changes on

the ancillary ligand affect the electron transfer lifetimes. The rapid formation of the ET state signifies that there must be strong electronic communication between the donor chromophore and acceptor moiety.

The effect of structural changes is also manifested in the lifetimes for back electron transfer, τ_{BET}, where a 150 mV difference in driving force between (**1**) and (**3**) leads to halving the lifetime of the ET photoproduct. However, counter to intuition the complex with the largest driving force for back ET (**1**) has the longest lifetime (8 ps). This leads to the assumption that the back electron transfer process is occurring in the Marcus inverted region where reaction rates decrease with increased driving force.[93,94] To determine if the back ET process is occurring the Marcus inverted region the value of total reorganization energy, λ, is needed. Total reorganization energy is energy required for structural rearrangements of both the reactants and solvent molecules in order to assume the configuration of the electron transfer product. The inverted region is characterized by having $\Delta G^0_{BET} > -\lambda$. Temperature dependent TA single wavelength kinetic studies are often used to measure λ. However, these experiments were not conducted on these systems. Therefore we will estimate λ from similar systems prepared by our group. It was found from temperature dependent studies on similar DBA systems with a methylene spacer in the bridging ligand (see **Figure 1.3**) that λ for back ET is about ~1.0 eV.[95] Since $-\lambda$ is less than ΔG^0_{BET} we assume that the back ET process is occurring in the inverted region. Admittedly, this is an estimate but we feel that the values of λ for the two DBA systems (directly linked vs. containing a methylene spacer) will not vary significantly.

4.4 Concluding Remarks

In this chapter the photophysics and photoinduced electron transfer processes for the complexes in the driving force series have been presented. The complexes were characterized by absorption, emission and ultrafast pump-probe spectroscopies as well as by quantum calculations. The UV-visible absorption spectra of the DBA complexes revealed that when compared to those of the respective donor an increase in absorption between 500 and 600 nm is observed. This effect is most pronounced for $[Ru(tmb)_2(bpy\text{-}phenyl\text{-}MV)](PF_6)_4$ (**3**) where the growth of a second peak is observed. Utilizing DFT and TD-DFT methods it was found that the increased absorbance was brought about by delocalization of the ^{3}MLCT excited state onto the asymmetric ligand. The TD-DFT calculations also predicted direct excitation from the metal center to the acceptor moiety.

It was established that there is sufficient driving force for electron transfer. Ultrafast pump-probe experiments confirmed the formation of the electron transfer photoproduct. The TA spectra provided information about the absorptive properties of the ET state while the TA single wavelength kinetics data were used to extract electron transfer lifetimes. From the fits of the TA single wavelength data it was revealed that in addition to the two lifetimes needed to describe the ET reaction (forward and back ET) a third component is needed. The third component was assigned as the lifetime of the vibrationally excited acceptor after direct excitation. The other two components were assigned as forward and back electron transfer lifetimes and it was established that ET dynamics exhibited normal kinetic behavior.

Analysis of τ_{ET} for the complexes in this series concluded that the electron transfer is very rapid in these systems and there is evidence validating our reasons for preparing

these complexes in that structural changes can determine ET lifetimes. Estimation of reorganization energy leads to the conclusion that τ_{BET} occurs in the Marcus inverted region. The extracted rate constants agree with the predictions of Marcus theory in that k_{BET} decreases with increased driving force.

This chapter focused on the effects of varying the structure of the ancillary ligand on the properties of DBA complexes. Differences in electron transfer lifetimes were observed. In the next chapter we explore the effect of systematic addition of steric bulk on the bridging ligand while not varying the ancillary ligand.

4.5 References

(1) Juris, A.; Balzani, V.; Barigelletti, F.; Campagna, S.; Belser, P.; Von Zelewsky, A. *Coord. Chem. Rev.* **1988**, *84*, 85.

(2) Kalyanasundaram, K. *Photochemistry of Polypyridine and Porphyrin Complexes*; Academic Press Inc.: San Diego, 1992.

(3) Lever, A. B. P. *Inorg. Chem.* **1990**, *29*, 1271.

(4) Sauvage, J.-P.; Collin, J.-P.; Chambron, J.-C.; Guillerez, S.; Coudret, C. *Chem. Rev.* **1994**, *94*, 993.

(5) Vos, J. G.; Kelly, J. M. *Dalton T* **2006**, 4869.

(6) Anderson, P. A.; Keene, F. R.; Meyer, T. J.; Moss, J. A.; Strouse, G. F.; Treadway, J. A. *J Chem Soc Dalton* **2002**, 3820.

(7) Ghosh, B. K.; Chakravorty, A. *Coord. Chem. Rev.* **1989**, *95*, 239.

(8) Meylemans, H. A.; Lei, C. F.; Damrauer, N. H. *Inorg. Chem.* **2008**, *47*, 4060.

(9) Meylemans, H. A.; Hewitt, J. T.; Abdelhaq, M.; Vallett, P. J.; Damrauer, N. H. *J. Am. Chem. Soc.* **2010**, *132*, 11464.

(10) McDaniel, A. M.; Tseng, H. W.; Damrauer, N. H.; Shores, M. P. *Inorg. Chem.* **2010**, *49*, 7981.

(11) Shao, Y.; Molnar, L. F.; Jung, Y.; Kussmann, J.; Ochsenfeld, C.; Brown, S. T.; Gilbert, A. T.; Slipchenko, L. V.; Levchenko, S. V.; O'Neill, D. P.; DiStasio, R. A., Jr.; Lochan, R. C.; Wang, T.; Beran, G. J.; Besley, N. A.; Herbert, J. M.; Lin, C. Y.; Van Voorhis, T.; Chien, S. H.; Sodt, A.; Steele, R. P.; Rassolov, V. A.; Maslen, P. E.; Korambath, P. P.; Adamson, R. D.; Austin, B.; Baker, J.; Byrd, E. F.; Dachsel, H.; Doerksen, R. J.; Dreuw, A.; Dunietz, B. D.; Dutoi, A. D.; Furlani, T. R.; Gwaltney, S. R.; Heyden, A.; Hirata, S.; Hsu, C. P.; Kedziora, G.; Khalliulin, R. Z.; Klunzinger, P.; Lee, A. M.; Lee, M. S.; Liang, W.; Lotan, I.; Nair, N.; Peters, B.; Proynov, E. I.; Pieniazek, P. A.; Rhee, Y. M.; Ritchie, J.; Rosta, E.; Sherrill, C. D.; Simmonett, A. C.; Subotnik, J. E.; Woodcock, H. L., 3rd; Zhang, W.; Bell, A. T.; Chakraborty, A. K.; Chipman, D. M.; Keil, F. J.; Warshel, A.; Hehre, W. J.; Schaefer, H. F., 3rd; Kong, J.; Krylov, A. I.; Gill, P. M.; Head-Gordon, M. *Physical chemistry chemical physics : PCCP* **2006**, *8*, 3172.

(12) Chai, J. D.; Head-Gordon, M. *J. Chem. Phys.* **2008**, *128*, 084106.

(13) Gordon, M. S.; Binkley, J. S.; Pople, J. A.; Pietro, W. J.; Hehre, W. J. *J. Am. Chem. Soc.* **1982**, *104*, 2797.
(14) Binkley, J. S.; Pople, J. A.; Hehre, W. J. *J. Am. Chem. Soc.* **1980**, *102*, 929.
(15) Andrae, D.; Dolg, M.; Stoll, H.; Preub, H. *Theoret. Chim. Acta* **1990**, 123.
(16) Andrae, D.; Hiuflermann, U.; Dolg, M.; Stoll, H.; Preull, H. *Theoret. Chim. Acta* **1991**, 247.
(17) Hirata, S.; Head-Gordon, M. *Chem. Phys. Lett.* **1999**, *3*, 291.
(18) Head-Gordon, M.; Grana, A. M.; Maurice, D.; White, C. A. *J. Phys. Chem.* **1995**, *1995*, 14261.
(19) Varetto, U.; 5.4.0.8 ed.; Swiss National Supercomputing Centre: Manno, Switzerland, 2009.
(20) Shirakawa, A.; Kobayashi, T. *Appl. Phys. Lett* **1998**, *72*, 147.
(21) Wilhelm, T.; Piel, J.; Riedle, E. *Opt. Lett.* **1997**, *22*, 1494.
(22) Megerle, U.; Pugliesi, I.; Schriever, C.; Sailer, C. F.; Riedle, E. *Appl. Phys. B* **2009**, *96*, 215.
(23) Grumstrup, E. M.; Johnson, J. C.; Damrauer, N. H. *Phys. Rev. Lett.* **2010**, *105*, 257403.
(24) Kovalenko, S. A.; Dobryakov, A. L.; Ruthmann, J.; Ernsting, N. P. *Phys. Rev. A* **1999**, *59*, 2369.
(25) Zhou, Q. X.; Lei, W. H.; Li, C.; Hou, Y. J.; Wang, X. S.; Zhang, B. W. *New Journal of Chemistry* **2010**, *34*, 137.
(26) Hayes, M. A.; Meckel, C.; Schatz, E.; Ward, M. D. *J Chem Soc Dalton* **1992**, 703.
(27) Sun, Y. J.; El Ojaimi, M.; Hammitt, R.; Thummel, R. P.; Turro, C. *J. Phys. Chem. B* **2010**, *114*, 14664.
(28) Henrich, J. D.; Zhang, H. Y.; Dutta, P. K.; Kohler, B. *J. Phys. Chem. B* **2010**, *114*, 14679.
(29) Strouse, G. F.; Schoonover, J. R.; Duesing, R.; Boyde, S.; Jones, W. E.; Meyer, T. J. *Inorg. Chem.* **1995**, *34*, 473.
(30) Benniston, A. C.; Harriman, A.; Grosshenny, V.; Ziessel, R. *New Journal of Chemistry* **1997**, *21*, 405.
(31) Demas, J. N.; Crosby, G. A. *J. Phys. Chem.* **1971**, *75*, 991.
(32) Suzuki, K.; Kobayashi, A.; Kaneko, S.; Takehira, K.; Yoshihara, T.; Ishida, H.; Shiina, Y.; Oishic, S.; Tobita, S. *Phys. Chem. Chem. Phys.* **2009**, *11*, 9850.
(33) Parker, C. A.; Rees, W. T. *Analyst (London)* **1960**, *85*, 587.
(34) Kober, E. M.; Caspar, J. V.; Lumpkin, R. S.; Meyer, T. J. *J. Phys. Chem.* **1986**, *90*, 3722.
(35) Claude, J. P. Ph.D., University of North Carolina, 1995.
(36) Claude, J. P.; Meyer, T. J. *J. Phys. Chem.* **1995**, *99*, 51.
(37) Caspar, J. V.; Meyer, T. J. *J. Am. Chem. Soc.* **1983**, *105*, 5583.
(38) Chen, P.; Meyer, T. J. *Chem. Rev.* **1998**, *98*, 1439.
(39) Caspar, J. V.; Meyer, T. J. *J. Phys. Chem.* **1983**, *87*, 952.
(40) Robinson, G. W.; Frosch, R. P. *J. Chem. Phys.* **1963**, *38*, 1187.
(41) Siebrand, W. *J. Chem. Phys.* **1967**, *47*, 2411.
(42) Damrauer, N. H.; Boussie, T. R.; Devenney, M.; McCusker, J. K. *J. Am. Chem. Soc.* **1997**, *119*, 8253.
(43) Weller, A. *Z. Phys. Chem.* **1982**, *133*, 93.

(44) Vleck, A.; Zalis, S. *Coord. Chem. Rev.* **2007**, *251*, 258.
(45) Charlot, M. F.; Pellegrin, Y.; Quaranta, A.; Leibl, W.; Aukauloo, A. *Chem. Eur. J.* **2006**, *12*, 796.
(46) Ciofini, I.; Laine, P. P.; Bedioui, F.; Adamo, C. *J. Am. Chem. Soc.* **2004**, *126*, 10763.
(47) Meylemans, H. A.; Damrauer, N. H. *Inorg. Chem.* **2009**, *48*, 11161.
(48) Vallett, P. J.; Damrauer, N. H. *J. Phys. Chem. A* **2011**, *115*, 3122.
(49) Jacquemin, D.; Perpete, E. A.; Ciofini, I.; Adamo, C. *J. Chem. Theor. Comput.* **2010**, *6*, 1532.
(50) Song, J. A.; Gao, F.; Shi, B.; Liang, W. Z. *Phys. Chem. Chem. Phys.* **2010**, *12*, 13070.
(51) McCusker, J. K. *Acc. Chem. Res.* **2003**, *36*, 876.
(52) Balzani, V.; Campagna, S.; Denti, G.; Juris, A.; Serroni, S.; Venturi, M. *Acc. Chem. Res.* **1998**, *31*, 26.
(53) Braterman, P. S.; Harriman, A.; Heath, G. A.; Yellowlees, L. J. *J Chem Soc Dalton* **1983**, 1801.
(54) Yoshimura, A.; Hoffman, M. Z.; Sun, H. *J. Photochem. Photobiol. Chem.* **1993**, *70*, 29.
(55) Wallin, S.; Davidsson, J.; Modin, J.; Hammarstrom, L. *J. Phys. Chem. A* **2005**, *109*, 4697.
(56) Zalis, S.; Consani, C.; El Nahhas, A.; Cannizzo, A.; Chergui, M.; Hartl, F.; Vlcek, A. *Inorg. Chim. Acta* **2011**, *374*, 578.
(57) Cannizzo, A.; van Mourik, F.; Gawelda, W.; Zgrablic, G.; Bressler, C.; Chergui, M. *Angew Chem Int Ed* **2006**, *45*, 3174.
(58) Bhasikuttan, A. C.; Suzuki, M.; Nakashima, S.; Okada, T. *J. Am. Chem. Soc.* **2002**, *124*, 8398.
(59) Damrauer, N. H.; Cerullo, G.; Yeh, A.; Boussie, T. R.; Shank, C. V.; McCusker, J. K. *Science* **1997**, *275*, 54.
(60) Yoon, S.; Kukura, P.; Stuart, C. M.; Mathies, R. A. *Mol. Phys.* **2006**, *104*, 1275.
(61) Cannizzo, A.; Milne, C. J.; Consani, C.; Gawelda, W.; Bressler, C.; van Mourik, F.; Chergui, M. *Coord. Chem. Rev.* **2010**, *254*, 2677.
(62) Yeh, A.; Shank, C. V.; McCusker, J. K. *Science* **2000**, *289*, 935.
(63) Damrauer, N. H.; McCusker, J. K. *J. Phys. Chem. A* **1999**, *103*, 8440.
(64) Shaw, G. B.; Styers-Barnett, D. J.; Gannon, E. Z.; Granger, J. C.; Papanikolas, J. M. *J. Phys. Chem. A* **2004**, *108*, 4998.
(65) Henry, W.; Coates, C. G.; Brady, C.; Ronayne, K. L.; Matousek, P.; Towrie, M.; Botchway, S. W.; Parker, A. W.; Vos, J. G.; Browne, W. R.; McGarvey, J. J. *J. Phys. Chem. A* **2008**, *112*, 4537.
(66) Dearmond, M. K.; Carlin, C. M. *Coord. Chem. Rev.* **1981**, *36*, 325.
(67) Braun, D.; Huber, P.; Wudy, J.; Schmidt, J.; Yersin, H. *J. Phys. Chem.* **1994**, *98*, 8044.
(68) Riesen, H.; Wallace, L.; Krausz, E. *J. Phys. Chem.* **1996**, *100*, 17138.
(69) Riesen, H.; Krausz, E. *Chem. Phys. Lett.* **1996**, *260*, 130.
(70) Riesen, H.; Krausz, E. *J. Chem. Phys.* **1993**, *99*, 7614.
(71) Huber, P.; Yersin, H. *J. Phys. Chem.* **1993**, *97*, 12705.

(72) Turro, C.; Chung, Y. C.; Leventis, N.; Kuchenmeister, M. E.; Wagner, P. J.; Leroi, G. E. *Inorg. Chem.* **1996**, *35*, 5104.
(73) Oh, D. H.; Boxer, S. G. *J. Am. Chem. Soc.* **1989**, *111*, 1130.
(74) Karki, L.; Hupp, J. T. *Inorg. Chem.* **1997**, *36*, 3318.
(75) Webb, M. A.; Knorr, F. J.; McHale, J. L. *J Raman Spectrosc* **2001**, *32*, 481.
(76) Kober, E. M.; Sullivan, B. P.; Meyer, T. J. *Inorg. Chem.* **1984**, *23*, 2098.
(77) Hoff, D. A.; Silva, R.; Rego, L. G. C. *J. Phys. Chem. C* **2011**, *115*, 15617.
(78) Moret, M. E.; Tavernelli, I.; Chergui, M.; Rothlisberger, U. *Chemistry-a European Journal* **2010**, *16*, 5889.
(79) Miller, S. A.; Moran, A. M. *J. Phys. Chem. A* **2010**, *114*, 2117.
(80) Baudin, H. B.; Davidsson, J.; Serroni, S.; Juris, A.; Balzani, V.; Campagna, S.; Hammarstrom, L. *J. Phys. Chem. A* **2002**, *106*, 4312.
(81) Johansson, O.; Borgstrom, M.; Lomoth, R.; Palmblad, M.; Bergquist, J.; Hammarstrom, L.; Sun, L. C.; Akermark, B. *Inorg. Chem.* **2003**, *42*, 2908.
(82) Laine, P. P.; Bedioui, F.; Loiseau, F.; Chiorboli, C.; Campagna, S. *J. Am. Chem. Soc.* **2006**, *128*, 7510.
(83) Laine, P. P.; Loiseau, F.; Campagna, S.; Ciofini, I.; Adamo, C. *Inorg. Chem.* **2006**, *45*, 5538.
(84) Monk, P. M. S. *The viologens : physicochemical properties, synthesis, and applications of the salts of 4,4'-bipyridine*; Wiley: Chichester ; New York, 1998.
(85) Haupl, T.; Lomoth, R.; Hammarstrom, L. *J. Phys. Chem. A* **2003**, *107*, 435.
(86) Yonemoto, E. H.; Riley, R. L.; Kim, Y. I.; Atherton, S. J.; Schmehl, R. H.; Mallouk, T. E. *J. Am. Chem. Soc.* **1992**, *114*, 8081.
(87) Lomoth, R.; Haupl, T.; Johansson, O.; Hammarstrom, L. *Chem. Eur. J.* **2002**, *8*, 102.
(88) Yonemoto, E. H.; Saupe, G. B.; Schmehl, R. H.; Hubig, S. M.; Riley, R. L.; Iverson, B. L.; Mallouk, T. E. *J. Am. Chem. Soc.* **1994**, *116*, 4786.
(89) Cooley, L. F.; Larson, S. L.; Elliott, C. M.; Kelley, D. F. *J. Phys. Chem.* **1991**, *95*, 10694.
(90) Cooley, L. F.; Headford, C. E. L.; Elliott, C. M.; Kelley, D. F. *J. Am. Chem. Soc.* **1988**, *110*, 6673.
(91) Elliott, C. M.; Freitag, R. A.; Blaney, D. D. *J. Am. Chem. Soc.* **1985**, *107*, 4647.
(92) Palacios, R. E.; Kodis, G.; Gould, S. L.; Garza, L. d. l.; Brune, A.; Gust, D.; Moore, T. A.; Moore, A. L. *ChemPhysChem* **2005**, *6*, 2359.
(93) Marcus, R. A. *J. Chem. Phys.* **1956**, *24*, 966.
(94) Marcus, R. A. *Annu. Rev. Phys. Chem.* **1964**, *15*, 155.
(95) Meylemans, H.M; Synthesis and Investigation of Ruthneium Polypyridyl based Donor-Bridge-Acceptor Complexes toward Control of Electron Transfer Photochemistry. PhD. Dissertation. University of Colorado, 2010.

Chapter Five

Photophysical Characterization and Photoinduced Electron Transfer Analysis for Complexes in the Sterics Series.

5.1 Introductory Remarks

In Chapter Four the photophysics and photoinduced intramolecular electron transfer (ET) lifetimes of donor-bridge-Acceptor (DBA) complexes with minimal steric bulk on the bridging subunit were discussed. For the complexes in the driving-force series it was determined that structural modifications on the ancillary ligands play a role in determining electron transfer lifetimes by modulating the energetics of the complexes. In this chapter we shift to a discussion of the photophysics and ET lifetimes of DBA complexes with varying degrees of steric bulk on the bridging subunit. The addition of steric bulk on the bridging subunit is not expected to alter the driving forces for ET. The complexes in the sterics series were prepared to investigate how structural changes on the bridging subunit can control excited-state delocalization dynamics[1-5] thereby dictating ET lifetimes. By preparing DBA complexes varying in number and position of methyl substituents on the bridging subunit one can establish if steric bulk can effectively localize the transferred electron on the acceptor thus elongating the ET photoproduct lifetime while not substantially altering the rate of photoproduct formation.

The complexes discussed in this chapter are presented below in **Figure 5.1** (where dimethylphenyl has been abbreviated with dmp) both donor and corresponding DBA complexes are shown. Preparation of the complexes was described in detail in Chapter Three.

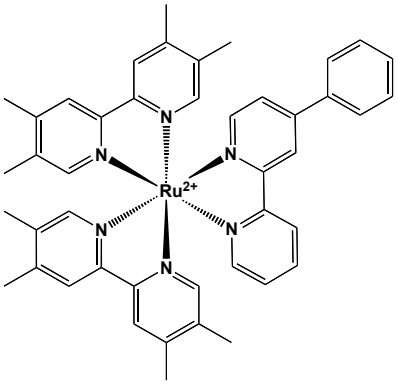

[Ru(tmb)$_2$(bpy-phenyl)]$^{2+}$(**3'**)

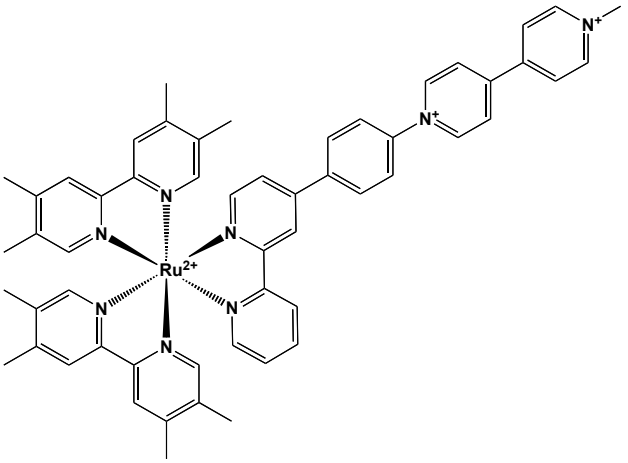

[Ru(tmb)$_2$(bpy-phenyl-MV)]$^{4+}$(**3**)

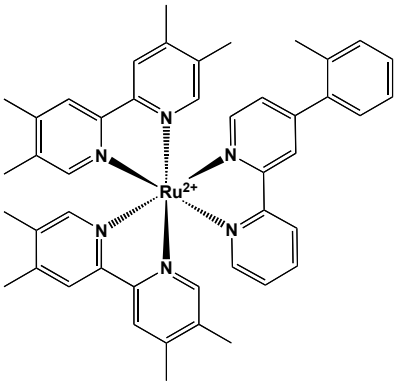

[Ru(tmb)$_2$(bpy-ortho)]$^{2+}$(**4'**)

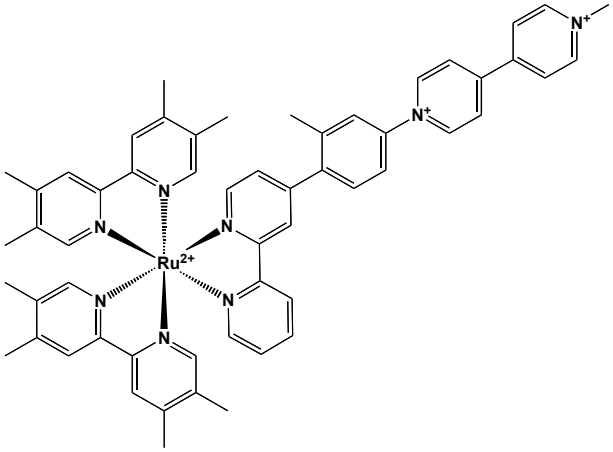

[Ru(tmb)$_2$(bpy-ortho-MV)]$^{4+}$(**4**)

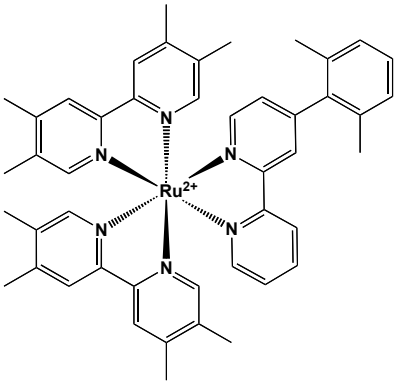

[Ru(tmb)$_2$(bpy-2,6-dmp)]$^{2+}$(**5'**)

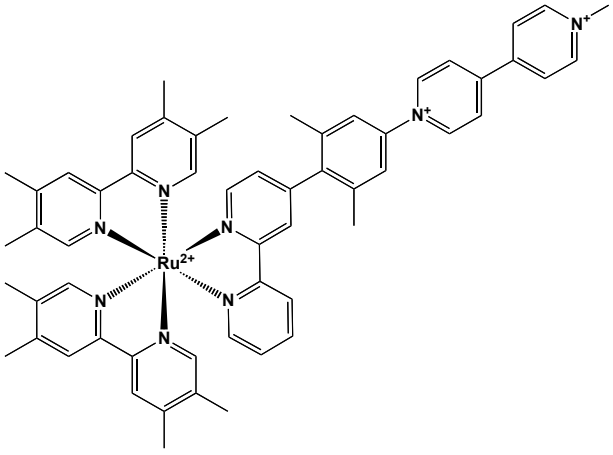

[Ru(tmb)$_2$(bpy-2,6-dmp-MV)]$^{4+}$(**5**)

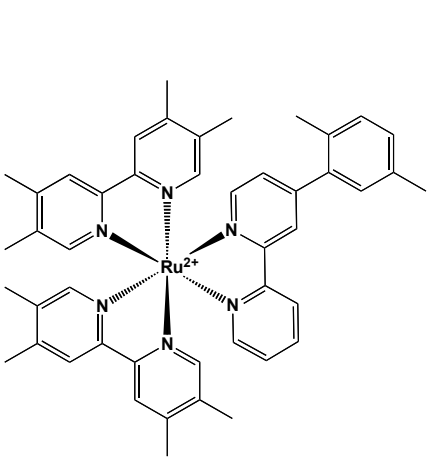

[Ru(tmb)$_2$(bpy-2,5-dmp)]$^{2+}$(**6'**)

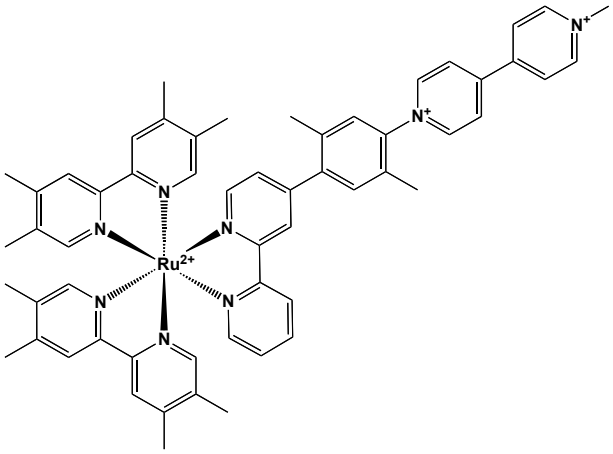

[Ru(tmb)$_2$(bpy-2,5-dmp)]$^{4+}$(**6**)

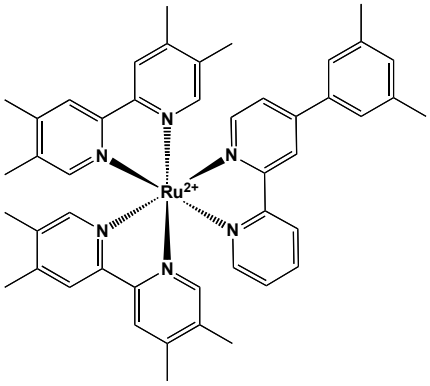

[Ru(tmb)$_2$(bpy-3,5-dmp)]$^{2+}$(**7'**)

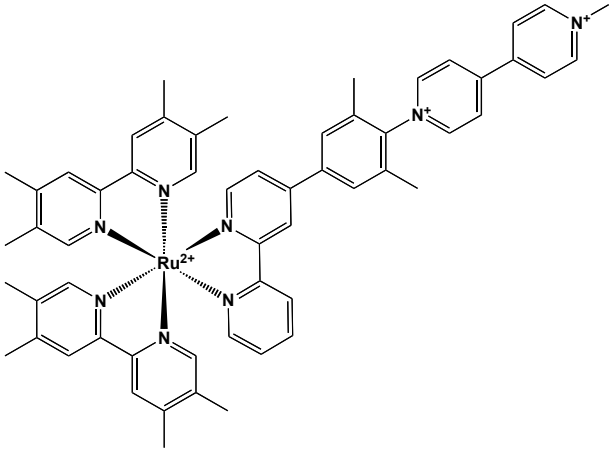

[Ru(tmb)$_2$(bpy-3,5-dmp)]$^{4+}$(**7**)

Figure 5.1 Donor (left) and Donor-Bridge-Acceptor (right) complexes in the sterics series. The complexes share ancillary ligands differ but differ by asymmetric aryl substituted ligand. The complexes were isolated as PF_6^- salts. Dimethylphenyl has been abbreviated by dmp.

The ligand 4,4',5,5'-tetramethyl-2,2'-bipyrdine (tmb) serves as the ancillary ligand for the complexes in this series. However, the complexes differ in asymmetric aryl substituted ligand. Five asymmetric electroactive ligands were prepared for the purpose of studying how number and position of methyl substituents affects ET lifetimes.

By choosing the same ancillary ligand for the complexes it is assumed that differences in driving forces for ET, ΔG^0_{ET} and ΔG^0_{BET}, will be minimal across the series[6]

implying that other factors are controlling ET lifetimes. Indeed we find differences in the ET lifetimes of these complexes, ultimately signifying that structural elements of the asymmetric ligand are playing a role in determining the lifetimes of photoinduced ET. This implies that steric bulk is influencing electronic communication between the donor and acceptor moieties by inhibiting excited state ring rotational dynamics that are known to bring out intraligand delocalization of the ^{3}MLCT state.

Building on the discussion presented in Chapter Four of the complexes with minimal steric bulk, steady state UV-visible absorption and emission experiments will be performed on the complexes to determine photophysical properties. The DBA complexes are found to be non-emissive in room temperature acetonitrile signifying that the complexes are utilizing other excited state deactivation pathways. Quantum calculations will be presented to aid in interpretation of the UV-visible absorption spectra. Driving forces for ET will be determined and ultrafast pump-probe spectroscopies will be utilized to detect and measure the lifetimes of the electron transfer photoproduct.

Experimental details have been described in **Section 4.2** of Chapter Four.

5.2 Results and Discussion

5.2.1 Steady State Absorption and Emission Spectroscopy

From **Figure 5.2** below we see that the complexes prepared in the sterics series exhibit the same ^{1}MLCT $\leftarrow$ ^{1}GS band as their parent complexes. **Figure 5.2** shows an overlay of the normalized UV-visible absorption spectra of the DBA complexes (black) with the corresponding donor complexes (red) recorded in room temperature acetonitrile. The normalized emission spectra of the donor complexes, also recorded in room temperature

acetonitrile, are also shown (blue). From top to bottom the spectra are presented in the following order $[Ru(tmb)_2(bpy\text{-}phenyl)](PF_6)_2$ (**3'**) and $[Ru(tmb)_2(bpy\text{-}phenyl\text{-}MV)](PF_6)_4$ (**3**), $[Ru(tmb)_2(bpy\text{-}ortho)](PF_6)_2$ (**4'**) and $[Ru(tmb)_2(bpy\text{-}ortho\text{-}MV)](PF_6)_4$ (**4**), $[Ru(tmb)_2(bpy\text{-}2,6\text{-}dimethylphenyl)](PF_6)_2$ (**5'**) and $[Ru(tmb)_2(bpy\text{-}2,6\text{-}dimethylphenyl\text{-}MV)](PF_6)_4$ (**5**), $[Ru(tmb)_2(bpy\text{-}2,5\text{-}dimethylphenyl)](PF_6)_2$ (**6'**) and $[Ru(tmb)_2(bpy\text{-}2,5\text{-}dimethylphenyl\text{-}MV)](PF_6)_4$ (**6**) and $[Ru(tmb)_2(bpy\text{-}3,5\text{-}dimethylphenyl)](PF_6)_2$ (**7'**) and $[Ru(tmb)_2(bpy\text{-}3,5\text{-}dimethylphenyl\text{-}MV)](PF_6)_4$ (**7**).

What is evident from the UV-visible spectra is that the appended acceptor moiety is perturbing the MLCT absorption of the DBA complexes as evidenced by the non-superimposable behavior of the DBA complexes with their corresponding donor complexes. The DBA complexes exhibit increased red-edge absorption (between 500-600 nm) when compared to their respective donor compounds. This phenomenon is most pronounced for $[Ru(tmb)_2(bpy\text{-}phenyl\text{-}MV)](PF_6)_4$ (**3**) (top panel) and $[Ru(tmb)_2(bpy\text{-}3,5\text{-}dimethylphenyl\text{-}MV)](PF_6)_4$ (**7**) (bottom panel) where the growth of a second peak is observed. For $[Ru(tmb)_2(bpy\text{-}ortho\text{-}MV)](PF_6)_4$ (**4**) (second panel), $[Ru(tmb)_2(bpy\text{-}2,6\text{-}dimethylphenyl\text{-}MV)](PF_6)_4$ (**5**) (third panel) and $[Ru(tmb)_2(bpy\text{-}2,5\text{-}dimethylphenyl\text{-}MV)](PF_6)_4$ (**6**) (fourth panel) the increased red edge absorption is manifested as a shoulder rather than an additional peak.

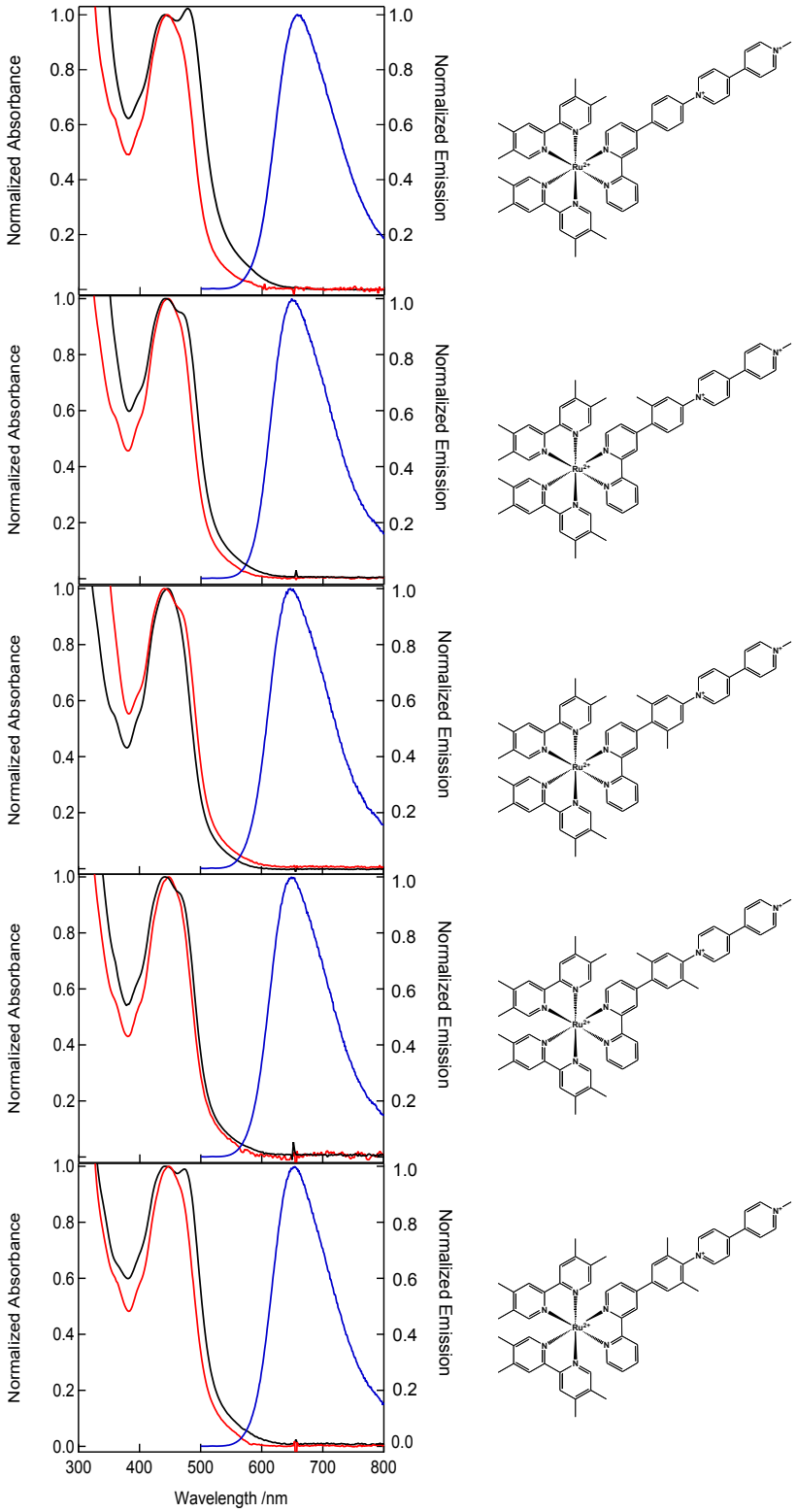

Figure 5.2 Normalized UV-visible absorption spectra of DBA (black) and donor (red) complexes in room temperature CH_3CN .The corrected emission spectra of the donor complexes recorded in room temperature CH_3CN are shown (blue). DBA complexes are shown to the right

Given that the donor complexes do not exhibit an increase in red-edge absorption it is clear that electroactive ligand is bringing about this observable. In the literature there are several examples where appending a ligand with an extended π-system leads to red shifting of the MLCT absorption band.[7-12] The red-edge non-superimposability of the UV-visible spectra of the donors with corresponding DBA complexes indicates that the lowest-energy ^{3}MLCT state of the DBA complexes lies on the asymmetric ligand. In Chapter Four TD-DFT calculations showed that the increased absorption between 500-600 nm in the UV-visible absorption spectra of the DBA complexes was attributed to delocalization of the ^{3}MLCT onto the asymmetric ligand with significant density localized to the bridging phenyl group. Again TD-DFT calculations will be used to explain why some DBA complexes in this series exhibit more absorbance between 500-600 nm than others (**Section 5.2.3**).

The emission spectra of the donor complexes, which were collected after electronic excitation at 450 nm, show a broad and featureless emission band, which is characteristic of the ^{3}MLCT $\rightarrow$ ^{1}GS transition of other ruthenium polypyridyl complexes[13] and of the homoleptic parent complex $[Ru(tmb)_3](PF_6)_2$. **Table 5.1** below lists relevant ground state and excited state properties of all the complexes in this series. It should be noted that the emission maxima for the five donor complexes are red shifted with respect to the parent complex indicating that the lowest-lying ^{3}MLCT state lies on the lower energy asymmetric donor ligand and not on the higher energy ancillary ligand.

Table 5.1 Photophysical Properties of Complexes in Room Temperature CH_3CN

Complex		λ_{max}^{MLCT} /nm	ε /10^3 M^{-1} cm^{-1}	λ_{max}^{em} /nm	Φ_{em}[a]	τ_{obs} $1/k_0$ /μs	k_r /10^5 s^{-1}	k_{nr} /10^5 s^{-1}
$[Ru(tmb)_3](PF_6)_2$		448	8.1	600	0.067	0.41	1.64	22.7
$[Ru(tmb)_2$(bpy-phenyl)$](PF_6)_2$	(**3'**)	444	12.6	658	0.064	0.85	0.76	11.0
$[Ru(tmb)_2$(bpy-phenyl-MV)$](PF_6)_4$	(**3**)	478	15.8	--	--	--	--	--
$[Ru(tmb)_2$(bpy-ortho)$](PF_6)_2$	(**4'**)	446	13.2	649	0.061	0.80	0.76	11.5
$[Ru(tmb)_2$(bpy-ortho-MV)$](PF_6)_4$	(**4**)	442	14.4	--	--	--	--	--
$[Ru(tmb)_2$(bpy-2,6-dmp)$](PF_6)_2$	(**5'**)	446	14.3	647	0.057	0.76	0.72	11.9
$[Ru(tmb)_2$(bpy-2,6-dmp-MV)$](PF_6)_4$	(**5**)	440	15.4	--	--	--	--	--
$[Ru(tmb)_2$(bpy-2,5-dmp)$](PF_6)_2$	(**6'**)	448	15.3	649	0.055	0.85	0.65	11.1
$[Ru(tmb)_2$(bpy-2,5-dmp-MV)$](PF_6)_4$	(**6**)	440	16.6	--	--	--	--	--
$[Ru(tmb)_2$(bpy-3,5-dmp)$](PF_6)_2$	(**7'**)	448	14.6	654	0.063	0.90	0.70	10.4
$[Ru(tmb)_2$(bpy-3,5-dmp-MV)$](PF_6)_4$	(**7**)	442	15.8	--	--	--	--	--

[a]The error bars on these measurements are ±0.003; they represent reproducibility within 2σ for three separate measurements for each complex. Dimethylphenyl has been abbreviated with dmp.

The emission maxima for $[Ru(tmb)_2$(bpy-ortho)$](PF_6)_2$ (**4'**), $[Ru(tmb)_2$(bpy-2,6-dimethylphenyl)$](PF_6)_2$ (**5'**) and $[Ru(tmb)_2$(bpy-2,5-dimethylphenyl)$](PF_6)_2$ (**6'**) are within 2 nm of each other demonstrating that the ^{3}MLCT states of these complexes are energetically similar. Whereas the ^{3}MLCT states of $[Ru(tmb)_2$(bpy-phenyl)$](PF_6)_2$ (**3'**) and $[Ru(tmb)_2$(bpy-3,5-dimethylphenyl)$](PF_6)_2$ (**7'**) must be energetically similar since their emission maxima are higher (lower in energy) than the other donor complexes and are within 4 nm of each other. It is apparent that the position of methyl group(s) affects the energy of the ^{3}MLCT state. Complexes with no methyl groups (**3**') or methyl groups in the 3- and 5- position (**7'**) of the aryl group have lower energy emission maxima than those with methyl substitution in the 6- and/or 2- position on the aryl group (**4**', **5**', or **6**'). These observations for (**3**') and (**7**') suggest the ^{3}MLCT state is delocalized onto the aryl group

thereby lowering its energy whereas for (**4'**), (**5'**) and (**6'**) the methyl substituents limit the extent of delocalization onto the aryl group hence raising the energy of the emission maximum. This is in line with observations of similar series of ruthenium (II) polypyridine complexes.[1,6]

Radiative quantum yields, Φ_{em}, and emission lifetimes, τ_{obs}, for the donor complexes are listed above in **Table 5.1**. Emission lifetimes were measured experimentally using the setup described above in **Section 4.2.2**. The emission lifetimes of the donor complexes are longer than that of the parent complex $[Ru(tmb)_3](PF_6)_2$. From the values of Φ_{em} and τ_{obs} radiative (k_r) and non-radiative (k_{nr}) rate constants for the donor complexes were determined. These quantities are also listed in **Table 5.1**. Like we saw in Chapter Four the trend in k_{nr} can be explained by a comparison of Huang-Rhys factors, S_M, among the compounds. Values for S_M are obtained from spectral fitting of the emission spectra.

Table 5.2 Emission Spectra Fitting Data for Complexes in Room Temperature CH_3CN

Complex	E_0 /cm^{-1}	ΔG^0_{MLCT} /cm^{-1}	$h\omega_M$ /cm^{-1}	S_M	$\Delta\overline{\nu}_{0,1/2}$ /cm^{-1}
$[Ru(tmb)_3](PF_6)_2$[a]	16580±70	17810±70	1350	0.97±0.05	1680±40
$[Ru(tmb)_2$(bpy-phenyl)$](PF_6)_2$ (**3'**)	15315±70	16780±70	1350	0.81±0.05	1840±40
$[Ru(tmb)_2$(bpy-ortho)$](PF_6)_2$ (**4'**)	15485±70	16856±70	1350	0.84±0.05	1774±40
$[Ru(tmb)_2$(bpy-2,6-dmp)$](PF_6)_2$ (**5'**)	15566±70	17099±70	1350	0.83±0.05	1876±40
$[Ru(tmb)_2$(bpy-2,5-dmp)$](PF_6)_2$ (**6'**)	15572±70	16982±70	1350	0.82±0.05	1800±40
$[Ru(tmb)_2$(bpy-3,5-dmp)$](PF_6)_2$ (**7'**)	15480±70	16937±70	1350	0.77±0.05	1829±40

The error bars for the parameters reported in this table represent 2σ determined from five separate measurements and fittings of emission of $[Ru(bpy)_2$(bpy-phenyl$](PF_6)_2$.[a] These data were taken from reference 2. Dimethylphenyl has been abbreviated by dmp.

The values of E_0 obtained from the fits confirm the observations stated above regarding the energetics of the ^{3}MLCT state of the donor complexes. Namely, that the energy of the lowest lying ^{3}MLCT state of all the donor complexes is lower than that of the

parent complex $[Ru(tmb)_3](PF_6)_2$ and that complexes where excited state delocalization is more amenable (**3'** and **7'**) have the lowest energy ^{3}MLCT states. The values of S_M obtained from the spectral emission fits are listed in **Table 5.2**. Clearly the new donor complexes have values of S_M that are lower than that of the parent complex. From the discussion above this indicates that the excited state and ground state surfaces for the donor complexes are more nested (less nuclear distortion between the two states) than those of the parent complex where complexes (**3'**) and (**7'**) are the most nested. The Energy Gap Law predicts that when surfaces are more nested it leads to a decrease in the non-radiative rate of decay from the ^{3}MLCT state. As can be can see from **Table 5.1** this is what is observed when comparing k_{nr} values among the donor complexes in this series.[1,14-17]

5.2.2 Determination of Driving Forces for Photoinduced Electron Transfer

Calculating driving forces for photoinduced ET will establish if it is energetically feasible to form the charge separated state, D^+-B-A^-, from the excited state donor, D^*-B-A. As described in detail in Chapter Four, there are two main quantities that are needed in order to determine free energies for ET. The first of these quantities is ΔG^0_{MLCT} which is usually described as the amount of energy stored in D^*-B-A. ΔG^0_{MLCT} is calculated from values summarized in **Table 5.2** above. The values of ΔG^0_{MLCT} for the donor complexes are lower than that of the parent complex. This is in line with our analysis that for the donor complexes the ^{3}MLCT lies on the lower energy asymmetric aryl substituted ligand. Consistent with the observations stated above the complexes where the ^{3}MLCT state can delocalize onto the aryl ring have lower emission maxima these complexes also have lower values of ΔG^0_{MLCT} when comparing complexes in the series.

The second quantity needed is ΔG^0_{IP}. This is the energy associated with forming the ion pair, D^+-B-A^-, from the ground state, D-B-A, and is determined primarily from electrochemical data. We use Weller's formulation[18] for finding ΔG^0_{IP}; summarized in dielectric constant of the solvent in which the ET measurements will be measured and R_{DA} is an estimate of the donor-to-acceptor distance. This distance is a through-space measurement from the Ru(II) center to 4,4'-carbon bond in the acceptor. These values were estimated from the geometry-optimized structures obtained from DFT calculations performed in Q-Chem 4.0.

Equation 5.1 and **Equation 5.2** summarize how driving forces for forward ET and back ET (BET) are calculated, respectively.

$$\Delta G^{\circ}_{ET} = -\Delta G^{\circ}_{MLCT} + \Delta G^{\circ}_{IP} \qquad \textbf{Equation 5.1}$$

$$\Delta G^{\circ}_{BET} = -\Delta G^{\circ}_{IP} \qquad \textbf{Equation 5.2}$$

Values for R_{DA}, ΔG^0_{IP}, ΔG^0_{ET} and ΔG^0_{BET} are summarized in **Table 5.3** and in **Figure 5.3**.

Table 5.3 Calculated Driving Forces for Photoinduced ET

Complex		R_{DA}/Å	ΔG^0_{IP}/eV	ΔG^0_{ET} /eV	ΔG^0_{BET} /eV
$[Ru(tmb)_2(bpy\text{-}phenyl\text{-}MV)](PF_6)_4$	(**3**)	14.1(3)	1.38	-0.70	-1.38
$[Ru(tmb)_2(bpy\text{-}ortho\text{-}MV)](PF_6)_4$	(**4**)	14.1(2)	1.37	-0.72	-1.37
$[Ru(tmb)_2(bpy\text{-}2,6\text{-}dmp\text{-}MV)](PF_6)_4$	(**5**)	14.1(2)	1.39	-0.73	-1.39
$[Ru(tmb)_2(bpy\text{-}2,5\text{-}dmp\text{-}MV)](PF_6)_4$	(**6**)	14.1(1)	1.40	-0.70	-1.40
$[Ru(tmb)_2(bpy\text{-}3,5\text{-}dmp\text{-}MV)](PF_6)_4$	(**7**)	14.1(1)	1.40	-0.70	-1.40

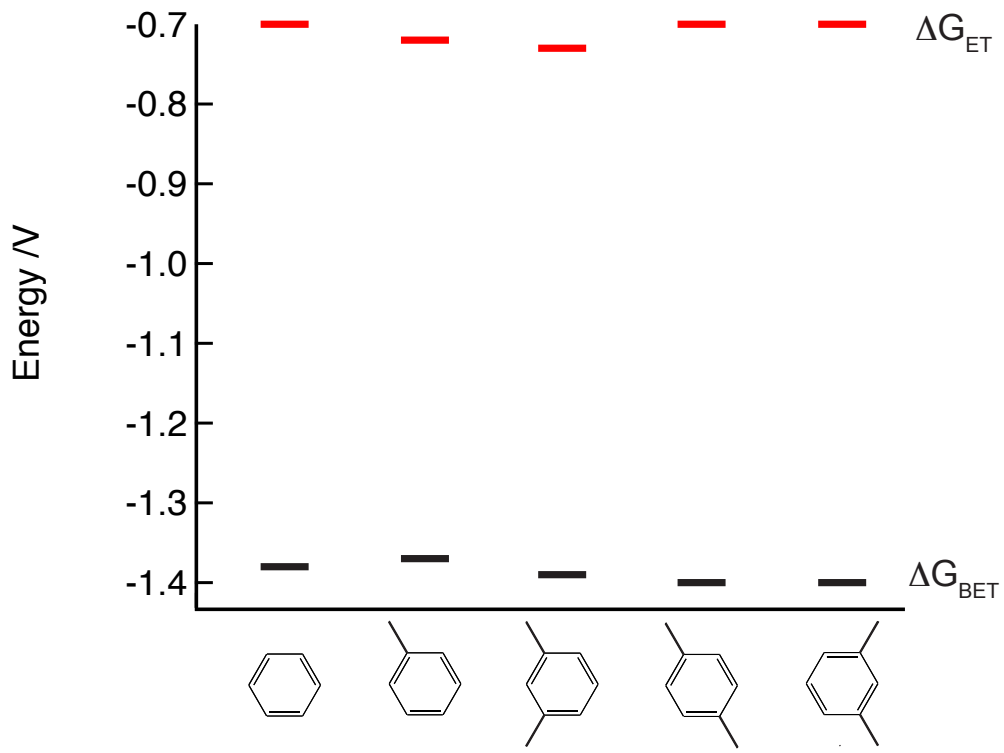

Figure 5.3 Energy level diagram summarizing the driving forces for electron transfer.

From **Table 5.3** we see that the assumption on which this work was founded generally holds; i.e., that there are minimal differences in driving forces for ET and BET for the complexes in the series. There is a 30 meV difference in both ΔG^0_{ET} and ΔG^0_{BET} among the complexes in the series. These differences are attributed to variations in oxidation potentials of the complexes as well as differences in ΔG^0_{MLCT}. We will see in **Section 5.2.4** that despite minor differences in ET driving forces significant differences in ET photoproduct lifetimes are observed.

5.2.3 Time-Dependent Density Functional Theory to Explain Absorption Spectra

In extension of the analysis presented in Chapter Four, Density Functional Theory (DFT) and Time-Dependent Density Functional Theory (TD-DFT) were used to determine the nature of the increased absorbance at the red edge of the UV-visible spectrum (between

500-600 nm) of the DBA complexes. This effect is most pronounced for $[Ru(tmb)_2(bpy\text{-}phenyl\text{-}MV)](PF_6)_4$ (**3**) and $[Ru(tmb)_2(bpy\text{-}3,5\text{-}mesiutyl\text{-}MV)](PF_6)_4$ (**7**) where the growth of a second peak is observed. The use of DFT and TD-DFT to understand charge transfer processes in d^6 transition metals have become more prevalent in the literature.[19-23] Here we use DFT to optimize ground-state geometries of the DBA and donor complexes followed by TD-DFT to predict the absorption spectra of the complexes.

Figure 5.4 below is a comparison of the experimental UV-visible absorption spectra (top panel) to the computed spectra (bottom panel) of the donor complexes and **Figure 5.5** makes the same comparison for the DBA complexes. It should be noted that the calculated spectra of the complexes have been red shifted by 1.4 eV for better comparison with experimental spectra.[24-26] In the calculated spectra below the solid lines are representative of the absorption envelope and the so-called sticks represent transitions within the envelope.

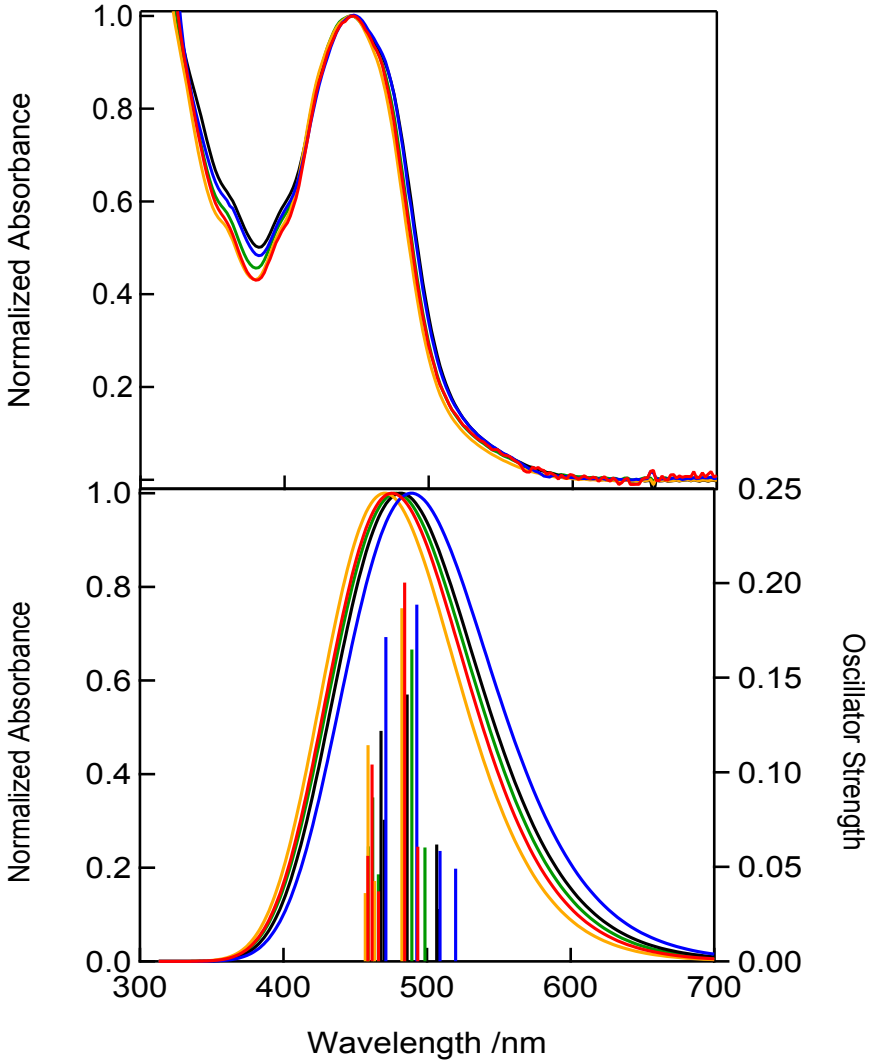

Figure 5.4 Comparison of experimental (top) and calculated (bottom) absorption spectra of [Ru(tmb)$_2$(bpy-phenyl)](PF$_6$)$_2$ (**3'**) (black), [Ru(tmb)$_2$(bpy-ortho)](PF$_6$)$_2$ (**4'**) (green), [Ru(tmb)$_2$(bpy-2,6-dimethylphenyl)](PF$_6$)$_2$ (**5'**) (orange), [Ru(tmb)$_2$(bpy-2,5-dimethylphenyl)](PF$_6$)$_2$ (**6'**) (red) and [Ru(tmb)$_2$(bpy-3,5-dimethylphenyl)](PF$_6$)$_4$ (**7'**) (blue). The calculated spectra have been red shifted by 1.4 eV for better comparison with experimental spectra.

As we can see when comparing the experimental visible absorption spectra (top panel above) with the calculated spectra (bottom panel above) there is qualitative agreement between the two data sets where both show broader spectra for [Ru(tmb)$_2$(bpy-phenyl)](PF$_6$)$_2$ (**3'**) (black) and [Ru(tmb)$_2$(bpy-phenyl-)](PF$_6$)$_2$ (**7'**) (blue).

From **Figure 5.5** below we see the calculated spectra for the DBA complexes qualitatively agree with the experimental absorption spectra. The calculated spectra (bottom panel) are broader than the experimental spectra (top panel) but the observed trend in red edge absorption is correctly reproduced by the calculations.

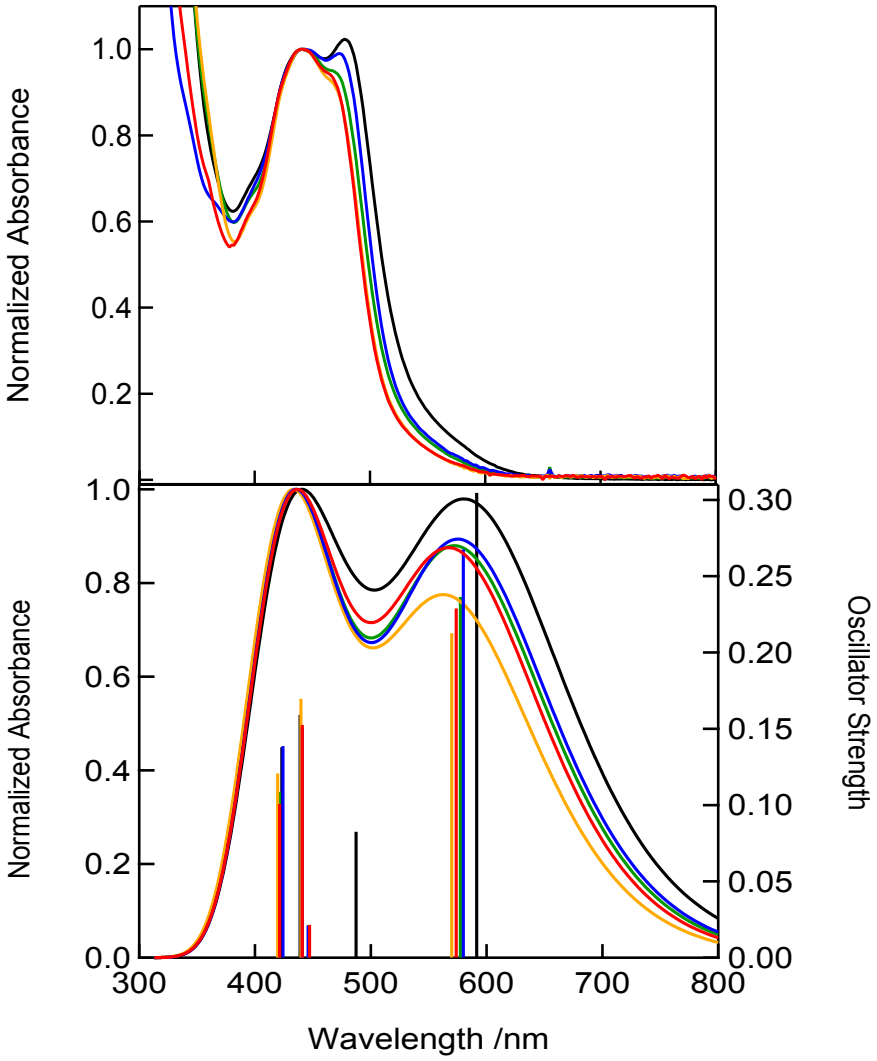

Figure 5.5 Comparison of experimental (top) and calculated (bottom) absorption spectra of [Ru(tmb)$_2$(bpy-phenyl-MV)](PF$_6$)$_4$ (**3**) (black), [Ru(tmb)$_2$(bpy-ortho-MV)](PF$_6$)$_4$ (**4**) (green), [Ru(tmb)$_2$(bpy-2,6-dimethylphenyl-MV)](PF$_6$)$_4$ (**5**) (orange), [Ru(tmb)$_2$(bpy-2,5-dimethylphenyl-MV)](PF$_6$)$_4$ (**6**) (red) and [Ru(tmb)$_2$(bpy-3,5-dimethylphenyl-MV)](PF$_6$)$_4$ (**7**) (blue). The calculated spectra have been red shifted by 1.4 eV for better comparison with experimental spectra. The DBA spectra were normalized at 440 nm for better comparison of red-edge peak intensity.

Consistent with experiment the red edge absorption becomes most prominent in the calculated spectra for [Ru(tmb)$_2$(bpy-phenyl-MV)](PF$_6$)$_4$ (**3**) (black trace) and [Ru(tmb)$_2$(bpy-3,5-dimethylphenyl-MV)](PF$_6$)$_4$ (**7**) (blue trace) and as steric bulk is added in the 2- and 6- positions of the aryl bridging ligand there is a reduction in red-edge absorption.

The so-called stick spectra provide information on the transitions that are occurring upon excitation as well as the orbital components comprising the transition. To visually represent the transitions we turned to detachment/attachment densities which are plots of regions depopulated and populated, respectively, after excitation.[19,24] For the donor complexes the stick spectra show the expected MLCT transitions where the detachment density is metal centered and the attachment density is localized on a polypyridine ligand. The lower energy transitions have electron density localized on the asymmetric ligands. In analyzing the attachment and detachment densities for the DBA complexes we find that the transitions between 400 and 500 nm are MLCT in character where the detachment density is centered on the metal center and the attachment density on an ancillary ligand or the 2,2'-bipyridine moiety of the asymmetric ligand.

Now we turn to the stick spectra to help explain the observed increase in red-edge absorption for the DBA complexes. Specifically we will look at the lowest energy transitions at 591 nm for [Ru(tmb)$_2$(bpy-phenyl-MV)](PF$_6$)$_4$ (**3**), 577 nm for [Ru(tmb)$_2$(bpy-ortho-MV)](PF$_6$)$_4$ (**4**), 570 nm for [Ru(tmb)$_2$(bpy-2,6-dimethylphenyl-MV)](PF$_6$)$_4$ (**5**), 574 nm for [Ru(tmb)$_2$(bpy-2,5-dimethylphenyl-MV)](PF$_6$)$_4$ (6) and 580 nm for [Ru(tmb)$_2$(bpy-3,5-dimethylphenyl-MV)](PF$_6$)$_4$ (**7**). **Figure 5.6** below shows the attachment densities in blue and detachment densities in red for these transitions. Isovalues of 0.002 were plotted.

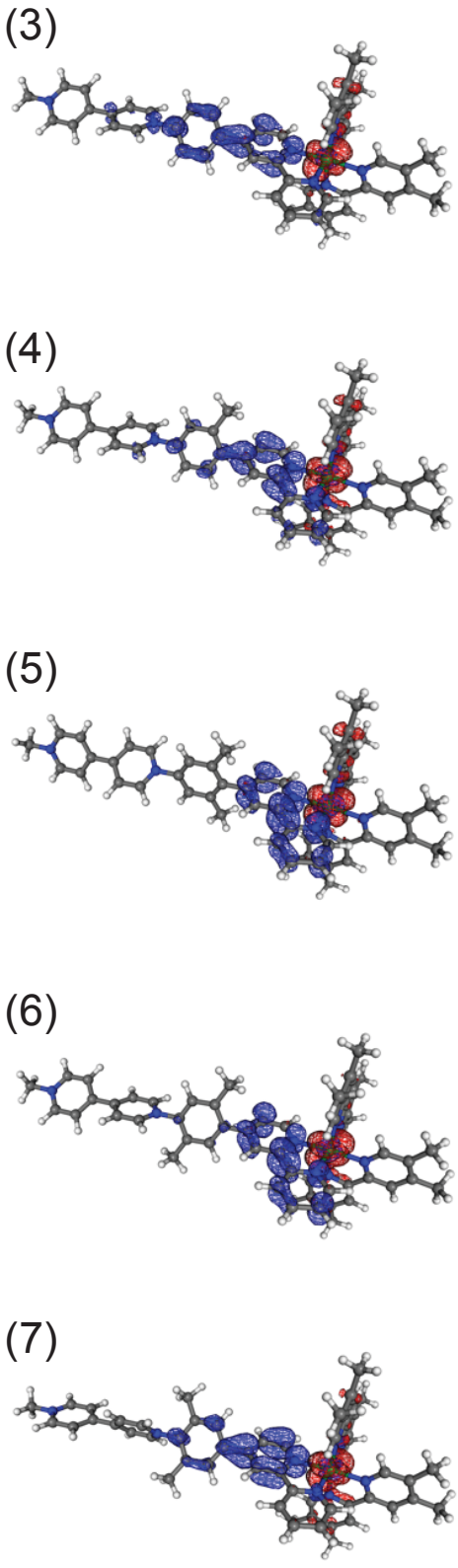

Figure 5.6 Attachment (blue) and detachment (red) densities for red edge transitions of the DBA complexes.

Looking at these densities we find the detachment density is metal centered for the complexes and the attachment density is localized only on the asymmetric ligand. Looking closely at the attachment densities we see that the density is not only localized on 2,2'-bipyrdine moiety of the ligand but is delocalized throughout the asymmetric ligand with some attachment density on the acceptor moiety for (**3**) and (**4**). We attribute this delocalization onto the asymmetric ligand as the cause for the increased absorption in the red edge of the spectra (between 500 and 600 nm). What is striking is that the extent of delocalization onto the asymmetric ligand moiety is determined by the position of methyl substituents. Looking at the attachment densities for the doubly methylated complexes we can clearly see this effect. For $[Ru(tmb)_2(bpy\text{-}2,6\text{-}dimethylphenyl\text{-}MV)](PF_6)_4$ (**5**) the attachment density is localized strictly on the 2,2'-bipyridine moiety of the asymmetric ligand here the methyl groups are disrupting electronic communication preventing delocalization across the entire ligand like $[Ru(tmb)_2(bpy\text{-}phenyl\text{-}MV)](PF_6)_4$ (**3**). Looking now at $[Ru(tmb)_2(bpy\text{-}3,5\text{-}dimethylphenyl\text{-}MV)](PF_6)_4$ (**7**) we see that the methyl substituents here are preventing delocalization of the attachment density onto the acceptor moiety but allowing for delocalization onto the 2,2'-bipyridine as well as the bridging aryl group. As might be expected, the attachment density for $[Ru(tmb)_2(bpy\text{-}2,5\text{-}dimethylphenyl\text{-}MV)](PF_6)_4$ (**6**) is somewhere in between the attachment densities of complexes (**5**) and (**7**), where a small fraction is present on the aryl bridging ligand and the remainder on the 2,2'-bipyridine moiety. Despite calculating the spectra for these complexes using the same basis sets and functionals as for complexes (**1**), (**2**) and (**3**) direct excitation from the metal center to the acceptor moiety was not observed in any of the sticks for complexes with methyl substituents on the bridging subunit. Here the methyl

groups are effectively disrupting electronic communication in the ground state controlling the extent of delocalization of the attachment density thereby determining the shape of the UV-visible spectra as well as preventing direct excitation to the acceptor.

5.2.4 Picosecond Transient Absorption Kinetics and Spectra

This body of work is centered on investigating the effects of structural elements on the rates of the photoinduced intramolecular electron transfer in directly-linked conformationally-active ruthenium (II) polypyridyl DBA complexes. Studying the ultrafast behavior of the complexes in this series affords a direct way of answering this question because the complexes essentially have the same driving forces for photoinduced ET. Therefore, any differences in ET lifetimes are attributable to differences in structure. From calculated driving forces it was concluded that forming the charge-separated electron transfer photoproduct, D^{+}-B-A^{-}, from the excited state donor, D*-B-A, is a free-energy downhill process. The reductive spectrorelectrochemical data presented in Chapter Three provide optical tags[27] for the absorptive properties of the electron transfer product. In this section, a discussion of the picosecond transient absorption techniques utilized to detect and measure the rates of photoinduced electron transfer for this series of DBA complexes will be presented. A discussion of transient absorption spectra will be followed by transient absorption single wavelength kinetics. Transient Absorption techniques have been described in Chapter Four.

The analysis of transient absorption experimental data presented here is an extension of the analysis presented in Chapter Four. Recall that the early time absorption feature centered at ~370 nm was assigned as intraligand transitions within the reduced polypyridine ligand from the excited ^{3}MLCT state (D*-B-A).[28-31] The absorption feature

between 500-600 nm is assigned as Ligand-to-Metal Charge Transfer (LMCT) transitions of the ^{3}MLCT state as well as intraligand transitions of the reduced polypyridine ligand.[32] From later time points it was concluded that the ET photophoduct has a broad absorptive features centered at 420 nm as well as between 500-600 nm. The bleach feature from ~450-500 is attributed to the loss of ^{1}MLCT ← ^{1}GS absorption. For the complexes in this series the same spectral features are observed in the TA spectra thereby affirming that the ET photoproduct is also formed. Below are the TA spectra recorded in room temperature acetonitrile after excitation with a ~500 nm pulse (~80 fs) for [Ru(tmb)$_2$(bpy-phenyl-MV)](PF$_6$)$_4$ (**3**), [Ru(tmb)$_2$(bpy-ortho-MV)](PF$_6$)$_4$ (**4**) and [Ru(tmb)$_2$(bpy-2,6-dimethylphenyl-MV)](PF$_6$)$_4$ (**5**) in **Figure 5.7**, **Figure 5.8** and **Figure 5.9**, respectively. The early time point is shown in red, the intermediate in blue and the long time point in green.

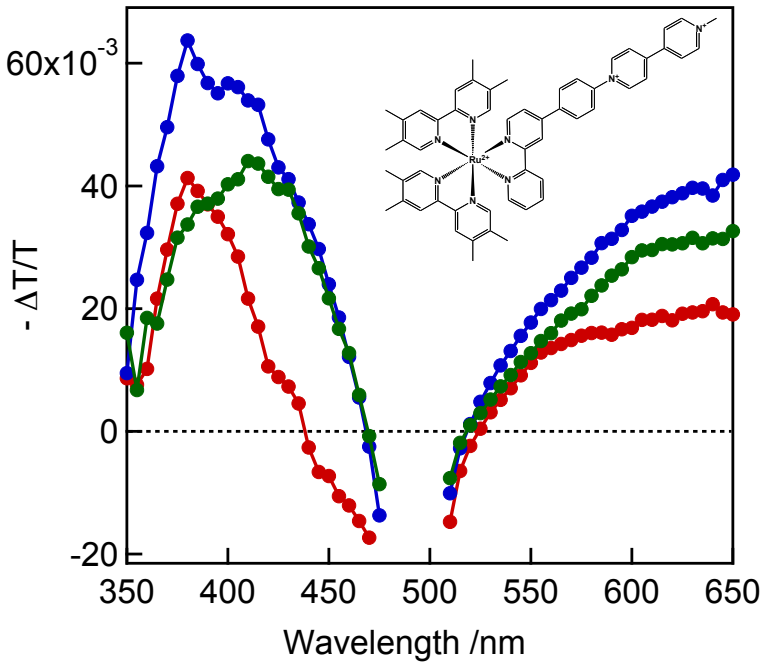

Figure 5.7 Transient Absorption Spectra of [Ru(tmb)$_2$(bpy-phenyl-MV)](PF$_6$)$_4$ (**3**) in room temperature acetonitrile collected 0.5 ps (red) 1.5 ps (blue) and 5.0 ps (green) following excitation with a 500 nm, ~80 fs pump pulse. Data between 475 and 515 nm has been removed since it was strongly contaminated with scatter from the pump pulse

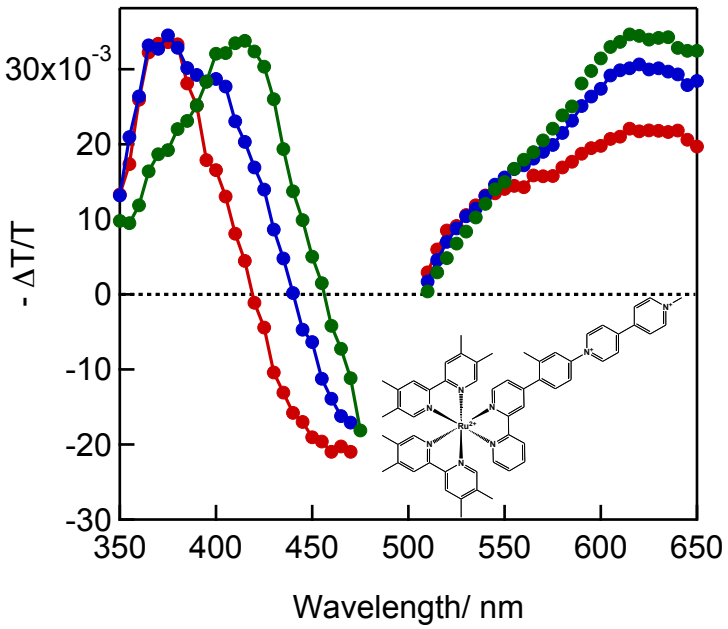

Figure 5.8 Transient Absorption Spectra of $[Ru(tmb)_2(bpy\text{-}ortho\text{-}MV)](PF_6)_4$ (**4**) in room temperature acetonitrile collected 0.5 ps (red) 1.5 ps (blue) and 5.0 ps (green) following excitation with a 500 nm, ~80 fs pump pulse. Data between 475 and 515 nm has been removed since it was strongly contaminated with scatter from the pump pulse

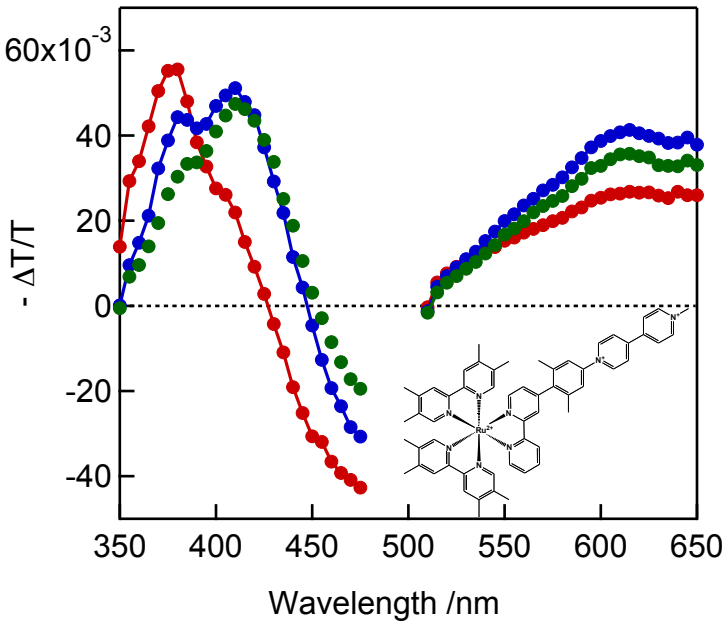

Figure 5.9 Transient Absorption Spectra of $[Ru(tmb)_2(bpy\text{-}2,6\text{-}dimethylphenyl\text{-}MV)](PF_6)_4$ (**5**) in room temperature acetonitrile collected 2.0 ps (red) 10.0 ps (blue) and 20.0 ps (green) following excitation with a 500 nm, ~80 fs pump pulse. Data between 475 and 515 nm has been removed since it was strongly contaminated with scatter from the pump pulse

The TA spectra recorded in room temperature acetonitrile after excitation with a ~500 nm (80 fs) pulse for $[Ru(tmb)_2(bpy\text{-}2,5\text{-}dimethylphenyl\text{-}MV)](PF_6)_4$ (**6**) and $[Ru(tmb)_2(bpy\text{-}3,5\text{-}dimethylphenyl\text{-}MV)](PF_6)_4$ (**7**) are shown below in **Figure 5.10** and **Figure 5.11**, respectively. The early time point (2.0 ps) is shown in red, the intermediate time point (10.0 ps) in blue and the long time point (20.0 ps) in green. In general, the spectral features of these two complexes are similar to those of complexes (**3**), (**4**) and (**5**) where signatures of the ET photoproduct are present. However, it is evident that the peak in the blue region of the spectrum for (**6**) and (**7**) is more narrow than that of the complexes (**3**), (**4**) and (**5**). For (**6**) and (**7**) this peak is centered at 395 nm rather than 420 nm for (**3**), (**4**) and (**5**). The observation of band narrowing and blue shifting of peak maximum is consistent with the reductive spectroelectrochemical data presented in Chapter Three (see **Section 3.3.3**) for the complexes where the reductive spectroelectrochemistry indicates that the methyl substituents were effectively localizing electron density onto the acceptor moiety of the electroactive ligand. The TA spectra for (**6**) and (**7**) indicate that the ET photoproducts of these complexes behave like the respective radical cation of the electroactive ligand and reduced complex. Namely, that electron density is localized on the acceptor moiety. This result indicates that our original claim for adding methyl substitution in the 3- and 5- positions of the bridging subunit is validated because spectral features in the TA spectra are indicative of an electron localized onto the acceptor.

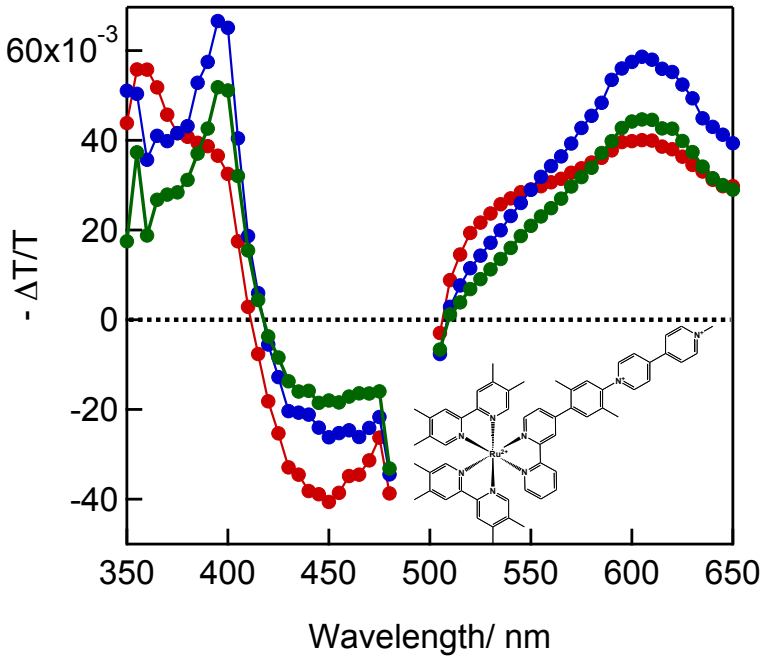

Figure 5.10 Transient Absorption Spectra of $[Ru(tmb)_2(bpy\text{-}2,5\text{-}dimethylphenyl\text{-}MV)](PF_6)_4$ (**6**) in room temperature acetonitrile collected 2.0 ps (red) 10.0 ps (blue) and 20.0 ps (green) following excitation with a 500 nm, ~80 fs pump pulse.

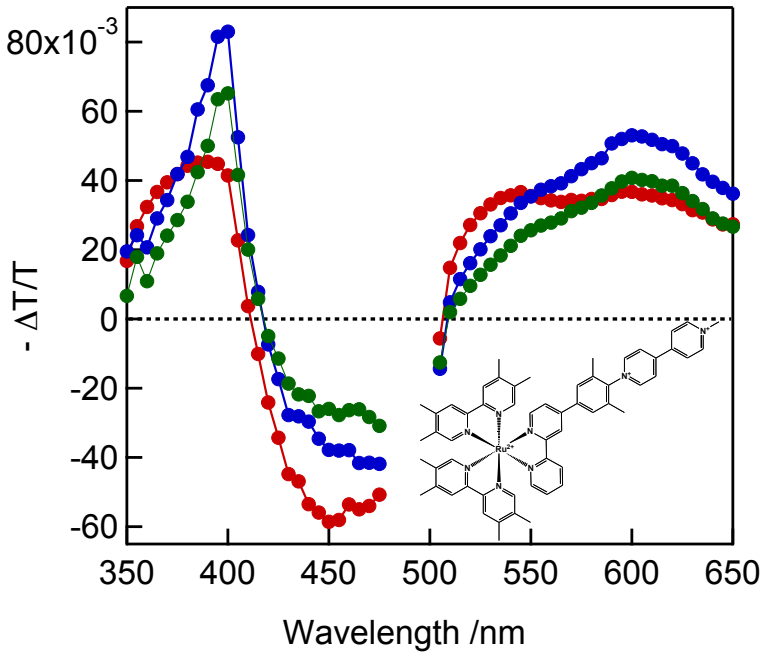

Figure 5.11 Transient Absorption Spectra of $[Ru(tmb)_2(bpy\text{-}3,5\text{-}dimethylphenyl\text{-}MV)](PF_6)_4$ (**7**) in room temperature acetonitrile collected 2.0 ps (red) 10.0 ps (blue) and 20.0 ps (green) following excitation with a 500 nm, ~80 fs pump pulse.

The TA spectra confirmed the formation of the ET photoproduct and now we turn to TA single wavelength kinetics for extraction of ET lifetimes. Ideally, one would choose probe wavelengths where all transient signal is attributed to the ET photoproduct however as discussed in Chapter Four there are no wavelengths available within our experimental setup that will allow for uniquely probing the ET photoproduct. From the discussion of the TA spectra above, probe wavelengths of ~380 nm, ~400 nm and ~607 nm were selected. Probing at ~400 nm and 607 nm allow for monitoring the dynamics at wavelengths where the ET product has significant absorbance while probing at ~380 allows for monitoring the dynamics that are attributed to both ^{3}MLCT and D^+-B-A^-.

The single wavelength kinetic data for $[Ru(tmb)_2(bpy\text{-}phenyl\text{-}MV)](PF_6)_4$ (**3**) collected in room temperature acetonitrile with an ~500 nm (80 fs fwhm) pump pulse are shown below in **Figure 5.12**. These data were presented and discussed in **Section 4.3.4**. The raw data are shown in blue and a fit of the data is shown in red. The data were fit with a triple exponential function. The extracted lifetimes are a fast component τ_1= ~0.7 ps, an intermediate component τ_2=~4 ps and a long component τ_3=~16 ps. As was stated in Chapter Four the data probing at 370 nm reveal only a decay feature that required two exponential functions to fit properly. The lifetimes extracted from the 370 nm probe data are commensurate with τ_1 and τ_2.

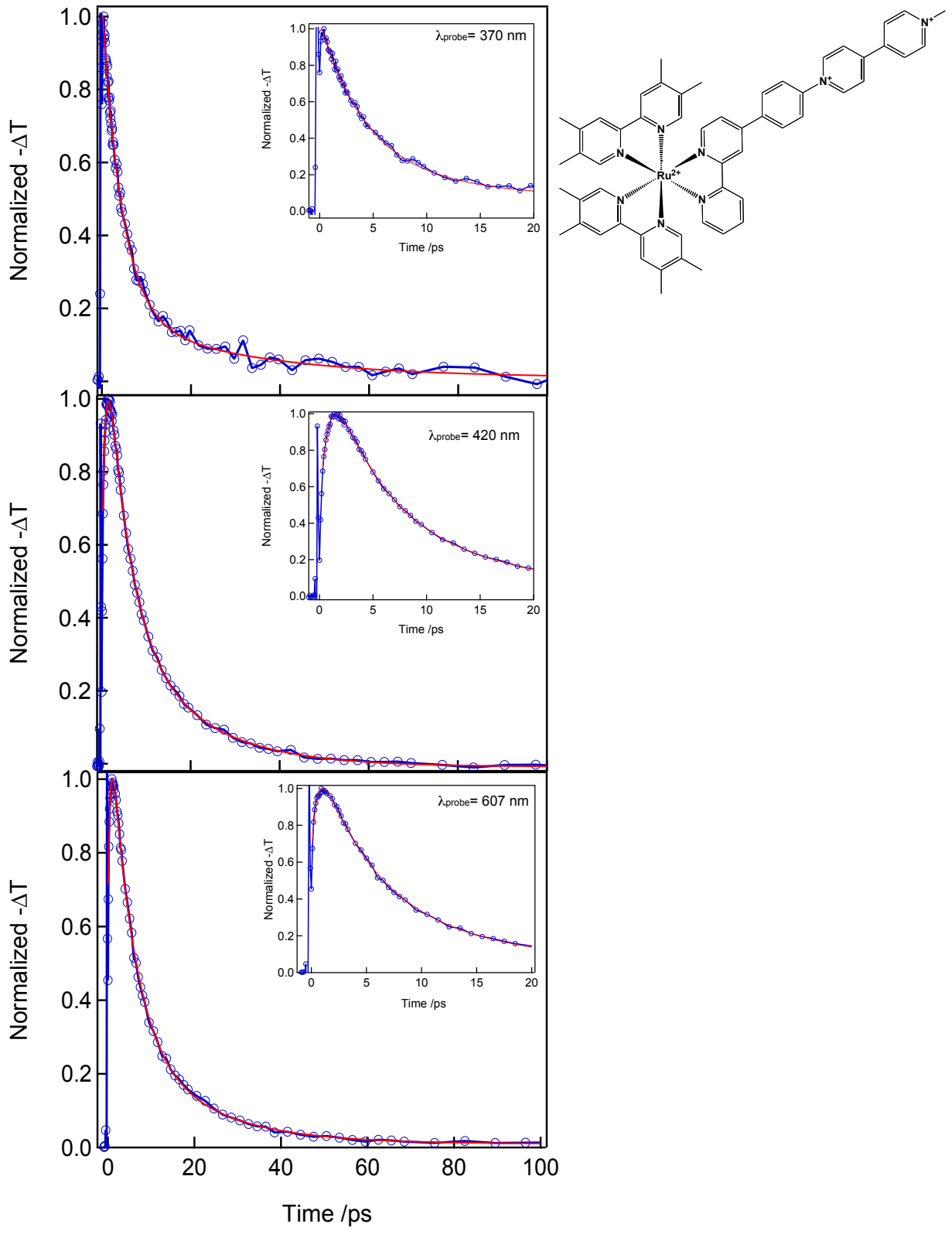

Figure 5.12 Transient absorption kinetics for (**3**) in room temperature acetonitrile collected with ~500 nm pump pulse and at a probe wavelength of 370 nm (top), 420 nm (middle) and 607 nm (bottom). The raw data (blue) were fit with a multi-exponential function (red).

The single wavelength TA experiments were repeated for the DBA complexes with steric bulk on the asymmetric ligand. **Figure 5.13** below shows the raw data in blue and a multi-exponential fit of the data in red for $[Ru(tmb)_2(bpy\text{-}ortho\text{-}MV)](PF_6)_4$ (**4**) collected in room temperature acetonitrile with an ~500 nm (80 fs fwhm) pump pulse. Data probing at 420 nm and 607 nm show a rise feature followed by a decay while the data probing at 380 nm (albeit noisy) shows a decay feature. This is consistent with the single wavelength data for $[Ru(tmb)_2(bpy\text{-}phenyl\text{-}MV)](PF_6)_4$ (**3**). Interestingly for complex (**4**) and the other complexes with steric bulk, a double exponential function is required to properly fit the data probing at 420 nm and 607 nm. The fits of $[Ru(tmb)_2(bpy\text{-}ortho\text{-}MV)](PF_6)_4$ (**4**) probing at 420 nm and 607 nm reveal that a fast component of ~1.5 ps and a long component of ~15 ps fit the data satisfactorily. The data probing at 380 nm, although noisy is fit with a single exponential component that is commensurate with the long time component.

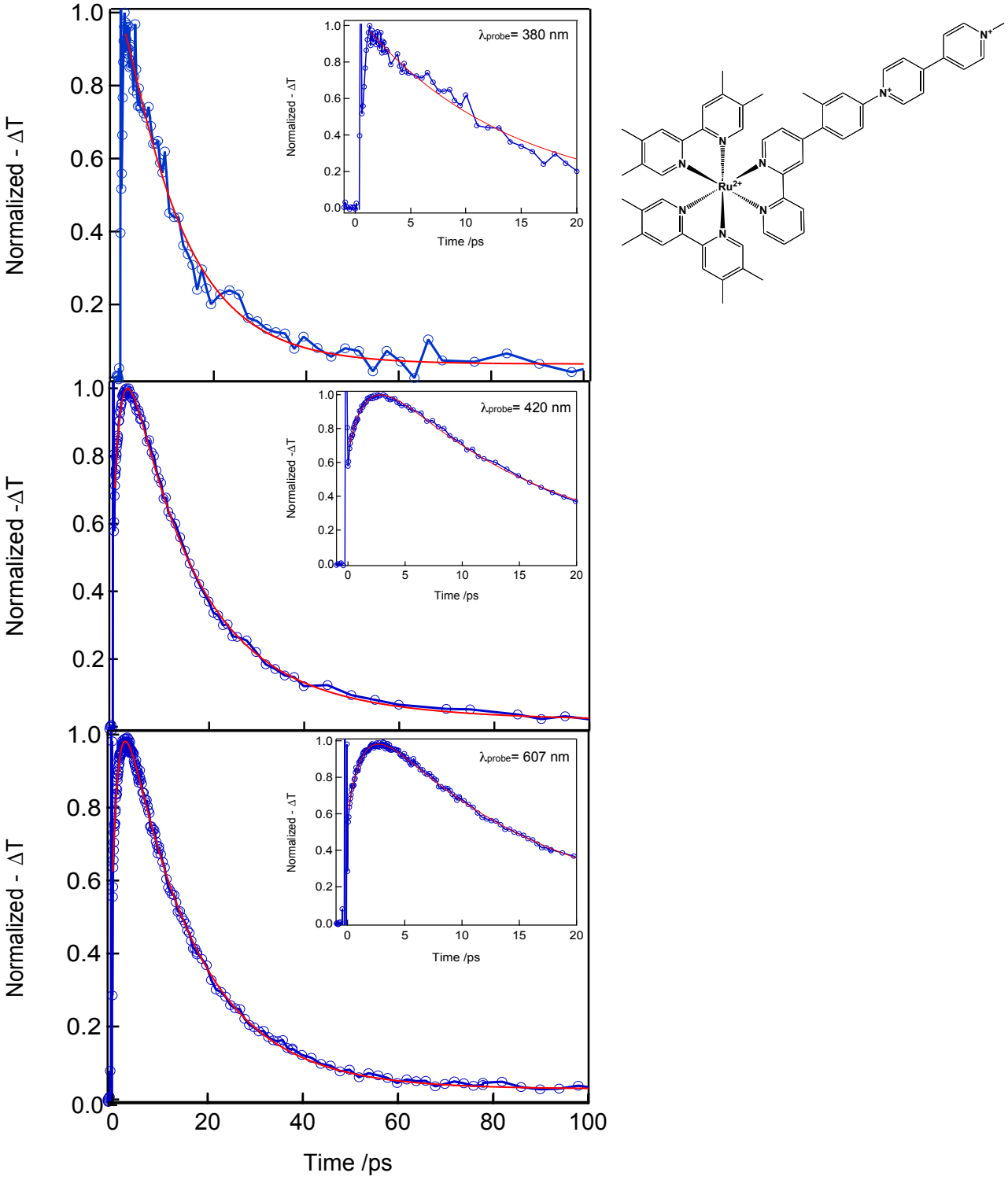

Figure 5.13 Transient absorption kinetics for (**4**) in room temperature acetonitrile collected with ~500 nm pump pulse and at a probe wavelength of 380 nm (top), 420 nm (middle) and 607 nm (bottom). The raw data (blue) were fit with a multi-exponential function (red).

The single wavelength data for complexes that are doubly methylated on the bridging aryl group are shown below. **Figure 5.14** shows the raw data in blue and a fit of the data in red for $[Ru(tmb)_2(bpy\text{-}2,6\text{-}dimethylphenyl\text{-}MV)](PF_6)_4$ (**5**) collected in room temperature acetonitrile with an ~500 nm (80 fs fwhm) pump pulse. Probe wavelengths of 420 nm (middle panel) and 607 nm (bottom panel) were again chosen to probe ET photoproduct dynamics while a probe wavelength of 380 nm (top panel) was selected to monitor dynamics at a wavelength where both the ^{3}MLCT and ET photoproduct absorb. Unlike the 380 probe nm data for (**3**) and (**4**) this data has a rise feature. We can see from the insets that the dynamics for this complex are slower than those of (**3**) and (**4**). As was the case for (**4**) a double exponential function successfully fit the data probing at 420 nm and 607 nm. Unlike the other complexes, the 380 nm probe data required a bi-exponential function to be fit. The fits of $[Ru(tmb)_2(bpy\text{-}2,6\text{-}dimethylphenyl\text{-}MV)](PF_6)_4$ (**5**) probing at 380, 420 nm and 607 reveal that a fast component of ~6 ps and a long component of ~30 ps fit the data satisfactorily.

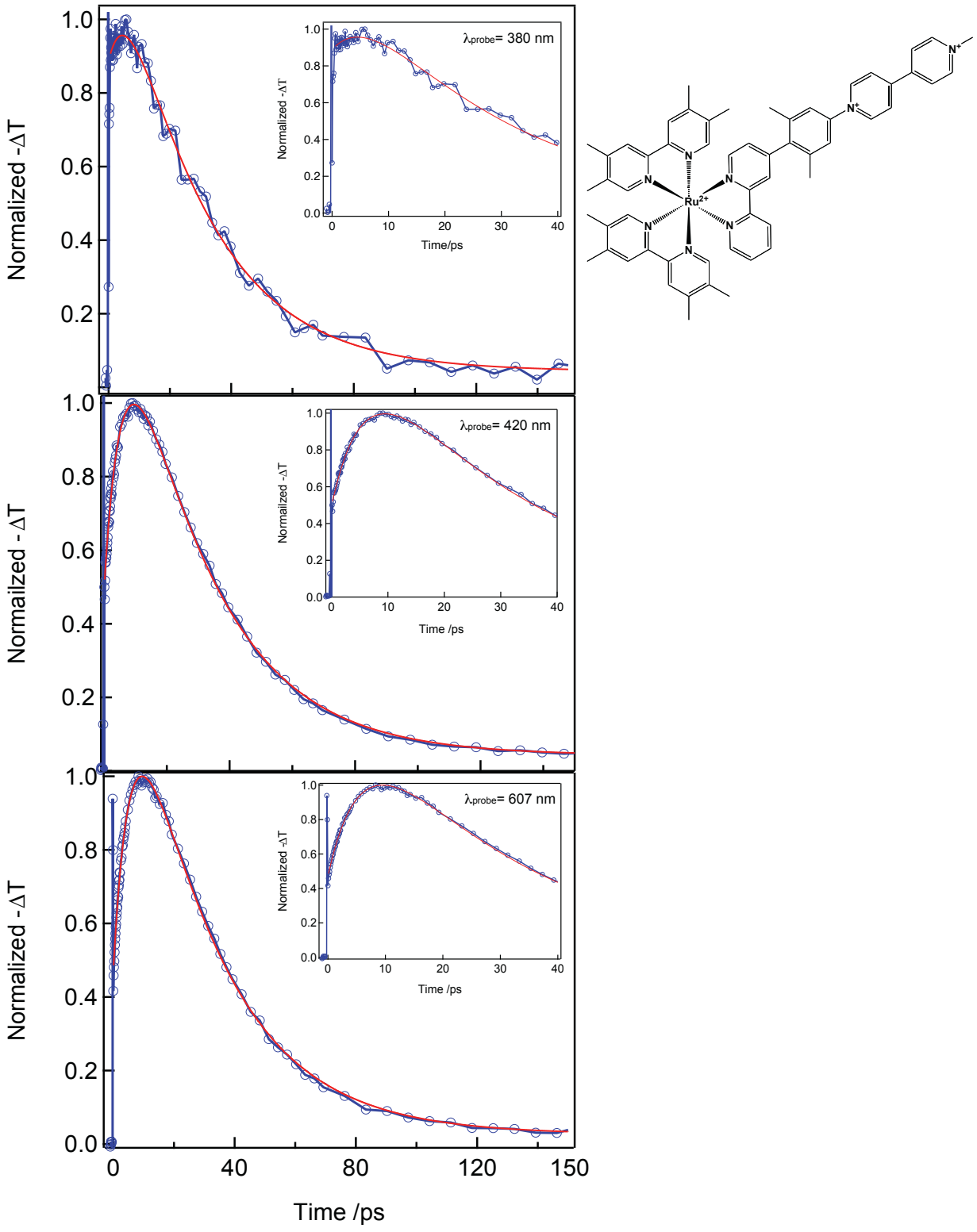

Figure 5.14 Transient absorption kinetics for (**5**) in room temperature acetonitrile collected with ~500 nm pump pulse and at a probe wavelength of 380 nm (top), 420 nm (middle) and 607 nm (bottom). The raw data (blue) were fit with a multi-exponential function (red).

Continuing the discussion of the single wavelength kinetics for doubly methylated complexes the data for $[Ru(tmb)_2(bpy\text{-}2,5\text{-}dimethylphenyl\text{-}MV)](PF_6)_4$ (**6**) are shown below in **Figure 5.15** where the raw data are shown in blue and a double exponential fit of the data in red. The data were collected in room temperature acetonitrile with an ~500 nm (80 fs fwhm) pump pulse. In this case, a probe wavelength of 390 nm (middle panel) along with 607 nm (bottom panel) were chosen to probe ET photoproduct dynamics while a probe wavelength of 380 nm was also selected. Like the data of $[Ru(tmb)_2(bpy\text{-}2,6\text{-}dimethylphenyl\text{-}MV)](PF_6)_4$ (**5**) the dynamics for this complex are slower than those of (**3**) and (**4**) and that the data probing at 380 nm has rise feature. Consistent with complexes (**4**) and (**5**) a double exponential function successfully fit the data probing at 380 nm, 390 nm and 607 nm The fits of $[Ru(tmb)_2(bpy\text{-}2,5\text{-}dimethylphenyl\text{-}MV)](PF_6)_4$ (**6**) reveal that a fast component of ~5 ps and a long component of ~25 ps fit the data satisfactorily.

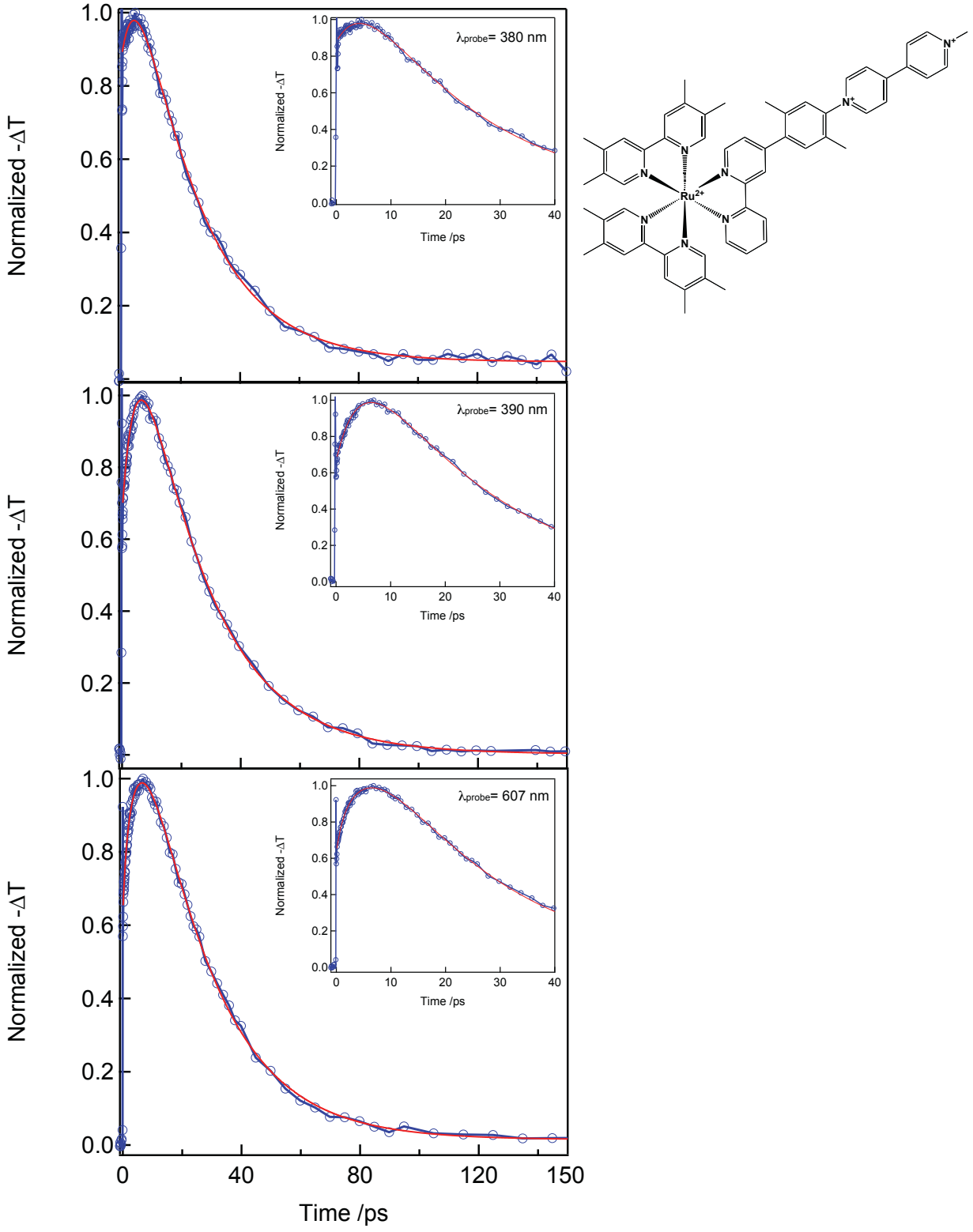

Figure 5.15 Transient absorption kinetics for (**6**) in room temperature acetonitrile collected with ~500 nm pump pulse and at a probe wavelength of 380 nm (top), 390 nm (middle) and 607 nm (bottom). The raw data (blue) were fit with a multi-exponential function (red).

Lastly, the single wavelength data for [Ru(tmb)$_2$(bpy-3,5-dimethylphenyl-MV)](PF$_6$)$_4$ (**7**) is presented. The data are shown below in **Figure 5.16** where the raw data are shown in blue and a double exponential fit of the data in red. The data were collected in room temperature acetonitrile with an ~500 nm (80 fs fwhm) pump pulse. Probe wavelengths of 390 nm (middle panel) and 607 nm (bottom panel) were chosen to probe ET photoproduct dynamics and a probe wavelength of 380 nm (top panel) was selected. We see here that the data probing at 380 nm is similar in shape to the data probing at 390 nm and 607 nm. Like the data of [Ru(tmb)$_2$(bpy-2,6-dimethylphenyl-MV)](PF$_6$)$_4$ (**5**) and [Ru(tmb)$_2$(bpy-2,5-dimethylphenyl-MV)](PF$_6$)$_4$ (**6**) we see from the insets that the dynamics for this complex are slower than those of (**3**) and (**4**). Consistent with complexes (**5**) and (**6**) a double exponential function successfully fit the data probing at 380, 390 nm and 607 nm The fits of [Ru(tmb)$_2$(bpy-3,5-dimethylphenyl-MV)](PF$_6$)$_4$ (**7**) reveal that a fast component of ~3 ps and a long component of ~25 ps fit the data satisfactorily.

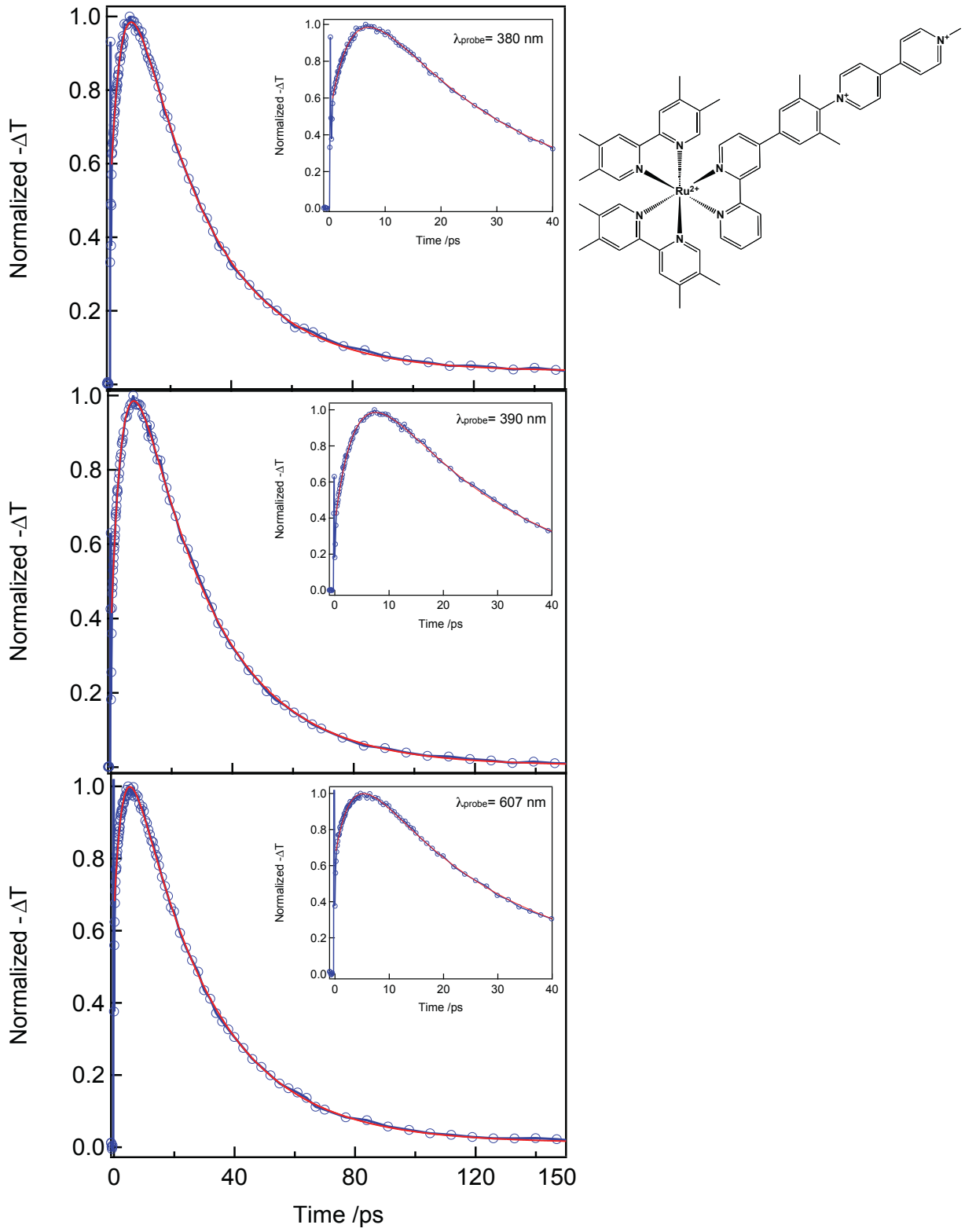

Figure 5.16 Transient absorption kinetics for (**7**) in room temperature acetonitrile collected with ~500 nm pump pulse and at a probe wavelength of 380 nm (top), 390 nm (middle) and 607 nm (bottom). The raw data (blue) were fit with a multi-exponential function (red).

Clearly $[Ru(tmb)_2(bpy\text{-}phenyl\text{-}MV)](PF_6)_4$ (**3**) undergoes an additional photo-excited process seeing as it is the only complex in this series that requires a triple exponential function to fit the single wavelength kinetic data. As was established in Chapter Four this component was assigned as the vibrationally excited lifetime of the directly excited acceptor moiety. The calculated absorption spectra of the complexes with steric bulk did not show any evidence for direct excitation to the acceptor and the single wavelength kinetic data show no signature of the component that is a result of the direct excitation process. Thereby for the remainder of the discussion pertaining to ET, lifetime τ_3 will not be discussed since it was found to be independent of the electron transfer process.

Consistent with the assignment of normal kinetics for ET that is described in Chapter Four and Appendix Two, we assign the fast component from the fits of the DBA complexes as τ_{ET} and the slow component as τ_{BET}. The lifetimes and rate constants for ET and BET are summarized below in **Table 5.5**. The error bars reported in this table represent 2σ determined from fitting three separate measurements of kinetics collected at λ_{probe} =607 nm for each complex.

Table 5.5 Electron Transfer Data of Complexes in Room Temperature Acetonitrile.

Complex		$k_{ET}/10^{11}$ s^{-1}	τ_{ET} /ps	$k_{BET}/10^{10}$ s^{-1}	τ_{BET} /ps
$[Ru(tmb)_2(bpy\text{-}phenyl\text{-}MV)](PF_6)_4$ [a]	(**3**)	14	0.74±0.1	22	4.5±1.0
$[Ru(tmb)_2(bpy\text{-}ortho\text{-}MV)](PF_6)_4$	(**4**)	7.1	1.4±0.1	6.8	14.8±0.2
$[Ru(tmb)_2(bpy\text{-}2,6\text{-}dmp\text{-}MV)](PF_6)_4$	(**5**)	1.8	5.7±0.9	3.6	27.9±2.7
$[Ru(tmb)_2(bpy\text{-}2,5\text{-}dmp\text{-}MV)](PF_6)_4$	(**6**)	2.2	4.6±0.4	4.1	24.4±1.0
$[Ru(tmb)_2(bpy\text{-}3,5\text{-}dmp\text{-}MV)](PF_6)_4$	(**7**)	2.9	3.4±0.8	3.9	25.6±1.2

The error bars reported in this table represent 2σ determined from fitting three separate measurements of kinetics collected at λ_{probe} =607 nm for each complex. [a]The non-electron transfer related component, τ_3, was not listed in the table. Dimethylphenyl has been abbreviated by dmp.

What is clear from the compiled ET data is that despite having very similar driving forces for ET and BET different electron transfer lifetimes are obtained. We see that going from a

complex with no steric bulk (**3**) to a complex that is doubly methylated (**5**) the forward electron transfer process is slowed by a factor of ~8 and the back electron transfer is slowed down by a factor of ~6. Steric bulk on the bridging ligand is undoubtedly determining the electron transfer lifetimes for both forward and back ET processes.

Intuitively, the electronic matrix coupling element, H_{ab}, should decrease across the series as steric bulk is added onto the bridging ligand because this quantity is governed by π-orbital overlap and orbital energy. It was assumed that steric bulk on the bridging ligand would hinder excited state ring-rotational dynamics that permit intraligand delocalization of the excited electron thus decreasing H_{ab}. To accurately determine H_{ab} requires temperature-dependent single wavelength kinetics data. However, these experiments were not conducted on these complexes therefore conclusions reached about the ET behavior of these complexes from H_{ab} are speculative. For the case of complex (**3**) where the electroactive ligand is non-methylated, H_{ab} is expected to be the largest since the ligand is fully conjugated and without steric bulk on the bridging subunit we expect this ligand to be most coplanar thereby permitting facile electronic communication between donor and acceptor moieties. As methyl groups are added to the electroactive ligand the conjugation is disrupted by steric bulk preventing co-planarization and it is expected that H_{ab} will decrease. From the compiled ET data in **Table 5.5** a systematic increase in τ_{ET} and τ_{BET} is observed going from a complex with no sterics (high H_{ab}) to a complex that has a doubly methylated electroactive ligand (low H_{ab}) suggesting that differences in H_{ab} are bringing about the changes in ET lifetimes. By preparing complexes with no, one or two methyl substituents on the bridging subunit we have systematically built in mechanisms for electronically disconnecting the different parts of the molecule.

Although H_{ab} is most likely contributing to the observed differences in forward electron transfer lifetimes for these complexes we now turn to the results of the TD-DFT calculations to offer an additional explanation for the observed differences in forward ET lifetimes. From the attachment densities of these complexes shown in **Figure 5.5** it is evident that steric bulk is effectively dictating the extent of the delocalization of the excited state. This is manifested experimentally by increased red-edge (500-600 nm) absorption in the UV-visible absorption spectra. The complex with no steric bulk on the electroactive ligand, (**3**), has the most delocalized excited state, where electron density is found on the bridging ligand and to some extent on the electroactive acceptor. Complex (**3**) also has the shortest forward electron transfer lifetime (0.74 ps). The complex with the least delocalized excited state is (**5**), where methylation in the 2- and 6- positions of the bridging subunit are restricting electron density onto the 2,2'-bipyridine moiety of the electroactive ligand. Complex (**5**) has the longest forward ET lifetime (5.7 ps). Therefore we conclude that by localizing electron density on certain portions of the electroactive ligands steric bulk is effectively leading to distance-dependent electron transfer, where compounds with most delocalization have the shortest forward ET lifetimes ((**3**) and (**4**)), 0.74 ps and 1.4 ps, respectively) and complexes with the least delocalization have the longest forward ET lifetimes ((**5**) and (**6**)), 5.7 ps and 4.6 ps, respectively). The complex with intermediate delocalization, (**7**), has an intermediate forward ET lifetime, 3.4 ps. One possible way of determining the validity of this explanation would be to prepare an analogous set of complexes with longer distances between donor and acceptor and measure ET lifetimes to see if the same trend persists.

The back electron transfer lifetimes of the complexes in this series plainly show that number of methyl substituents is determining the lifetimes of back electron transfer. The complex with minimal steric bulk on the bridging ligand (**3**) has the shortest back ET lifetime, 4.5 ps. While the three DBA complexes with doubly methylated electroactive ligands, (**5**), (**6**) and (**7**), have the longest back ET lifetimes, 27.9 ps, 24.4 ps and 25.5 ps, respectively. The back ET lifetime of the complex with a singly methylated electroactive ligand, (**4**), falls between the other complexes at 14.8 ps. The spectral features from reductive spectroelectrochemistry and TA spectra of these complexes indicate that the methyl substituents are effectively localizing electron density on different parts of the electroactive ligand. However, looking at the back ET lifetimes for the three complexes with doubly methylated electroactive ligands we find that within the error of the measurement no discernable difference exists. Therefore, delocalization of the ET photoproduct is not the only factor determining back ET lifetimes. To explain what is bringing about the differences in back ET lifetimes we turn to the timescale of ring rotation and how rotational barrier heights are affected by the addition of steric bulk.

Back electron transfer is thought to occur via a superexchange mechanism that is governed by π-orbital overlap between the electron acceptor and ground state.[33-35] π-orbital overlap is affected by the conformation between acceptor and ground state where more planar conformations are more amenable to π-orbital overlap. We propose that the addition of steric bulk reduces the number of conformations that lead to geometries that are amenable to π-orbital overlap thereby slowing back ET. Along these lines, experimental and computational studies on biphenyl and substituted biphenyls[36,37] indicate that rotational barrier height increases as steric bulk is added. A higher rotational barrier will

lead to slower conformational sampling which will in turn lead to slower back ET processes. The fastest back ET is measured for complex (**3**); this complex has no steric bulk to impede conformational sampling. While back ET is slowed as the number of conformational-limiting methyl substituents is increased (14.8 ps for (**4**) and ~30 ps for (**5**), (**6**) and (**7**)). The observation that complexes (**5**), (**6**) and (**7**) essentially have the same back ET lifetime signifies that number of bulky groups is more of a determining factor of restricting conformational sampling than position of bulk. However, looking closely at the back ET lifetimes of complexes (**5**), (**6**) and (**7**) indicates that if two methyl groups are on the same side of the bridging subunit like complexes (**5**) and (**7**) the back ET is longer than if the methyl groups are staggered as in (**6**). Rotation barriers are expected to be higher for complexes with methylation on the same side of the bridging subunit. Thereby indicating that methyl substituent position has some affect on back ET lifetimes but the largest contributing factor to back ET lifetime elongation in these directly linked systems is number of methyl groups.

One of the reasons for systematically methylating various positions of the bridging subunit was to establish if steric bulk can effectively give way to a longer-lived ET photoproduct while not altering the forward ET lifetime. It was speculated that complexes (**6**) and (**7**) would be more effective at trapping the transferred electron onto the acceptor the other complexes. However we find that as methylation increases both ET and back ET are slowed, considerably. As explained above it seems that doubly methylating the electroactive ligand leads to longer back ET lifetimes by restricting conformational sampling but it also limits the delocalization of the initial excited state slowing forward ET. Compared to (**3**), complex (**4**) seems to afford the best ratio of back ET elongation with

respect to slowing forward ET, where the forward ET process is slowed by a factor of two and the back ET process is elongated by a factor of three. Although this was not what was expected when the systems were designed it is evident that in these directly linked systems the addition of one methyl substituent gives more a favorable ratio of back ET lifetime to forward ET lifetime.

5.3 Concluding Remarks

In this chapter the photophysics of a series of complexes that were designed to address the role of structural elements on the rates of photoinduced electron transfer were presented. Systematic methylation of the bridging subunit led to the preparation of five DBA complexes that differed in number and position of methyl substituents. By designing and measuring the ET lifetimes of these DBA complexes one can establish how both number and position of methyl groups affect ET lifetimes. This series of complexes allows for simultaneous determination of whether position of methylation can lead to the formation of longer-lived ET photoproducts while not slowing the forward ET process. The complexes were characterized by UV-visible absorption and emission spectroscopies, DFT and TD-DFT methods and ultrafast pump-probe experiments. Driving forces for ET and BET were also determined. Calculating ET driving forces for the complexes in this series confirmed the expectation that there would be little to no difference in these values.

UV-visible absorption experiments revealed that the spectra for the DBA complexes showed increased red-edge absorption (between 500-600 nm) when overlaid with respective donor complexes. The UV-visible absorption spectra also showed that the extent of red-edge absorption was dependent on number and position of methyl substituent(s) on the bridging aryl group of the electroactive ligand. Results from TD-DFT calculations

showed that the increase in red-edge absorption is explained by delocalization of the MLCT state onto the asymmetric ligand. Complexes where delocalization over the bridging subunit and acceptor moiety was available showed larger increases in red edge absorption than complexes where little or no delocalization was available. This delocalization of the excited state is cited as a possible explanation for the observed forward ET lifetimes; where restricting electron density on certain parts of the electroactive ligand steric bulk is effectively bringing about distance dependent ET.

Back ET lifetimes show that steric bulk on the electroactive ligand can bring about longer ET photoproduct lifetimes. The back ET lifetimes were found to be dependent on the number of methyl substituents and their ability to limit conformational sampling within the electron transfer state. However, it was established that the addition of two methyl groups on the bridging subunit slows forward ET more than it elongates back ET with respect to complex (**3**). Thus, the doubly methylated systems are less efficient for producing and storing charge separated redox equivalents than complex (**4**).

5.4 References

(1) Damrauer, N. H.; Boussie, T. R.; Devenney, M.; McCusker, J. K. *J. Am. Chem. Soc.* **1997**, *119*, 8253.

(2) Damrauer, N. H.; Weldon, B. T.; McCusker, J. K. *J. Phys. Chem. A* **1998**, *102*, 3382.

(3) Damrauer, N. H.; McCusker, J. K. *J. Phys. Chem. A* **1999**, *103*, 8440.

(4) Damrauer, N. H.; McCusker, J. K. *Inorg. Chem.* **1999**, *38*, 4268.

(5) Lyubimova, O. O.; Baranovskii, V. I. *Journal of Structural Chemistry* **2003**, *44*, 728.

(6) Meylemans, H. A.; Hewitt, J. T.; Abdelhaq, M.; Vallett, P. J.; Damrauer, N. H. *J. Am. Chem. Soc.* **2010**, *132*, 11464.

(7) Zhou, Q. X.; Lei, W. H.; Li, C.; Hou, Y. J.; Wang, X. S.; Zhang, B. W. *New Journal of Chemistry* **2010**, *34*, 137.

(8) Hayes, M. A.; Meckel, C.; Schatz, E.; Ward, M. D. *J Chem Soc Dalton* **1992**, 703.

(9) Sun, Y. J.; El Ojaimi, M.; Hammitt, R.; Thummel, R. P.; Turro, C. *J. Phys. Chem. B* **2010**, *114*, 14664.

(10) Henrich, J. D.; Zhang, H. Y.; Dutta, P. K.; Kohler, B. *J. Phys. Chem. B* **2010**, *114*, 14679.
(11) Strouse, G. F.; Schoonover, J. R.; Duesing, R.; Boyde, S.; Jones, W. E.; Meyer, T. J. *Inorg. Chem.* **1995**, *34*, 473.
(12) Benniston, A. C.; Harriman, A.; Grosshenny, V.; Ziessel, R. *New Journal of Chemistry* **1997**, *21*, 405.
(13) Juris, A.; Balzani, V.; Barigelletti, F.; Campagna, S.; Belser, P.; Von Zelewsky, A. *Coord. Chem. Rev.* **1988**, *84*, 85.
(14) Kober, E. M.; Caspar, J. V.; Lumpkin, R. S.; Meyer, T. J. *J. Phys. Chem.* **1986**, *90*, 3722.
(15) Caspar, J. V.; Meyer, T. J. *J. Phys. Chem.* **1983**, *87*, 952.
(16) Robinson, G. W.; Frosch, R. P. *J. Chem. Phys.* **1963**, *38*, 1187.
(17) Siebrand, W. *J. Chem. Phys.* **1967**, *47*, 2411.
(18) Weller, A. *Z. Phys. Chem.* **1982**, *133*, 93.
(19) Vleck, A.; Zalis, S. *Coord. Chem. Rev.* **2007**, *251*, 258.
(20) Charlot, M. F.; Pellegrin, Y.; Quaranta, A.; Leibl, W.; Aukauloo, A. *Chem. Eur. J.* **2006**, *12*, 796.
(21) Ciofini, I.; Laine, P. P.; Bedioui, F.; Adamo, C. *J. Am. Chem. Soc.* **2004**, *126*, 10763.
(22) Meylemans, H. A.; Damrauer, N. H. *Inorg. Chem.* **2009**, *48*, 11161.
(23) Vallett, P. J.; Damrauer, N. H. *J. Phys. Chem. A* **2011**, *115*, 3122.
(24) Head-Gordon, M.; Grana, A. M.; Maurice, D.; White, C. A. *J. Phys. Chem.* **1995**, *1995*, 14261.
(25) Song, J. A.; Gao, F.; Shi, B.; Liang, W. Z. *Phys. Chem. Chem. Phys.* **2010**, *12*, 13070.
(26) Jacquemin, D.; Perpete, E. A.; Ciofini, I.; Adamo, C. *J. Chem. Theor. Comput.* **2010**, *6*, 1532.
(27) McCusker, J. K. *Acc. Chem. Res.* **2003**, *36*, 876.
(28) Balzani, V.; Campagna, S.; Denti, G.; Juris, A.; Serroni, S.; Venturi, M. *Acc. Chem. Res.* **1998**, *31*, 26.
(29) Braterman, P. S.; Harriman, A.; Heath, G. A.; Yellowlees, L. J. *J Chem Soc Dalton* **1983**, 1801.
(30) Yoshimura, A.; Hoffman, M. Z.; Sun, H. *J. Photochem. Photobiol. Chem.* **1993**, *70*, 29.
(31) Wallin, S.; Davidsson, J.; Modin, J.; Hammarstrom, L. *J. Phys. Chem. A* **2005**, *109*, 4697.
(32) Zalis, S.; Consani, C.; El Nahhas, A.; Cannizzo, A.; Chergui, M.; Hartl, F.; Vlcek, A. *Inorg. Chim. Acta* **2011**, *374*, 578.
(33) Wasielewski, M. R. *Chem. Rev.* **1992**, *92*, 435.
(34) Wenger, O. S. *Coord. Chem. Rev.* **2009**, *253*, 1439.
(35) Albinsson, B.; Martensson, J. *J. Photochem. Photobiol. C-Photochem. Rev.* **2008**, *9*, 138.
(36) Deeg, F. W.; Stankus, J. J.; Greenfield, S. R.; Newell, V. J.; Fayer, M. D. *J. Chem. Phys.* **1989**, *90*, 6893.
(37) Mazzanti, A.; Lunazzi, L.; Minzoni, M.; Anderson, J. E. *J Org Chem* **2006**, *71*, 5474.

Bibliography

(1) Lewis, N. S.; Nocera, D. G. *Proc. Natl. Acad. Sci. U.S.A.* **2006**, *103*, 15729.

(2) *IPCC Fourth Assessment Report; Climate Change 2007: The Physical Science Basis*; Cambridge University Press: Cambridge, 2007.

(3) Hoffert, M. I.; Caldeira, K.; Jain, A. K.; Haites, E. F.; Harvey, L. D. D.; Potter, S. D.; Schlesinger, M. E.; Schneider, S. H.; Watts, R. G.; Wigley, T. M. L.; Wuebbles, D. J. *Nature* **1998**, *395*, 881.

(4) *Basic Research Needs for Solar Energy Utilization*; Office of Science; US Department of Energy: Washington DC, 2005.

(5) Nozik, A. J. *Annu. Rev. Phys. Chem.* **1978**, *29*, 189.

(6) Gray, H. B.; Maverick, A. W. *Science* **1981**, *214*, 1201.

(7) Meyer, T. J. *Acc. Chem. Res.* **1989**, *22*, 163.

(8) O'Regan, B.; Gratzel, M. *Nature* **1991**, *353*, 737.

(9) Wasielewski, M. R. *Chem. Rev.* **1992**, *92*, 435.

(10) Kalyanasundaram, K.; Gratzel, M. *Coord. Chem. Rev.* **1998**, *177*, 347.

(11) Gosztola, D.; Niemczyk, M. P.; Svec, W.; Lukas, A. S.; Wasielewski, M. R. *J. Phys. Chem. A* **2000**, *104*, 6545.

(12) Gust, D.; Moore, T. A.; Moore, A. L. *Acc. Chem. Res.* **2001**, *34*, 40.

(13) Gratzel, M. *J. Photochem. Photobiol., C* **2003**, *4*, 145.

(14) Nozik, A. J. *Inorg. Chem.* **2005**, *44*, 6893.

(15) Wenger, O. S.; Leigh, B. S.; Villahermosa, R. M.; Gray, H. B.; Winkler, J. R. *Science* **2005**, *307*, 99.

(16) Alstrum-Acevedo, J. H.; Brennaman, M. K.; Meyer, T. J. *Inorg. Chem.* **2005**, *44*, 6802.

(17) Meyer, G. J. *Inorg. Chem.* **2005**, *44*, 6852.

(18) Wasielewski, M. R. *J. Org. Chem.* **2006**, *71*, 5051.

(19) Crabtree, G. W.; Lewis, N. S. *Physics Today* **2007**, *60*, 37.

(20) Kamat, P. V. *J. Phys. Chem. C* **2007**, *111*, 2834.

(21) Wasielewski, M. R. *Chem. Rev.* **1992**, *92*, 435.

(22) Balch, A. L.; Olmstead, M. M. *Chem. Rev.* **1998**, *98*, 2123.

(23) Barbara, P. F.; Meyer, T. J.; Ratner, M. A. *J. Phys. Chem.* **1996**, *100*, 13148.

(24) Benniston, A. C.; Harriman, A. *Chem. Soc. Rev.* **2006**, *35*, 169.

(25) Johansson, O.; Borgstrom, M.; Lomoth, R.; Palmblad, M.; Bergquist, J.; Hammarstrom, L.; Sun, L. C.; Akermark, B. *Inorg. Chem.* **2003**, *42*, 2908.

(26) Collin, J. P.; Guillerez, S.; Sauvage, J. P.; Barigelletti, F.; Decola, L.; Flamigni, L.; Balzani, V. *Inorg. Chem.* **1991**, *30*, 4230.

(27) Cukier, R. I.; Nocera, D. G. *Annu. Rev. Phys. Chem.* **1998**, *49*, 337.

(28) Damrauer, N. H.; Hodgkiss, J. M.; Rosenthal, J.; Nocera, D. G. *J. Phys. Chem. B* **2004**, *108*, 6315.

(29) Davis, W. B.; Svec, W. A.; Ratner, M. A.; Wasielewski, M. R. *Nature* **1998**, *396*, 60.

(30) Davis, W. B.; Ratner, M. A.; Wasielewski, M. R. *J. Am. Chem. Soc.* **2001**, *123*, 7877.

(31) Heimer, T. A.; Heilweil, E. J.; Bignozzi, C. A.; Meyer, G. J. *J. Phys. Chem. A* **2000**, *104*, 4256.

(32) Laine, P. P.; Loiseau, F.; Campagna, S.; Ciofini, I.; Adamo, C. *Inorg. Chem.* **2006**, *45*, 5538.
(33) Macqueen, D. B.; Schanze, K. S. *J. Am. Chem. Soc.* **1991**, *113*, 7470.
(34) Newton, M. D. *Chem. Rev.* **1991**, *91*, 767.
(35) Oevering, H.; Paddonrow, M. N.; Heppener, M.; Oliver, A. M.; Cotsaris, E.; Verhoeven, J. W.; Hush, N. S. *J. Am. Chem. Soc.* **1987**, *109*, 3258.
(36) Yonemoto, E. H.; Riley, R. L.; Kim, Y. I.; Atherton, S. J.; Schmehl, R. H.; Mallouk, T. E. *J. Am. Chem. Soc.* **1992**, *114*, 8081.
(37) Weller, A. *Z. Phys. Chem.* **1982**, *133*, 93.
(38) Weber, J. M.; Rawls, M. T.; MacKenzie, V. J.; Limoges, B. R.; Elliott, C. M. *J. Am. Chem. Soc.* **2007**, *129*, 313.
(39) Watson, D. F.; Meyer, G. J. *Annu. Rev. Phys. Chem.* **2005**, *56*, 119.
(40) Sauvage, J.-P.; Collin, J.-P.; Chambron, J.-C.; Guillerez, S.; Coudret, C. *Chem. Rev.* **1994**, *94*, 993.
(41) Rubtsov, I. V.; Susumu, K.; Rubtsov, G. I.; Therien, M. J. *J. Am. Chem. Soc.* **2003**, *125*, 2687.
(42) Opperman, K. A.; Mecklenburg, S. L.; Meyer, T. J. *Inorg. Chem.* **1994**, *33*, 5295.
(43) Juris, A.; Balzani, V.; Barigelletti, F.; Campagna, S.; Belser, P.; Vonzelewsky, A. *Coord. Chem. Rev.* **1988**, *84*, 85.
(44) Demas, J. N.; Crosby, G. A. *J. Phys. Chem.* **1971**, *75*, 991.
(45) Kalyanasundaram, K. **1992**.
(46) Anderson, P. A.; Keene, F. R.; Meyer, T. J.; Moss, J. A.; Strouse, G. F.; Treadway, J. A. *J Chem Soc Dalton* **2002**, 3820.
(47) Meylemans, H. A.; Lei, C. F.; Damrauer, N. H. *Inorg. Chem.* **2008**, *47*, 4060.
(48) Laine, P. P.; Bedioui, F.; Loiseau, F.; Chiorboli, C.; Campagna, S. *J. Am. Chem. Soc.* **2006**, *128*, 7510.
(49) Sauvage, J. P.; Collin, J. P.; Chambron, J. C.; Guillerez, S.; Coudret, C.; Balzani, V.; Barigelletti, F.; Decola, L.; Flamigni, L. *Chem. Rev.* **1994**, *94*, 993.
(50) Laine, P. P.; Campagna, S.; Loiseau, F. *Coord. Chem. Rev.* **2008**, 2552.
(51) Phifer, C. C.; McMillin, D. R. *Inorg. Chem.* **1986**, *25*, 1329.
(52) Boyde, S.; Strouse, G. F.; Jones, W. E.; Meyer, T. J. *J. Am. Chem. Soc.* **1990**, *112*, 7395.
(53) Strouse, G. F.; Schoonover, J. R.; Duesing, R.; Boyde, S.; Jones, W. E.; Meyer, T. J. *Inorg. Chem.* **1995**, *34*, 473.
(54) Treadway, J. A.; Loeb, B.; Lopez, R.; Anderson, P. A.; Keene, F. R.; Meyer, T. J. *Inorg. Chem.* **1996**, *35*, 2242.
(55) Damrauer, N. H.; Boussie, T. R.; Devenney, M.; McCusker, J. K. *J. Am. Chem. Soc.* **1997**, *119*, 8253.
(56) Hammarstrom, L.; Barigelletti, F.; Flamigni, L.; Indelli, M. T.; Armaroli, N.; Calogero, G.; Guardigli, M.; Sour, A.; Collin, J. P.; Sauvage, J. P. *J. Phys. Chem. A* **1997**, *101*, 9061.
(57) Feliz, M. R.; Rodriguez-Nieto, F.; Ruiz, G.; Wolcan, E. *J Photochem Photobiol a-Chem* **1998**, *117*, 185.
(58) Damrauer, N. H.; McCusker, J. K. *J. Phys. Chem. A* **1999**, *103*, 8440.
(59) Damrauer, N. H.; McCusker, J. K. *Inorg. Chem.* **1999**, *38*, 4268.
(60) Miller, M. T.; Gantzel, P. K.; Karpishin, T. B. *Inorg. Chem.* **1999**, *38*, 3414.

(61) Michalec, J. F.; Bejune, S. A.; McMillin, D. R. *Inorg. Chem.* **2000**, *39*, 2708.
(62) Berg, K. E.; Tran, A.; Raymond, M. K.; Abrahamsson, M.; Wolny, J.; Redon, S.; Andersson, M.; Sun, L. C.; Styring, S.; Hammarstrom, L.; Toftlund, H.; Akermark, B. *Eur. J. Inorg. Chem.* **2001**, 1019.
(63) Michalec, J. F.; Bejune, S. A.; Cuttell, D. G.; Summerton, G. C.; Gertenbach, J. A.; Field, J. S.; Haines, R. J.; McMillin, D. R. *Inorg. Chem.* **2001**, *40*, 2193.
(64) Walters, K. A.; Ley, K. D.; Cavalaheiro, C. S. P.; Miller, S. E.; Gosztola, D.; Wasielewski, M. R.; Bussandri, A. P.; van Willigen, H.; Schanze, K. S. *J. Am. Chem. Soc.* **2001**, *123*, 8329.
(65) Walters, K. A.; Premvardhan, L. L.; Liu, Y.; Peteanu, L. A.; Schanze, K. S. *Chem. Phys. Lett.* **2001**, *339*, 255.
(66) Wang, Y. S.; Liu, S. X.; Pinto, M. R.; Dattelbaum, D. M.; Schoonover, J. R.; Schanze, K. S. *J. Phys. Chem. A* **2001**, *105*, 11118.
(67) Balazs, G. C.; del Guerzo, A.; Schmehl, R. H. *Photochem. Photobiol. Sci.* **2005**, *4*, 89.
(68) Goze, C.; Sabatini, C.; Barbieri, A.; Barigelletti, F.; Ziessel, R. *Inorg. Chem.* **2007**, *46*, 7341.
(69) Clark, M. L.; Diring, S.; Retailleau, P.; McMillin, D. R.; Ziessel, R. *Chem. Eur. J.* **2008**, *14*, 7168.
(70) Strouse, G. F.; Schoonover, J. R.; Duesing, R.; Boyde, S.; Jones, W. E.; Meyer, T. J. *Inorg. Chem.* **1995**, *34*, 473.
(71) Damrauer, N. H.; Weldon, B. T.; McCusker, J. K. *J. Phys. Chem. A* **1998**, *102*, 3382.
(72) Lyubimova, O. O.; Baranovskii, V. I. *Journal of Structural Chemistry* **2003**, *44*, 728.
(73) Almenningen, A.; Bastiansen, O.; Fernholt, L.; Cyvin, B. N.; Cyvin, S. J.; Samdal, S. *J Mol Struct* **1985**, *128*, 59.
(74) Brock, C. P.; Minton, R. P. *J. Am. Chem. Soc.* **1989**, *111*, 4586.
(75) Rubio, M.; Merchan, M.; Orti, E. *Theoretica Chimica Acta* **1995**, *91*, 17.
(76) Rubio, M.; Merchan, M.; Orti, E.; Roos, B. O. *Chem. Phys. Lett.* **1995**, *234*, 373.
(77) Meylemans, H. A.; Hewitt, J. T.; Abdelhaq, M.; Vallett, P. J.; Damrauer, N. H. *J. Am. Chem. Soc.* **2010**, *132*, 11464.
(78) Meylemans, H.; Damrauer, N. H., In preparation.
(79) Larsson, S. *J. Am. Chem. Soc.* **1981**, *103*, 4034.
(80) Helms, A.; Heiler, D.; McLendon, G. *J. Am. Chem. Soc.* **1991**, *113*, 4325.
(81) Gourdon, A. *New J. Chem.* **1992**, *16*, 953.
(82) Dong, T. Y.; Huang, C. H.; Chang, C. K.; Wen, Y. S.; Lee, S. L.; Chen, J. A.; Yeh, W. Y.; Yeh, A. *J. Am. Chem. Soc.* **1993**, *115*, 6357.
(83) Ward, M. D. *Chem. Soc. Rev.* **1995**, *24*, 121.
(84) Sachs, S. B.; Dudek, S. P.; Hsung, R. P.; Sita, L. R.; Smalley, J. F.; Newton, M. D.; Feldberg, S. W.; Chidsey, C. E. D. *J. Am. Chem. Soc.* **1997**, *119*, 10563.
(85) Newton, M. D. *International Journal of Quantum Chemistry* **2000**, *77*, 255.
(86) Toutounji, M. M.; Ratner, M. A. *J. Phys. Chem. A* **2000**, *104*, 8566.
(87) Nelsen, S. F.; Li, G. Q.; Konradsson, A. *Org. Lett.* **2001**, *3*, 1583.
(88) Nelsen, S. F.; Blomgren, F. *J. Org. Chem.* **2001**, *66*, 6551.
(89) Kyrychenko, A.; Albinsson, B. *Chem. Phys. Lett.* **2002**, *366*, 291.

(90) Benniston, A. C.; Harriman, A.; Li, P.; Sams, C. A.; Ward, M. D. *J. Am. Chem. Soc.* **2004**, *126*, 13630.
(91) Rubtsov, I. V.; Redmore, N. P.; Hochstrasser, R. M.; Therien, M. J. *J. Am. Chem. Soc.* **2004**, *126*, 2684.
(92) Joachim, C.; Ratner, M. A. *Nanotechnology* **2004**, *15*, 1065.
(93) Smalley, J. F.; Sachs, S. B.; Chidsey, C. E. D.; Dudek, S. P.; Sikes, H. D.; Creager, S. E.; Yu, C. J.; Feldberg, S. W.; Newton, M. D. *J. Am. Chem. Soc.* **2004**, *126*, 14620.
(94) Benniston, A. C.; Harriman, A.; Li, P. Y.; Patel, P. V.; Sams, C. A. *Phys. Chem. Chem. Phys.* **2005**, *7*, 3677.
(95) Holman, M. W.; Yan, P.; Ching, K. C.; Liu, R. C.; Ishak, F. I.; Adams, D. M. *Chem. Phys. Lett.* **2005**, *413*, 501.
(96) Weiss, E. A.; Tauber, M. J.; Kelley, R. F.; Ahrens, M. J.; Ratner, M. A.; Wasielewski, M. R. *J. Am. Chem. Soc.* **2005**, *127*, 11842.
(97) Welter, S.; Salluce, N.; Belser, P.; Groeneveld, M.; De Cola, L. *Coord. Chem. Rev.* **2005**, *249*, 1360.
(98) Valasek, M.; Pecka, J.; Jindrich, J.; Calleja, G.; Craig, P. R.; Michl, J. *J. Org. Chem.* **2005**, *70*, 405.
(99) Benniston, A. C.; Harriman, A.; Li, P. Y.; Patel, P. V.; Sams, C. A. *J. Org. Chem.* **2006**, *71*, 3481.
(100) Eng, M. P.; Ljungdahl, T.; Martensson, J.; Albinsson, B. *J. Phys. Chem. B* **2006**, *110*, 6483.
(101) Venkataraman, L.; Klare, J. E.; Nuckolls, C.; Hybertsen, M. S.; Steigerwald, M. L. *Nature* **2006**, *442*, 904.
(102) Albinsson, B.; Eng, M.; Pettersson, K.; Winters, M. *Phys. Chem. Chem. Phys.* **2007**, *9*, 5847.
(103) Kilsa, K.; Kajanus, J.; Martensson, J.; Albinsson, B. *J. Phys. Chem. B* **1999**, *103*, 7329.
(104) Indelli, M. T.; Chiorboli, C.; Flamigni, L.; De Cola, L.; Scandola, F. *Inorg. Chem.* **2007**, *46*, 5630.
(105) Albinsson, B.; Martensson, J. *J. Photochem. Photobiol. C-Photochem. Rev.* **2008**, *9*, 138.
(106) Benniston, A.; Harriman, A.; Li, P.; Patel, P.; Sams, C. *Chem. Eur. J.* **2008**, *14*, 1710.
(107) Eng, M.; Albinsson, B. *Chem. Phys.* **2009**, *357*, 132.
(108) Ciofini, I.; Laine, P. P.; Bedioui, F.; Adamo, C. *J. Am. Chem. Soc.* **2004**, *126*, 10763.
(109) Monk, P. M. S. *The viologens : physicochemical properties, synthesis, and applications of the salts of 4,4'-bipyridine*; Wiley: Chichester ; New York, 1998.
(110) *Electron Transfer in Chemistry*; Balzani, V., Ed.; Wiley-VCH: Weinheim, 2001.
(111) Cooley, L. F.; Headford, C. E. L.; Elliott, C. M.; Kelley, D. F. *J. Am. Chem. Soc.* **1988**, *110*, 6673.
(112) Cooley, L. F.; Larson, S. L.; Elliott, C. M.; Kelley, D. F. *J. Phys. Chem.* **1991**, *95*, 10694.
(113) Elliott, C. M.; Freitag, R. A.; Blaney, D. D. *J. Am. Chem. Soc.* **1985**, *107*, 4647.
(114) Kelly, L. A.; Rodgers, M. A. J. *J. Phys. Chem.* **1995**, *99*, 13132.

(115) Lomoth, R.; Haupl, T.; Johansson, O.; Hammarstrom, L. *Chem. Eur. J.* **2002**, *8*, 102.
(116) Yonemoto, E. H.; Saupe, G. B.; Schmehl, R. H.; Hubig, S. M.; Riley, R. L.; Iverson, B. L.; Mallouk, T. E. *J. Am. Chem. Soc.* **1994**, *116*, 4786.
(117) Meylemans, H. a.; Lei, C.-F.; Damrauer, N. H. *Inorg. Chem.* **2008**, *47*, 4060.
(118) Meylemans, H. A.; Damrauer, N. H. *Inorg. Chem.* **2009**, *48*, 11161.
(119) Henrich, J. D.; Zhang, H. Y.; Dutta, P. K.; Kohler, B. *J. Phys. Chem. B* **2010**, *114*, 14679.
(120) BergBrennan, C.; Subramanian, P.; Absi, M.; Stern, C.; Hupp, J. T. *Inorg. Chem.* **1996**, *35*, 3719.
(121) Cordaro, J. G.; McCusker, J. K.; Bergman, R. G. *Chem. Commun.* **2002**, 1496.
(122) Borgstrom, M.; Johansson, O.; Lomoth, R.; Baudin, H. B.; Wallin, S.; Sun, L. C.; Akermark, B.; Hammarstrom, L. *Inorg. Chem.* **2003**, *42*, 5173.
(123) Zhang, Z.; Dong, Y. W.; Wang, G. W. *Chem. Lett.* **2003**, *32*, 966.
(124) Coe, B. J.; Harris, J. A.; Harrington, L. J.; Jeffery, J. C.; Rees, L. H.; Houbrechts, S.; Persoons, A. *Inorg. Chem.* **1998**, *37*, 3391.
(125) Pavlishchuk, V. *Inorg. Chim. Acta* **2000**, *298*, 97.
(126) Li, J. J. *Name reactions in heterocyclic chemistry*; Wiley-Interscience: Hoboken, N.J., 2005.
(127) Cheng, W. C.; Kurth, M. J. *Org Prep Proced Int* **2002**, *34*, 585.
(128) Coe, B. J.; Harris, J. A.; Jones, L. A.; Brunschwig, B. S.; Song, K.; Clays, K.; Garin, J.; Orduna, J.; Coles, S. J.; Hursthouse, M. B. *J. Am. Chem. Soc.* **2005**, *127*, 4845.
(129) Freitag, M.; Gundlach, L.; Piotrowiak, P.; Galoppini, E. *J. Am. Chem. Soc.* **2012**, *134*, 3358.
(130) Coe, B. J.; Foxon, S. P.; Harper, E. C.; Helliwell, M.; Raftery, J.; Swanson, C. A.; Brunschwig, B. S.; Clays, K.; Franz, E.; Garin, J.; Orduna, J.; Horton, P. N.; Hursthouse, M. B. *J. Am. Chem. Soc.* **2010**, *132*, 1706.
(131) Coe, B. J.; Fielden, J.; Foxon, S. P.; Brunschwig, B. S.; Asselberghs, I.; Clays, K.; Samoc, A.; Samoc, M. *J. Am. Chem. Soc.* **2010**, *132*, 3496.
(132) Marvell, E. N.; Caple, G.; Shahidi, T. *J. Am. Chem. Soc.* **1970**, *92*, 5641.
(133) Ise, N.; Okubo, T.; Kitano, H.; Kunugi, S. *J. Am. Chem. Soc.* **1975**, *97*, 2882.
(134) Kunugi, S.; Okubo, T.; Ise, N. *J. Am. Chem. Soc.* **1976**, *98*, 2282.
(135) Miyaura, N.; Yamada, K.; Suzuki, A. *Tetrahedron Lett.* **1979**, *20*, 3437.
(136) Miyaura, N.; Suzuki, A. *J Chem Soc Chem Comm* **1979**, 866.
(137) Miyaura, N.; Suzuki, A. *Chem. Rev.* **1995**, *95*, 2457.
(138) Kocienski, P. J. *Protecting groups*; Corr. ed.; G. Thieme: Stuttgart ; New York, 2000.
(139) Saika, T.; Iyoda, T.; Shimidzu, T. *Chem. Lett.* **1990**, 1955.
(140) McCusker, J. K. *Acc. Chem. Res.* **2003**, *36*, 876.
(141) Watanabe, T.; Honda, K. *J. Phys. Chem.* **1982**, *86*, 2617.
(142) Haupl, T.; Lomoth, R.; Hammarstrom, L. *J. Phys. Chem. A* **2003**, *107*, 435.
(143) Kalyanasundaram, K. *Photochemistry of Polypyridine and Porphyrin Complexes*; Academic Press Inc.: San Diego, 1992.
(144) Lever, A. B. P. *Inorg. Chem.* **1990**, *29*, 1271.
(145) Vos, J. G.; Kelly, J. M. *Dalton T* **2006**, 4869.
(146) Ghosh, B. K.; Chakravorty, A. *Coord. Chem. Rev.* **1989**, *95*, 239.

(147) Damrauer, N. H.; Cerullo, G.; Yeh, A.; Boussie, T. R.; Shank, C. V.; McCusker, J. K. *Science* **1997**, *275*, 54.

(148) Bhasikuttan, A. C.; Suzuki, M.; Nakashima, S.; Okada, T. *J. Am. Chem. Soc.* **2002**, *124*, 8398.

(149) Cannizzo, A.; van Mourik, F.; Gawelda, W.; Zgrablic, G.; Bressler, C.; Chergui, M. *Angew Chem Int Ed* **2006**, *45*, 3174.

(150) Yoon, S.; Kukura, P.; Stuart, C. M.; Mathies, R. A. *Mol. Phys.* **2006**, *104*, 1275.

(151) Mines, G. A.; Bjerrum, M. J.; Hill, M. G.; Casimiro, D. R.; Chang, I. J.; Winkler, J. R.; Gray, H. B. *J. Am. Chem. Soc.* **1996**, *118*, 1961.

(152) Togano, T.; Nagao, N.; Tsuchida, M.; Kumakura, H.; Hisamatsu, K.; Howell, F. S.; Mukaida, M. *Inorg. Chim. Acta* **1992**, *195*, 221.

(153) Sullivan, B. P.; Salmon, D. J.; Meyer, T. J. *Inorg. Chem.* **1978**, *17*, 3334.

(154) Juris, A.; Balzani, V.; Barigelletti, F.; Campagna, S.; Belser, P.; Von Zelewsky, A. *Coord. Chem. Rev.* **1988**, *84*, 85.

(155) McDaniel, A. M.; Tseng, H. W.; Damrauer, N. H.; Shores, M. P. *Inorg. Chem.* **2010**, *49*, 7981.

(156) Shao, Y.; Molnar, L. F.; Jung, Y.; Kussmann, J.; Ochsenfeld, C.; Brown, S. T.; Gilbert, A. T.; Slipchenko, L. V.; Levchenko, S. V.; O'Neill, D. P.; DiStasio, R. A., Jr.; Lochan, R. C.; Wang, T.; Beran, G. J.; Besley, N. A.; Herbert, J. M.; Lin, C. Y.; Van Voorhis, T.; Chien, S. H.; Sodt, A.; Steele, R. P.; Rassolov, V. A.; Maslen, P. E.; Korambath, P. P.; Adamson, R. D.; Austin, B.; Baker, J.; Byrd, E. F.; Dachsel, H.; Doerksen, R. J.; Dreuw, A.; Dunietz, B. D.; Dutoi, A. D.; Furlani, T. R.; Gwaltney, S. R.; Heyden, A.; Hirata, S.; Hsu, C. P.; Kedziora, G.; Khalliulin, R. Z.; Klunzinger, P.; Lee, A. M.; Lee, M. S.; Liang, W.; Lotan, I.; Nair, N.; Peters, B.; Proynov, E. I.; Pieniazek, P. A.; Rhee, Y. M.; Ritchie, J.; Rosta, E.; Sherrill, C. D.; Simmonett, A. C.; Subotnik, J. E.; Woodcock, H. L., 3rd; Zhang, W.; Bell, A. T.; Chakraborty, A. K.; Chipman, D. M.; Keil, F. J.; Warshel, A.; Hehre, W. J.; Schaefer, H. F., 3rd; Kong, J.; Krylov, A. I.; Gill, P. M.; Head-Gordon, M. *Physical chemistry chemical physics : PCCP* **2006**, *8*, 3172.

(157) Chai, J. D.; Head-Gordon, M. *J. Chem. Phys.* **2008**, *128*, 084106.

(158) Gordon, M. S.; Binkley, J. S.; Pople, J. A.; Pietro, W. J.; Hehre, W. J. *J. Am. Chem. Soc.* **1982**, *104*, 2797.

(159) Binkley, J. S.; Pople, J. A.; Hehre, W. J. *J. Am. Chem. Soc.* **1980**, *102*, 929.

(160) Andrae, D.; Dolg, M.; Stoll, H.; Preub, H. *Theoret. Chim. Acta* **1990**, 123.

(161) Andrae, D.; Hiuflermann, U.; Dolg, M.; Stoll, H.; Preull, H. *Theoret. Chim. Acta* **1991**, 247.

(162) Hirata, S.; Head-Gordon, M. *Chem. Phys. Lett.* **1999**, *3*, 291.

(163) Head-Gordon, M.; Grana, A. M.; Maurice, D.; White, C. A. *J. Phys. Chem.* **1995**, *1995*, 14261.

(164) Varetto, U.; 5.4.0.8 ed.; Swiss National Supercomputing Centre: Manno, Switzerland, 2009.

(165) Shirakawa, A.; Kobayashi, T. *Appl. Phys. Lett* **1998**, *72*, 147.

(166) Wilhelm, T.; Piel, J.; Riedle, E. *Opt. Lett.* **1997**, *22*, 1494.

(167) Megerle, U.; Pugliesi, I.; Schriever, C.; Sailer, C. F.; Riedle, E. *Appl. Phys. B* **2009**, *96*, 215.

(168) Grumstrup, E. M.; Johnson, J. C.; Damrauer, N. H. *Phys. Rev. Lett.* **2010**, *105*, 257403.

(169) Kovalenko, S. A.; Dobryakov, A. L.; Ruthmann, J.; Ernsting, N. P. *Phys. Rev. A* **1999**, *59*, 2369.
(170) Zhou, Q. X.; Lei, W. H.; Li, C.; Hou, Y. J.; Wang, X. S.; Zhang, B. W. *New Journal of Chemistry* **2010**, *34*, 137.
(171) Hayes, M. A.; Meckel, C.; Schatz, E.; Ward, M. D. *J Chem Soc Dalton* **1992**, 703.
(172) Sun, Y. J.; El Ojaimi, M.; Hammitt, R.; Thummel, R. P.; Turro, C. *J. Phys. Chem. B* **2010**, *114*, 14664.
(173) Benniston, A. C.; Harriman, A.; Grosshenny, V.; Ziessel, R. *New Journal of Chemistry* **1997**, *21*, 405.
(174) Suzuki, K.; Kobayashi, A.; Kaneko, S.; Takehira, K.; Yoshihara, T.; Ishida, H.; Shiina, Y.; Oishic, S.; Tobita, S. *Phys. Chem. Chem. Phys.* **2009**, *11*, 9850.
(175) Parker, C. A.; Rees, W. T. *Analyst (London)* **1960**, *85*, 587.
(176) Kober, E. M.; Caspar, J. V.; Lumpkin, R. S.; Meyer, T. J. *J. Phys. Chem.* **1986**, *90*, 3722.
(177) Claude, J. P. Ph.D., University of North Carolina, 1995.
(178) Claude, J. P.; Meyer, T. J. *J. Phys. Chem.* **1995**, *99*, 51.
(179) Caspar, J. V.; Meyer, T. J. *J. Am. Chem. Soc.* **1983**, *105*, 5583.
(180) Chen, P.; Meyer, T. J. *Chem. Rev.* **1998**, *98*, 1439.
(181) Caspar, J. V.; Meyer, T. J. *J. Phys. Chem.* **1983**, *87*, 952.
(182) Robinson, G. W.; Frosch, R. P. *J. Chem. Phys.* **1963**, *38*, 1187.
(183) Siebrand, W. *J. Chem. Phys.* **1967**, *47*, 2411.
(184) Vleck, A.; Zalis, S. *Coord. Chem. Rev.* **2007**, *251*, 258.
(185) Charlot, M. F.; Pellegrin, Y.; Quaranta, A.; Leibl, W.; Aukauloo, A. *Chem. Eur. J.* **2006**, *12*, 796.
(186) Vallett, P. J.; Damrauer, N. H. *J. Phys. Chem. A* **2011**, *115*, 3122.
(187) Jacquemin, D.; Perpete, E. A.; Ciofini, I.; Adamo, C. *J. Chem. Theor. Comput.* **2010**, *6*, 1532.
(188) Song, J. A.; Gao, F.; Shi, B.; Liang, W. Z. *Phys. Chem. Chem. Phys.* **2010**, *12*, 13070.
(189) Balzani, V.; Campagna, S.; Denti, G.; Juris, A.; Serroni, S.; Venturi, M. *Acc. Chem. Res.* **1998**, *31*, 26.
(190) Braterman, P. S.; Harriman, A.; Heath, G. A.; Yellowlees, L. J. *J Chem Soc Dalton* **1983**, 1801.
(191) Yoshimura, A.; Hoffman, M. Z.; Sun, H. *J. Photochem. Photobiol. Chem.* **1993**, *70*, 29.
(192) Wallin, S.; Davidsson, J.; Modin, J.; Hammarstrom, L. *J. Phys. Chem. A* **2005**, *109*, 4697.
(193) Zalis, S.; Consani, C.; El Nahhas, A.; Cannizzo, A.; Chergui, M.; Hartl, F.; Vlcek, A. *Inorg. Chim. Acta* **2011**, *374*, 578.
(194) Cannizzo, A.; Milne, C. J.; Consani, C.; Gawelda, W.; Bressler, C.; van Mourik, F.; Chergui, M. *Coord. Chem. Rev.* **2010**, *254*, 2677.
(195) Yeh, A.; Shank, C. V.; McCusker, J. K. *Science* **2000**, *289*, 935.
(196) Shaw, G. B.; Styers-Barnett, D. J.; Gannon, E. Z.; Granger, J. C.; Papanikolas, J. M. *J. Phys. Chem. A* **2004**, *108*, 4998.

(197) Henry, W.; Coates, C. G.; Brady, C.; Ronayne, K. L.; Matousek, P.; Towrie, M.; Botchway, S. W.; Parker, A. W.; Vos, J. G.; Browne, W. R.; McGarvey, J. J. *J. Phys. Chem. A* **2008**, *112*, 4537.

(198) Dearmond, M. K.; Carlin, C. M. *Coord. Chem. Rev.* **1981**, *36*, 325.

(199) Braun, D.; Huber, P.; Wudy, J.; Schmidt, J.; Yersin, H. *J. Phys. Chem.* **1994**, *98*, 8044.

(200) Riesen, H.; Wallace, L.; Krausz, E. *J. Phys. Chem.* **1996**, *100*, 17138.

(201) Riesen, H.; Krausz, E. *Chem. Phys. Lett.* **1996**, *260*, 130.

(202) Riesen, H.; Krausz, E. *J. Chem. Phys.* **1993**, *99*, 7614.

(203) Huber, P.; Yersin, H. *J. Phys. Chem.* **1993**, *97*, 12705.

(204) Turro, C.; Chung, Y. C.; Leventis, N.; Kuchenmeister, M. E.; Wagner, P. J.; Leroi, G. E. *Inorg. Chem.* **1996**, *35*, 5104.

(205) Oh, D. H.; Boxer, S. G. *J. Am. Chem. Soc.* **1989**, *111*, 1130.

(206) Karki, L.; Hupp, J. T. *Inorg. Chem.* **1997**, *36*, 3318.

(207) Webb, M. A.; Knorr, F. J.; McHale, J. L. *J Raman Spectrosc* **2001**, *32*, 481.

(208) Kober, E. M.; Sullivan, B. P.; Meyer, T. J. *Inorg. Chem.* **1984**, *23*, 2098.

(209) Hoff, D. A.; Silva, R.; Rego, L. G. C. *J. Phys. Chem. C* **2011**, *115*, 15617.

(210) Moret, M. E.; Tavernelli, I.; Chergui, M.; Rothlisberger, U. *Chemistry-a European Journal* **2010**, *16*, 5889.

(211) Miller, S. A.; Moran, A. M. *J. Phys. Chem. A* **2010**, *114*, 2117.

(212) Baudin, H. B.; Davidsson, J.; Serroni, S.; Juris, A.; Balzani, V.; Campagna, S.; Hammarstrom, L. *J. Phys. Chem. A* **2002**, *106*, 4312.

(213) Laine, P. P.; Loiseau, F.; Campagna, S.; Ciofini, I.; Adamo, C. *Inorg. Chem.* **2006**, *45*, 5538.

(214) Palacios, R. E.; Kodis, G.; Gould, S. L.; Garza, L. d. l.; Brune, A.; Gust, D.; Moore, T. A.; Moore, A. L. *ChemPhysChem* **2005**, *6*, 2359.

(215) Marcus, R. A. *J. Chem. Phys.* **1956**, *24*, 966.

(216) Marcus, R. A. *Annu. Rev. Phys. Chem.* **1964**, *15*, 155.

(217) Meylemans, H.M; Synthesis and Investigation of Ruthneium Polypyridyl based Donor-Bridge-Acceptor Complexes toward Control of Electron Transfer Photochemistry. PhD. Dissertation. University of Colorado, 2010.

(218) Deeg, F. W.; Stankus, J. J.; Greenfield, S. R.; Newell, V. J.; Fayer, M. D. *J. Chem. Phys.* **1989**, *90*, 6893.

(219) Mazzanti, A.; Lunazzi, L.; Minzoni, M.; Anderson, J. E. *J Org Chem* **2006**, *71*, 5474.

Appendix One - ^{1}H NMR Spectra for Novel Ligands and Complexes Reported in Chapters Two & Three

1. N-(Methyl) -N'-(2,4-dinitrophenyl)-4,4'-bipyridinium Chloride Iodide (modified Zincke Salt) in D_2O

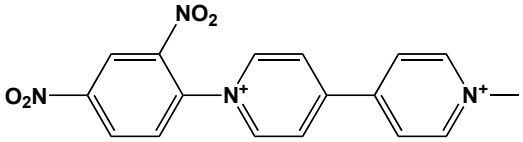

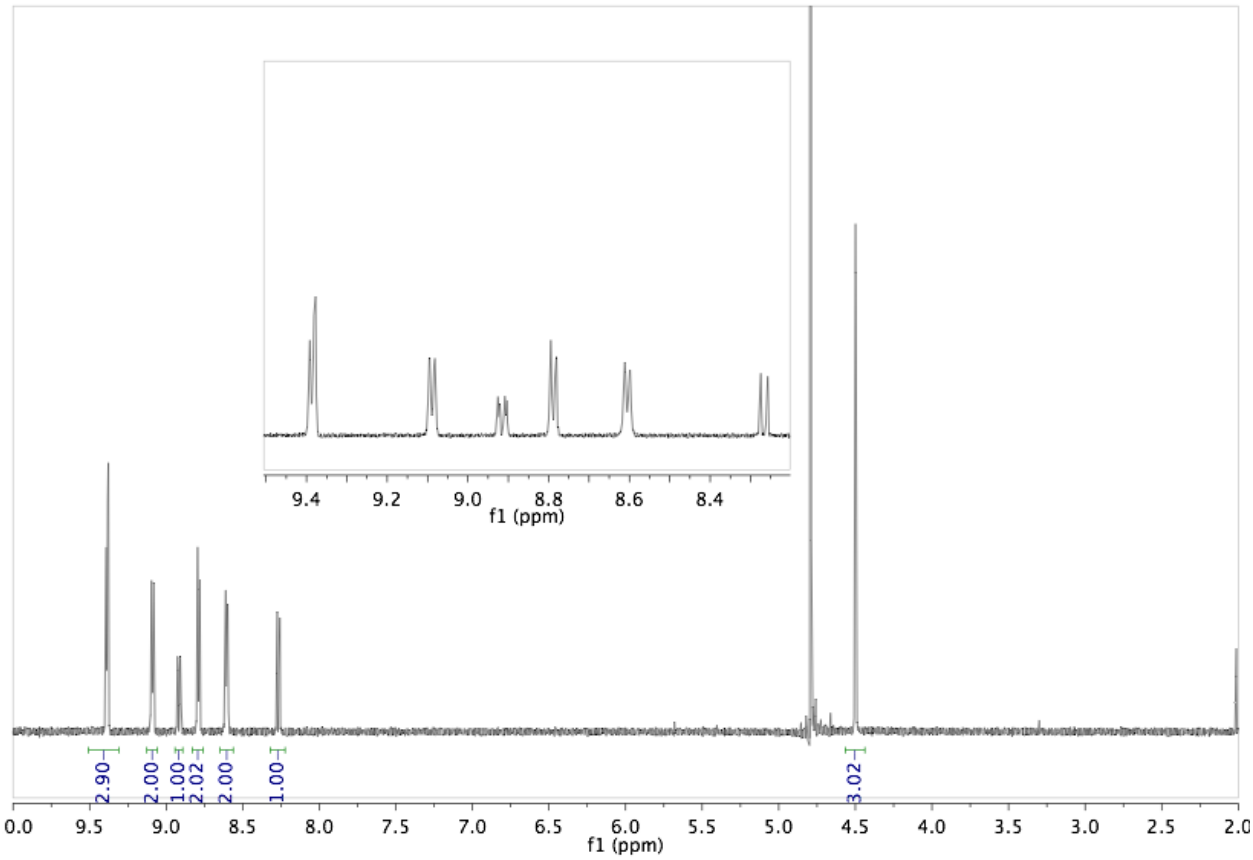

2. 4-(2-methylphenyl)-2,2'-bipyrdine in $CDCl_3$

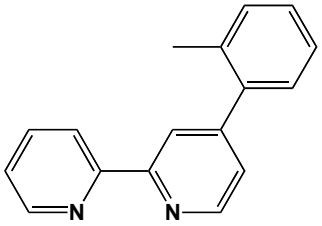

This compound is contaminated with excess triphenylphosphine. These peaks have not been integrated.

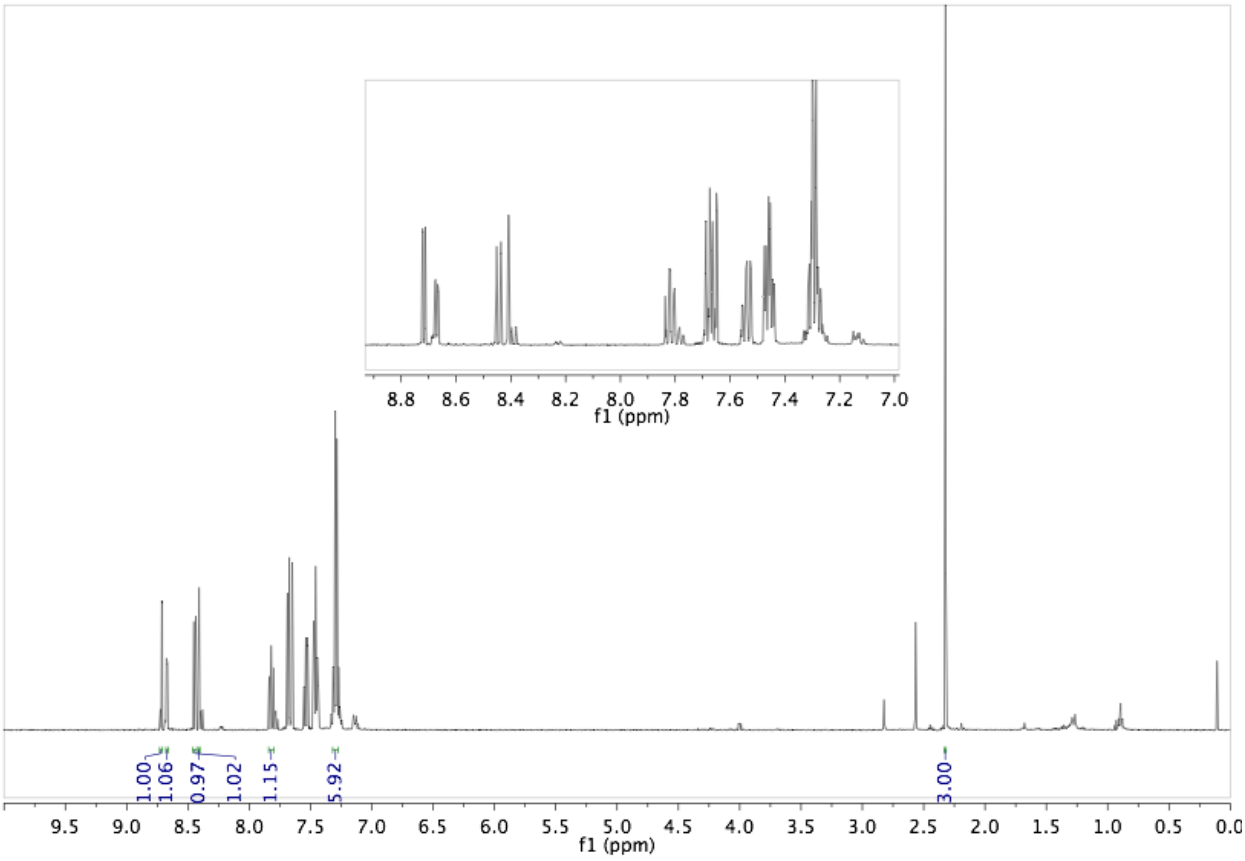

3. 4-(2,6-dimethylphenyl)-2,2'-bipyrdine in $CDCl_3$

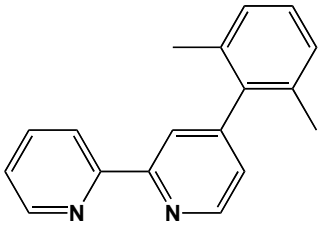

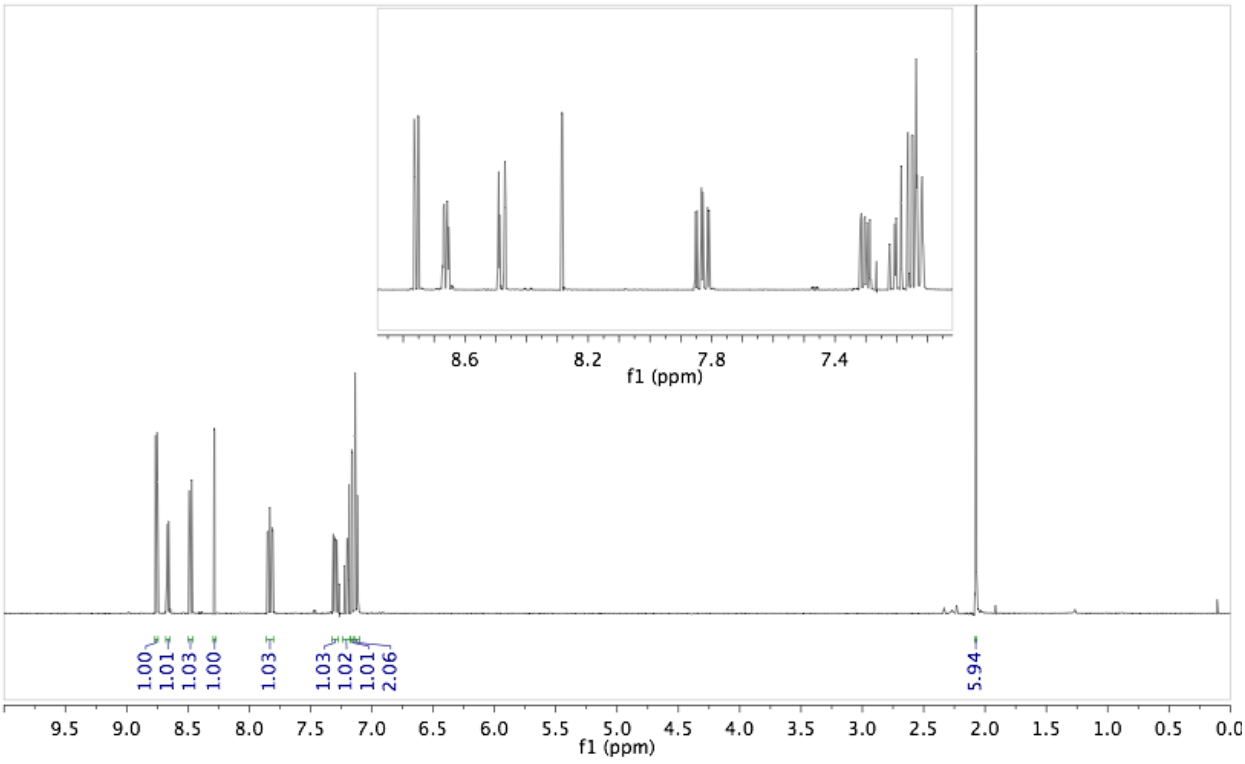

4. 4-(2,5-dimethylphenyl)-2,2'-bipyrdine in $CDCl_3$

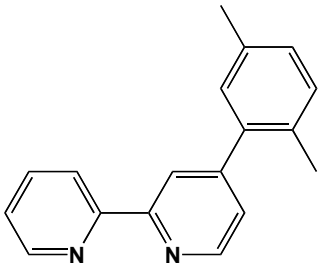

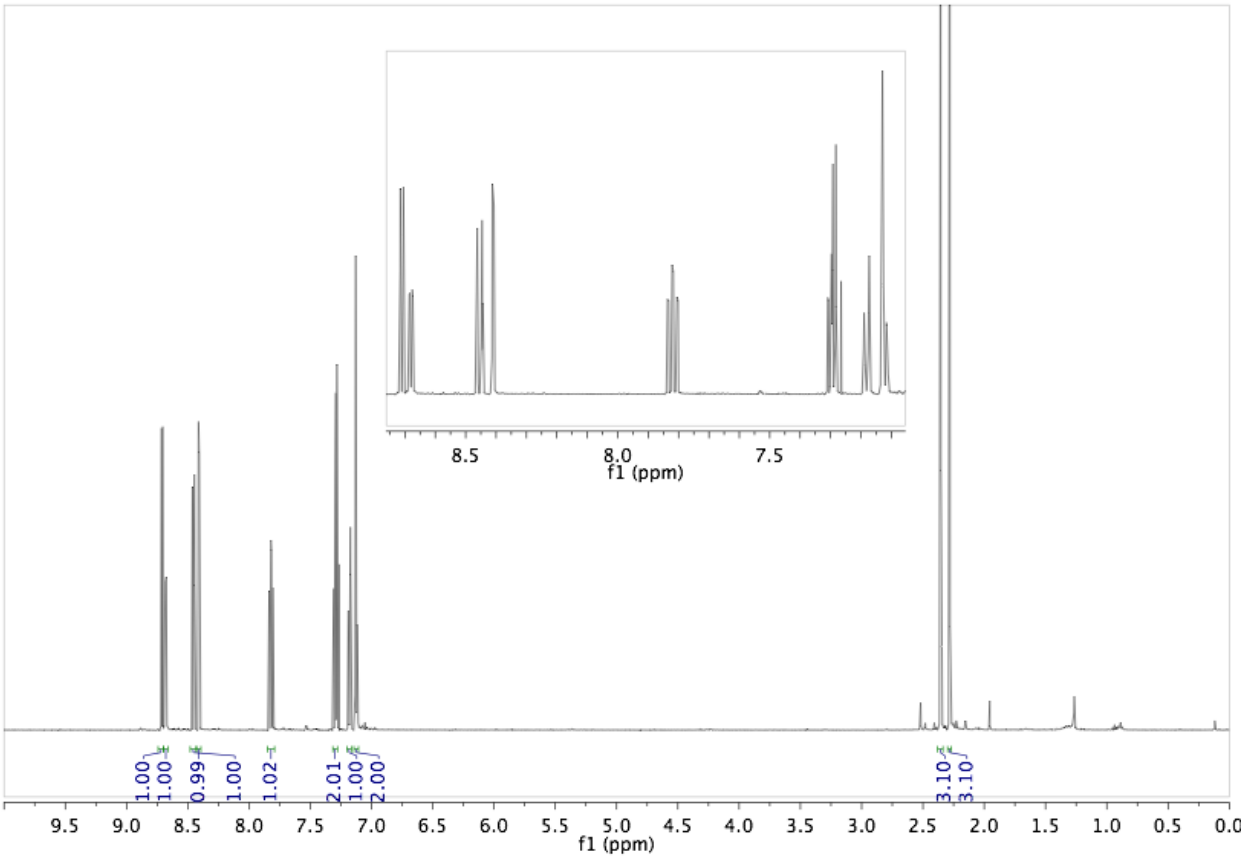

5. 4-(3,5-dimethylphenyl)-2,2'-bipyrdine in $CDCl_3$

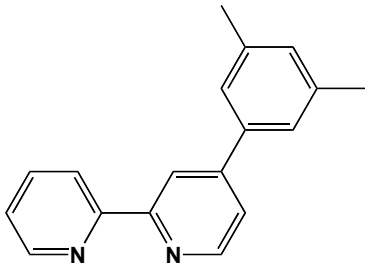

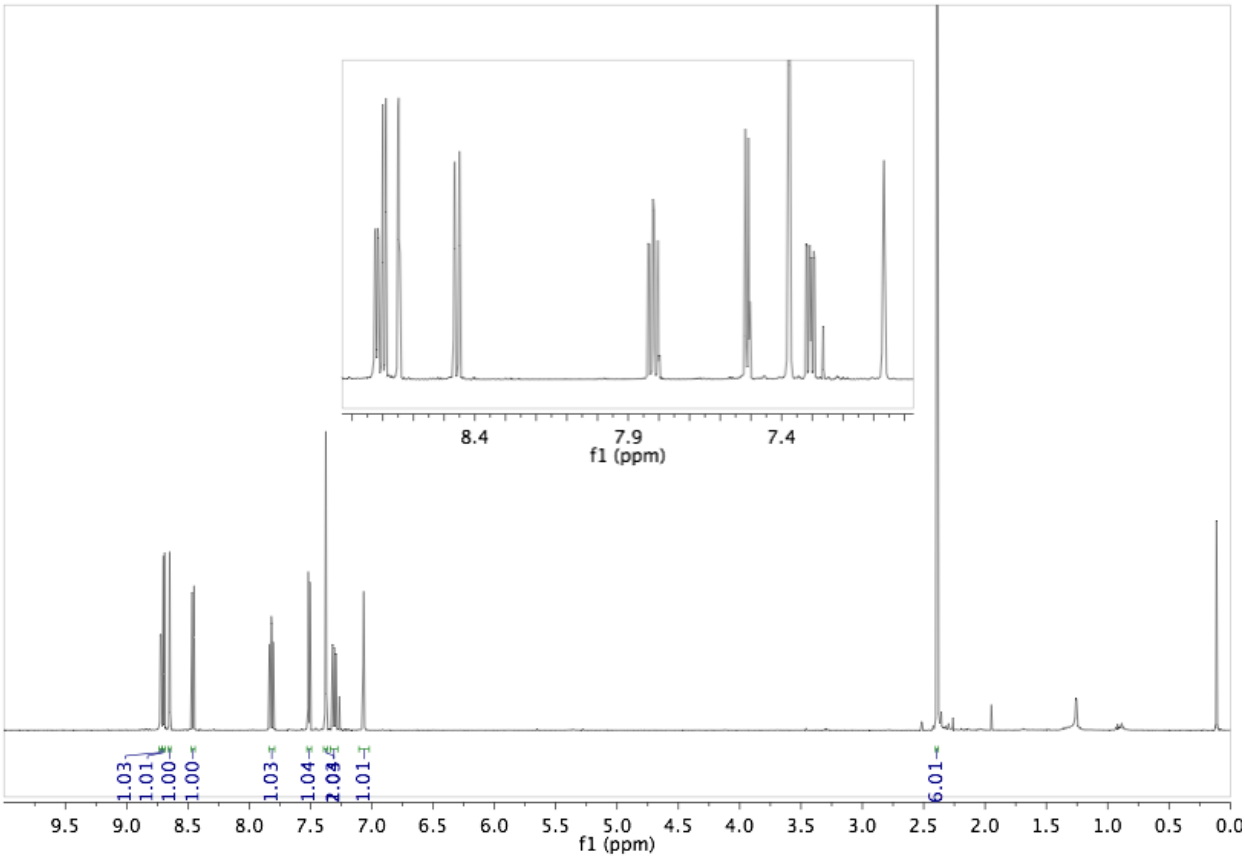

6. 4-(4-Amino-2-methylphenyl)-2,2'-bipyridine in $CDCl_3$

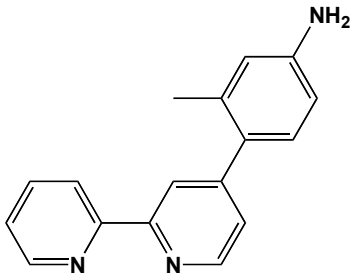

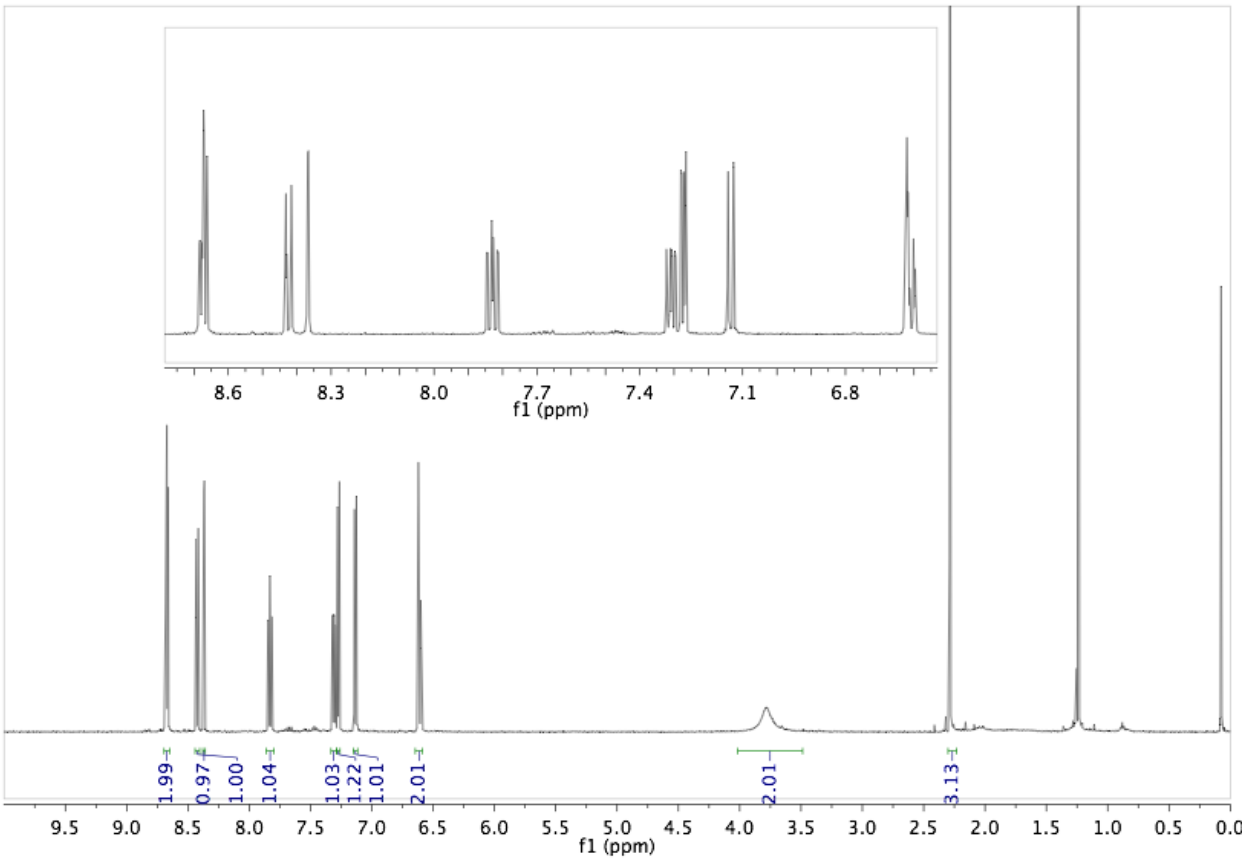

7. 4-(4-Amino-2,6-dimethylphenyl)-2,2'-bipyridine in $CDCl_3$

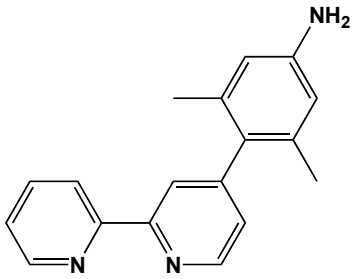

It should be noted that resonance centered at 7.26 ppm also contains the solvent.

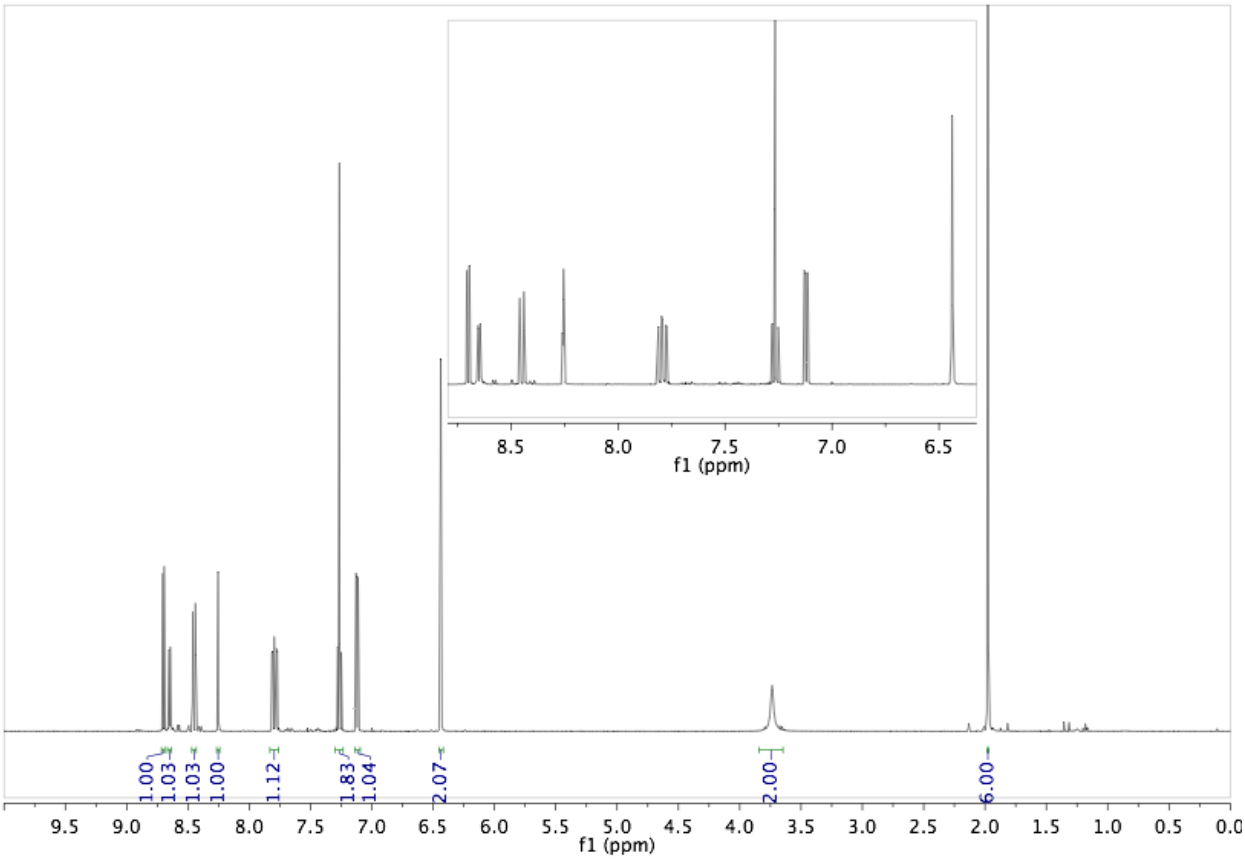

8. 4-(4-Amino-2,5-dimethylphenyl)-2,2'-bipyridine in $CDCl_3$

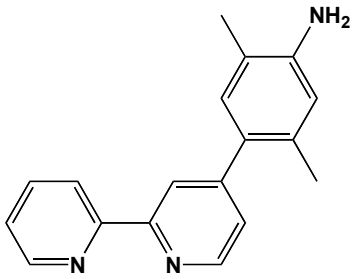

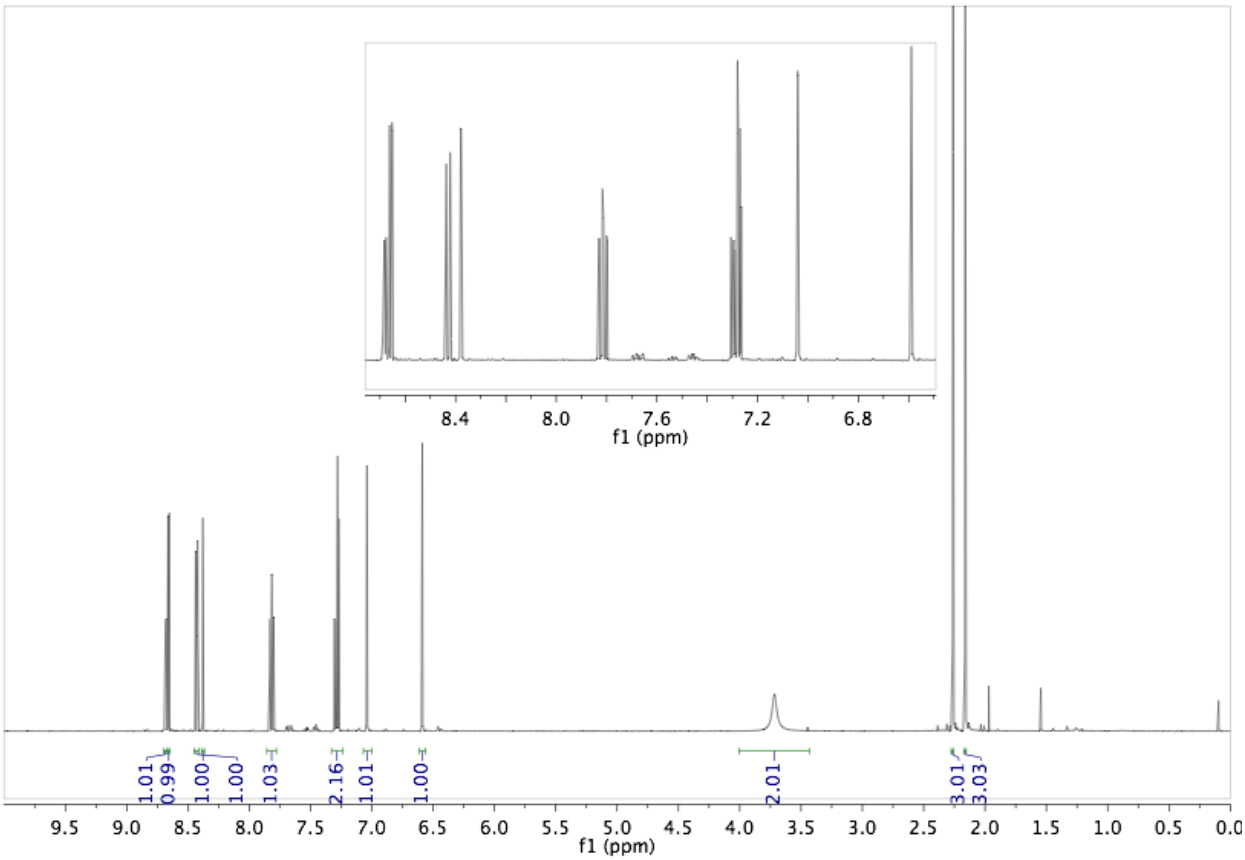

9. 4-(4-Amino-3,5-dimethylphenyl)-2,2'-bipyridine in $CDCl_3$

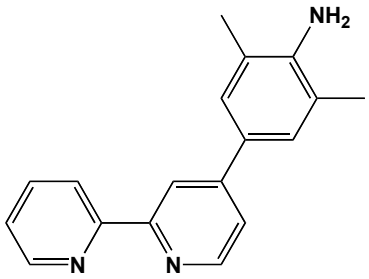

This compound is contaminated with excess triphenylphosphine. These peaks have not been integrated.

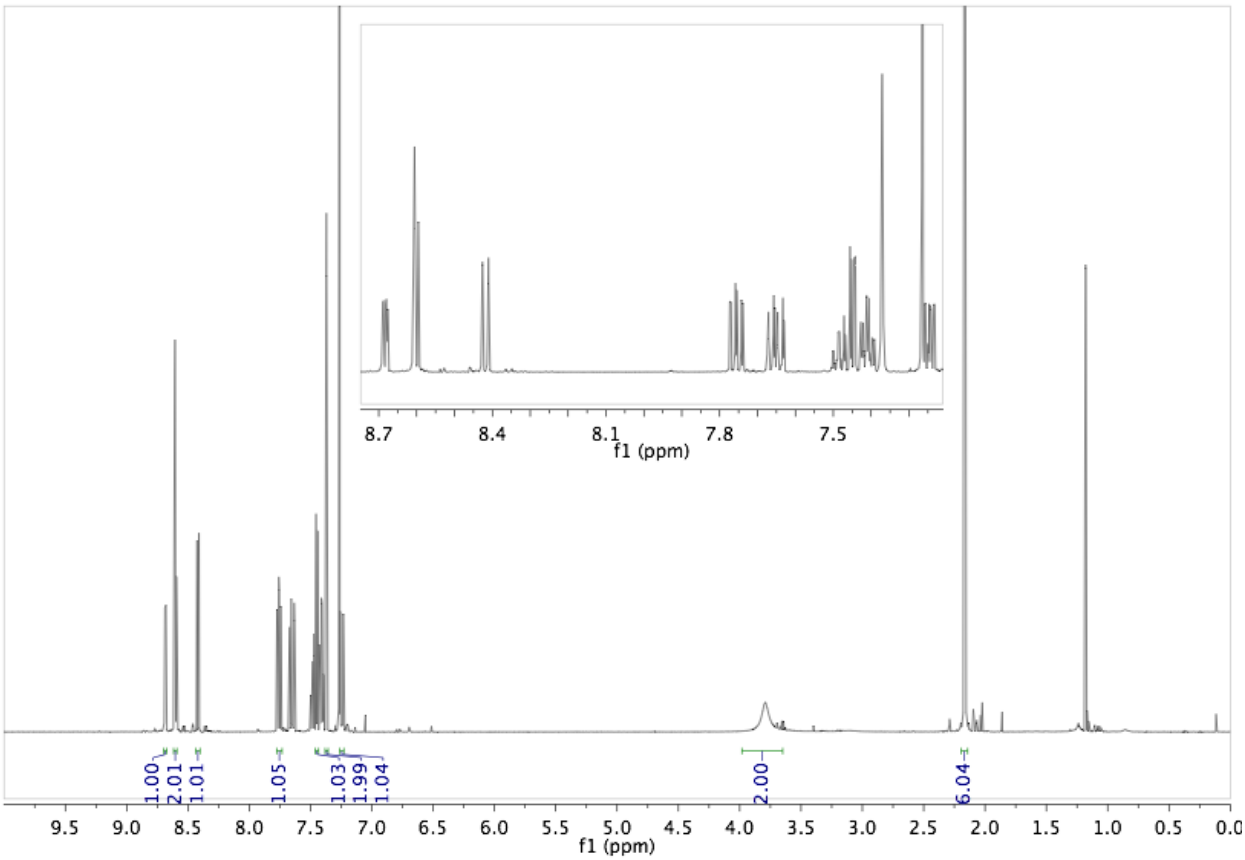

10. N-Methyl-N'-phenyl-4,4'-bipyridinium Hexafluorophosphate

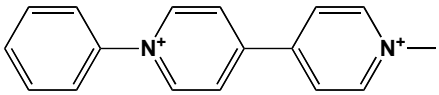

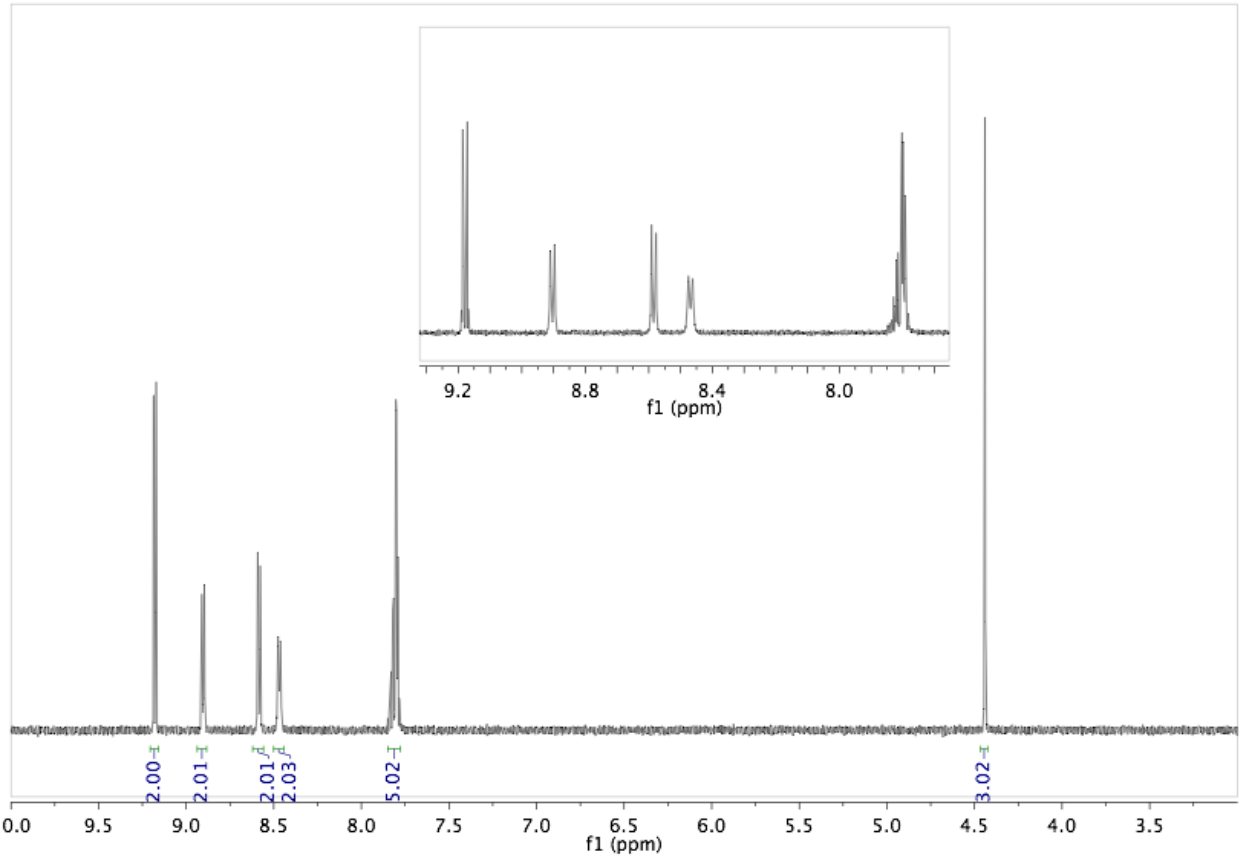

11. N-Methyl-N'-(2,5-dimethylphenyl-4,4'-bipyridinium Hexafluorophosphate

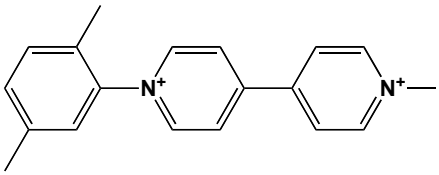

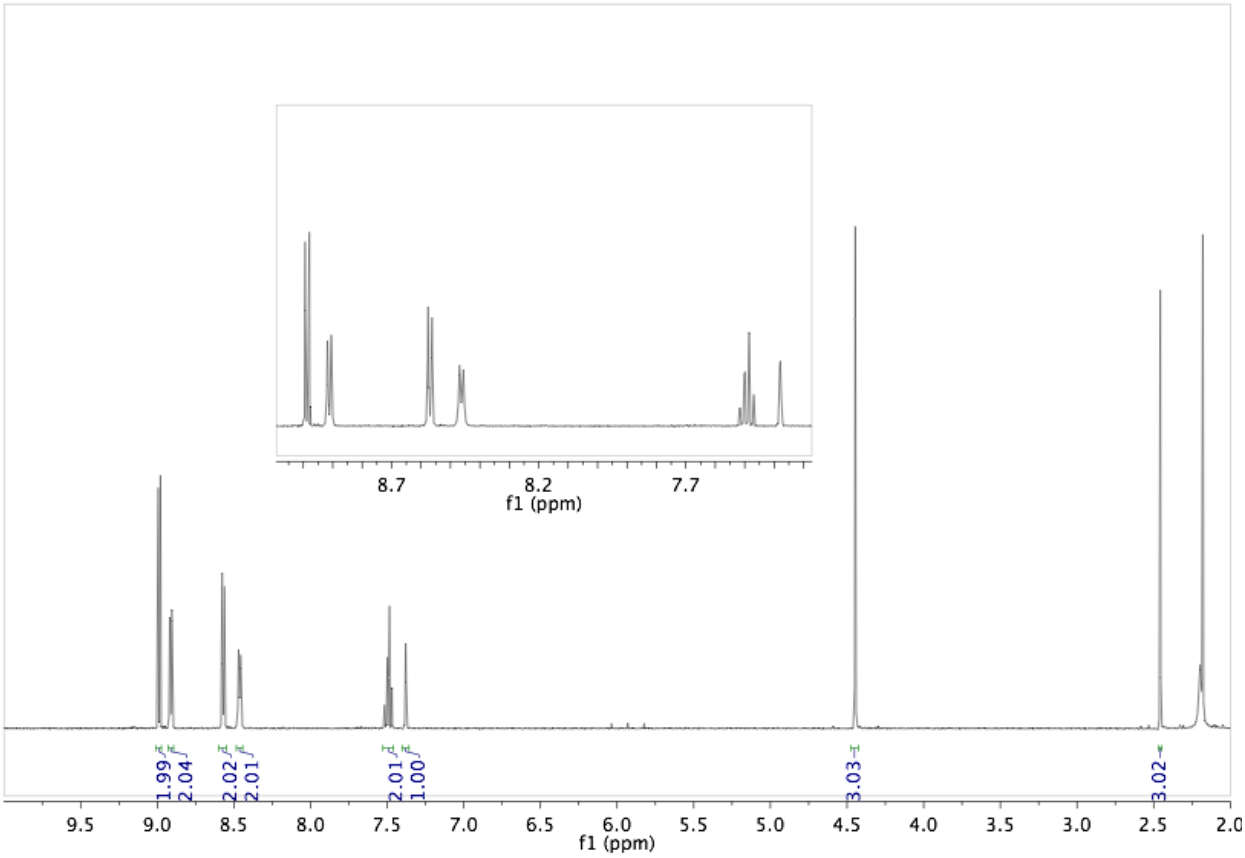

12. N-Methyl-N'-(2,6-dimethylphenyl-4,4'-bipyridinium Hexafluorophosphate (3,5-acceptor)

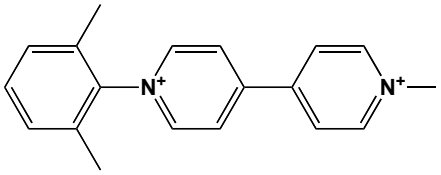

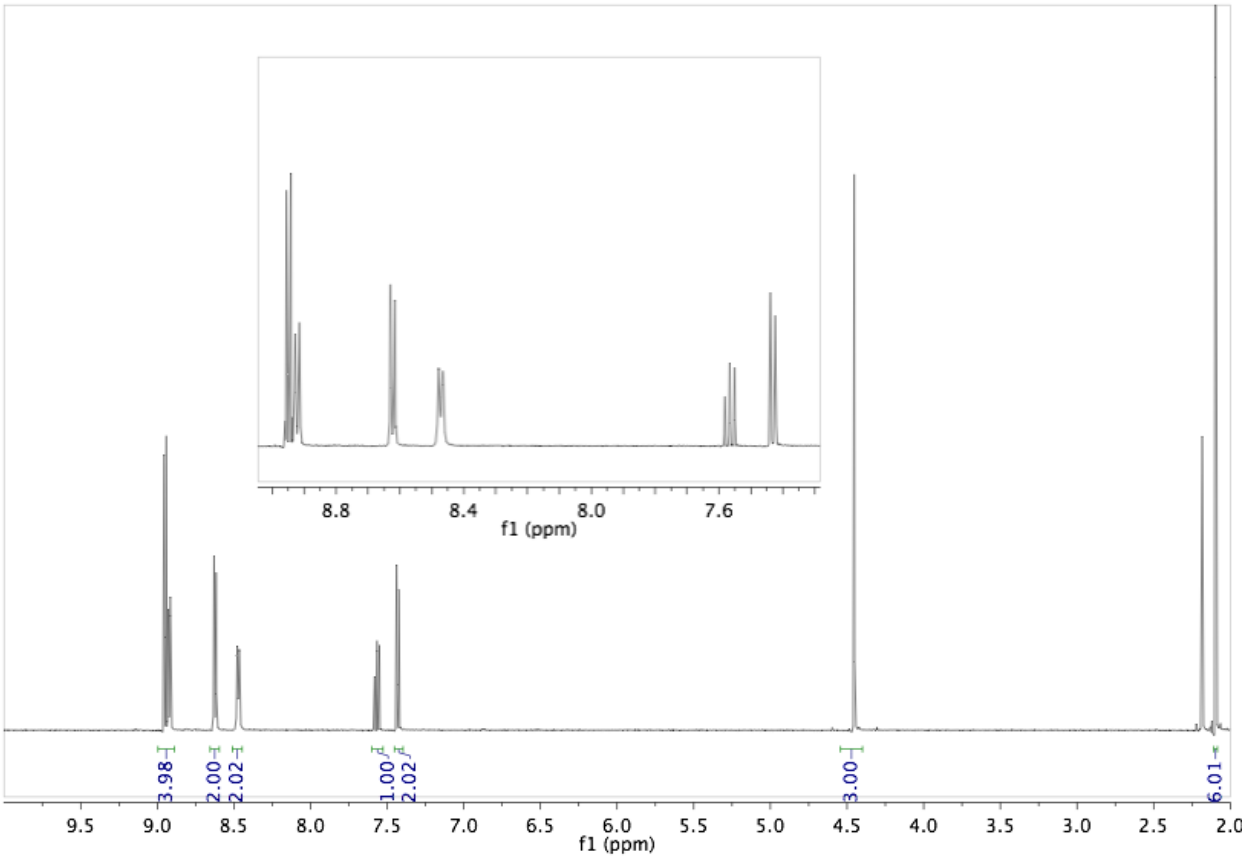

13.4-(1-(1'-Methyl-4,4'-bipyridinium-1-yl)-phenyl)-2,2'-bipyridine Hexafluorophosphate in. CD_3CN

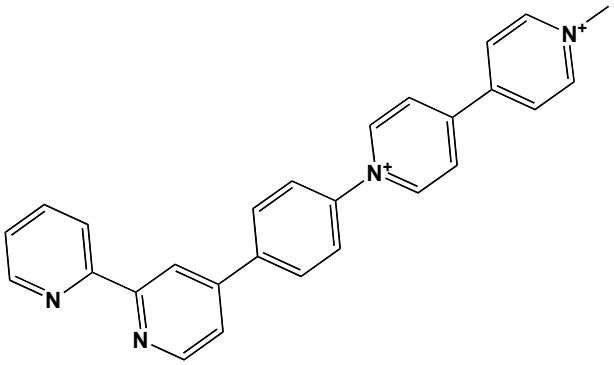

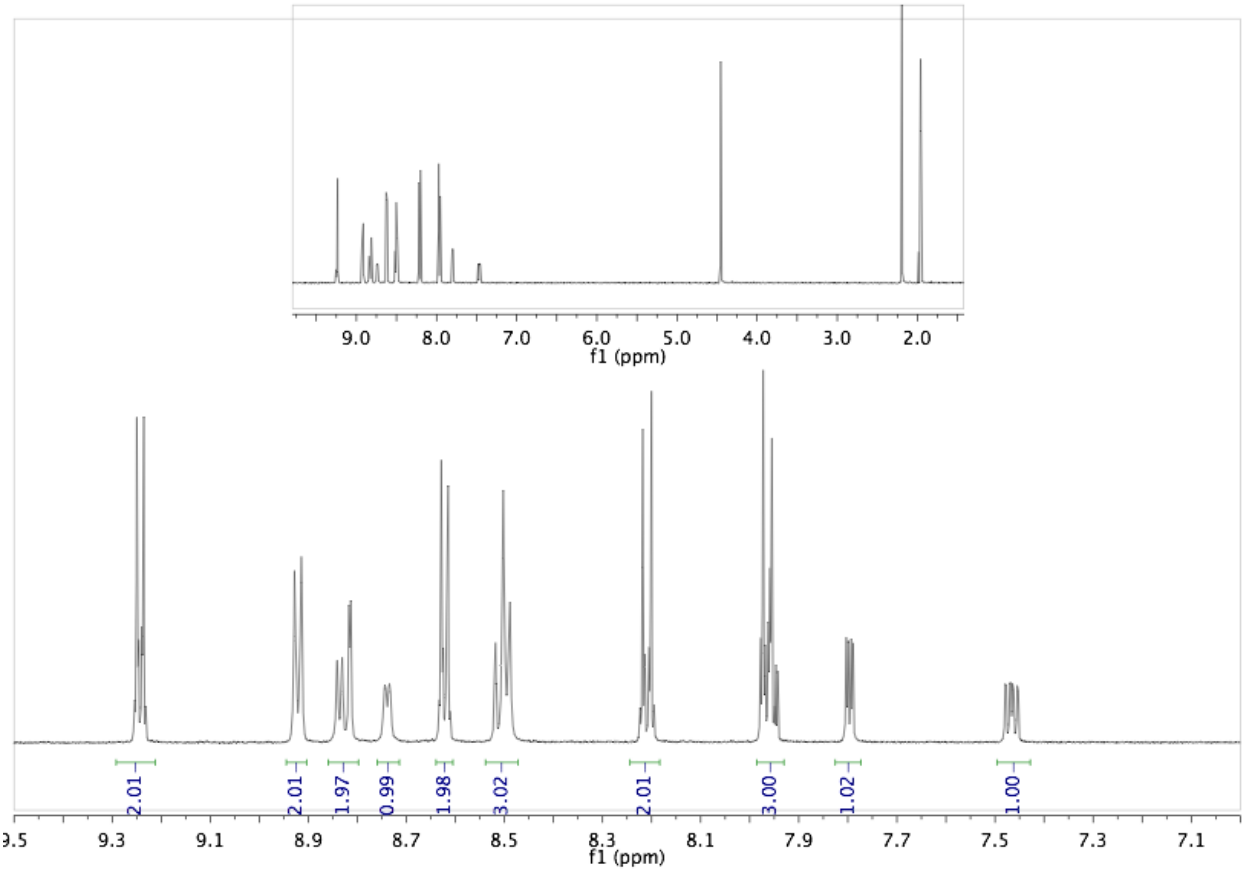

14. 4-(1-(1'-Methyl-4,4'-bipyridinium-1-yl)-phenyl)-2,2':6',2''-terpyridine hexafluorophosphate in CD_3CN.

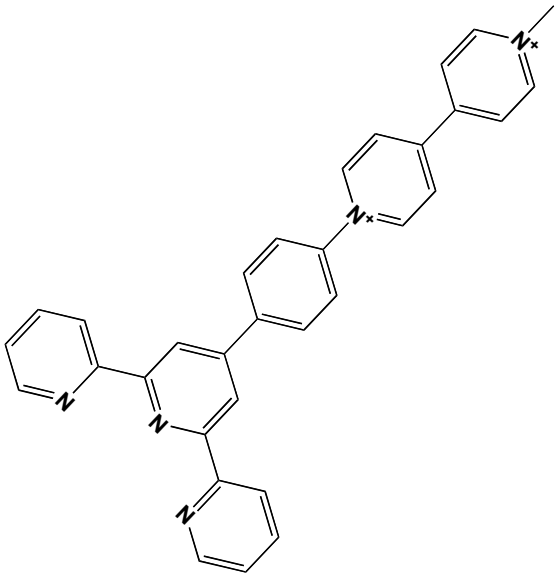

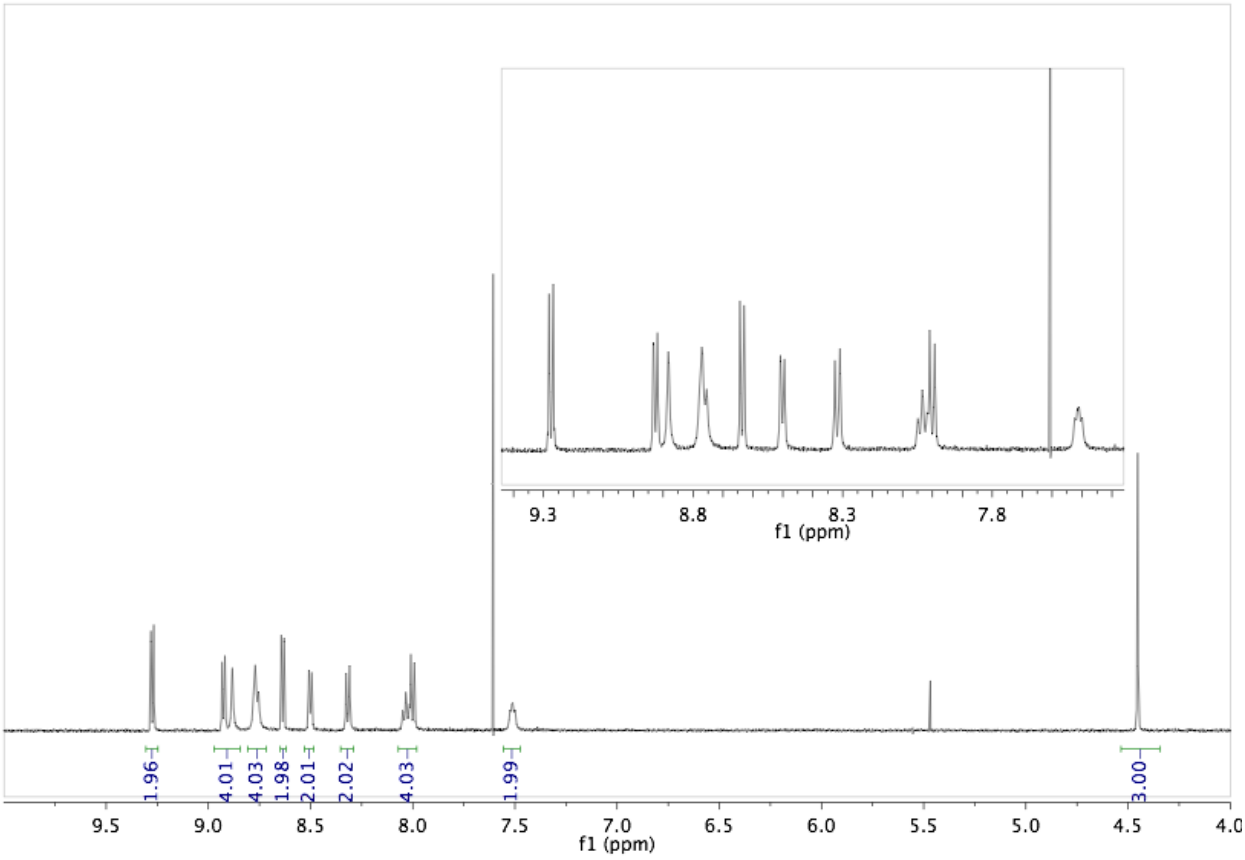

15. 4-(1-(1'-Methyl-4,4'-bipyridinium-1-yl)-3-methyphenyl)-2,2'-bipyridine Hexafluorophosphate in CD_3CN.

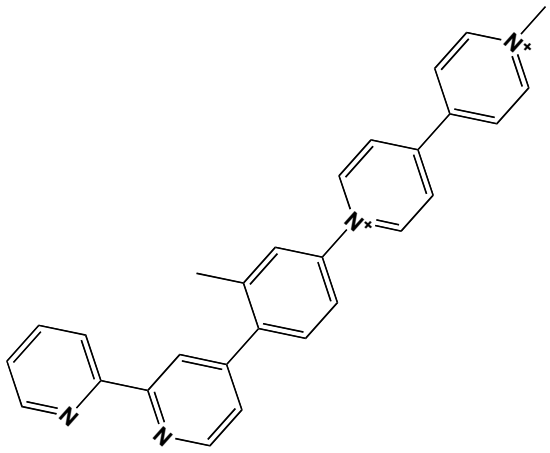

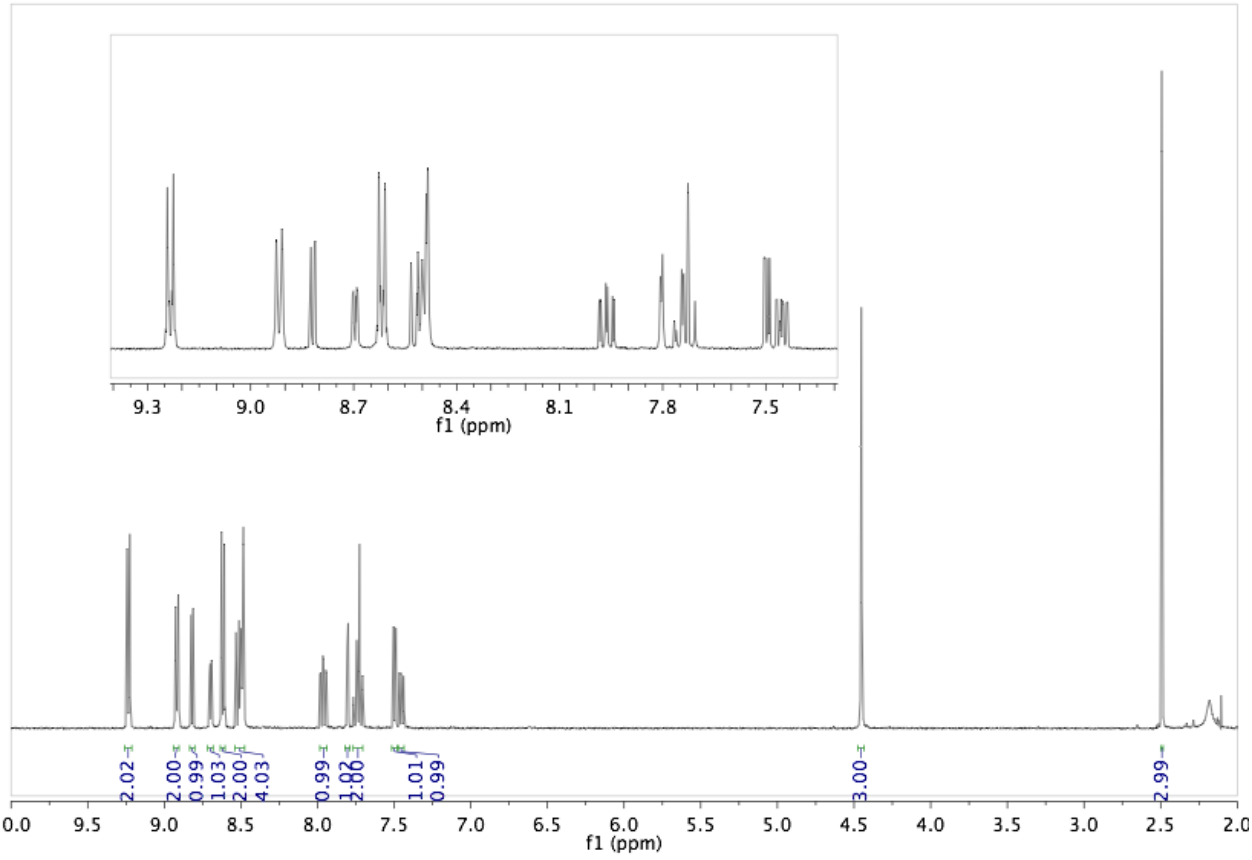

16. 4-(1-(1'-Methyl-4,4'-bipyridinium-1-yl)-3,5-dimethyphenyl)-2,2'-bipyridine Hexafluorophosphate in CD_3CN.

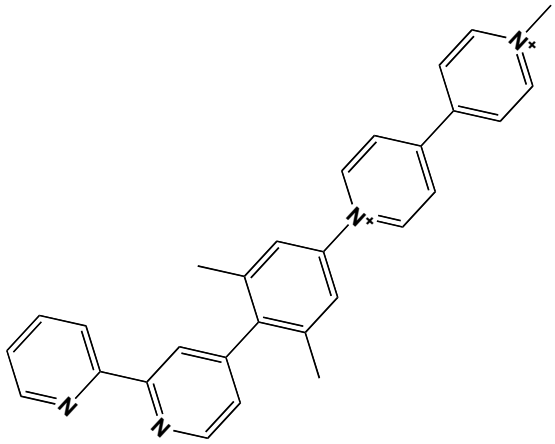

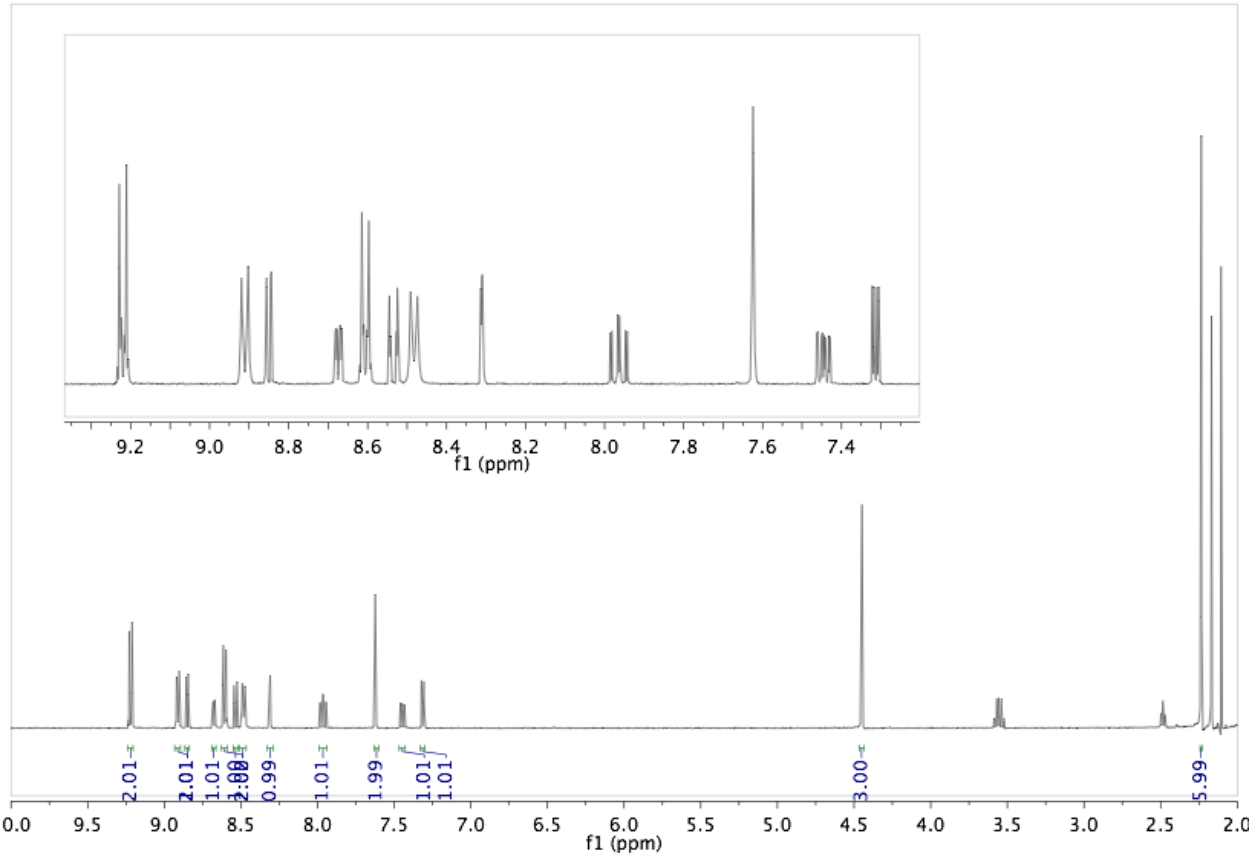

17. 4-(1-(1'-Methyl-4,4'-bipyridinium-1-yl)-2,5-dimethyphenyl)-2,2'-bipyridine Hexafluorophosphate in CD_3CN.

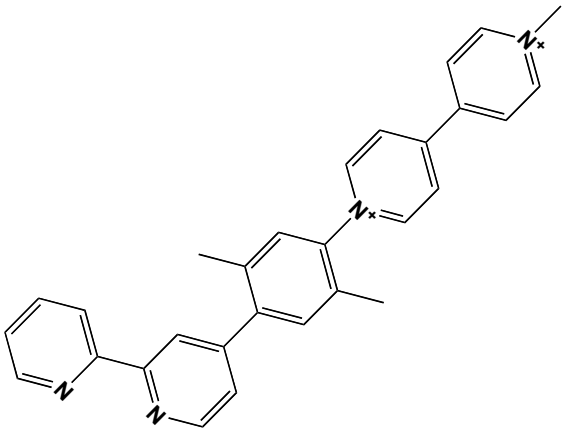

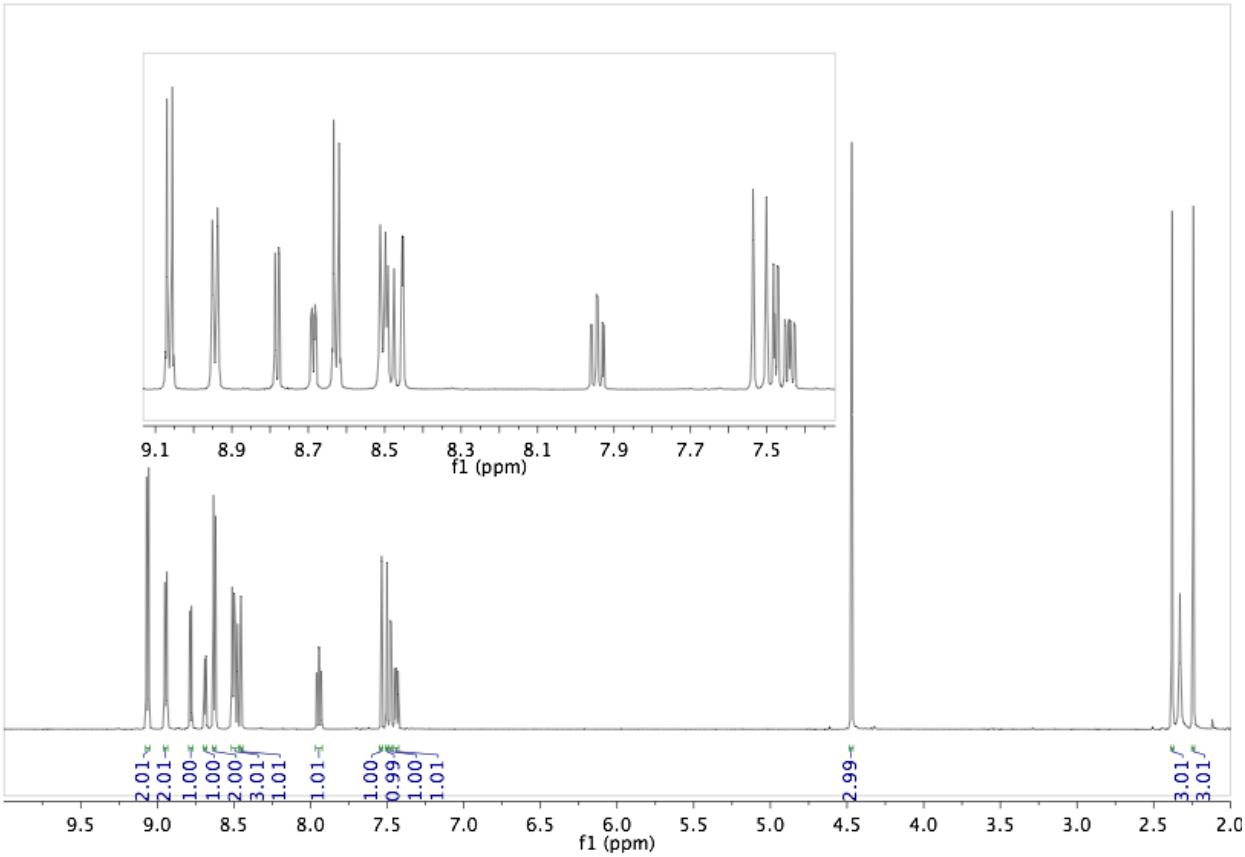

18. 4-(1-(1'-Methyl-4,4'-bipyridinium-1-yl)-2,6-dimethyphenyl)-2,2'-bipyridine Hexafluorophosphate in CD_3CN.

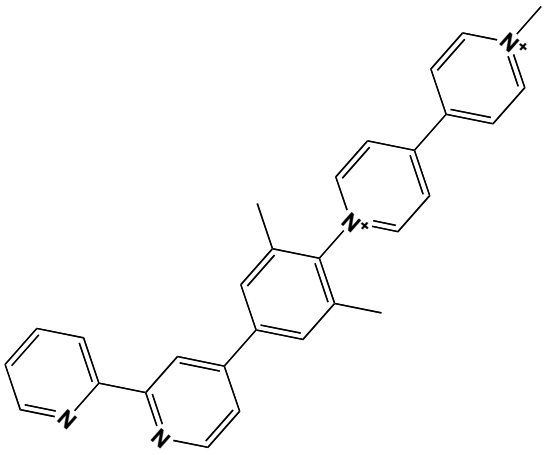

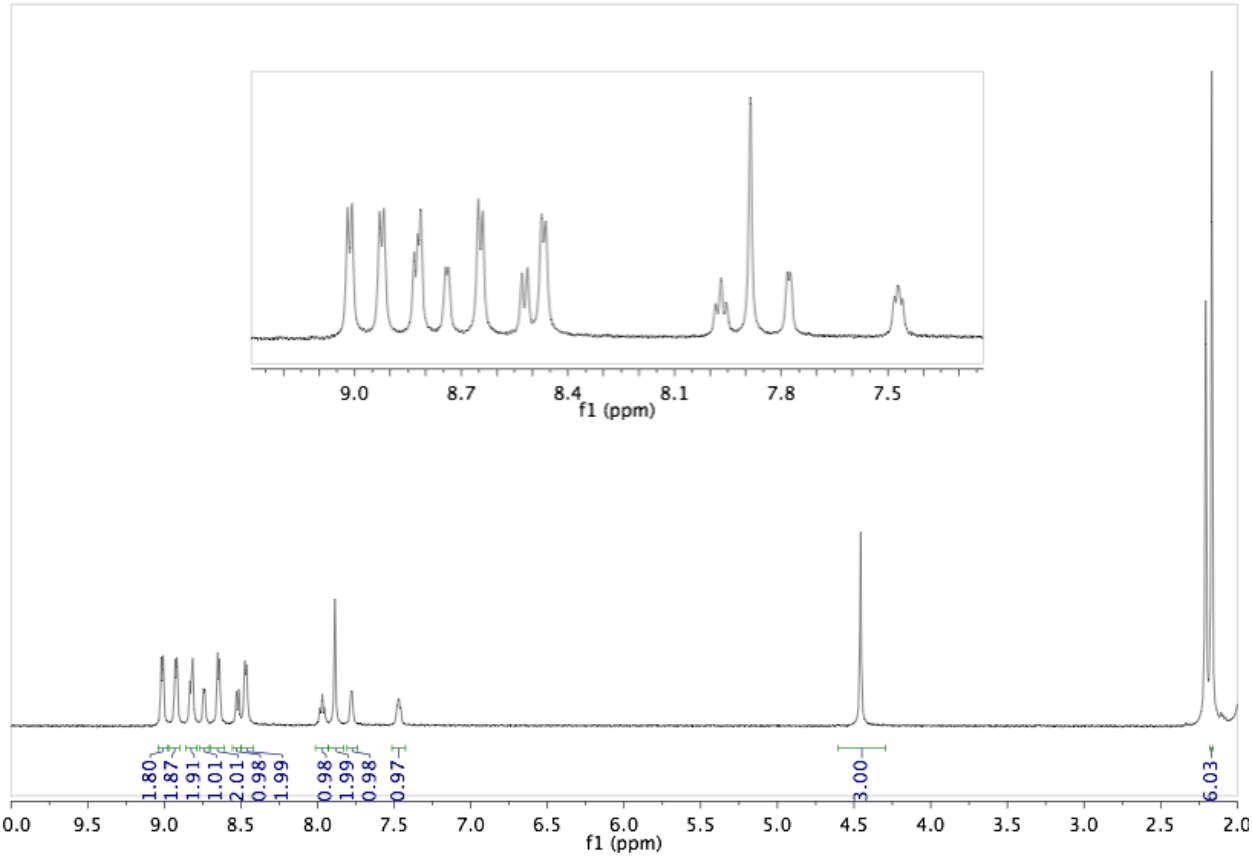

19. $[Ru(bpy)_2(bpy\text{-}phenyl)](PF_6)_2$ in CD_3CN

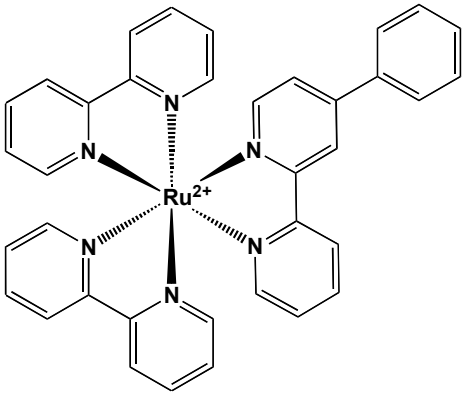

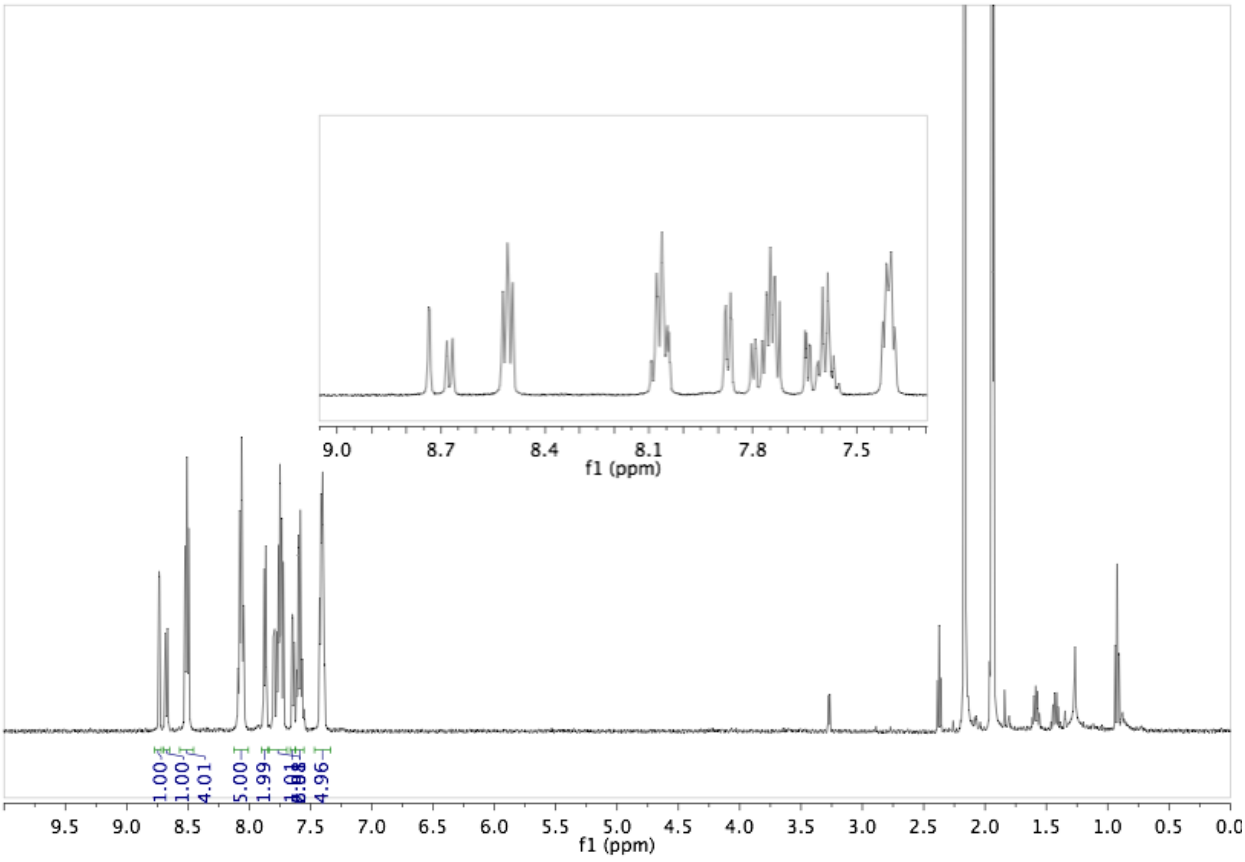

20. $[Ru(dmb)_2(bpy\text{-}phenyl)](PF_6)_2$ in CD_3CN

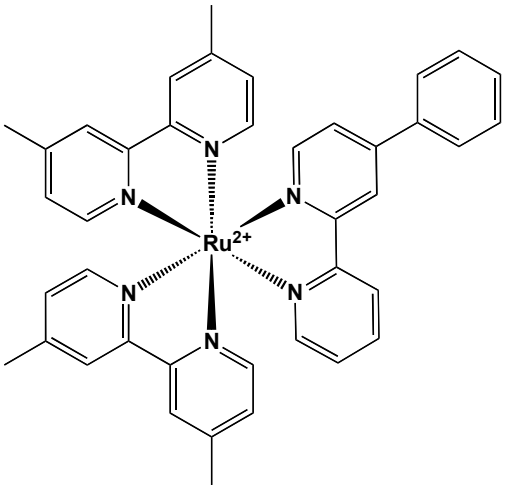

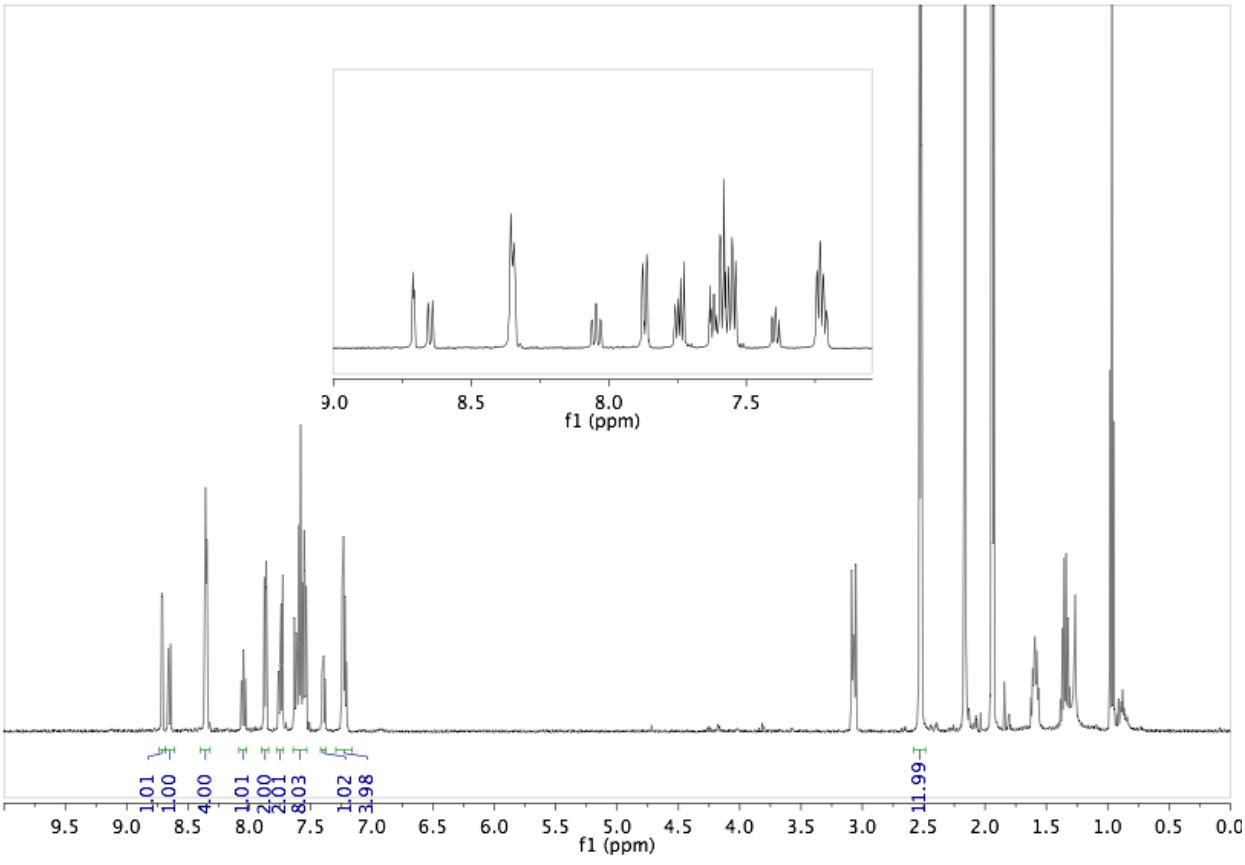

21. $[Ru(tmb)_2(bpy\text{-}phenyl)](PF_6)_2$ in CD_3CN

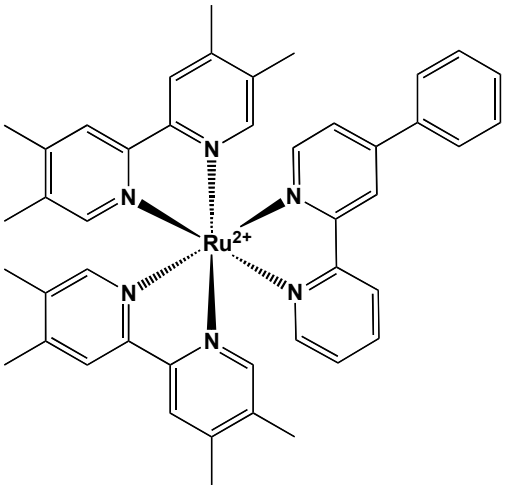

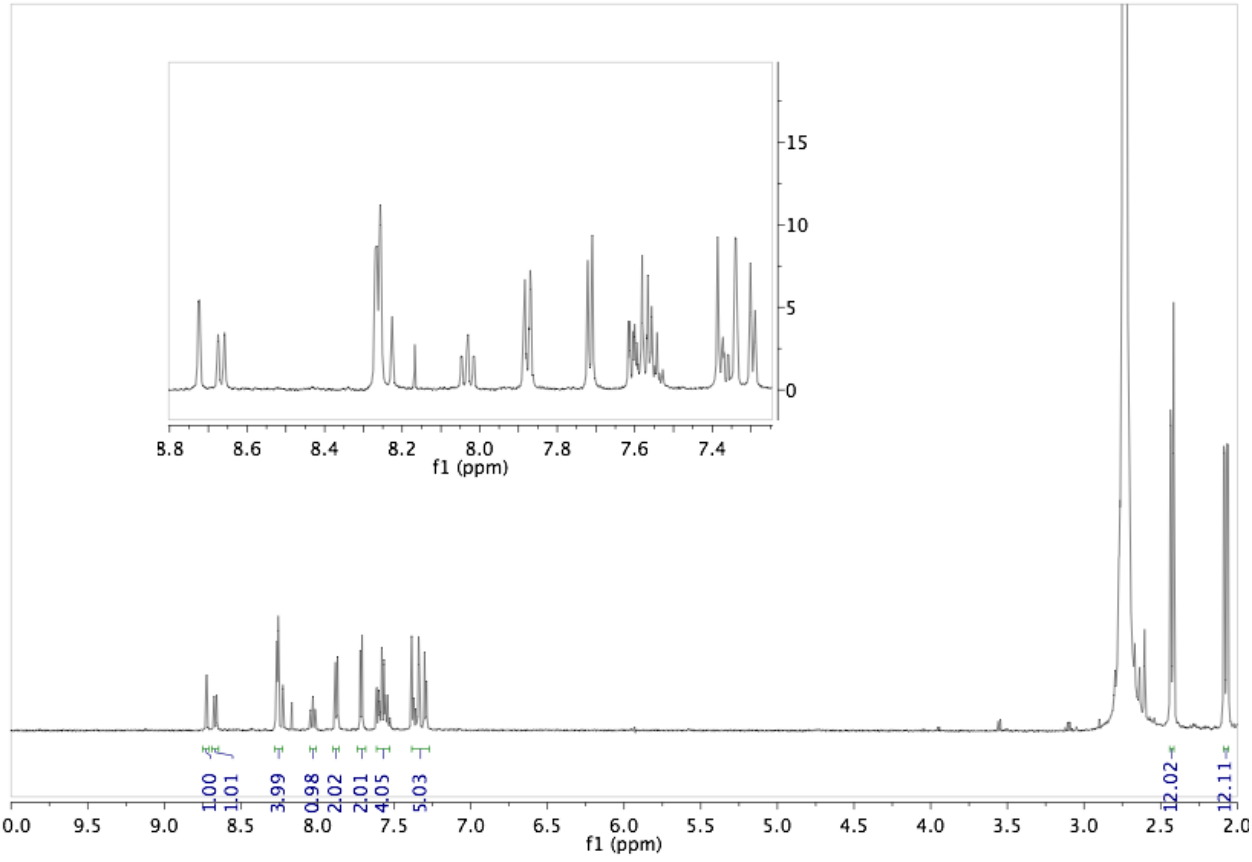

22. $[Ru(tmb)_2(bpy\text{-}ortho)](PF_6)_2$ in CD_3CN

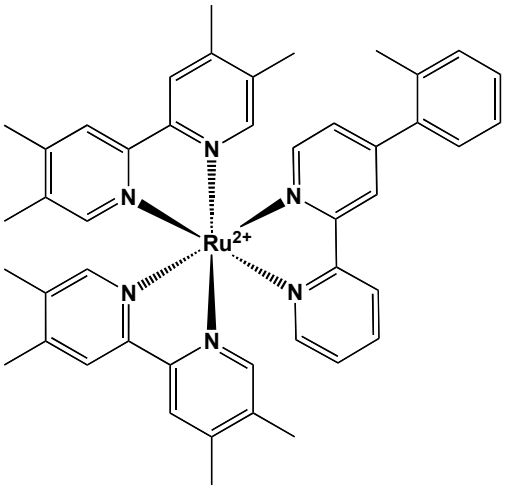

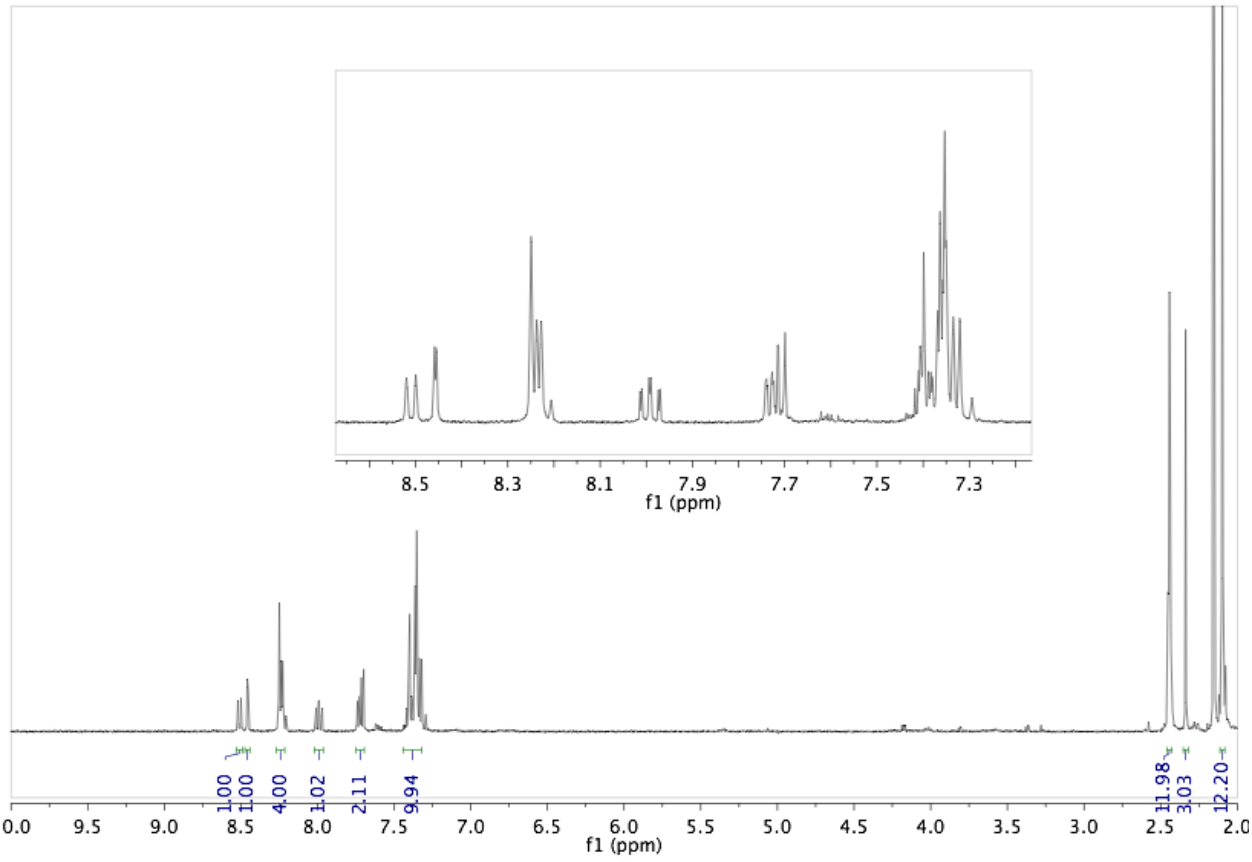

23. $[Ru(tmb)_2(bpy\text{-}2,6\text{-}mesityl)](PF_6)_2$ in CD_3CN

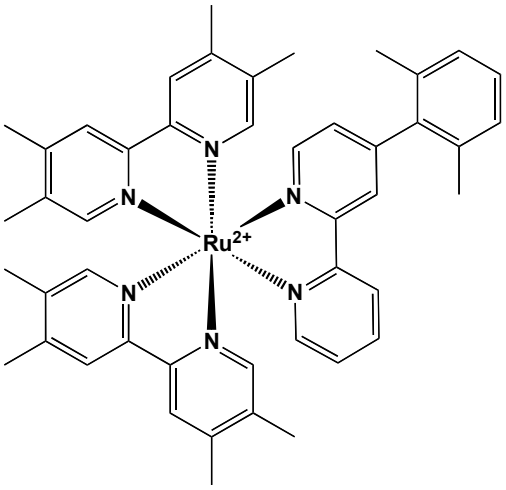

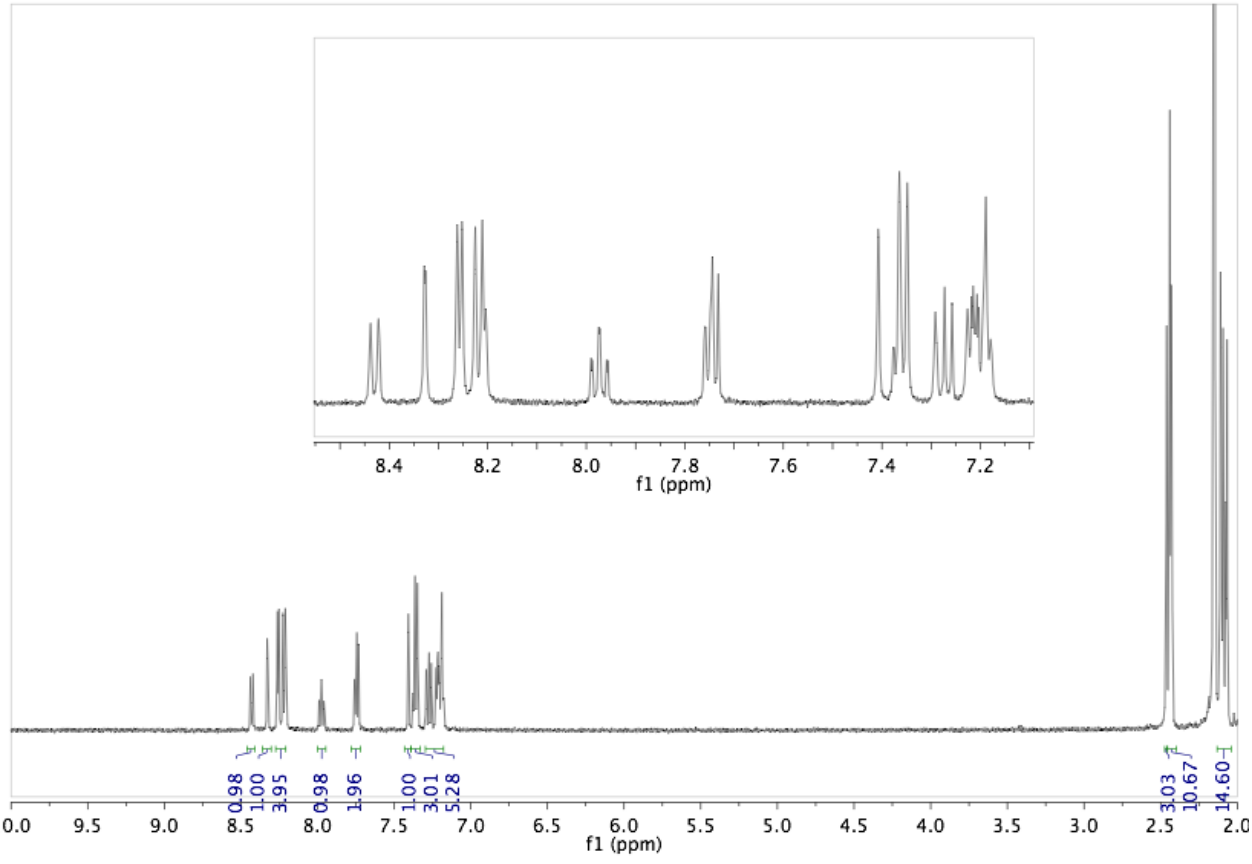

24. $[Ru(tmb)_2(bpy\text{-}2,5\text{-}mesityl)](PF_6)_2$ in CD_3CN

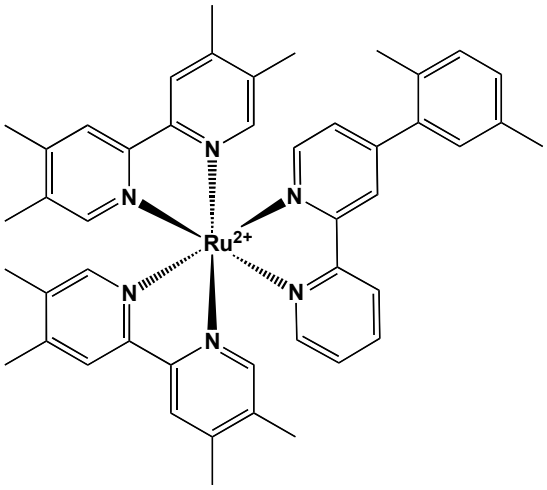

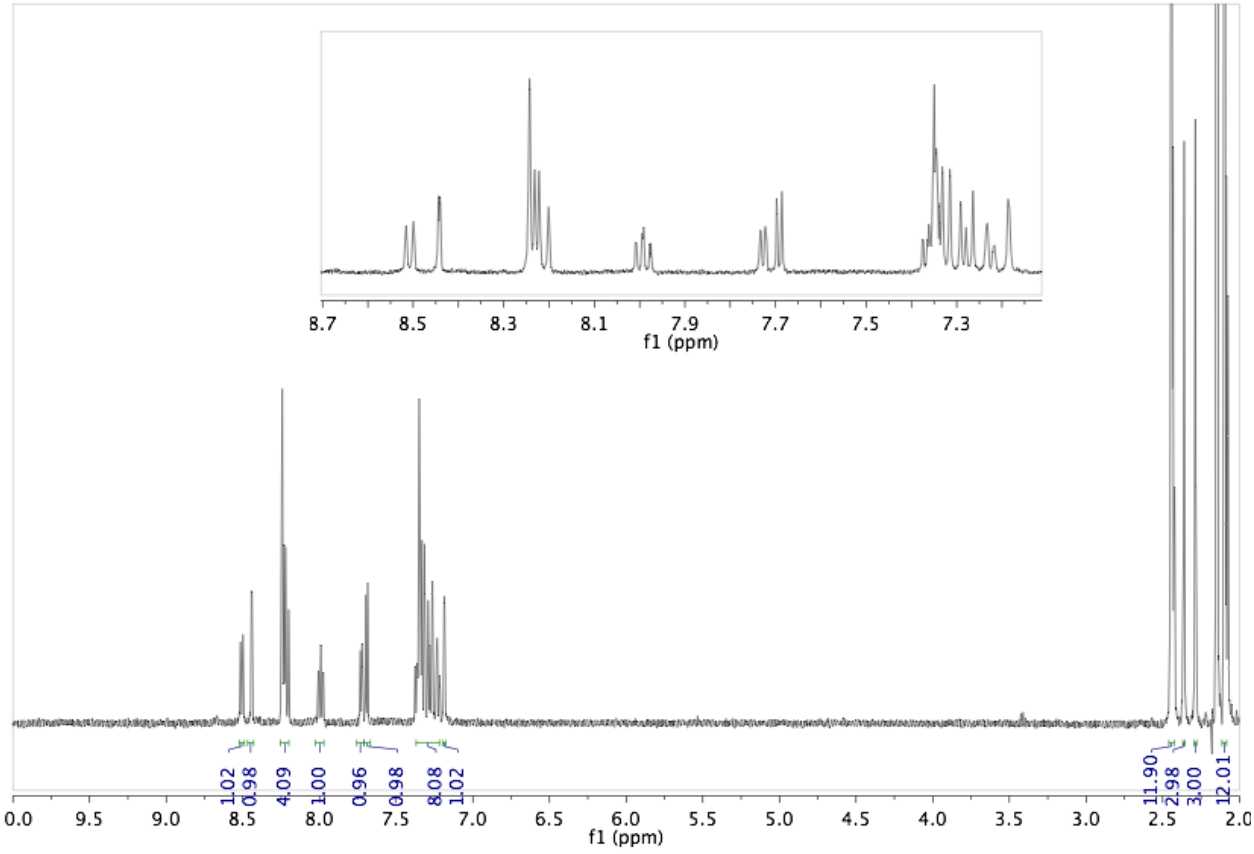

25. $[Ru(tmb)_2(bpy\text{-}3,5\text{-}mesityl)](PF_6)_2$ in CD_3CN

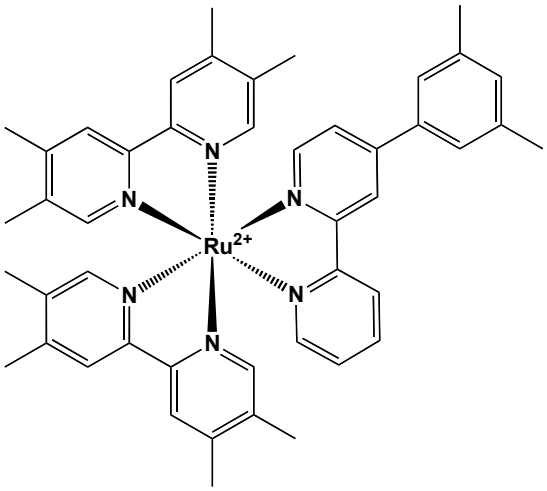

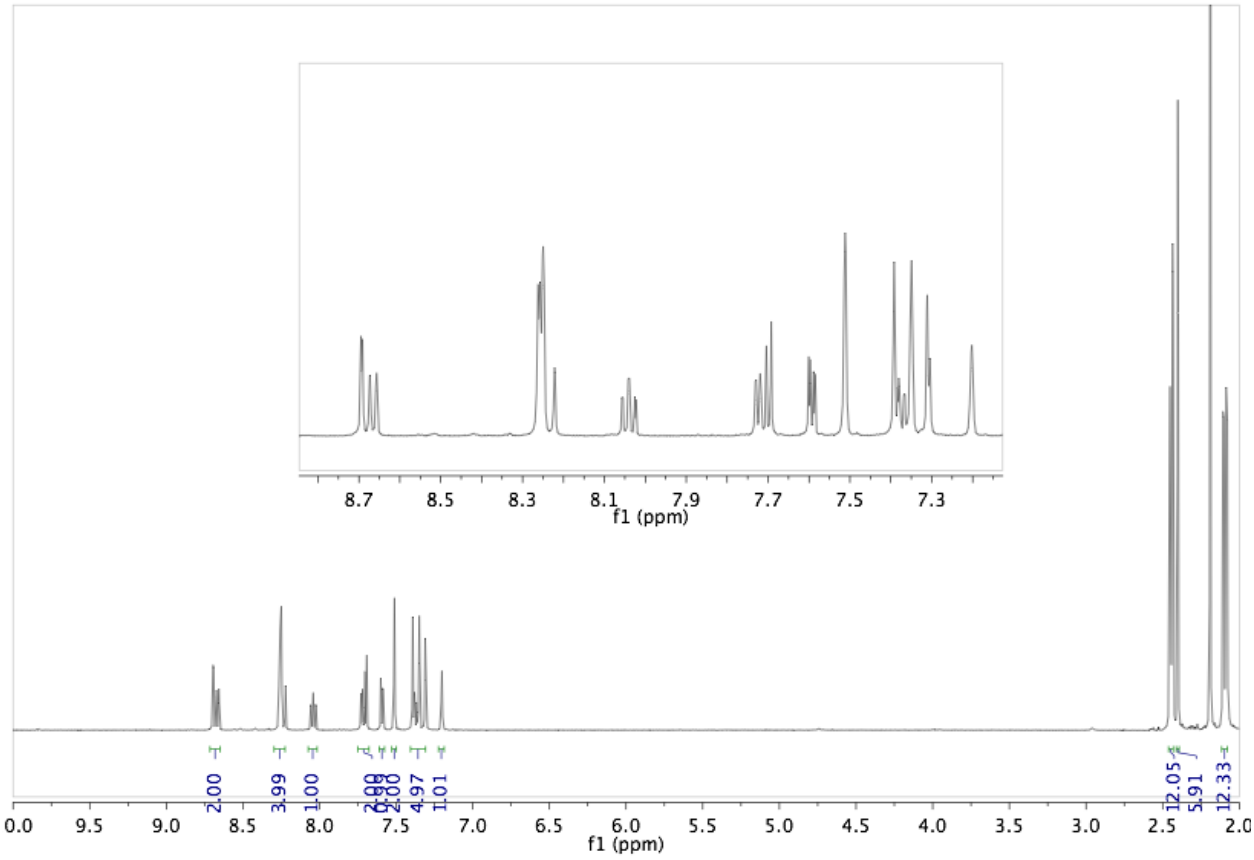

26. $[Ru(bpy)_2(bpy\text{-}phenyl\text{-}MV)](PF_6)_4$ in CD_3CN

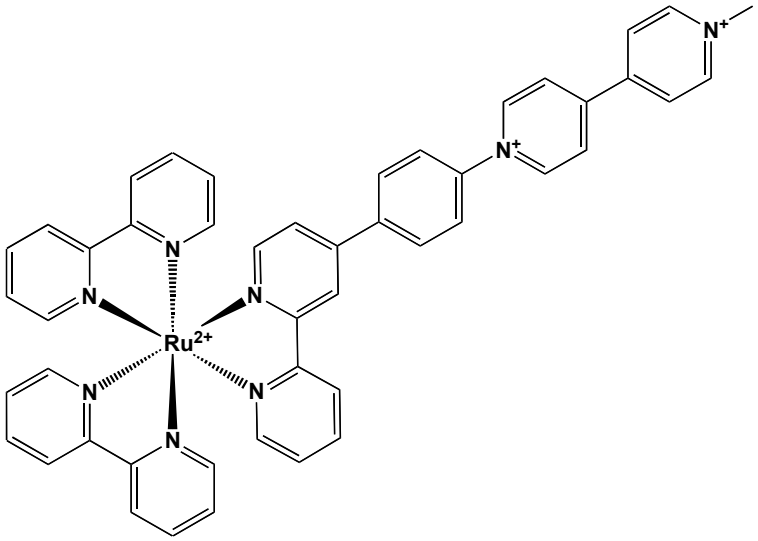

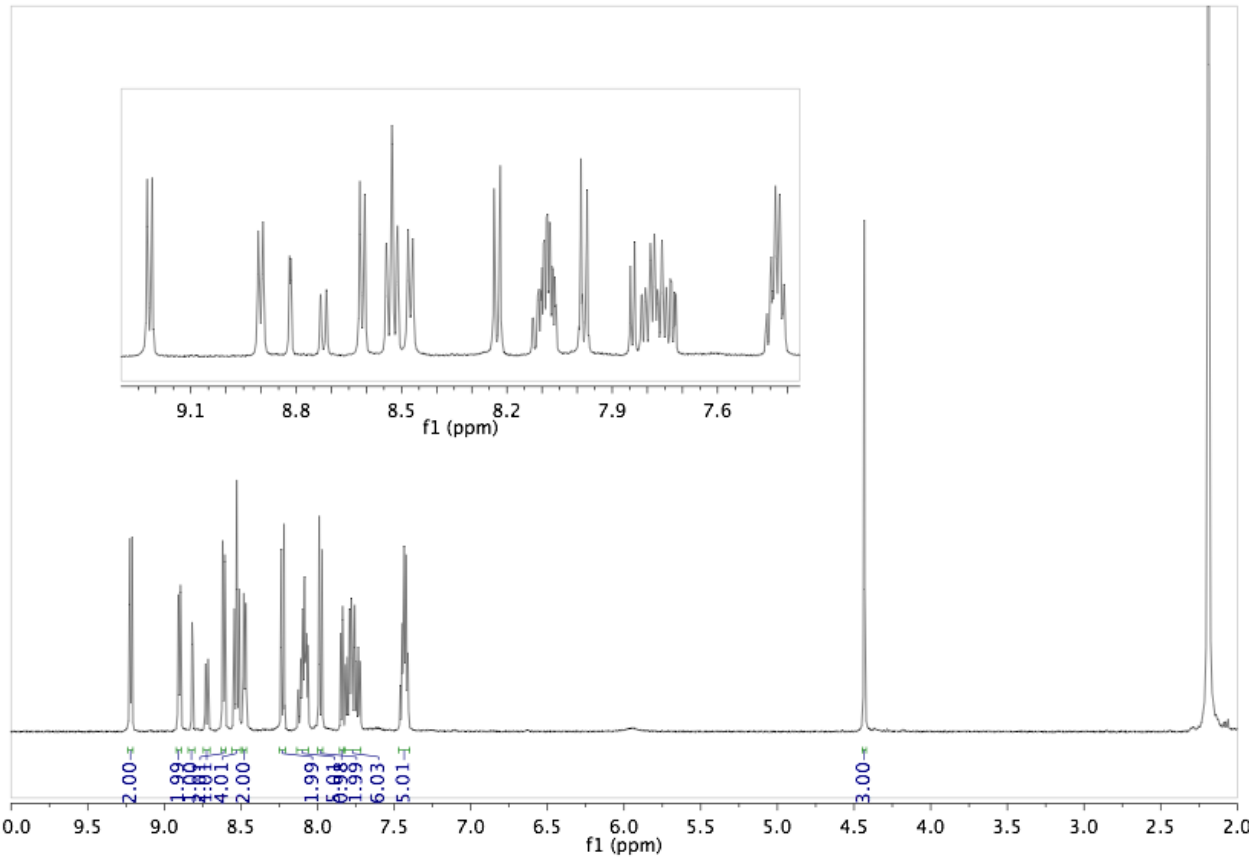

27. $[Ru(dmb)_2(bpy\text{-}phenyl\text{-}MV)](PF_6)_4$ in CD_3CN

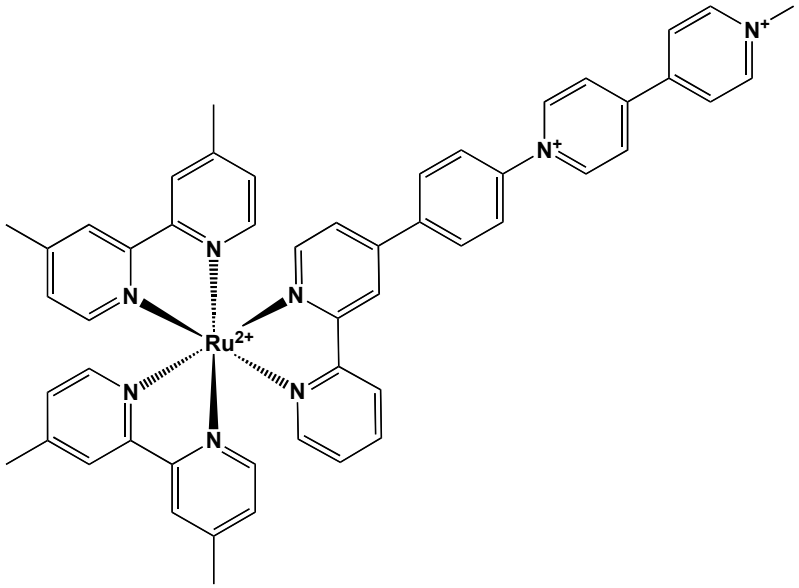

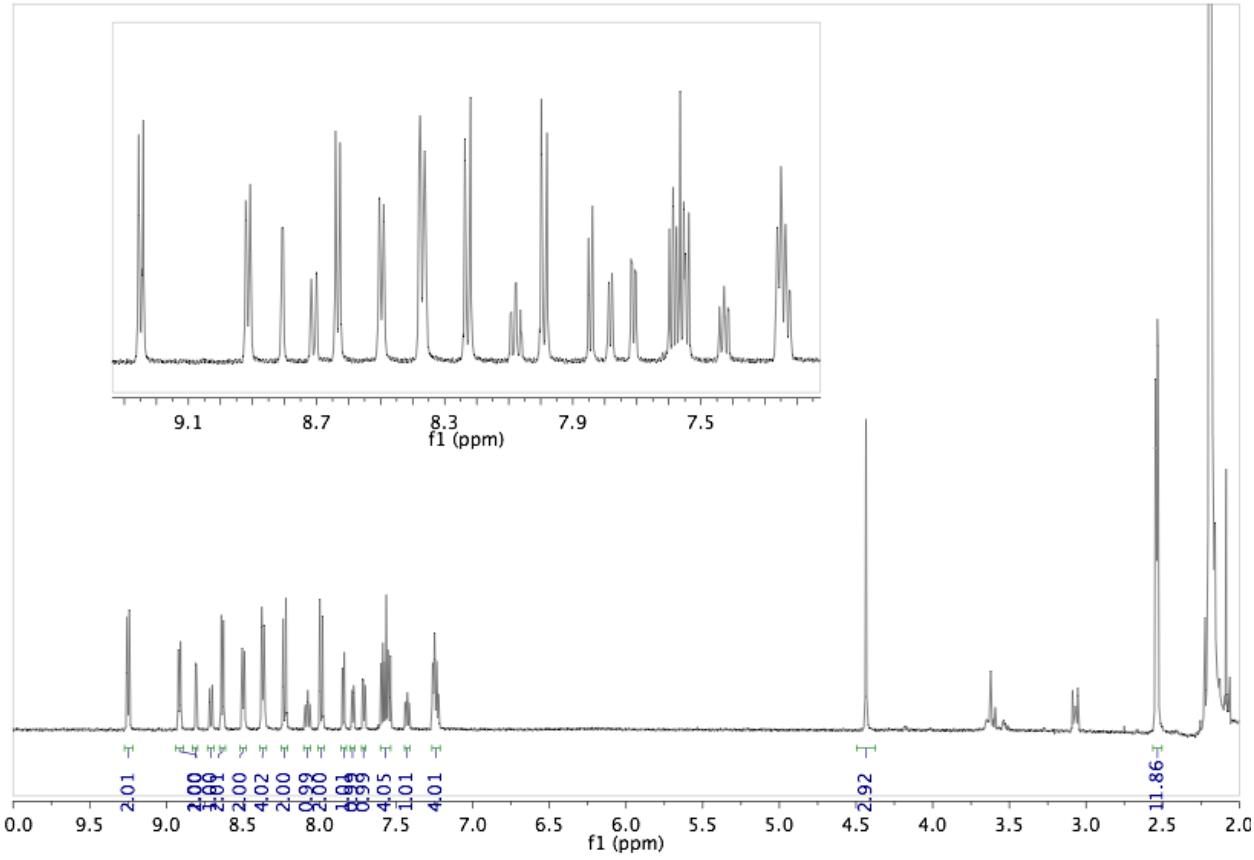

28. $[Ru(tmb)_2(bpy\text{-}phenyl\text{-}MV)](PF_6)_4$ in CD_3CN

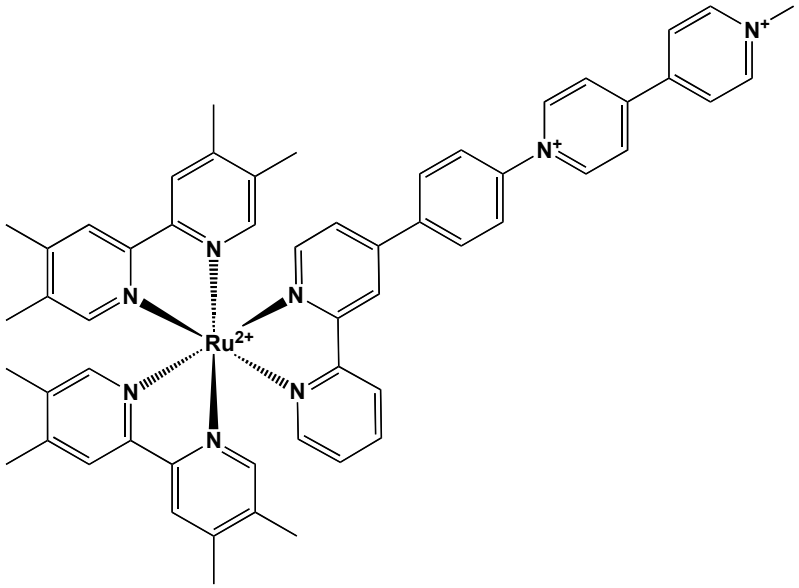

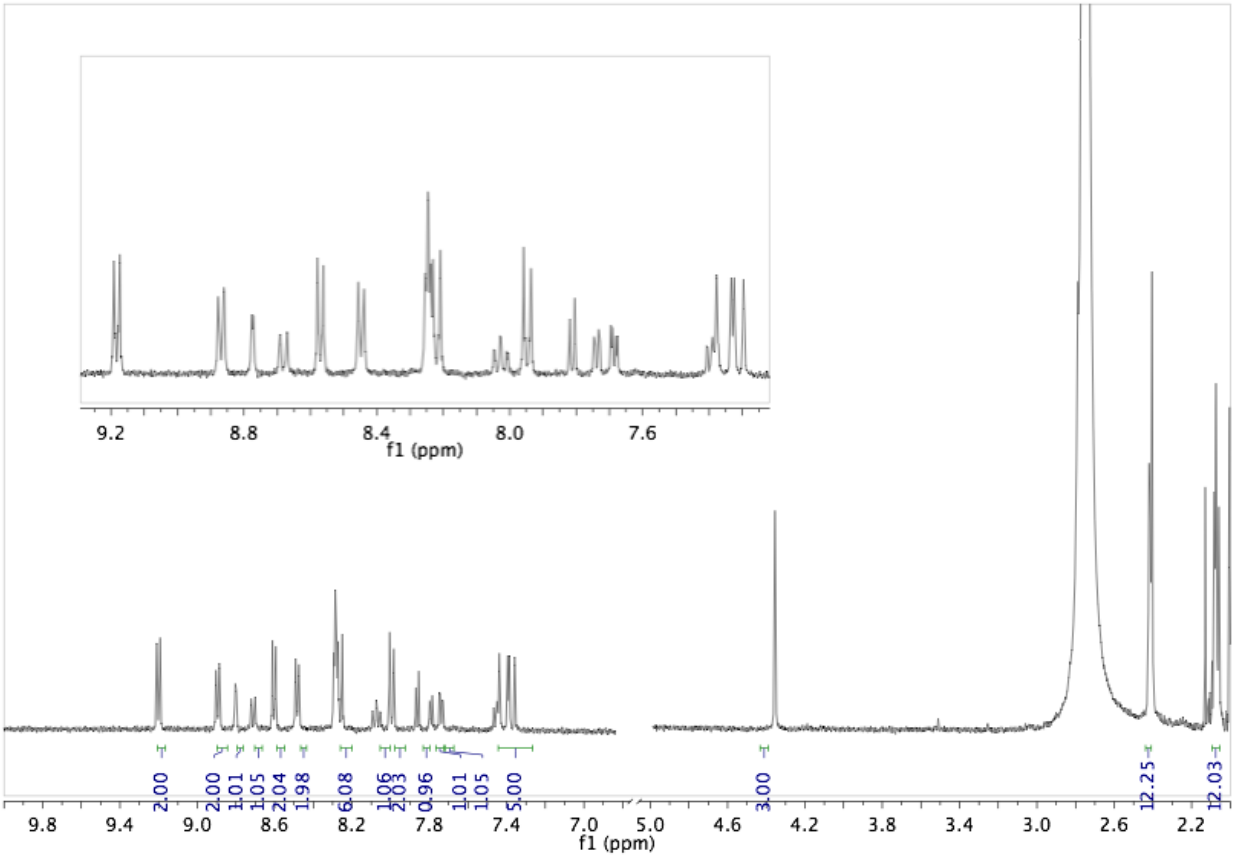

29. $[Ru(tmb)_2(bpy\text{-}ortho\text{-}MV)](PF_6)_4$ in CD_3CN

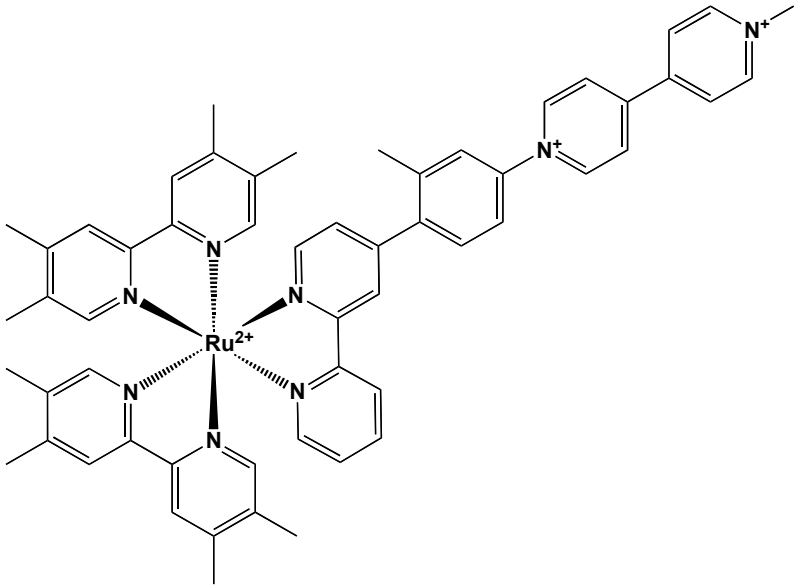

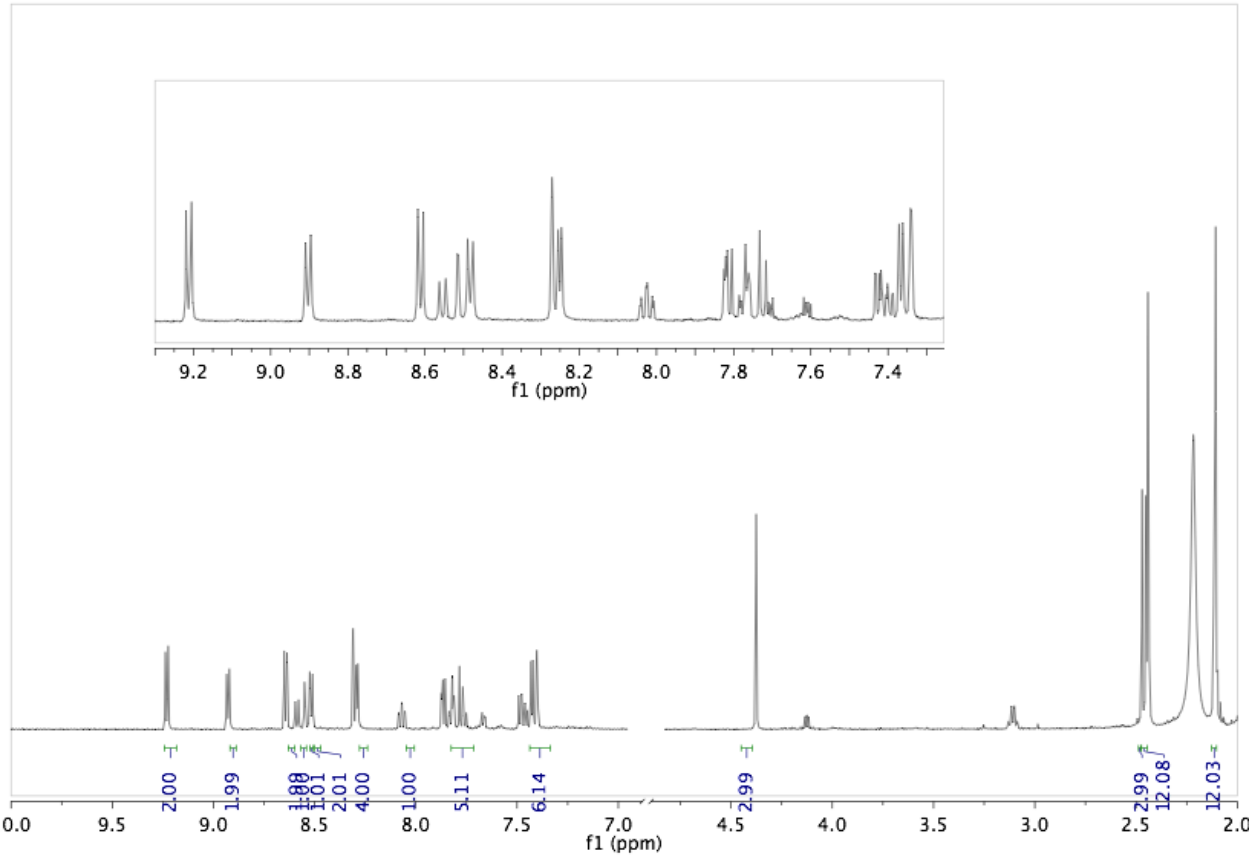

30. $[Ru(tmb)_2(bpy\text{-}2,6\text{-}mesityl\text{-}MV)](PF_6)_4$ in CD_3CN

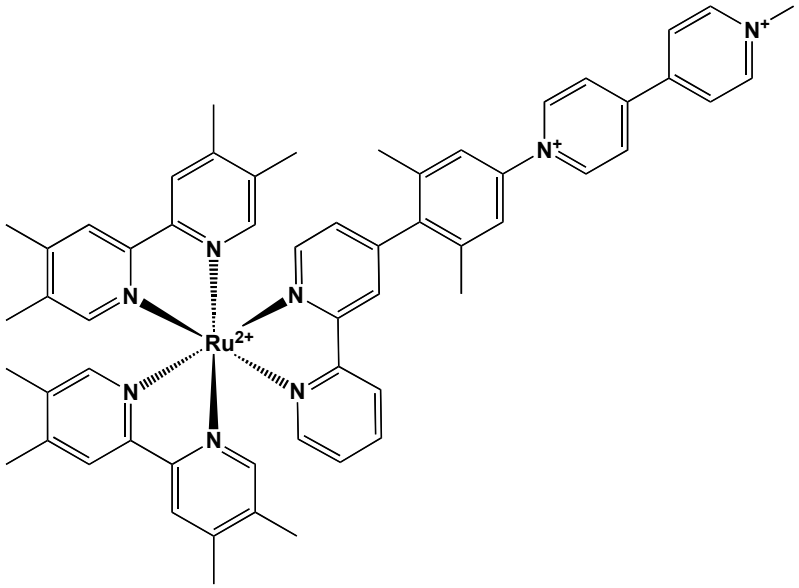

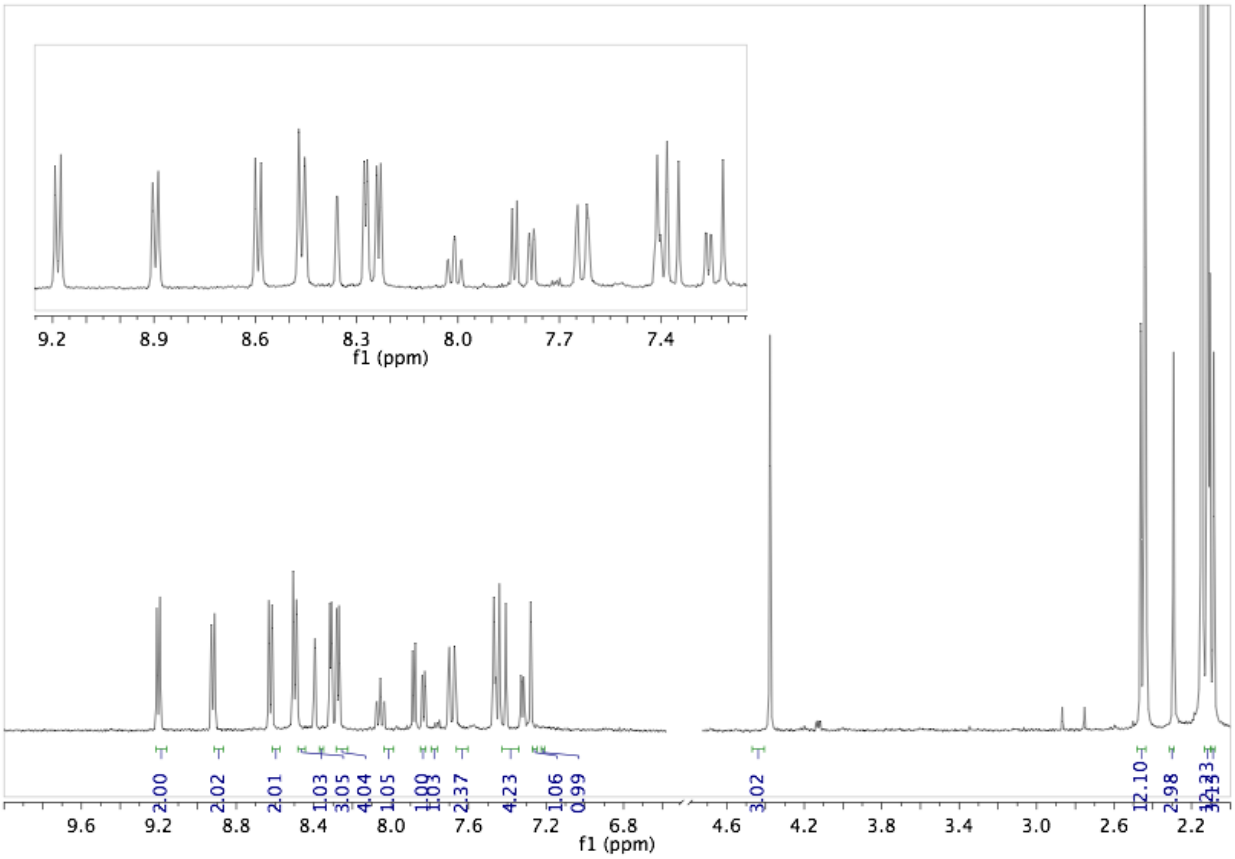

31. $[Ru(tmb)_2(bpy\text{-}2,5\text{-}mesityl\text{-}MV)](PF_6)_4$ in CD_3CN

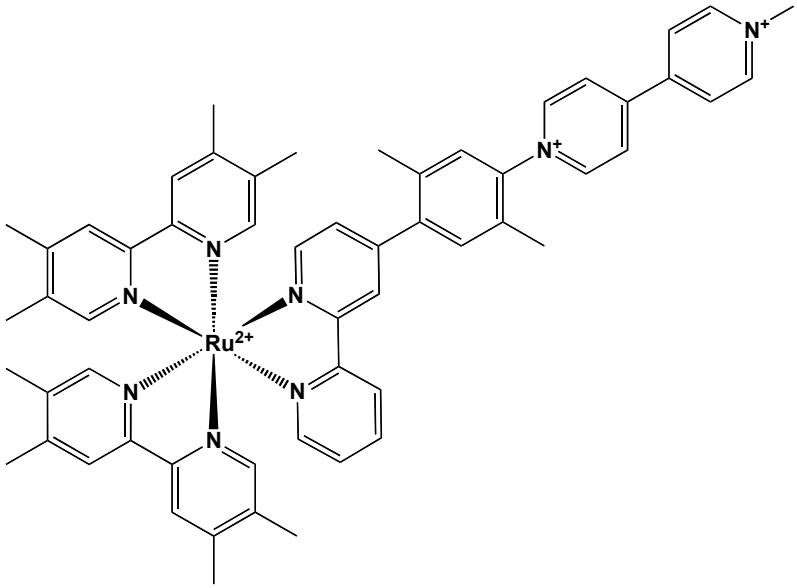

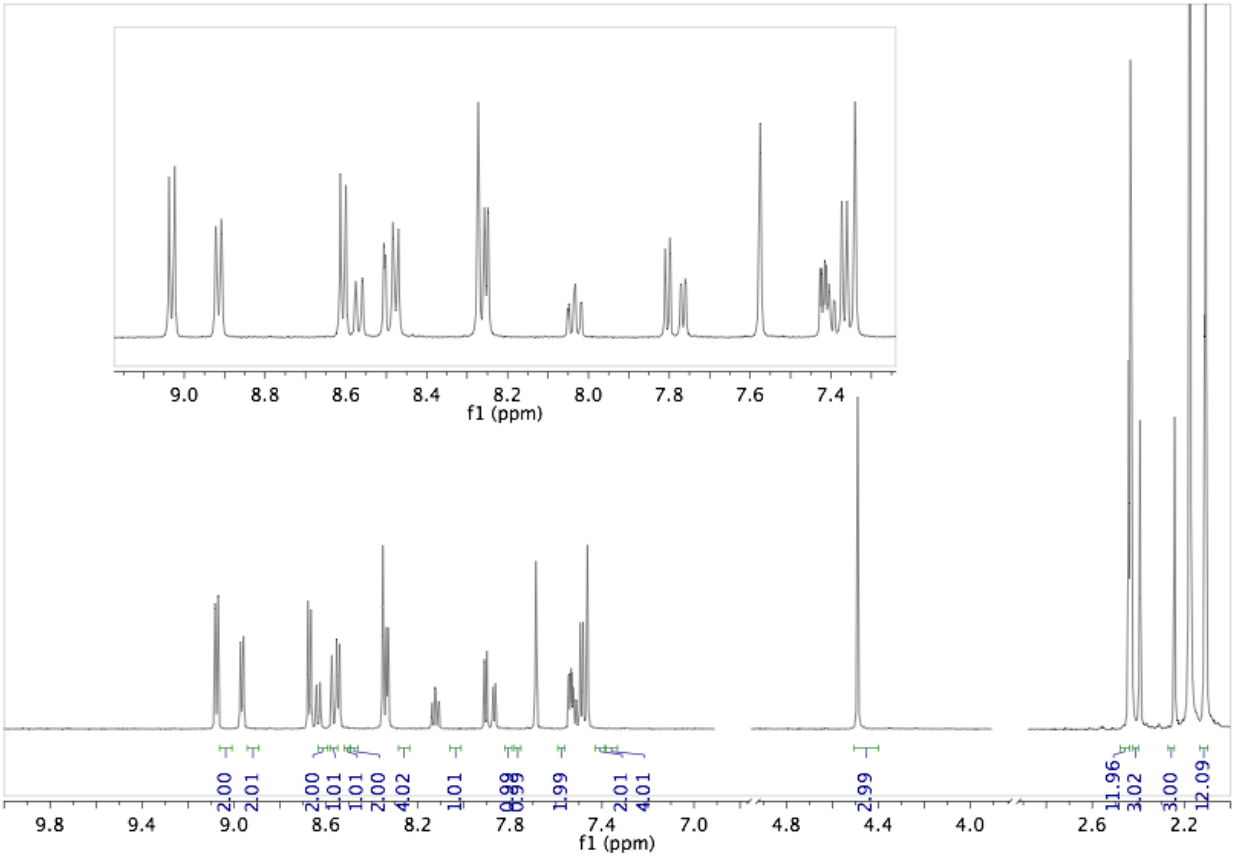

32. $[Ru(tmb)_2(bpy\text{-}3,5\text{-}mesityl\text{-}MV)](PF_6)_4$ in CD_3CN

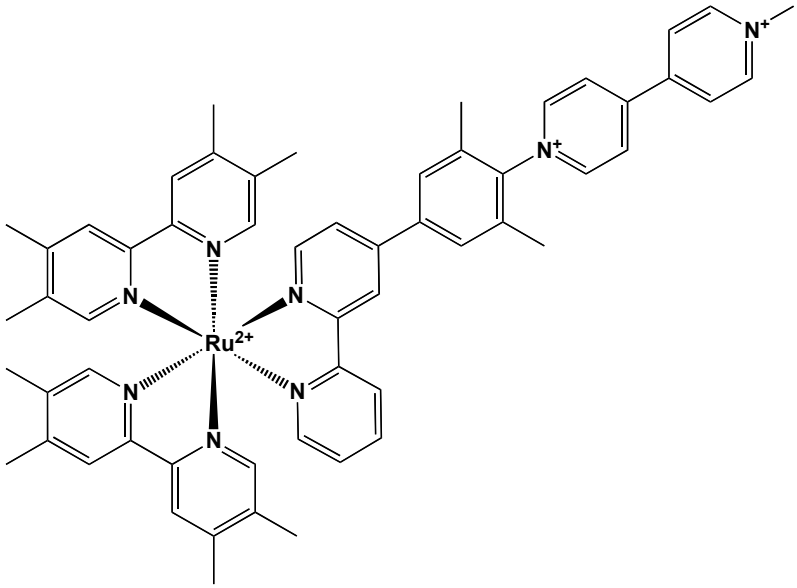

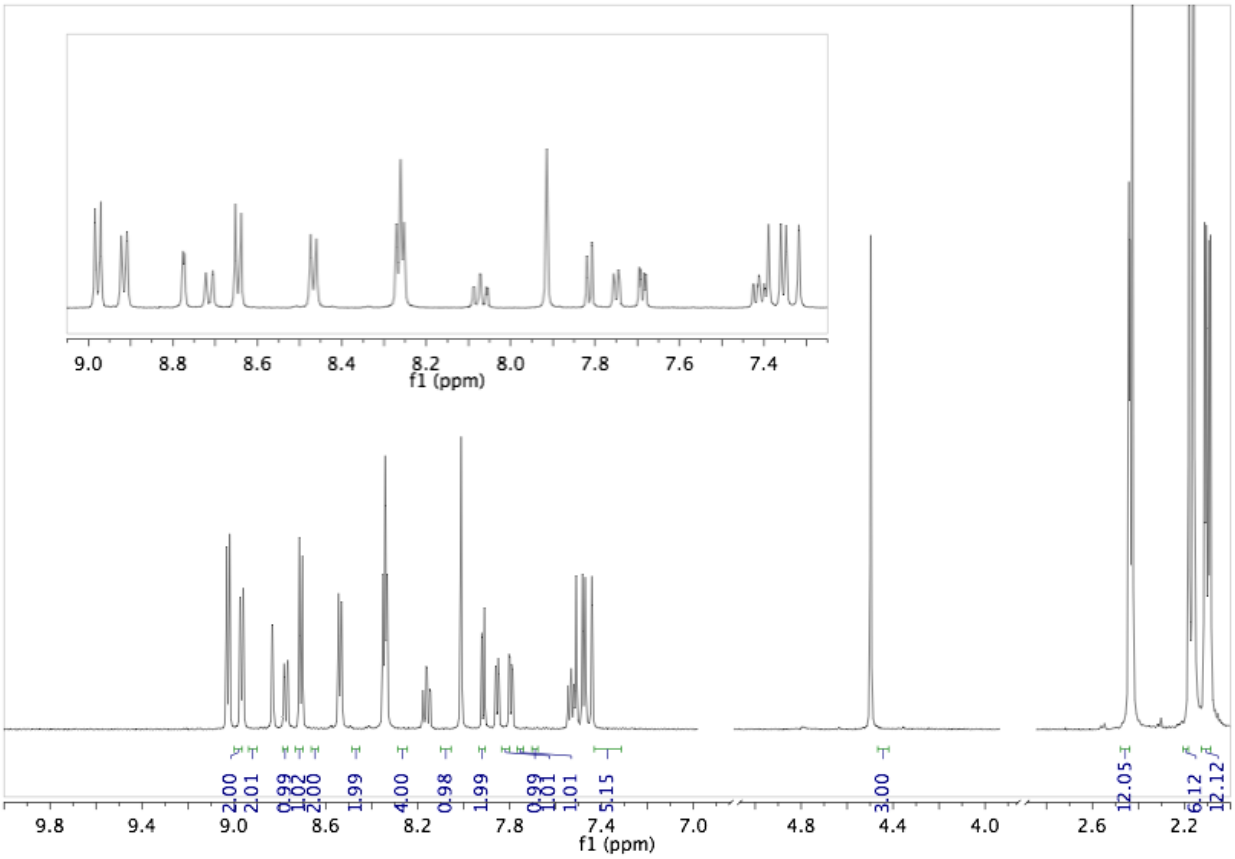

Appendix Two- Details of the Fitting Process Used to Extract Electron Transfer (ET) Lifetimes and Details Regarding the Generation of Simulated Transient Absorption Spectra and Kinetics

A2.1 Fitting Single Wavelength Kinetic Data.

Processing and fitting raw single wavelength kinetic data was performed in Igor Pro 6.0 and fitting functions were programmed in-house. The data is plotted as a negative change in transmittance (-ΔT) versus time in picoseconds. The signal maximum is normalized to 1.The beginning of the experiment, t_0, is manually set to occur after the coherent solvent spike see **Figure A2.1** below.

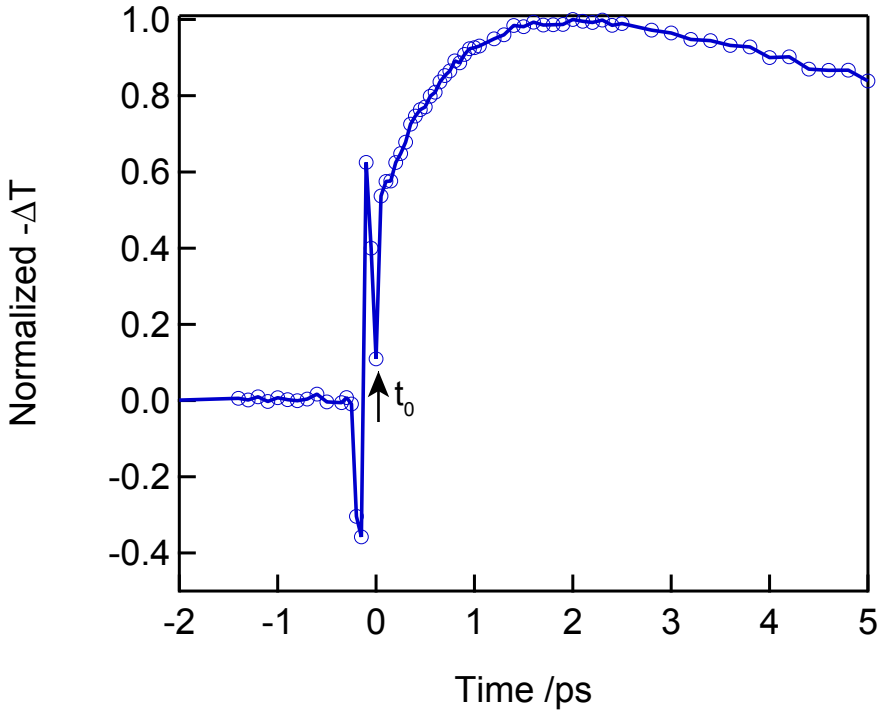

Figure A2.1 A representative single wavelength kinetic trace. The raw data was normalized and t_0 was manually set to occur after the coherent solvent spike as indicated by the arrow.

The range over which the data was fit was set manually. The fit begins at the first data point after the coherent solvent spike (usually ~50 fs) and ends at 100 ps. The extracted fitting parameters were not dependent on the position of the long time cursor as long as it was

placed after the conclusion of dynamics but the 100 ps data point was used throughout for fitting all seven DBA complexes. **Figure A2.2** below highlight these data points.

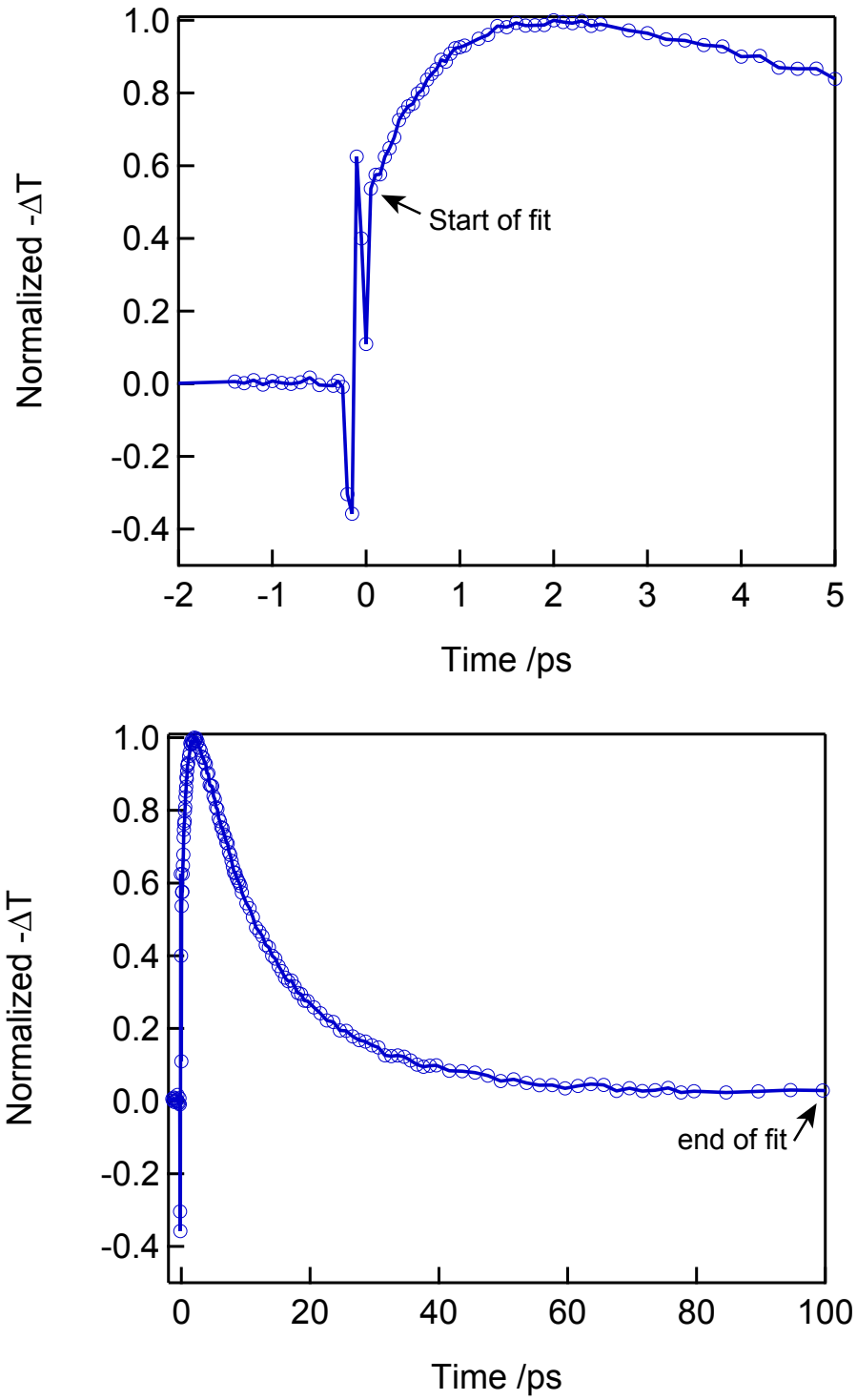

Figure A2.2 The first data point after the coherent solvent spike is selected as the starting point of the fit (top panel) and the data point at 100 ps is selected as the end point (bottom panel). The 100 ps end point was selected when fitting data for all DBA complexes.

In order to fit the single wavelength kinetic data a multi-exponential function with a time independent y-offset was used. Without the y-offset the data cannot be properly fit, the value of the offset was never greater than 0.02 (or 2 percent of the total signal). The time dependent values obtained from fits were not dependent on the value of the y-offset. The best fit was determined by visual inspection and by minimizing the error from the extracted lifetimes for each individual fit. Three separate data sets were fit for each complex; the average value for extracted lifetimes was reported.

A2.2 Transient Absorption Spectra Simulation Details

In order to assign the directionality of electron transfer i.e. which of the extracted lifetimes corresponds to forward ET, τ_{ET}, and which corresponds to back ET, τ_{BET}, the TA spectra were simulated. If $\tau_{ET} < \tau_{BET}$ then the kinetics are regarded as normal and a build up of the ET photoproduct is observed. Conversely if $\tau_{ET} > \tau_{BET}$ then the kinetics are regarded as inverted and no buildup of the ET product is observed. The two cases, normal versus inverted, lead to drastically different TA spectral profiles and by simulating the two scenarios we can match the experimental spectra with the simulation that best reproduces it. The directionality of ET will be assigned based on the simulation that best reproduces the experimental spectra.

As seen in Chapter Four the TA spectra of the DBA complexes in the driving force series are distinctive and reveal interesting dynamics in the spectral region between 350 and 500 nm. In our attempt to simulate these dynamics we chose to focus on the data in this wavelength region. Recall that a third exponential component, τ_3, was needed to fit the data probing at ~400 nm but this component was found to be independent of the ET process and therefore was not included in the simulations. Simulations of the TA spectra

were performed in Mathematica 8 utilizing the basic functions available in the software. To begin the simulations two Gaussian functions were defined to describe the two peaks observed in the experimental TA spectra. As discussed in Chapter Four the first peak centered at ~370 nm is assigned to absorbance of the ^{3}MLCT state of the donor and the second peak centered at ~400 nm is assigned as absorbance from the ET photoproduct. To generate accurate Gaussians peak widths and relative heights were estimated from the experimental spectra. Also for best agreement with experimental TA spectra the Gaussians were centered at their respective experimental maxima (370 nm and 400 nm for donor absorbance and ET absorbance, respectively).

To introduce time dependence each Gaussian was multiplied by the solution to the rate law describing its respective state. The rate law describing the disappearance of the ^{3}MLCT state is shown below in **Equations A2.1**. It is assumed that the ^{3}MLCT state decays via formation of the ET photoproduct alone with the rate constant k_{ET}. On the time scale of the forward ET process this is a valid approximation.

$$\frac{d\,[MLCT]}{dt} = -k_{ET}[MLCT] \qquad \textbf{Equation A2.1}$$

The rate law for the formation and subsequent loss of the ET photoproduct is shown below in **Equation A2.2**. It is assumed that the ET photoproduct is formed from the ^{3}MLCT state with the rate constant k_{ET} and is lost via decay back to the ground state with the rate constant k_{BET}.

$$\frac{d\,[ET]}{dt} = k_{ET}[MLCT] - k_{BET}[ET] \qquad \textbf{Equation A2.2}$$

At t_0 the ^{3}[MLCT] is set to one and [ET] set to zero. The Gaussian centered at 370 nm was multiplied by the solution to the rate law describing the depletion of the ^{3}MLCT state. The

peak centered at 400 nm was multiplied by the solution to the rate law describing the formation and subsequent loss of the ET photoproduct.

For each of the complexes in the driving force series, $[Ru(bpy)_2(bpy\text{-}phenyl\text{-}MV)](PF_6)_4$ (**1**), $Ru(dmb)_2(bpy\text{-}phenyl\text{-}MV)](PF_6)_4$ (**2**) and $[Ru(tmb)_2(bpy\text{-}phenyl\text{-}MV)](PF_6)_4$ (**3**) both normal and inverted kinetics were simulated. To simulate normal kinetics τ_{ET} (or $1/k_{ET}$) was set to the fast lifetime obtained from the fits of the single wavelength kinetics data and τ_{BET} (or $1/k_{BET}$) was set to the intermediate lifetime obtained from the same fit. Below in **Figure A2.3** simulated normal kinetics for complexes (**1**) (top panel), (**2**) (middle panel) and (**3**) (bottom panel) are shown below. What is obvious from these simulations is that the same dynamics are observed for these complexes and the differences in electron transfer lifetimes are not enough to alter the dynamics of one complex from another. These simulations of normal kinetics successfully reproduce the experimental TA spectra observed in Chapter Four wherein at early times a peak centered is 370 is the dominant spectral feature but as time progresses a broader peak centered at 400 nm is the dominant spectral feature.

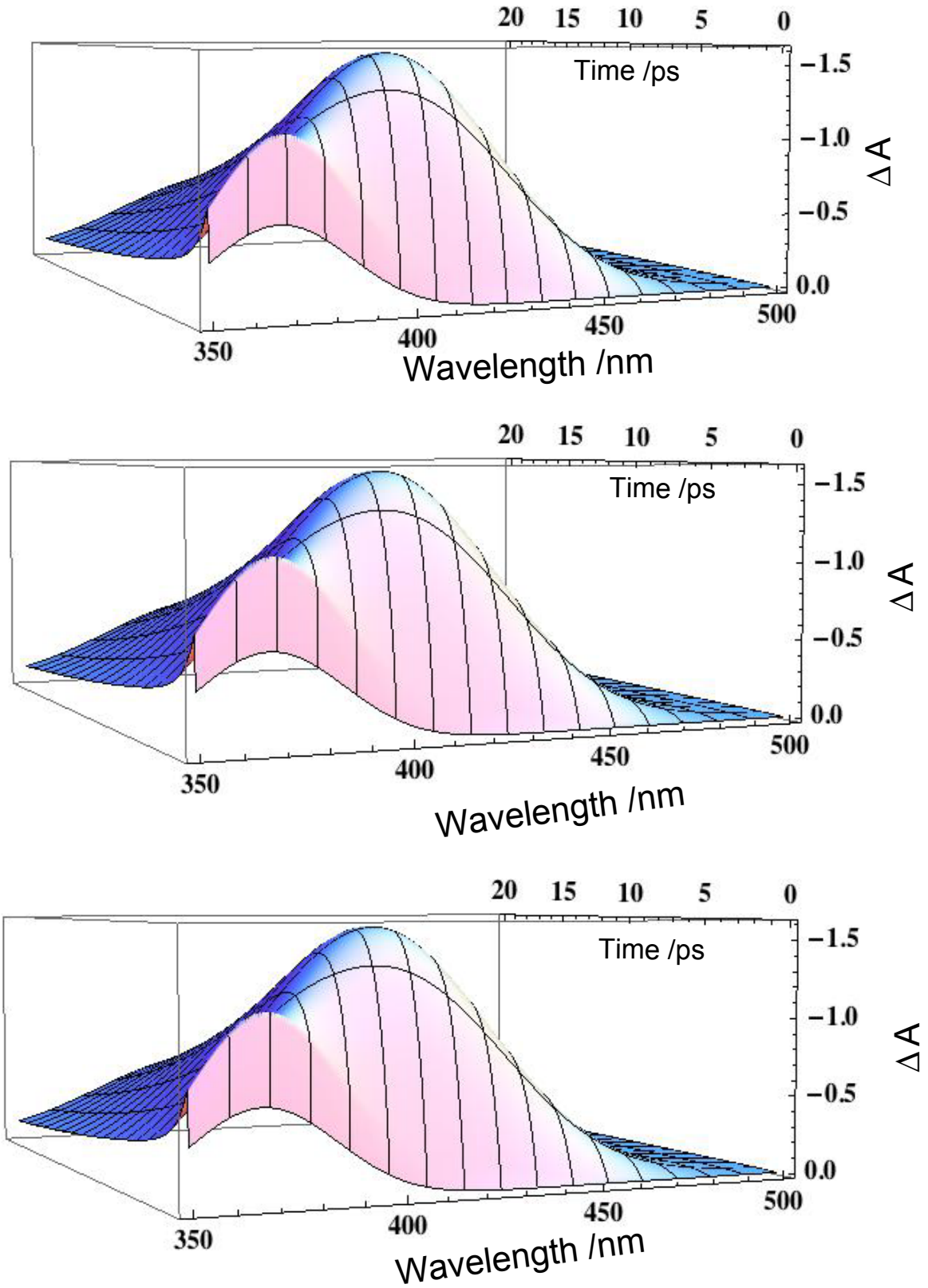

Figure A2.3 Simulated TA spectra for complexes (**1**) (top), (**2**) (middle) and (**3**) (bottom) under normal kinetic conditions.

The inverted kinetics were simulated for each complex with τ_{ET} (or $1/k_{ET}$) set as the intermediate lifetime obtained from the fits of the single wavelength kinetics data of complexes (**1**), (**2**) and (**3**) and τ_{BET} (or $1/k_{BET}$) set as the fast lifetime obtained from the same fits. These simulations are shown below in **Figure A2.4** below where (**1**) is shown in the top panel, (**2**) in the middle panel and (**3**) in the bottom panel. As we can also see from these simulations is that similar dynamics are predicted for the three complexes in this series. However what is obvious is that dynamics predicted for the inverted kinetics scenario do not match those seen in the experimental TA spectra. The simulations predict the presence of a single peak centered at 370 nm over the course of the experiment and never the presence of the second peak centered at 400 nm that is observed in the experimental data. Therefore it is concluded that the ET dynamics observed for the complexes in this series are following normal kinetics.

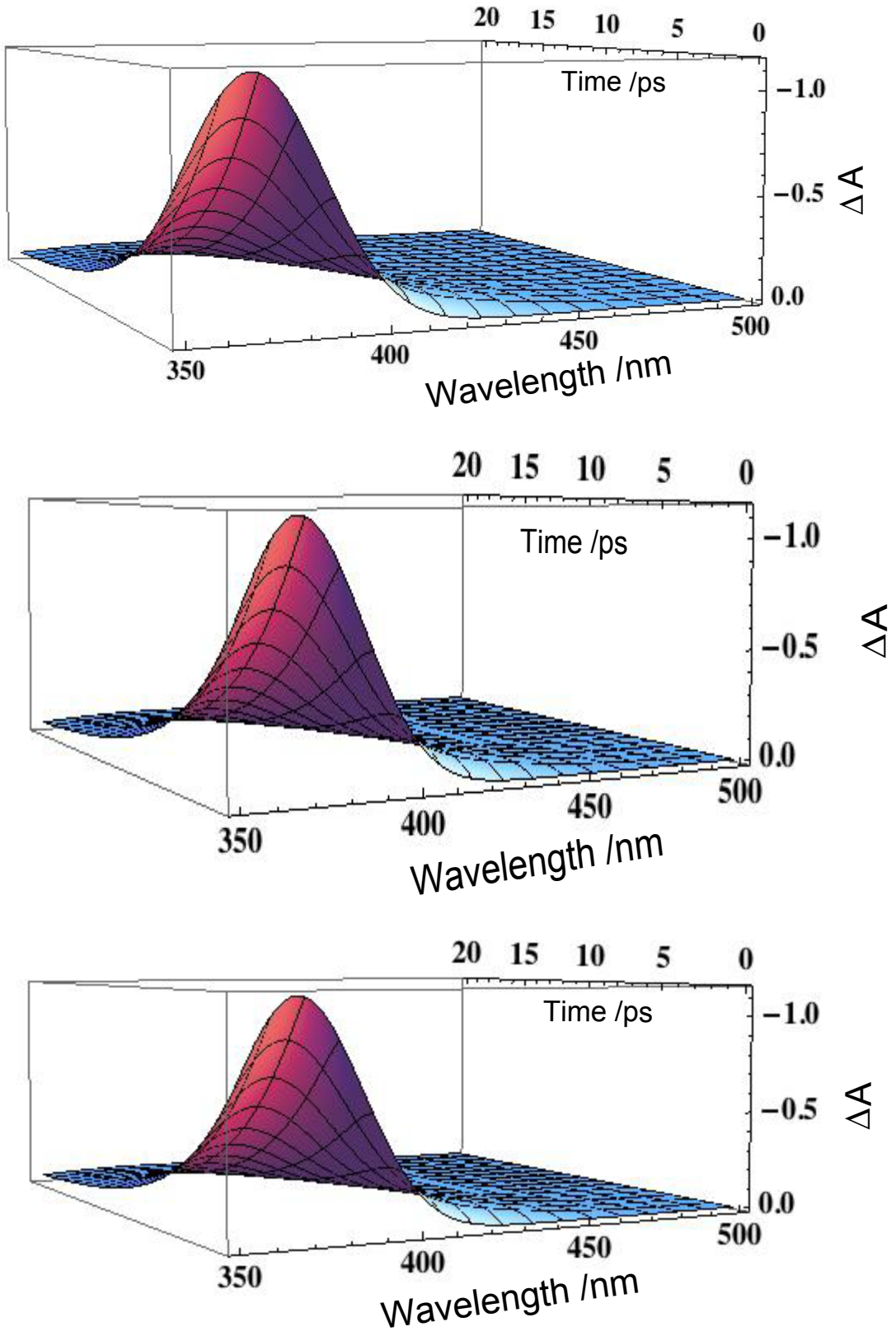

Figure A2.4 Simulated TA spectra for complexes (**1**) (top), (**2**) (middle) and (**3**) (bottom) under inverted kinetic conditions.

A2.3 Validating Vibrational Cooling in the Fitting of Single Wavelength Kinetic Data

Mathematica was used to simulate the single wavelength kinetic for compounds requiring a third exponential component to be fit. The third component was assigned as vibrational cooling of the directly excited acceptor. It was concluded that even though the cooling process is longer than the back electron transfer process the cooling component is still be detected in the single wavelength kinetic data. The following kinetic scheme was simulated.

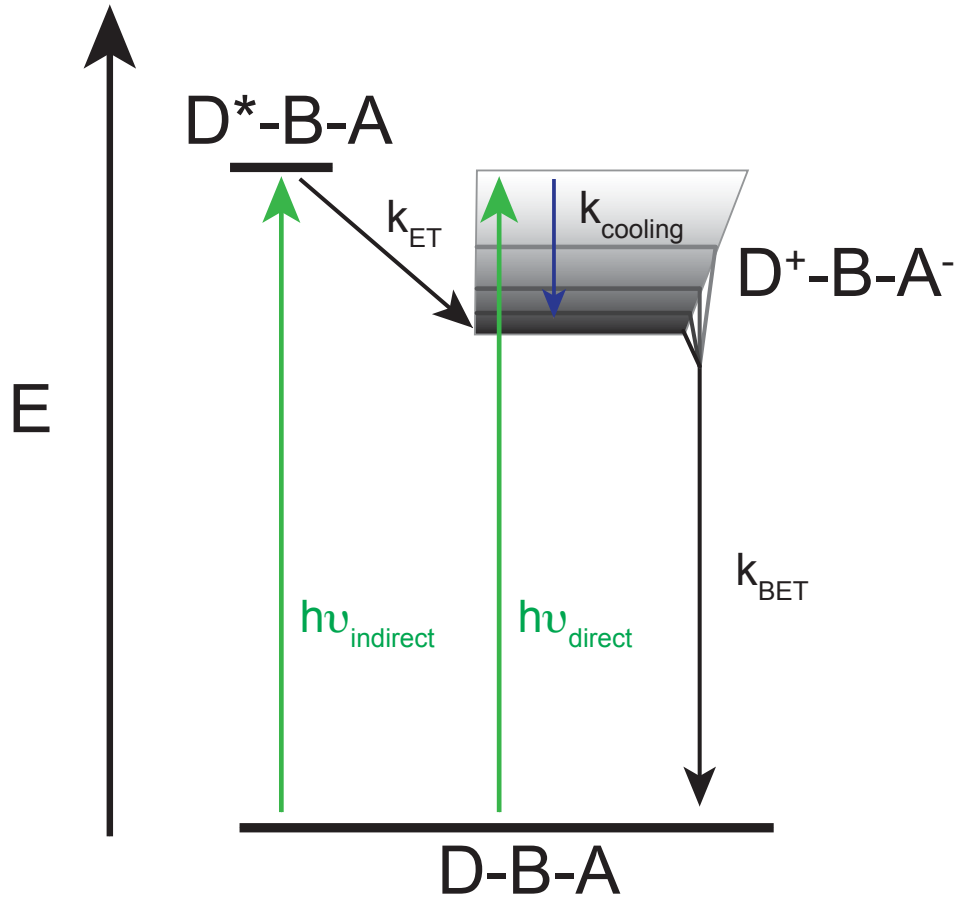

Figure A2.4 Simulated kinetic scheme including cooling dynamics.

In the scheme above excitation to both the ^{1}MLCT and acceptor occurs (the intersystem crossing is not shown and D*-B-A is assumed to be a ^{3}MLCT state. The directly excited state

is vibrationally hot. The ^{3}MLCT decays via formation of the electron transfer (ET) state. Back electron transfer (BET) can occur from both the hot and 'cool' ET states. In the simulation the cooling lifetime was set to 20 ps, BET from the cool state was set to 5 ps and BET from the hot state was set to 30 ps. The value of 30 ps is just an estimate but this lifetime must be longer than BET from the cool state since BET is occurring the Marcus inverted region (where reaction rates decrease with increased driving force). The simulated single wavelength kinetic data are shown below.

Simulated data 'probing' at 607 nm is shown below in Figures **A2.5** and **A2.6**. The figures below show the simulated 607 nm data fit with a double and a triple exponential function, respectively. As seen below the data are not fit satisfactorily with a double an exponential function.

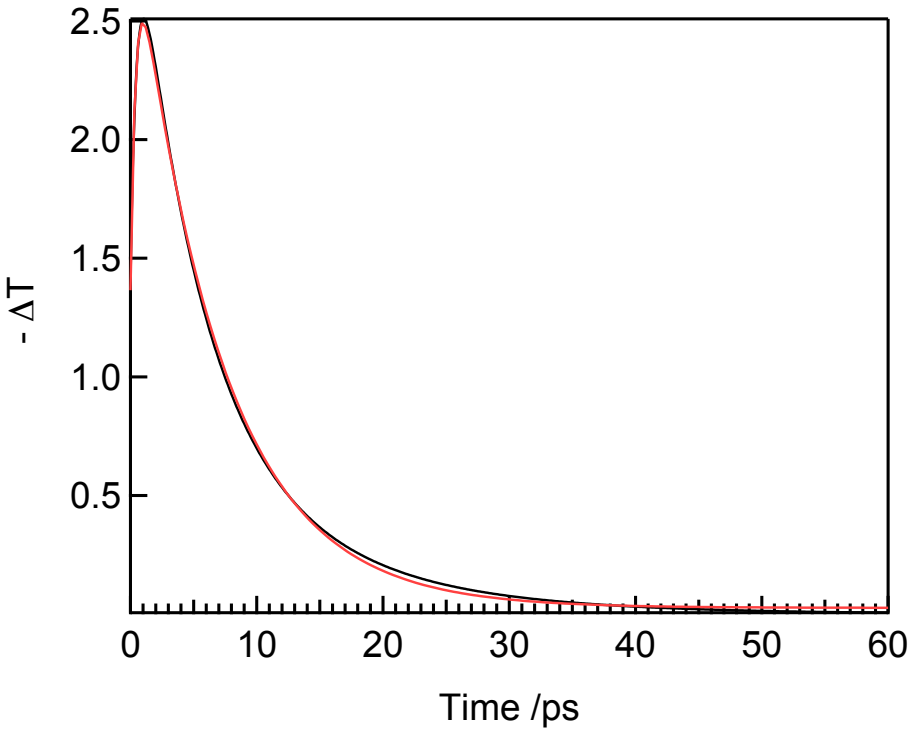

Figure A2.6 Simulated 607 nm data (black) fit with a double exponential (red). Clearly the data do not fit to a double exponential.

The simulated 607 nm probe data fit with a triple exponential function is shown below.

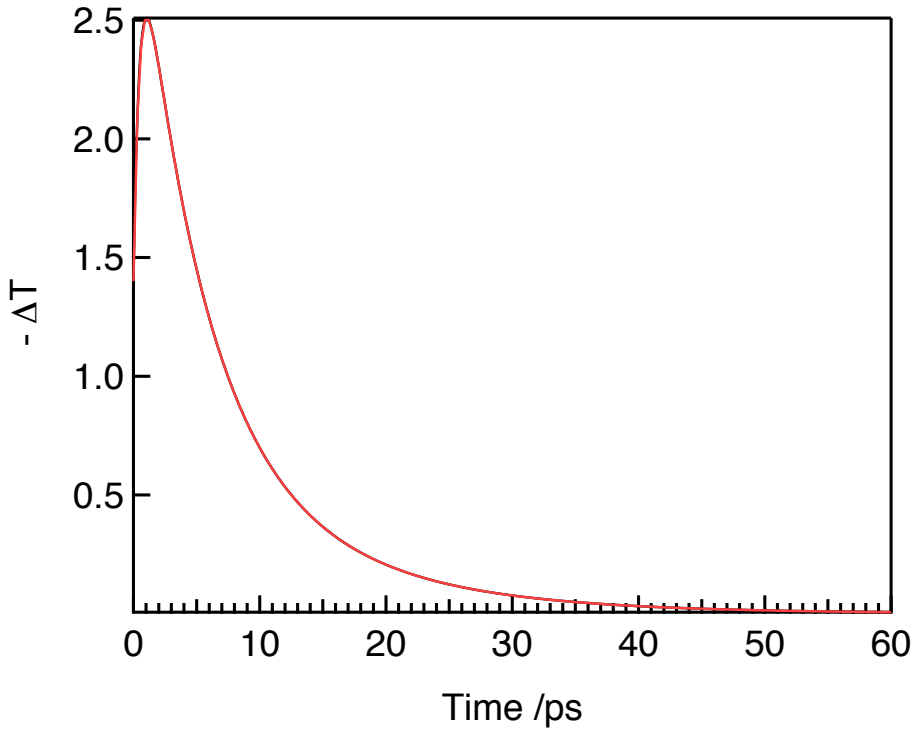

Figure A2.6 Simulated 607 nm data (black) fit with a triple exponential (red). Clearly the data fit nicely to a triple exponential

A triple exponential function fits the data very nicely. The extracted lifetimes are a fast component of ~0.5 ps, an intermediate component of ~5 ps and a long component of ~12 ps. If holding the long component to 20 ps the data is still fit satisfactorily and a fast component of ~0.5 ps and an intermediate component is ~6 ps are obtained. These simulations show that even though the cooling component is longer than BET it should be detected in the data. One might be tempted to assign the long component to be BET from the directly excited acceptor state but experimentally differences in this lifetime for complexes (**2**) and (**3**) should be present since there would be driving force dependence but 16 ps is obtained for both complexes.

Appendix Three-Cartesian Coordinates for Geometry Optimized Complexes.
Donor Complexes

$[Ru(bpy)_2(bpy\text{-}phenyl)](PF_6)_2$ (1') (Å)

Atom	X	Y	Z
C	5.74392	-0.83200	0.65519
C	5.15507	0.19422	1.38405
C	3.79825	0.42911	1.21946
N	3.03284	-0.28791	0.38385
C	3.60263	-1.28016	-0.33915
C	4.95733	-1.57678	-0.21564
C	1.84039	1.49906	-2.49092
C	2.17387	2.59049	-3.27886
C	2.10666	3.85965	-2.71714
C	1.70746	3.98819	-1.39242
C	1.38409	2.84972	-0.65947
N	1.45167	1.61602	-1.21303
C	2.68741	-2.00186	-1.26153
C	0.94071	2.88787	0.75826
N	1.40836	-1.55703	-1.27436
C	0.52404	-2.14195	-2.09530
C	0.86221	-3.18796	-2.94105
C	2.17224	-3.65068	-2.93213
C	3.09325	-3.05035	-2.08228
C	0.74976	4.07042	1.46752
C	0.32430	4.01545	2.78909
C	0.10392	2.77460	3.37424
C	0.31568	1.63601	2.61053
N	0.72288	1.68237	1.33342
C	-1.78354	0.85962	-1.07305
C	1.07171	-2.20397	2.22095
C	0.57276	-3.17705	3.07393
C	-0.80095	-3.38600	3.10683
C	-1.61815	-2.61725	2.28779
C	-1.05041	-1.65807	1.45333
N	0.28763	-1.45711	1.42935
C	-1.84551	-0.79507	0.54046
N	-1.12197	0.04967	-0.23241
C	-3.23088	-0.83318	0.47541
C	-3.93115	0.00562	-0.39985
C	-3.16203	0.86830	-1.18879

Ru	0.96766	0.00982	0.06820
C	-5.40695	-0.01965	-0.47688
C	-6.10385	-1.22516	-0.33393
C	-7.49113	-1.24610	-0.40311
C	-8.19739	-0.06300	-0.60575
C	-7.51226	1.14126	-0.74790
C	-6.12427	1.16339	-0.68876
H	-1.23391	-4.13732	3.76051
H	1.24897	-3.75617	3.69349
H	-0.23284	2.68423	4.40152
H	0.11031	-3.62509	-3.58969
H	2.48272	2.44148	-4.30819
H	5.73196	0.80603	2.06921
H	-8.06087	2.06643	-0.89873
H	-8.02260	-2.18817	-0.30421
H	-5.59983	2.11245	-0.77620
H	-5.56128	-2.15922	-0.20433
H	-3.63388	1.53203	-1.90650
H	-3.79259	-1.49647	1.12358
H	-2.69118	-2.77010	2.30076
H	0.92109	5.03224	0.99723
H	-0.48601	-1.74437	-2.06636
H	1.65573	4.97224	-0.94072
H	2.13720	-2.00129	2.16156
H	-1.16793	1.51717	-1.67994
H	0.15785	0.64345	3.02184
H	1.87633	0.48805	-2.88541
H	3.29061	1.21514	1.77066
H	4.11893	-3.40134	-2.06681
H	5.40420	-2.37829	-0.79323
H	-9.28226	-0.08005	-0.65392
H	2.47647	-4.46701	-3.58034
H	6.80253	-1.05169	0.75671
H	2.36090	4.73955	-3.30043
H	0.16758	4.93149	3.35071

[Ru(dmb)$_2$(bpy-phenyl)](PF$_6$)$_2$ (2') (Å)

Atom	**X**	**Y**	**Z**

C	5.44207	-0.82806	0.94726
C	4.84031	0.30917	1.49232
C	3.48822	0.52768	1.29567
N	2.70482	-0.31321	0.60209
C	3.26431	-1.42606	0.07555
C	4.61984	-1.69770	0.23235
C	1.54251	0.74268	-2.64320
C	1.92258	1.59458	-3.66446
C	1.94369	2.97378	-3.44258
C	1.56822	3.41605	-2.17468
C	1.19551	2.50839	-1.18797
N	1.18422	1.17786	-1.42477
C	2.33442	-2.31850	-0.66651
C	0.78563	2.91417	0.18307
N	1.05389	-1.89039	-0.73464
C	0.16209	-2.65002	-1.38963
C	0.49545	-3.84518	-2.00103
C	1.81272	-4.30788	-1.94367
C	2.73101	-3.51388	-1.25687
C	0.72243	4.23951	0.60113
C	0.33258	4.55885	1.90122
C	0.00906	3.49210	2.74366
C	0.09130	2.19524	2.26920
N	0.47782	1.89687	1.01916
C	-2.06131	0.53029	-1.16635
C	0.67405	-1.59708	2.87409
C	0.13901	-2.26471	3.96527
C	-1.23919	-2.42977	4.03125
C	-2.02723	-1.92717	3.00378
C	-1.42396	-1.26848	1.93528
N	-0.08164	-1.10225	1.88277
C	-2.18294	-0.68532	0.79758
N	-1.43368	-0.04300	-0.12866
C	-3.56346	-0.77418	0.68102
C	-4.22722	-0.19056	-0.40431
C	-3.43317	0.48153	-1.33954
Ru	0.64687	-0.04601	0.20736
C	-5.69778	-0.27668	-0.54028
C	-6.38021	-1.43449	-0.14968
C	-7.76258	-1.50920	-0.26896
C	-8.47785	-0.42580	-0.77265

C	-7.80711	0.72994	-1.16404
C	-6.42376	0.80340	-1.05427
H	-1.69822	-2.93900	4.87345
H	0.79502	-2.63989	4.74384
H	-0.31065	3.66646	3.76714
H	-0.26974	-4.41242	-2.52322
H	2.20687	1.18196	-4.62844
H	5.42307	1.02323	2.06700
H	-8.36308	1.57913	-1.55048
H	-8.28141	-2.41617	0.02752
H	-5.91237	1.71989	-1.33999
H	-5.82879	-2.29626	0.22059
H	-3.87694	0.94204	-2.21657
H	-4.14678	-1.27997	1.44253
H	-3.10420	-2.04431	3.04259
H	0.97494	5.04072	-0.08538
H	-0.85305	-2.26492	-1.42003
H	1.57530	4.48036	-1.96428
H	1.74412	-1.43693	2.78008
H	-1.42325	1.03917	-1.88283
H	-0.15249	1.34908	2.90522
H	1.51750	-0.33354	-2.78750
H	2.99645	1.40648	1.70354
H	3.76295	-3.84271	-1.19239
H	5.05141	-2.59440	-0.20003
C	0.27434	5.97982	2.38334
H	1.02768	6.14980	3.16012
H	0.45661	6.69050	1.57357
H	-0.70364	6.20051	2.82260
C	2.35088	3.93169	-4.52537
H	2.41402	4.95741	-4.15443
H	3.32360	3.65365	-4.94308
H	1.62403	3.91097	-5.34483
C	2.21441	-5.60531	-2.58445
H	1.85325	-5.65530	-3.61624
H	3.29958	-5.73269	-2.59046
H	1.77449	-6.45065	-2.04383
C	6.91227	-1.08604	1.11276
H	7.19320	-2.07857	0.75200
H	7.49195	-0.34592	0.55013
H	7.21033	-1.00461	2.16267

H	-9.55930	-0.48080	-0.85793

[Ru(tmb)$_2$(bpy-phenyl)](PF$_6$)$_2$ (3') (Å)

RuTmb Phenyl Donor (Å)

Atom	X	Y	Z
C	5.28018	-0.76853	1.20491
C	4.76270	0.53324	1.32436
C	3.41814	0.72355	1.03248
N	2.58760	-0.25283	0.63716
C	3.08196	-1.50184	0.50156
C	4.41562	-1.77648	0.78643
C	1.37542	0.00905	-2.77317
C	1.71617	0.55196	-4.00563
C	1.71811	1.95279	-4.12299
C	1.38403	2.70235	-2.99817
C	1.05311	2.08227	-1.79803
N	1.04824	0.73602	-1.69492
C	2.11564	-2.52363	0.02691
C	0.69470	2.81973	-0.56064
N	0.86908	-2.07377	-0.23005
C	-0.04425	-2.94487	-0.68537
C	0.20705	-4.29263	-0.91102
C	1.49975	-4.77031	-0.63301
C	2.44445	-3.86105	-0.16572
C	0.63716	4.20721	-0.47792
C	0.30605	4.83943	0.71765
C	0.03166	4.03154	1.83527
C	0.10673	2.65479	1.67010
N	0.42791	2.05090	0.51639
C	-2.18941	0.22239	-1.24522
C	0.57627	-0.87667	3.17266
C	0.04643	-1.24412	4.40033
C	-1.33480	-1.33190	4.52646
C	-2.12929	-1.05269	3.42185
C	-1.53104	-0.69209	2.21728
N	-0.18568	-0.60267	2.10345
C	-2.30009	-0.38527	0.98230
N	-1.55358	-0.05838	-0.09789
C	-3.68622	-0.42860	0.92143
C	-4.36003	-0.14782	-0.27277
C	-3.56615	0.18261	-1.37661
Ru	0.53346	-0.03351	0.20149

C	-5.83630	-0.19806	-0.35509
C	-6.55878	-1.12708	0.40270
C	-7.94543	-1.16823	0.33222
C	-8.62861	-0.27806	-0.49232
C	-7.91873	0.64831	-1.25200
C	-6.53149	0.68726	-1.18680
H	-1.79002	-1.61600	5.47054
H	0.70819	-1.45615	5.23350
H	-8.45039	1.34739	-1.89091
H	-8.49632	-1.89693	0.91950
H	-5.98873	1.43083	-1.76574
H	-6.03380	-1.84525	1.02885
H	-4.01447	0.38734	-2.34353
H	-4.26503	-0.66225	1.80817
H	-3.20824	-1.11732	3.50384
H	0.85087	4.81517	-1.35144
H	-1.03106	-2.53127	-0.88025
H	1.38619	3.78528	-3.06928
H	1.64886	-0.79102	3.02495
H	-1.55194	0.47565	-2.08741
H	-0.09782	1.99068	2.50626
H	1.36064	-1.06939	-2.63397
H	2.97433	1.71244	1.11741
H	3.44751	-4.21399	0.05220
H	4.80061	-2.78576	0.68266
C	-0.87473	-5.20034	-1.42518
H	-1.80945	-4.65653	-1.58735
H	-0.58289	-5.66212	-2.37512
H	-1.07471	-6.01321	-0.71830
C	1.85358	-6.21554	-0.83528
H	1.19966	-6.86566	-0.24372
H	1.73319	-6.50729	-1.88480
H	2.88666	-6.41867	-0.54300
C	6.72143	-1.06003	1.50943
H	6.96692	-0.78226	2.54080
H	6.95683	-2.11857	1.37565
H	7.38095	-0.47607	0.85741
C	5.62391	1.69030	1.74571
H	6.07105	1.51790	2.73092
H	6.44695	1.84386	1.03883
H	5.04918	2.61922	1.79610
C	-0.33964	4.62059	3.16710

H	-0.49141	3.84092	3.91840
H	0.43953	5.29848	3.53278
H	-1.26516	5.20297	3.09434
C	0.25004	6.33666	0.81343
H	-0.74115	6.67312	1.13783
H	0.97047	6.70445	1.55323
H	0.47582	6.80954	-0.14526
C	2.06591	2.62084	-5.42194
H	2.07332	3.70908	-5.32508
H	3.05113	2.30178	-5.77943
H	1.34077	2.35521	-6.19999
C	2.06801	-0.34247	-5.16085
H	1.36636	-0.20730	-5.99171
H	3.06955	-0.11860	-5.54450
H	2.04777	-1.39537	-4.86719
H	-9.71319	-0.30630	-0.54204

$[Ru(tmb)_2(bpy\text{-}ortho](PF_6)_2$ (4') (Å)

Atom	**X**	**Y**	**Z**
C	5.37969	0.10716	1.41986
C	4.62053	1.28877	1.49924
C	3.28659	1.22534	1.11784
N	2.68314	0.10930	0.68419
C	3.40769	-1.02843	0.59021
C	4.74995	-1.04417	0.95471
C	1.62454	0.11941	-2.75911
C	1.95053	0.71511	-3.97102
C	1.77610	2.10656	-4.08433
C	1.27338	2.79063	-2.98031
C	0.95152	2.11901	-1.80618
N	1.13675	0.78389	-1.70161
C	2.66353	-2.21162	0.10712
C	0.36703	2.76961	-0.61393
N	1.37361	-1.98145	-0.22308
C	0.63208	-3.00198	-0.67832
C	1.10302	-4.30062	-0.81636
C	2.43765	-4.55741	-0.45158
C	3.20621	-3.48832	0.00244
C	0.02117	4.11523	-0.55129
C	-0.54848	4.65571	0.59820
C	-0.76114	3.79951	1.69435

C	-0.38651	2.46965	1.55661
N	0.16126	1.95576	0.44481
C	-1.98492	-0.17874	-1.39201
C	0.77556	-0.97869	3.08034
C	0.28200	-1.50727	4.26296
C	-1.06893	-1.82763	4.33643
C	-1.87498	-1.59490	3.22944
C	-1.31788	-1.05011	2.07509
N	0.00231	-0.75440	2.00667
C	-2.09188	-0.77179	0.84438
N	-1.35366	-0.39760	-0.22849
C	-3.47408	-0.87440	0.77234
C	-4.14497	-0.62094	-0.42729
C	-3.35783	-0.29007	-1.53463
Ru	0.67138	-0.05038	0.15421
C	-5.62005	-0.71755	-0.52883
C	-6.16163	-1.57066	-1.49800
C	-7.53694	-1.71295	-1.62866
C	-8.37916	-0.97969	-0.79875
C	-7.84370	-0.11508	0.14974
H	-1.48914	-2.25607	5.23978
H	0.95160	-1.67252	5.09903
H	-8.50947	0.47010	0.77728
H	-7.94610	-2.38901	-2.37212
H	-3.81829	-0.08623	-2.49532
H	-4.05081	-1.15461	1.64566
H	-2.92577	-1.85534	3.26397
H	0.18462	4.76176	-1.40620
H	-0.39182	-2.75201	-0.93872
H	1.13801	3.86441	-3.04661
H	1.82245	-0.71700	2.97466
H	-1.35036	0.10717	-2.22386
H	-0.53073	1.76676	2.37094
H	1.74567	-0.95103	-2.62335
H	2.65433	2.10602	1.17244
H	4.23651	-3.66676	0.28944
H	5.32096	-1.96322	0.88261
C	0.19617	-5.38475	-1.32614
H	-0.78722	-4.99057	-1.59499
H	0.62038	-5.86421	-2.21506
H	0.05349	-6.16706	-0.57261
C	3.01128	-5.94227	-0.53290

H	2.41658	-6.63988	0.06645
H	3.00220	-6.31417	-1.56336
H	4.04038	-5.97010	-0.16860
C	6.82181	0.08866	1.83668
H	6.93009	0.45261	2.86434
H	7.24434	-0.91674	1.78462
H	7.42272	0.74643	1.19922
C	5.21160	2.58661	1.97031
H	5.60479	2.50432	2.98931
H	6.04478	2.89052	1.32694
H	4.46704	3.38671	1.96004
C	-1.36424	4.29264	2.97815
H	-1.50968	3.47831	3.69275
H	-0.72137	5.04261	3.45284
H	-2.33690	4.76532	2.80452
C	-0.94392	6.10296	0.65820
H	-2.03231	6.19829	0.74675
H	-0.50466	6.59580	1.53193
H	-0.62705	6.64225	-0.23717
C	2.09006	2.82973	-5.36174
H	2.03461	3.91359	-5.23920
H	3.09051	2.57573	-5.72657
H	1.38007	2.54291	-6.14655
C	2.46177	-0.12115	-5.10995
H	1.79406	-0.05069	-5.97595
H	3.45094	0.21591	-5.43802
H	2.53693	-1.17327	-4.82440
C	-6.46427	0.03280	0.31031
C	-5.94512	1.01195	1.33891
H	-5.72334	0.52098	2.29465
H	-5.03270	1.51592	1.00340
H	-6.69637	1.77891	1.54359
H	-5.49707	-2.14755	-2.13533
H	-9.45653	-1.07244	-0.89098

[Ru(tmb)$_2$(bpy-2,6-mesityl)](PF$_6$)$_2$ (5') (Å)

Atom	**X**	**Y**	**Z**
C	5.51845	-0.57244	1.22788
C	4.96951	0.72101	1.27495
C	3.61665	0.85858	0.99228
N	2.80590	-0.16173	0.67609

C	3.32688	-1.40606	0.62249
C	4.67276	-1.62786	0.89654
C	1.61317	-0.22809	-2.73238
C	1.96345	0.20546	-4.00459
C	1.94797	1.58936	-4.25082
C	1.58381	2.43432	-3.20575
C	1.24553	1.92139	-1.95774
N	1.26100	0.59074	-1.73023
C	2.37502	-2.48017	0.24392
C	0.86225	2.76336	-0.79640
N	1.11642	-2.07469	-0.02857
C	0.21391	-2.99421	-0.40202
C	0.48869	-4.35015	-0.52901
C	1.79367	-4.78149	-0.23289
C	2.72618	-3.82269	0.15376
C	0.76953	4.15053	-0.84327
C	0.42738	4.88345	0.29029
C	0.18194	4.17741	1.48114
C	0.28548	2.79309	1.44370
N	0.61374	2.09233	0.34853
C	-1.97087	0.12339	-1.23378
C	0.80300	-0.61972	3.25445
C	0.27620	-0.90892	4.50428
C	-1.10370	-1.01012	4.63536
C	-1.90053	-0.82014	3.51359
C	-1.30490	-0.53568	2.28756
N	0.03902	-0.43198	2.16828
C	-2.07763	-0.32280	1.03594
N	-1.33702	-0.07441	-0.06856
C	-3.46568	-0.37812	0.97848
C	-4.13369	-0.1767	-0.23063
C	-3.35018	0.07905	-1.35756
Ru	0.75009	-0.01039	0.22639
C	-5.62331	-0.22938	-0.30429
C	-6.25551	-1.44456	-0.61174
C	-7.64836	-1.47294	-0.66604
C	-8.39319	-0.32506	-0.42251
C	-7.75220	0.87138	-0.12483

H	-1.55618	-1.23297	5.59696
H	0.93958	-1.05261	5.35065
H	-8.33747	1.76889	0.06023
H	-8.15248	-2.40683	-0.90279
H	-3.81367	0.24189	-2.32609
H	-4.05268	-0.57905	1.86904
H	-2.97862	-0.89620	3.59795
H	0.96508	4.67919	-1.7708
H	-0.78246	-2.61323	-0.61448
H	1.57212	3.50598	-3.37716
H	1.87450	-0.52792	3.10228
H	-1.33264	0.32149	-2.09018
H	0.10126	2.20496	2.33983
H	1.61295	-1.28836	-2.49166
H	3.14921	1.83977	1.01919
H	3.73751	-4.14007	0.38749
H	5.08169	-2.63189	0.84867
C	-0.58092	-5.31119	-0.96578
H	-1.53096	-4.79845	-1.14056
H	-0.29732	-5.82252	-1.89272
H	-0.74924	-6.08551	-0.20922
C	2.17742	-6.22949	-0.33802
H	1.52394	-6.85795	0.27656
H	2.08574	-6.58327	-1.37132
H	3.20810	-6.39313	-0.01419
C	6.97290	-0.80490	1.51973
H	7.22323	-0.48108	2.53660
H	7.24257	-1.85917	1.42224
H	7.60436	-0.22424	0.83791
C	5.80439	1.92531	1.60799
H	6.26183	1.83119	2.59899
H	6.61826	2.05079	0.88521
H	5.20583	2.84048	1.59989
C	-0.18282	4.88138	2.75793
H	-0.31985	4.17128	3.57799
H	0.59390	5.59563	3.05264
H	-1.11372	5.44804	2.64309
C	0.32481	6.38045	0.24354

H	-0.68134	6.71193	0.52493
H	1.02199	6.84312	0.95142
H	0.54585	6.76913	-0.75346
C	2.31171	2.13990	-5.59973
H	2.30655	3.23248	-5.60020
H	3.30614	1.80125	-5.91039
H	1.60288	1.79725	-6.36264
C	2.34839	-0.78275	-5.06905
H	1.67768	-0.71290	-5.93286
H	3.36455	-0.59701	-5.43462
H	2.31075	-1.80877	-4.69331
C	-6.36134	0.93976	-0.05973
C	-5.67654	2.24564	0.26793
H	-5.15585	2.19717	1.23254
H	-4.93515	2.51945	-0.49203
H	-6.40644	3.05701	0.32994
H	-9.47790	-0.36237	-0.46675
C	-5.45627	-2.69909	-0.87557
H	-4.73649	-2.55817	-1.69109
H	-4.88990	-3.01108	0.01138
H	-6.11592	-3.52537	-1.15263

[Ru(tmb)$_2$(bpy-2,5-mesityl)](PF$_6$)$_2$ (6') (Å)

Atom	**X**	**Y**	**Z**
C	5.57285	-0.40405	1.33509
C	5.00063	0.87984	1.30533
C	3.64866	0.97622	1.00259
N	2.85909	-0.07527	0.73963
C	3.40115	-1.31138	0.76580
C	4.74875	-1.49225	1.06069
C	1.72575	-0.39685	-2.67870
C	2.08664	-0.04829	-3.97380
C	2.06130	1.31505	-4.31566
C	1.67440	2.22594	-3.33636
C	1.32363	1.79638	-2.06059
N	1.35133	0.48543	-1.74021
C	2.47007	-2.42317	0.44913
C	0.90885	2.71254	-0.96853
N	1.20902	-2.05555	0.13751

C	0.32440	-3.01071	-0.18535
C	0.62148	-4.36717	-0.22317
C	1.92908	-4.75878	0.11403
C	2.84256	-3.76318	0.45004
C	0.79978	4.09158	-1.11494
C	0.42517	4.89765	-0.04325
C	0.16532	4.27378	1.18964
C	0.28589	2.89172	1.25181
N	0.64494	2.12000	0.21554
C	-1.88135	0.00371	-1.27772
C	0.80368	-0.39269	3.30456
C	0.25420	-0.60050	4.56058
C	-1.12759	-0.70066	4.67172
C	-1.90323	-0.59255	3.52470
C	-1.28552	-0.38918	2.29336
N	0.06005	-0.28345	2.19372
C	-2.03314	-0.27305	1.01371
N	-1.26913	-0.09510	-0.08842
C	-3.41704	-0.36096	0.92992
C	-4.06555	-0.27214	-0.30647
C	-3.25438	-0.08057	-1.42953
Ru	0.80913	0.016	0.24369
C	-5.54474	-0.35062	-0.39142
C	-6.19872	-1.19676	-1.30245
C	-7.59543	-1.19684	-1.29286
C	-8.32426	-0.38698	-0.43386
C	-7.68101	0.45767	0.47445
H	-1.59745	-0.85967	5.63764
H	0.90132	-0.68314	5.42747
H	-8.12596	-1.85898	-1.97344
H	-3.68933	0.01605	-2.41863
H	-4.01648	-0.52267	1.81960
H	-2.98234	-0.66920	3.59364
H	1.00644	4.55600	-2.07385
H	-0.67417	-2.65846	-0.43358
H	1.65305	3.28276	-3.58258
H	1.87744	-0.30387	3.16701
H	-1.22902	0.15760	-2.13249
H	0.08984	2.36553	2.18327
H	1.73357	-1.43752	-2.36438
H	3.16383	1.94874	0.96774

H	3.85520	-4.04905	0.71630
H	5.17506	-2.49003	1.07255
C	-0.42717	-5.36975	-0.61522
H	-1.38260	-4.88384	-0.83165
H	-0.12300	-5.92927	-1.50718
H	-0.59388	-6.10158	0.18282
C	2.33734	-6.20387	0.10127
H	1.68419	-6.80624	0.74165
H	2.26806	-6.61863	-0.91088
H	3.36536	-6.32976	0.44951
C	7.02895	-0.59147	1.64999
H	7.26045	-0.21788	2.65424
H	7.32336	-1.64251	1.60217
H	7.65517	-0.02716	0.95004
C	5.81049	2.11626	1.57740
H	6.26238	2.08388	2.57485
H	6.62688	2.21882	0.85385
H	5.19384	3.01735	1.51622
C	-0.23190	5.06092	2.40669
H	-0.37701	4.40893	3.27242
H	0.53188	5.80291	2.66460
H	-1.16627	5.60736	2.23564
C	0.30329	6.38590	-0.19737
H	-0.70079	6.72633	0.08008
H	1.00817	6.90758	0.46023
H	0.49932	6.70333	-1.22442
C	2.43711	1.77620	-5.69452
H	2.43329	2.86647	-5.76551
H	3.43363	1.41742	-5.97419
H	1.73434	1.38529	-6.43968
C	2.49115	-1.10265	-4.96516
H	1.83296	-1.09274	-5.84133
H	3.51182	-0.93653	-5.32766
H	2.45127	-2.10238	-4.52443
C	-6.29090	0.45032	0.48446
H	-9.41121	-0.41626	-0.46179
C	-5.47404	-2.12137	-2.25346
H	-5.24281	-1.62716	-3.20533
H	-4.53457	-2.49958	-1.83747
H	-6.10269	-2.98455	-2.48990
H	-5.76426	1.11052	1.17284

C	-8.47245	1.35108	1.39381
H	-7.84453	1.76647	2.18804
H	-8.91073	2.19087	0.84273
H	-9.29690	0.80579	1.86415

[Ru(tmb)$_2$(bpy-3,5-mesityl)](PF$_6$)$_2$ (7') (Å)

Atom	X	Y	Z
C	5.64129	-0.30993	1.22374
C	5.02398	0.95411	1.25051
C	3.66694	1.01524	0.96329
N	2.91222	-0.05414	0.67118
C	3.49545	-1.27286	0.64499
C	4.85276	-1.41544	0.91582
C	1.73567	-0.30066	-2.70292
C	2.07614	0.10394	-3.98682
C	2.02449	1.47945	-4.27723
C	1.62458	2.34477	-3.26225
C	1.28978	1.86183	-2.00145
N	1.35280	0.53974	-1.72955
C	2.59414	-2.39414	0.30330
C	0.86169	2.71742	-0.87416
N	1.31844	-2.04385	0.02557
C	0.45011	-3.00259	-0.32933
C	0.78043	-4.34754	-0.43626
C	2.10071	-4.72455	-0.12883
C	2.99556	-3.72417	0.24206
C	0.69281	4.09566	-0.95902
C	0.31824	4.84188	0.15525
C	0.12053	4.15724	1.36864
C	0.28853	2.77888	1.36873
N	0.64753	2.06622	0.29098
C	-1.84353	0.06477	-1.21772
C	0.98602	-0.62655	3.22880
C	0.48840	-0.98249	4.47251
C	-0.88443	-1.15157	4.61498
C	-1.70330	-0.95817	3.51035

C	-1.13887	-0.60675	2.28663
N	0.19977	-0.44044	2.15714
C	-1.92521	-0.38843	1.05096
N	-1.19302	-0.13707	-0.06111
C	-3.31124	-0.44277	1.01000
C	-4.00158	-0.22672	-0.18836
C	-3.22198	0.03103	-1.32296
Ru	0.87222	-0.01120	0.22555
C	-5.47579	-0.26414	-0.24291
C	-6.12705	-0.78923	-1.36114
C	-7.52163	-0.82976	-1.42041
C	-8.24412	-0.32177	-0.34155
C	-7.61999	0.21658	0.78838
H	-1.31333	-1.43225	5.57097
H	1.16888	-1.12705	5.30358
H	-3.68685	0.22635	-2.28266
H	-3.87676	-0.66958	1.90572
H	-2.77451	-1.08780	3.60448
H	0.84743	4.60431	-1.90381
H	-0.55623	-2.65897	-0.54821
H	1.58351	3.40820	-3.46945
H	2.04885	-0.48369	3.06711
H	-1.21951	0.27013	-2.08051
H	0.13799	2.20675	2.27901
H	1.76585	-1.34883	-2.42491
H	3.14913	1.96873	0.96950
H	4.01614	-3.99837	0.48462
H	5.31113	-2.39695	0.88403
C	-0.24647	-5.35028	-0.87916
H	-1.21600	-4.87795	-1.05733
H	0.06463	-5.84467	-1.80643
H	-0.38712	-6.13509	-0.12810
C	2.54724	-6.15534	-0.21573
H	1.90144	-6.81130	0.37652
H	2.50725	-6.51159	-1.25130
H	3.57214	-6.27203	0.14363

C	7.10535	-0.45702	1.51940
H	7.32843	-0.12740	2.54089
H	7.44318	-1.49028	1.41640
H	7.70540	0.16887	0.85017
C	5.78955	2.20656	1.57129
H	6.24073	2.14851	2.56755
H	6.60101	2.36858	0.85353
H	5.14006	3.08561	1.54527
C	-0.25949	4.87630	2.63170
H	-0.35663	4.18340	3.47149
H	0.49012	5.62952	2.89743
H	-1.21524	5.39939	2.51627
C	0.13466	6.32852	0.06698
H	-0.87133	6.61860	0.39042
H	0.83812	6.85209	0.72413
H	0.28126	6.69750	-0.95069
C	2.38647	2.00285	-5.63698
H	2.38522	3.09487	-5.65577
H	3.37757	1.65547	-5.94707
H	1.67333	1.65091	-6.39162
C	2.48697	-0.90413	-5.02175
H	1.81179	-0.87583	-5.88443
H	3.49700	-0.70328	-5.39547
H	2.47497	-1.92073	-4.62077
C	-6.22931	0.23370	0.82743
H	-9.33110	-0.34262	-0.37857
H	-5.73082	0.67550	1.68734
C	-8.43982	0.78301	1.91913
H	-7.82109	1.00016	2.79450
H	-8.92855	1.71449	1.61288
H	-9.22521	0.08303	2.22140
H	-5.55071	-1.20289	-2.18594
C	-8.22017	-1.42432	-2.61662
H	-7.75405	-1.09847	-3.55185
H	-8.18419	-2.51941	-2.59153
H	-9.27223	-1.12877	-2.64377

Donor-Bridge-Acceptor Complexes
$[Ru(bpy)_2(bpy\text{-}phenyl\text{-}MV)](PF_6)_4$ (1) (Å)

Atom	X	Y	Z
C	8.68427	-0.45342	0.53888
C	8.01257	0.45467	1.34904
C	6.63322	0.54484	1.24534
N	5.91769	-0.20739	0.39390
C	6.56375	-1.10520	-0.39022
C	7.94734	-1.24573	-0.33398
C	4.80037	1.48636	-2.45091
C	5.26744	2.57326	-3.17455
C	5.28986	3.82189	-2.56433
C	4.83439	3.93572	-1.25621
C	4.37816	2.80522	-0.58481
N	4.36821	1.58872	-1.18364
C	5.69508	-1.88837	-1.29781
C	3.88818	2.82532	0.81254
N	4.38687	-1.52949	-1.29307
C	3.53518	-2.16148	-2.11519
C	3.93374	-3.17018	-2.97788
C	5.26986	-3.55580	-2.97831
C	6.15705	-2.90585	-2.12941
C	3.74961	3.98947	1.56445
C	3.28624	3.91409	2.87187
C	2.96490	2.66774	3.39882
C	3.12685	1.54695	2.59851
N	3.57864	1.61334	1.33609
C	1.10165	0.80110	-1.03671
C	4.05815	-2.26145	2.14115
C	3.60029	-3.28978	2.95281
C	2.24038	-3.57614	2.96318
C	1.39016	-2.81431	2.17006
C	1.91256	-1.78793	1.38911
N	3.24160	-1.52354	1.37314
C	1.08861	-0.91097	0.52662
N	1.78510	-0.03667	-0.24033
C	-0.30434	-0.94000	0.50703
C	-1.01894	-0.06010	-0.30602
C	-0.28248	0.82469	-1.09843
Ru	3.86286	-0.02066	0.05873

C	-2.50794	-0.05815	-0.30976
C	-3.22400	-1.25513	-0.43336
C	-4.61484	-1.25965	-0.42604
C	-5.28772	-0.05017	-0.28189
C	-4.60470	1.15593	-0.15714
C	-3.21442	1.14380	-0.17921
N	-6.74417	-0.04404	-0.25215
C	-7.40241	-0.81673	0.64237
C	-8.78191	-0.82146	0.69663
C	-9.52195	-0.00591	-0.16842
C	-8.81353	0.78409	-1.08243
C	-7.43378	0.74255	-1.11059
C	-11.00983	0.02764	-0.10964
C	-11.75155	-1.14304	0.07239
C	-13.13287	-1.07970	0.13328
N	-13.77624	0.09840	0.02513
C	-13.08476	1.24312	-0.15396
C	-11.70529	1.23683	-0.22670
C	-15.25947	0.15920	0.08709
H	-15.54752	0.91753	0.81638
H	-15.64623	-0.80966	0.39916
H	-15.64248	0.41565	-0.90248
H	1.84674	-4.38002	3.57590
H	4.29823	-3.85514	3.55912
H	-13.66606	2.15557	-0.22969
H	-13.74591	-1.96318	0.26819
H	-11.19459	2.18620	-0.34346
H	-11.28218	-2.11788	0.14194
H	-9.32635	1.41512	-1.80026
H	-9.26543	-1.43934	1.44573
H	-6.84324	1.31650	-1.81420
H	-6.78814	-1.40317	1.31413
H	-5.13822	2.09078	-0.01276
H	-5.15679	-2.19097	-0.56156
H	-2.67875	2.08034	-0.06004
H	-2.69626	-2.19434	-0.56708
H	-0.77544	1.51686	-1.77269
H	-0.84543	-1.61890	1.15580
H	0.32905	-3.03234	2.16327
H	4.00434	4.95370	1.14192
H	2.50658	-1.82041	-2.08144
H	4.85064	4.90393	-0.77160

H	5.10935	-2.00042	2.10005
H	1.70366	1.46785	-1.64347
H	2.90028	0.55360	2.97037
H	4.77718	0.49085	-2.87845
H	6.06538	1.23455	1.85847
H	7.19851	-3.20331	-2.11664
H	8.46105	-1.95328	-0.97334
H	5.61848	2.43886	-4.19127
H	2.59961	2.56267	4.41388
H	3.21040	-3.64458	-3.63096
H	8.54809	1.09087	2.04393
H	5.61803	-4.34434	-3.63686
H	9.76436	-0.54247	0.58164
H	5.66198	4.69453	-3.09034
H	3.17841	4.81441	3.46735

$[Ru(dmb)_2(bpy\text{-}phenyl\text{-}MV)](PF_6)_4$ (2) (Å)

Atom	**X**	**Y**	**Z**
C	8.21547	-0.72458	0.84701
C	7.57867	0.36669	1.44661
C	6.22219	0.55990	1.25530
N	5.46375	-0.26691	0.51614
C	6.05650	-1.33729	-0.06559
C	7.41833	-1.57695	0.08237
C	4.27317	0.87125	-2.63306
C	4.68919	1.77474	-3.59394
C	4.74114	3.13869	-3.29093
C	4.35449	3.51256	-2.00335
C	3.95010	2.55717	-1.07624
N	3.90748	1.24206	-1.39431
C	5.15303	-2.21117	-0.84900
C	3.55178	2.88070	0.31421
N	3.85779	-1.81730	-0.87988
C	2.98296	-2.55856	-1.57880
C	3.34423	-3.70035	-2.26885
C	4.67513	-4.13150	-2.24833
C	5.57524	-3.35597	-1.51690
C	3.51695	4.17418	0.82545
C	3.15927	4.40997	2.15293
C	2.83311	3.29092	2.92663
C	2.88015	2.02896	2.36288

N	3.23781	1.81294	1.08630
C	0.64355	0.65025	-0.96301
C	3.61676	-1.83534	2.64906
C	3.18274	-2.75695	3.59068
C	1.84221	-3.12207	3.59693
C	0.98002	-2.52728	2.68281
C	1.47638	-1.59316	1.77705
N	2.79335	-1.27276	1.75210
C	0.64427	-0.85613	0.79917
N	1.33429	-0.08390	-0.07638
C	-0.74877	-0.89473	0.78856
C	-1.47177	-0.12869	-0.12709
C	-0.73991	0.65715	-1.02248
Ru	3.41293	-0.05944	0.16831
C	-2.96005	-0.12921	-0.13411
C	-3.68119	-1.31364	0.06524
C	-5.07233	-1.31455	0.06633
C	-5.74001	-0.11227	-0.13948
C	-5.05690	1.08160	-0.34414
C	-3.66665	1.06362	-0.33799
N	-7.19991	-0.09952	-0.14060
C	-7.87267	-0.30541	1.01388
C	-9.25363	-0.29118	1.03928
C	-9.97302	-0.05904	-0.14023
C	-9.24763	0.15094	-1.32008
C	-7.86665	0.12496	-1.29504
C	-11.46241	-0.03458	-0.13893
C	-12.19894	-0.92116	0.65260
C	-13.58115	-0.87694	0.63651
N	-14.23689	0.01270	-0.13359
C	-13.55271	0.87950	-0.90855
C	-12.17163	0.87713	-0.92994
C	-15.72122	0.02717	-0.16323
H	-16.06811	1.06053	-0.14270
H	-16.10295	-0.49600	0.71256
H	-16.06047	-0.46800	-1.07562
H	1.47319	-3.85611	4.30514
H	3.88874	-3.17973	4.29645
H	-14.14407	1.56460	-1.50506
H	-14.18885	-1.54742	1.23207
H	-11.66575	1.60802	-1.55112

H	-11.71783	-1.66844	1.27405
H	-9.73977	0.30279	-2.27446
H	-9.74943	-0.42620	1.99417
H	-7.25891	0.26527	-2.18126
H	-7.26839	-0.46123	1.89975
H	-5.59225	2.01646	-0.48009
H	-5.61988	-2.24276	0.19939
H	-3.13168	1.99930	-0.46561
H	-3.15896	-2.25689	0.19042
H	-1.23405	1.26157	-1.77563
H	-1.27720	-1.48846	1.52574
H	-0.06673	-2.80717	2.67534
H	3.77420	5.01523	0.19233
H	1.96020	-2.19820	-1.58298
H	4.38614	4.56046	-1.72864
H	4.65403	-1.52524	2.60007
H	1.23961	1.25140	-1.63988
H	2.64154	1.14370	2.94253
H	4.23224	-0.19212	-2.84070
H	5.70894	1.40191	1.70633
H	6.61462	-3.66043	-1.48141
H	7.87562	-2.43787	-0.39120
C	5.10686	-5.37156	-2.97478
H	4.68663	-6.26227	-2.49461
H	4.74622	-5.35956	-4.00767
H	6.19398	-5.47347	-2.98858
C	9.69005	-0.95026	1.00607
H	9.98642	-0.90434	2.05841
H	10.00098	-1.91732	0.60443
H	10.25008	-0.17206	0.47568
C	3.13902	5.79436	2.73126
H	2.16716	6.01348	3.18495
H	3.89391	5.89014	3.51919
H	3.34424	6.55462	1.97441
C	5.19184	4.14876	-4.30581
H	5.25052	5.15249	-3.88001
H	6.17508	3.88113	-4.70524
H	4.49303	4.17730	-5.14910
H	4.98487	1.41297	-4.57359
H	2.54447	3.39775	3.96743
H	2.59369	-4.25200	-2.82547

H	8.13919	1.06229	2.06212

[Ru(tmb)$_2$(bpy-phenyl-MV)](PF$_6$)$_4$ (3) (Å)

Atom	X	Y	Z
C	7.93379	-0.63691	0.82920
C	7.38221	0.64585	1.00612
C	6.00942	0.78793	0.84888
N	5.17922	-0.21788	0.53031
C	5.70255	-1.45046	0.34307
C	7.06647	-1.67460	0.49546
C	3.76680	-0.27498	-2.75550
C	4.10748	0.16040	-4.02981
C	4.20691	1.54828	-4.24209
C	3.96093	2.39128	-3.16059
C	3.62939	1.87830	-1.91160
N	3.52999	0.54368	-1.71870
C	4.72779	-2.50083	-0.01894
C	3.37997	2.71099	-0.71438
N	3.43934	-2.09799	-0.09022
C	2.50087	-3.00821	-0.39580
C	2.76858	-4.34396	-0.66246
C	4.11068	-4.76662	-0.61852
C	5.07672	-3.82028	-0.28750
C	3.46361	4.09955	-0.70284
C	3.25618	4.82149	0.47007
C	2.94724	4.10162	1.64038
C	2.87026	2.71841	1.54642
N	3.08482	2.02855	0.41472
C	0.33704	0.18826	-1.02638
C	3.38291	-0.75220	3.20877
C	2.95021	-1.08923	4.48338
C	1.58373	-1.16996	4.72316
C	0.70212	-0.90965	3.68084
C	1.20158	-0.57953	2.42394
N	2.53661	-0.50186	2.19853
C	0.35342	-0.30817	1.24082
N	1.03307	-0.06397	0.09375
C	-1.04116	-0.29994	1.26924
C	-1.76865	-0.03752	0.10770
C	-1.04649	0.20982	-1.06380

Ru	3.11492	-0.05670	0.24217
C	-3.25695	-0.02022	0.10412
C	-3.98902	-1.01648	0.76126
C	-5.37965	-1.01814	0.73341
C	-6.03558	-0.00121	0.04641
C	-5.33806	1.01040	-0.60650
C	-3.94845	0.99118	-0.57530
N	-7.49169	-0.00084	-0.00315
C	-8.20643	-0.02596	1.14460
C	-9.58738	-0.03885	1.11928
C	-10.26525	-0.00636	-0.10542
C	-9.49989	0.03102	-1.27730
C	-8.12098	0.02196	-1.20074
C	-11.75349	-0.01068	-0.15847
C	-12.50151	-0.82577	0.69617
C	-13.88306	-0.80890	0.63201
N	-14.52567	-0.01200	-0.24330
C	-13.82922	0.78457	-1.08065
C	-12.44829	0.80302	-1.06106
C	-16.00872	-0.02124	-0.31899
H	-16.36783	1.00662	-0.37555
H	-16.41052	-0.49267	0.57682
H	-16.31281	-0.58013	-1.20662
H	1.20805	-1.43860	5.70462
H	3.67605	-1.28683	5.26359
H	-14.41224	1.40167	-1.75476
H	-14.49919	-1.42749	1.27326
H	-11.93071	1.47410	-1.73765
H	-12.02826	-1.49714	1.40446
H	-9.95805	0.02399	-2.26012
H	-10.11578	-0.03550	2.06633
H	-7.48489	0.01056	-2.07766
H	-7.63971	-0.01234	2.06775
H	-5.85900	1.82129	-1.10686
H	-5.93140	-1.82338	1.20952
H	-3.40266	1.79191	-1.06421
H	-3.47515	-1.82773	1.26727
H	-1.54762	0.39842	-2.00733
H	-1.56395	-0.47196	2.20347
H	-0.36549	-0.97247	3.85419
H	3.70548	4.63837	-1.61212

H	1.48312	-2.63262	-0.43158
H	4.03614	3.46321	-3.30432
H	4.43786	-0.68155	2.96900
H	0.92812	0.36863	-1.91720
H	2.64384	2.11888	2.42257
H	3.68448	-1.33675	-2.54429
H	5.54417	1.75907	0.98102
H	6.11402	-4.13160	-0.24549
H	7.47415	-2.66956	0.35843
C	1.65565	-5.29908	-0.98650
H	0.68230	-4.80109	-0.98099
H	1.79285	-5.75454	-1.97316
H	1.61862	-6.11512	-0.25651
C	4.49563	-6.18747	-0.91055
H	4.08888	-6.86475	-0.15040
H	4.10114	-6.51751	-1.87734
H	5.58045	-6.31058	-0.92451
C	9.40513	-0.87711	0.99231
H	9.73548	-0.61241	2.00345
H	9.66974	-1.92123	0.81163
H	9.98375	-0.25633	0.29969
C	8.23655	1.83198	1.34962
H	8.77632	1.67138	2.28934
H	8.98961	2.00975	0.57433
H	7.63918	2.74113	1.45549
C	2.72363	4.79085	2.95630
H	2.45001	4.07862	3.73893
H	3.62986	5.31319	3.28364
H	1.92962	5.54136	2.88327
C	3.37016	6.31756	0.49044
H	2.42276	6.77655	0.79437
H	4.12585	6.63743	1.21634
H	3.64789	6.71540	-0.48773
C	4.56811	2.10137	-5.58911
H	4.61499	3.19225	-5.58026
H	5.53934	1.71999	-5.92290
H	3.83175	1.79996	-6.34285
C	4.35651	-0.83032	-5.13075
H	3.64139	-0.69514	-5.94951
H	5.35921	-0.71008	-5.55436
H	4.27058	-1.85738	-4.76681

[Ru(tmb)$_2$(bpy-ortho-MV)](PF$_6$)$_4$ (4) (Å)

Atom	X	Y	Z
C	7.99149	-0.66212	0.79116
C	7.43339	0.60603	1.03774
C	6.05727	0.74423	0.90354
N	5.22877	-0.25484	0.55995
C	5.75629	-1.47838	0.32960
C	7.12524	-1.69417	0.43906
C	3.82768	-0.31666	-2.73620
C	4.16343	0.11719	-4.01228
C	4.25735	1.50493	-4.22776
C	4.01258	2.34918	-3.14692
C	3.68695	1.83744	-1.89576
N	3.59120	0.50313	-1.70017
C	4.78125	-2.53156	-0.02282
C	3.43668	2.67231	-0.70037
N	3.49034	-2.13384	-0.07583
C	2.55115	-3.04907	-0.36384
C	2.81995	-4.38538	-0.62662
C	4.16385	-4.80358	-0.59765
C	5.13105	-3.85163	-0.28725
C	3.52325	4.06081	-0.69088
C	3.31410	4.78545	0.47989
C	3.00034	4.06852	1.65062
C	2.91987	2.68524	1.55867
N	3.13616	1.99255	0.42880
C	0.39871	0.13415	-1.03819
C	3.40734	-0.78201	3.22853
C	2.96290	-1.10212	4.50346
C	1.59402	-1.16421	4.73541
C	0.72174	-0.90297	3.68537
C	1.23282	-0.58838	2.42914
N	2.57019	-0.52908	2.21123
C	0.39520	-0.31837	1.23838
N	1.08408	-0.09939	0.09268
C	-1.00051	-0.28955	1.25801
C	-1.71522	-0.03651	0.08811
C	-0.98402	0.17095	-1.08499
Ru	3.16555	-0.09335	0.25945
C	-3.20898	-0.00801	0.07982
C	-3.90981	-1.17177	0.41074
C	-5.30054	-1.21210	0.38915

C	-5.97548	-0.05380	0.03004
C	-5.30765	1.12354	-0.28576
N	-7.43500	-0.06649	-0.01382
C	-8.13772	-0.19413	1.13331
C	-9.51884	-0.21291	1.11793
C	-10.20678	-0.09699	-0.09671
C	-9.45083	0.03588	-1.26837
C	-8.07087	0.04651	-1.20123
C	-11.69567	-0.11371	-0.13948
C	-12.43146	-0.94892	0.70622
C	-13.81355	-0.94380	0.65191
N	-14.46948	-0.14182	-0.20848
C	-13.78578	0.67439	-1.03739
C	-12.40526	0.70821	-1.02348
C	-15.95371	-0.12424	-0.23872
H	-16.30494	0.80088	0.22301
H	-16.33451	-0.98461	0.30976
H	-16.28990	-0.18145	-1.27459
H	1.20975	-1.41996	5.71694
H	3.68192	-1.30065	5.28977
H	-14.37872	1.29378	-1.70041
H	-14.41952	-1.57355	1.29200
H	-11.90081	1.39517	-1.69397
H	-11.94900	-1.62917	1.39947
H	-9.91708	0.09330	-2.24573
H	-10.04060	-0.28575	2.06584
H	-7.43765	0.12811	-2.07670
H	-7.55827	-0.26195	2.04637
H	-5.86829	2.02251	-0.52829
H	-5.83259	-2.12973	0.61998
H	-1.47944	0.35129	-2.03281
H	-1.53646	-0.44860	2.18710
H	-0.34767	-0.95344	3.85137
H	3.76986	4.59762	-1.59989
H	1.53157	-2.67773	-0.38792
H	4.08247	3.42109	-3.29374
H	4.46433	-0.72670	2.99460
H	0.99900	0.29129	-1.92734
H	2.68925	2.08734	2.43475
H	3.74770	-1.37833	-2.52350
H	5.58721	1.70622	1.08041
H	6.16932	-4.16041	-0.25204
H	7.53824	-2.67802	0.24722
C	1.70536	-5.34626	-0.92621

H	0.73039	-4.85168	-0.90582
H	1.82607	-5.80645	-1.91288
H	1.68463	-6.15913	-0.19194
C	4.54925	-6.22602	-0.88163
H	4.15237	-6.89765	-0.11132
H	4.14497	-6.56496	-1.84135
H	5.63417	-6.34691	-0.90605
C	9.46801	-0.89764	0.90990
H	9.81079	-0.72979	1.93737
H	9.73921	-1.91724	0.62740
H	10.03053	-0.21085	0.26846
C	8.28461	1.78025	1.42703
H	8.83293	1.57901	2.35393
H	9.03010	1.99718	0.65437
H	7.68297	2.68017	1.57861
C	2.77629	4.76025	2.96509
H	2.50553	4.04990	3.75039
H	3.68152	5.28564	3.29002
H	1.98049	5.50898	2.89140
C	3.43139	6.28148	0.49746
H	2.48521	6.74296	0.80166
H	4.18847	6.60160	1.22171
H	3.70864	6.67652	-0.48190
C	4.60979	2.05675	-5.57762
H	4.64881	3.14798	-5.57294
H	5.58288	1.68131	-5.91286
H	3.87360	1.74668	-6.32800
C	4.41147	-0.87441	-5.11271
H	3.69238	-0.74360	-5.92869
H	5.41196	-0.75087	-5.54068
H	4.33095	-1.90124	-4.74676
C	-3.91154	1.16615	-0.26342
C	-3.20221	2.45853	-0.58304
H	-2.38298	2.64690	0.11650
H	-2.78066	2.43952	-1.59305
H	-3.89178	3.30435	-0.53006
H	-3.36088	-2.07296	0.66649

[Ru(tmb)$_2$(bpy-2,6-mesityl-MV)](PF$_6$)$_4$ (5) (Å)

Atom	**X**	**Y**	**Z**
C	8.00825	-0.66702	0.92185
C	7.48043	0.63561	0.99542

C	6.11357	0.79223	0.80381
N	5.26983	-0.21704	0.53963
C	5.77169	-1.46897	0.44231
C	7.12760	-1.70911	0.63914
C	3.92790	-0.36188	-2.74047
C	4.31123	0.02501	-4.01842
C	4.42261	1.40347	-4.28026
C	4.14418	2.28852	-3.24144
C	3.77406	1.82318	-1.98405
N	3.66362	0.49705	-1.74384
C	4.78328	-2.51807	0.11567
C	3.50329	2.69838	-0.82262
N	3.50658	-2.09135	-0.01106
C	2.55522	-2.99382	-0.29596
C	2.79582	-4.34767	-0.48338
C	4.12475	-4.79869	-0.37401
C	5.10537	-3.85894	-0.06815
C	3.58450	4.08695	-0.85705
C	3.36016	4.84762	0.28821
C	3.03863	4.16731	1.47837
C	2.96786	2.78180	1.43118
N	3.19627	2.05508	0.32593
C	0.44014	0.20675	-1.06226
C	3.45134	-0.64060	3.22051
C	3.00678	-0.95866	4.49599
C	1.63821	-1.04511	4.72204
C	0.76691	-0.80900	3.66545
C	1.27856	-0.49845	2.40868
N	2.61501	-0.41609	2.19588
C	0.44107	-0.24847	1.21388
N	1.12778	-0.02448	0.06765
C	-0.95420	-0.24618	1.23148
C	-1.67077	-0.01309	0.05969
C	-0.94438	0.21832	-1.11092
Ru	3.21193	-0.03415	0.23052
C	-3.16816	-0.01206	0.04908
C	-3.85649	-1.21697	-0.18249
C	-5.25251	-1.20294	-0.20855
C	-5.92481	-0.00559	-0.00431
C	-5.25529	1.18832	0.22625

N	-7.38185	-0.00246	-0.03958
C	-8.07645	-0.81737	0.78623
C	-9.45668	-0.84080	0.76437
C	-10.15953	-0.00381	-0.11100
C	-9.41344	0.83476	-0.94807
C	-8.03351	0.81243	-0.89938
C	-11.64800	-0.00819	-0.15221
C	-12.36690	-1.20215	-0.04644
C	-13.74988	-1.17933	-0.08993
N	-14.41820	-0.01894	-0.23147
C	-13.74954	1.14878	-0.33452
C	-12.36934	1.18285	-0.29971
C	-15.90260	-0.00001	-0.26412
H	-16.26830	0.51821	0.62440
H	-16.27547	-1.02271	-0.27034
H	-16.23030	0.51158	-1.17040
H	1.25292	-1.29890	5.70382
H	3.72545	-1.13893	5.28698
H	-14.35206	2.04416	-0.44129
H	-14.34362	-2.08305	-0.01663
H	-11.88040	2.14860	-0.35993
H	-11.87572	-2.16480	0.04020
H	-9.89270	1.48771	-1.66954
H	-9.97343	-1.49345	1.45958
H	-7.41287	1.41923	-1.54674
H	-7.48782	-1.42605	1.46126
H	-5.80466	2.10735	0.41155
H	-5.79861	-2.11816	-0.42053
H	-1.44678	0.40622	-2.05410
H	-1.49024	-0.42418	2.15704
H	-0.30236	-0.87577	3.82715
H	3.83857	4.59402	-1.78116
H	1.54746	-2.59788	-0.37490
H	4.23087	3.35409	-3.42277
H	4.50848	-0.56589	2.99187
H	1.03818	0.38163	-1.94968
H	2.73621	2.21237	2.32609
H	3.83688	-1.41359	-2.48802
H	5.66711	1.77922	0.85874
H	6.13399	-4.19090	0.01510

H	7.51673	-2.71906	0.58058
C	1.66955	-5.28890	-0.80061
H	0.70806	-4.76929	-0.83775
H	1.82389	-5.78028	-1.76748
H	1.59435	-6.07956	-0.04611
C	4.47356	-6.24529	-0.56820
H	3.96304	-6.87037	0.17330
H	4.15341	-6.59857	-1.55479
H	5.54830	-6.41564	-0.47798
C	9.47219	-0.91958	1.12888
H	9.79335	-0.57276	2.11763
H	9.72094	-1.97964	1.04485
H	10.06946	-0.36768	0.39449
C	8.34775	1.82917	1.27477
H	8.82935	1.74762	2.25523
H	9.14453	1.91903	0.52881
H	7.77105	2.75780	1.26151
C	2.79512	4.90055	2.76714
H	2.50292	4.21395	3.56579
H	3.69799	5.42883	3.09398
H	2.00718	5.65220	2.65285
C	3.47024	6.34390	0.25925
H	2.51610	6.81054	0.52929
H	4.21149	6.69032	0.98790
H	3.76608	6.71096	-0.72569
C	4.83258	1.90296	-5.63452
H	4.89803	2.99280	-5.65743
H	5.80571	1.49521	-5.92867
H	4.11100	1.59124	-6.39841
C	4.60163	-1.00676	-5.06971
H	3.92627	-0.89660	-5.92539
H	5.62304	-0.90859	-5.45274
H	4.49177	-2.02044	-4.67613
C	-3.85902	1.19617	0.25476
C	-3.11242	-2.50849	-0.41120
H	-2.37555	-2.40301	-1.21350
H	-2.57230	-2.81289	0.49240
H	-3.79574	-3.31676	-0.68047
C	-3.11882	2.48217	0.52166
H	-2.60519	2.44139	1.48843

H	-2.36189	2.67372	-0.24486
H	-3.80213	3.33412	0.54495

[Ru(tmb)$_2$(bpy-2,5-mesityl-MV)](PF$_6$)$_4$ (6) (Å)

Atom	**X**	**Y**	**Z**
C	8.09188	-0.66480	0.73503
C	7.53802	0.59858	1.01334
C	6.16098	0.74158	0.89332
N	5.32780	-0.24926	0.53740
C	5.85120	-1.46911	0.27956
C	7.22082	-1.68843	0.37064
C	3.90781	-0.24566	-2.75284
C	4.23103	0.21182	-4.02395
C	4.32114	1.60343	-4.21512
C	4.08670	2.42765	-3.11676
C	3.77418	1.89253	-1.87193
N	3.68052	0.55509	-1.70007
C	4.87120	-2.51523	-0.08057
C	3.53410	2.70513	-0.65947
N	3.58139	-2.11294	-0.12318
C	2.63811	-3.02196	-0.41725
C	2.90154	-4.35643	-0.69443
C	4.24407	-4.77974	-0.67370
C	5.21569	-3.83392	-0.35858
C	3.62590	4.09281	-0.62334
C	3.42770	4.79502	0.56283
C	3.11858	4.05645	1.72127
C	3.03143	2.67571	1.60254
N	3.23813	2.00454	0.45805
C	0.49212	0.17973	-1.03381
C	3.51425	-0.82459	3.20321
C	3.07376	-1.16280	4.47468
C	1.70560	-1.22135	4.71174
C	0.82998	-0.93892	3.67005
C	1.33721	-0.60651	2.41678
N	2.67386	-0.55010	2.19414
C	0.49545	-0.31236	1.23457
N	1.18090	-0.07608	0.09010
C	-0.89990	-0.27871	1.26014
C	-1.61818	-0.00204	0.09778

C	-0.89058	0.22281	-1.07421
Ru	3.26319	-0.07773	0.24925
C	-3.11182	0.03648	0.09488
C	-3.81742	-1.13386	0.38373
C	-5.21320	-1.19888	0.36806
C	-5.86776	-0.00775	0.05215
C	-5.19853	1.17902	-0.22511
N	-7.33012	0.00781	-0.00703
C	-9.43003	-0.00756	1.10264
C	-10.09810	0.02119	-0.12768
C	-9.32652	0.04790	-1.29567
C	-7.94719	0.03529	-1.20827
C	-11.58653	0.02589	-0.18824
C	-12.34246	-0.77599	0.67171
C	-13.72360	-0.75309	0.60132
N	-14.35816	0.03674	-0.28610
C	-13.65388	0.82169	-1.12812
C	-12.27301	0.83414	-1.10202
C	-15.84156	0.07713	-0.32871
H	-16.18285	1.00458	0.13591
H	-16.23933	-0.78119	0.21095
H	-16.17070	0.03099	-1.36734
H	1.32425	-1.49016	5.69084
H	3.79512	-1.37709	5.25476
H	-14.23151	1.43559	-1.80970
H	-14.34484	-1.36039	1.24824
H	-11.74862	1.49341	-1.78466
H	-11.87629	-1.44396	1.38785
H	-9.77981	0.04297	-2.28067
H	-9.96585	0.00252	2.04541
H	-7.29891	0.03787	-2.07661
H	-5.76351	2.08154	-0.44360
H	-1.38945	0.42337	-2.01621
H	-1.43349	-0.45245	2.18791
H	-0.23894	-0.98616	3.83993
H	3.86911	4.64688	-1.52284
H	1.61973	-2.64696	-0.43404
H	4.15354	3.50204	-3.24465
H	4.57051	-0.77110	2.96539
H	1.08948	0.34976	-1.92254
H	2.80343	2.06092	2.46754

H	3.82987	-1.31093	-2.55866
H	5.69440	1.70057	1.09415
H	6.25282	-4.14680	-0.32872
H	7.63043	-2.66827	0.15283
C	1.78250	-5.31060	-0.99886
H	0.81017	-4.81083	-0.97906
H	1.90273	-5.76907	-1.98621
H	1.75579	-6.12500	-0.26617
C	4.62306	-6.20118	-0.97103
H	4.21541	-6.87913	-0.21215
H	4.22401	-6.52586	-1.93788
H	5.70736	-6.32867	-0.98894
C	9.56902	-0.90478	0.83561
H	9.92085	-0.75723	1.86302
H	9.83574	-1.91951	0.53170
H	10.12714	-0.20691	0.20242
C	8.39425	1.76272	1.42130
H	8.94384	1.54282	2.34326
H	9.13885	1.99083	0.65099
H	7.79610	2.66183	1.59033
C	2.90840	4.72262	3.05109
H	2.64035	3.99844	3.82459
H	3.81868	5.23707	3.37897
H	2.11574	5.47650	2.99938
C	3.55132	6.29002	0.60851
H	2.60862	6.74936	0.92623
H	4.31336	6.59373	1.33451
H	3.82458	6.70244	-0.36494
C	4.65853	2.18057	-5.55822
H	4.69501	3.27165	-5.53488
H	5.62951	1.81344	-5.90864
H	3.91653	1.88133	-6.30711
C	4.46986	-0.75847	-5.14520
H	3.74546	-0.61085	-5.95364
H	5.46768	-0.62730	-5.57733
H	4.39044	-1.79224	-4.79923
C	-3.80490	1.22536	-0.20845
H	-3.26251	-2.04154	0.60576
C	-5.94466	-2.48295	0.66839
H	-6.38048	-2.47136	1.67384
H	-6.74810	-2.67741	-0.04979

H	-5.25831	-3.33098	0.62463
C	-3.09189	2.52278	-0.49744
H	-2.27657	2.69624	0.21085
H	-2.66392	2.52408	-1.50491
H	-3.78079	3.36828	-0.43100
C	-8.04888	-0.01008	1.13543
H	-7.48337	-0.01222	2.05960

[Ru(tmb)$_2$(bpy-3,5-mesityl-MV)](PF$_6$)$_4$ (7) (Å)

Atom	**X**	**Y**	**Z**
C	8.13760	-0.63458	0.77070
C	7.58261	0.63656	1.00878
C	6.20665	0.77673	0.87631
N	5.37558	-0.22257	0.53998
C	5.90014	-1.44818	0.31457
C	7.26870	-1.66665	0.42491
C	3.95985	-0.28059	-2.74934
C	4.29353	0.15364	-4.02584
C	4.39171	1.54122	-4.23990
C	4.15243	2.38509	-3.15764
C	3.82833	1.87305	-1.90628
N	3.72899	0.53879	-1.71175
C	4.92217	-2.49956	-0.03556
C	3.58343	2.70755	-0.70951
N	3.63225	-2.09882	-0.08740
C	2.69070	-3.01126	-0.37659
C	2.95650	-4.34763	-0.64222
C	4.29927	-4.76911	-0.61382
C	5.26891	-3.82012	-0.30163
C	3.67292	4.09576	-0.69953
C	3.46803	4.82014	0.47211
C	3.15535	4.10319	1.64306
C	3.07230	2.72019	1.55074
N	3.28496	2.02768	0.42019
C	0.53504	0.16212	-1.03216
C	3.57096	-0.74025	3.21832
C	3.13469	-1.05524	4.49721
C	1.76730	-1.11535	4.73816
C	0.88865	-0.85891	3.69249
C	1.39148	-0.55153	2.43114

N	2.72723	-0.49183	2.20527
C	0.54630	-0.29142	1.24310
N	1.22902	-0.06646	0.09407
C	-0.84798	-0.28061	1.26849
C	-1.57463	-0.04422	0.10043
C	-0.84843	0.17756	-1.07387
Ru	3.31117	-0.05799	0.24942
C	-3.06314	-0.02948	0.09469
C	-5.18399	-1.00406	0.80094
C	-5.81977	-0.01447	0.04374
C	-5.14561	0.97175	-0.68478
N	-7.28479	-0.01492	-0.00073
C	-9.36285	0.83439	0.77838
C	-10.05337	-0.00037	-0.10829
C	-9.30474	-0.84421	-0.93712
C	-7.92496	-0.83255	-0.86333
C	-11.54243	0.00301	-0.16438
C	-12.30246	-0.06516	1.00620
C	-13.68414	-0.07006	0.92773
N	-14.30912	-0.00130	-0.26330
C	-13.59857	0.07059	-1.40832
C	-12.21727	0.06876	-1.38877
C	-15.79281	-0.01351	-0.33879
H	-16.12485	0.85593	-0.90817
H	-16.20107	0.03511	0.66895
H	-16.11376	-0.93746	-0.82371
H	1.38877	-1.36588	5.72333
H	3.85831	-1.25147	5.27982
H	-14.16756	0.13029	-2.32962
H	-14.31276	-0.13403	1.80814
H	-11.68751	0.14174	-2.33240
H	-11.84252	-0.13034	1.98599
H	-9.78410	-1.52900	-1.62864
H	-9.88947	1.52322	1.42986
H	-7.29582	-1.46721	-1.47578
H	-1.34717	0.34255	-2.02297
H	-1.37258	-0.43321	2.20493
H	-0.17971	-0.90704	3.86651
H	3.91772	4.63264	-1.60896
H	1.67214	-2.63713	-0.39999
H	4.22581	3.45688	-3.30318

H	4.62643	-0.68575	2.97711
H	1.12786	0.32727	-1.92473
H	2.84201	2.12237	2.42698
H	3.87708	-1.34225	-2.53761
H	5.73878	1.74070	1.04812
H	6.30648	-4.13132	-0.26752
H	7.67915	-2.65269	0.23905
C	1.83988	-5.30510	-0.94546
H	0.86603	-4.80854	-0.92387
H	1.96018	-5.76219	-1.93359
H	1.81728	-6.12051	-0.21395
C	4.68115	-6.19185	-0.90092
H	4.28338	-6.86412	-0.13171
H	4.27578	-6.52792	-1.86108
H	5.76584	-6.31511	-0.92616
C	9.61355	-0.87296	0.89134
H	9.95500	-0.70460	1.91923
H	9.88309	-1.89350	0.61057
H	10.17853	-0.18818	0.25017
C	8.43623	1.81239	1.38776
H	8.98680	1.61733	2.31472
H	9.18019	2.02322	0.61197
H	7.83588	2.71392	1.53464
C	2.93472	4.79478	2.95818
H	2.66062	4.08479	3.74269
H	3.84232	5.31588	3.28339
H	2.14210	5.54684	2.88507
C	3.58844	6.31587	0.49021
H	2.64337	6.77924	0.79480
H	4.34661	6.63394	1.21417
H	3.86605	6.71066	-0.48924
C	4.74327	2.09358	-5.58983
H	4.78849	3.18456	-5.58315
H	5.71329	1.71333	-5.92851
H	4.00332	1.78923	-6.33875
C	4.53555	-0.83744	-5.12802
H	3.81683	-0.70131	-5.94344
H	5.53655	-0.71861	-5.55626
H	4.44966	-1.86443	-4.76374
C	-3.75228	0.93916	-0.64118
C	-5.95341	-2.04786	1.56950

H	-6.67547	-1.59479	2.25839
H	-6.50782	-2.72247	0.90721
H	-5.28079	-2.66337	2.16891
C	-7.98165	0.80940	0.81020
H	-7.39229	1.44092	1.46436
H	-3.19926	1.70091	-1.18294
C	-5.87508	2.02634	-1.47704
H	-6.58968	1.58555	-2.18148
H	-6.43133	2.71372	-0.82964
H	-5.17686	2.62693	-2.06246
C	-3.78898	-0.98543	0.81039
H	-3.26454	-1.75633	1.36769